University of Alberta

Fine-Scale Structure/Function Analysis of the Voltage-Sensing Domain in Voltage-Gated Potassium Channels

by

Tara Leah Klassen

A thesis submitted to the Faculty of Graduate Studies and Research
in partial fulfillment of the requirements for the degree of

Doctor of Philosophy

in

Physiology and Cell Biology

Department of Biological Sciences

Edmonton, Alberta
Spring 2007

Library and Archives Canada

Published Heritage Branch

395 Wellington Street
Ottawa ON K1A 0N4
Canada

Bibliothèque et Archives Canada

Direction du Patrimoine de l'édition

395, rue Wellington
Ottawa ON K1A 0N4
Canada

Your file Votre référence
ISBN: 978-0-494-29701-8
Our file Notre référence
ISBN: 978-0-494-29701-8

NOTICE:
The author has granted a non-exclusive license allowing Library and Archives Canada to reproduce, publish, archive, preserve, conserve, communicate to the public by telecommunication or on the Internet, loan, distribute and sell theses worldwide, for commercial or non-commercial purposes, in microform, paper, electronic and/or any other formats.

The author retains copyright ownership and moral rights in this thesis. Neither the thesis nor substantial extracts from it may be printed or otherwise reproduced without the author's permission.

AVIS:
L'auteur a accordé une licence non exclusive permettant à la Bibliothèque et Archives Canada de reproduire, publier, archiver, sauvegarder, conserver, transmettre au public par télécommunication ou par l'Internet, prêter, distribuer et vendre des thèses partout dans le monde, à des fins commerciales ou autres, sur support microforme, papier, électronique et/ou autres formats.

L'auteur conserve la propriété du droit d'auteur et des droits moraux qui protège cette thèse. Ni la thèse ni des extraits substantiels de celle-ci ne doivent être imprimés ou autrement reproduits sans son autorisation.

In compliance with the Canadian Privacy Act some supporting forms may have been removed from this thesis.

While these forms may be included in the document page count, their removal does not represent any loss of content from the thesis.

Conformément à la loi canadienne sur la protection de la vie privée, quelques formulaires secondaires ont été enlevés de cette thèse.

Bien que ces formulaires aient inclus dans la pagination, il n'y aura aucun contenu manquant.

Canada

This thesis is dedicated to my family.

For my mother Dolores, through your dignity, perseverance, support, and infectious smile, you have taught me that perfection is not a requirement for happiness, but pride in one's self is.

And for my husband Tim, you are my world.

ABSTRACT

Potassium channels are ubiquitous in animal and plant kingdoms, are found in both eukaryotic and prokaryotic cells, and have large structural variation allowing for a range of function. Members of the six transmembrane domain (6TM) Shaker-superfamily of voltage-gated (K_v) ion channels are major determinants of the electrical phenotype of excitable cells such as neurons, myocytes, and some epithelial cells. These channels have two functional domains, the ion selective pore which has strong similarity to the two transmembrane (2TM) bacterial channels, and a voltage-sensing domain formed by four transmembrane helices, including the evolutionarily conserved voltage sensor. These domains allow a voltage-gated channel to detect changes in transmembrane voltage and become activated through conformational changes that ultimately allow ions to pass through a selective pore.

Here I have explored the underlying structural interactions within voltage-sensing domains of two invertebrate channels, *jShak1* and *N.at-K_v3.2*. The detailed energetics and permeability of these channels was evaluated for a range of site-directed mutants. The *jShak1* mutants demonstrated fine mechanical tolerances in the voltage sensing domain; small differences in side chain structure for several interesting amino acids yielded significant changes in the energetics of voltage response. Despite an apparent conservation in structure, I found that *N.at-K_v3.2* channels allow ion flow through a non canonical ion pore. This alternative permeation flows through a gap in the gating pore created by movement of the voltage sensing-helix through this region. Extensive mutagenesis of the voltage sensing helix and the resulting changes in relative ionic

permeability identified constraints on the shape and flexibility of the voltage sensing helix within this aqueous gating pore.

The plasticity within these channel proteins demonstrates that the core function can be quantitatively modified to a minor or major extent by changes in protein packing and structural interactions within the functional domains. This information provides dynamic constraints on functional models of ion channels that can be applied in combination with energetic modeling of 3-D structures of homologous proteins. This combination of detailed structural modeling with functional energetic data will yield new insights into voltage-gated channel function in particular, and dynamics of protein function in general.

ACKNOWLEDGMENTS

First, I would like to thank Dr. Warren Gallin for being my supervisor. I had no idea that when we first met that a Hyundai accent, Monty Python, A & W burgers, and zebrafish would turn into this. I thank you for the opportunity that you gave me, but I am even more grateful for your support and guidance. You have taught me many things about science and life, and have instilled in me a great love of science and learning. For these things and the others that are too innumerable to count, you have my enduring gratitude.

I would also like to thank Dr. Andrew Spencer for being a teacher, a mentor, and a wonderful collaborator. Your knowledge of electrophysiology, neurobiology, and love of invertebrates has helped me countless ways. Our long discussions, your probing questions, and the chalk-board brainstorming sessions provided clarity and direction, and catalyzed so many rounds of experiments. Thank-you for the science, the guidance, and the friendship, it has made all the difference to me.

I would like to thank the many wonderful scientists who provided guidance, ideas, reagents and beer when needed. To the members of my committee, Dr. Declan Ali, and Dr. Peter Light, I would like to thank-you for your interest in my project, your constructive input, and your support through the course of my degree. It has been my distinct pleasure to work with you. I would also like to thank Dr. Greg Goss for all of his knowledge on *Xenopus* surgery and oocyte expression, and for use of his lab space and hemostats when I was learning.

I would like to thank the members of the Gallin Lab for their assistance, ideas, and the many sounding-off coffee sessions that helped resolve so many technical details. Specifically, I would like to thank Donna Atherton for all of the little things she did that kept things running smoothly that we always forget to thank her for. With her organization, patience and wry sense of humor, Donna taught me how to run a PCR, then how to run my project, and eventually how to run an undergrad student, and feel comfortable with their results. Ultimately, Donna provided me with the tools that will allow me to implement thought and theory at the bench. I would like to thank Rheanna,

Cindy, Alex and Brad for all of their help, and to say the stimulating environment that I had to work in, was a direct result of these wonderful people.

I would like to thank Ron Koss for acting as a wonderful teaching mentor, and an even better friend. A special thank-you goes to Dawn Kieller who laughed through the stress with me in my final semester of teaching. I would also like to thank Tad and Clarence in the aquatics facility for taking wonderful care of my frogs during my return to molecular work.

Finally, I must thank my family and friends for their constant support. Without them in my life, my accomplishments would be meaningless. I would particularly like to thank Amanda, Shandra, Claire, Glen and Tara who are intelligent articulate fantastic scientists, for always understanding and being supportive even during the tough decisions. I would like to end with a big thank-you to my family, Dolores, Shell, Tricia and Curt, Tracey, and Lois. I know we do not always talk in the same language, but your unconditional love and support always lets us communicate. Finally, I would like to thank my husband Dr. Tim Chen for all of his constant love and support, his ability to make me smile never ceases to amaze me. On the science side, I thank-you for being willing to brainstorm with me, for talking potassium channels whenever I wanted and for teaching me all about the role of K^+ channels in vascular tissue, it helped put things in perspective.

TABLE OF CONTENTS

CHAPTER 1: INTRODUCTION 1

1.1 Ion Channels and Membrane Potential 1

1.2 Cation Channel Relationships 1

1.2.1 Diversity, Structure and Evolution 1

1.2.2 2TM Single Pore Potassium Channels 1

1.2.3 4TM Two Pore Potassium Channels 2

1.2.4 6TM Single Pore Potassium Channels 2

1.2.4.1 General Structure 2

1.2.4.2 KCNH – *erg, elk, eag* 2

1.2.4.3 Calcium Activated Potassium Channels -K_{CA} 3

1.2.4.4 KCNQ 3

1.2.4.5 *Shaker* 3

1.2.5 24TM Single Pore Calcium and Sodium Channels 5

1.3 Potassium Channel Structure 5

1.3.1 Structural Components and Mechanisms 5

1.3.1.1 Selectivity Filter and the Pore 6

1.3.1.2 Voltage Sensor 8

1.3.1.3 Activation Gate 13

1.3.1.4 N-terminal Inactivation Peptide 14

1.4 Structure-Function Studies: Applications, advantages and limitations 15

1.4.1 Structure-function studies on K_v channels 15

1.4.2 Mutagenesis 16

1.4.3 Energetic Perturbation Analysis 18

1.4.4 Crystal Structure 19

1.4.5 Bioinformatic Comparative Analysis 20

1.4.6 Homology Models and Molecular Dynamics 21

1.5 Objectives of Thesis **23**

1.5.1 Intramolecular Interactions Determine Voltage-sensitivity in a Cnidarian Voltage-gated Potassium Channel, *jShak1* 24

1.5.2 Atypical Phenotypes from Flatworm K_v3 channels 25

1.5.3 A Natural Alternative Permeation Pathway in *N.at-K_v3.2* 26

CHAPTER 2: MATERIALS AND METHODS: **36**

2.1 Creation of an N-inactive form of *jShak1* in pXT7 ..... **36**

2.2 Isolation of Notoplana channels **36**

2.2.1 Collection and Isolation of DNA and RNA 36

2.2.2 Cloning and Sequencing 37

2.2.3 Phylogenetic Analysis of Notoplana channels 37

2.3 Mutagenesis **38**

2.3.1 Site-directed Mutagenesis 38

2.3.1.1 *jShak1 Mutants* 38

2.3.1.2 *N.at-K_v3.2 Mutants* 39

2.3.2 Overlapping Extension 39

2.3.3 *N.at-K_v3.2* Double Mutant Cut and Paste 40

2.4 Electrophysiological Methods **40**

2.4.1 Channel Expression 40

2.4.1.1 mRNA Creation 40

2.4.1.2 Oocyte Preparation 40

2.4.1.2.1 Oocyte Extraction 40

2.4.1.2.2 Biochemical Oocyte Preparation for Mutagenesis Experiments 41

2.4.1.2.3 Manual Oocyte Preparation for N.at-K_v3.1 and N.at-K_v3.2 Channel Characterization 41

2.4.1.3 Channel Injection and Incubation 41

2.4.1.3.1 jShak1 Mutant Channels 41

2.4.1.3.2 Wild-type Flatworm K_v3 Channels 41

2.4.1.3.3 N.at-K_v3.2 Mutant Channels 42
2.4.2 Acquisition of Data 42
2.4.2.1 General Methods 42
2.4.2.2 *jShak1* N-truncated Mutant Characterization 43
2.4.2.3 *N.at-K_v3.2* Current/Voltage Protocols 43
2.4.2.3.1 Inward Rectifier and Combination Delayed/Inward Rectifier Channels 43
2.4.2.3.2 Delayed Rectifier Channels 43
2.4.2.4 Inward Rectifier Permeability 44
2.5 Data Analysis 44
2.5.1.1 Gibb's Free Energy Analysis 44
2.5.1.2 Calculated Conductance for *N.at-K_v3.2* mutants 45
2.6 Molecular modeling 46
CHAPTER 3: INTRAMOLECULAR INTERACTIONS DETERMINE VOLTAGE-SENSITIVITY IN A CNIDARIAN VOLTAGE-GATED POTASSIUM CHANNEL, *jShak1* 57
3.1 Results 57
3.1.1 Relationship between V_{50} and Equivalent Charge 57
3.1.2 S2 Mutants 58
3.1.3 S4 Mutants 58
3.1.3.1 Triplet Insertions 58
3.1.3.2 S4 Single Mutants 59
3.1.3.3 S4 Double Mutants 60
3.1.4 Double Mutant Cycle Analysis 60
3.1.4.1 QIF Mutations 60
3.1.4.2 IFR Mutations 61
3.1.4.3 RIF Mutations 62
3.1.4.4 K294R Mutations 62
3.1.4.5 K294Q Mutations 63

3.1.5 Homology Modeling of *jShak1* on the *RatK_v1.2* template 64

3.2 Discussion 66

3.2.1 Single mutations in S2 stabilize the open state 68

3.2.2 Double mutants changing charge content in the S4 are different than the triplet insertion mutants 69

3.2.3 Acidic residue mutations at position N227 stabilize interactions with a longer S4 71

3.2.4 Acidic mutations at position N227 stabilize protein structure in single K294 mutants 73

3.2.5 Homology Modeling 74

3.2.6 Conclusions 75

CHAPTER 4: ATYPICAL PHENOTYPES FROM FLATWORM K_V3 CHANNELS 89

4.1 Results 89

4.1.1 *N.at-K_v3.1* and *N.at-K_v3.2* are Shaw-type channels 89

4.1.2 *N.at-K_v3.1* expresses a non-inactivating K+ current with slow, early opening transitions 91

4.1.2.1 Voltage-sensitivity 91

4.1.2.2 Activation Kinetics 91

4.1.3 *N.at-K_v3.2* expresses an inward rectifying K^+ current 93

4.1.3.1 Current-Voltage Relationships 93

4.1.3.2 Inactivation Kinetics 94

4.1.3.3 Channel Permeability 94

4.2 Discussion 95

4.2.1 *N.at-K_v3.1* Activation Kinetics 95

4.2.2 *N.at-K_v3.2* is an Inward Rectifier 96

4.2.3 Conclusions 99

CHAPTER 5: A NATURAL ALTERNATIVE PERMEATION PATHWAY IN *N.at-K_v3.2* 110

5.1 RESULTS 110

5.1.1 Single S4 Mutations 110
5.1.1.1 H325A/C/S/R/V/E Mutants 110
5.1.1.2 G331P/A/R/K Mutants 111
5.1.2 Double S4 Mutants 112
5.1.2.1 G331P with H325 Mutants 112
5.1.2.2 G331A with H325 Mutants 113
5.1.2.3 G331R with H325 Mutants 114
5.1.2.4 G331K with H325 Mutants 115
5.1.3 Channel Permeability 116
5.1.3.1 H325E and H325V Permeation Profiles 116
5.1.3.2 G331P and G331A Permeation Profiles 117
5.1.3.3 H325R with G331P/A/R Permeation Profiles 117
5.1.3.4 4-AP Block of the Omega Path 118
5.2 DISCUSSION 118
5.2.1 Proposed Structural Model of the Gating Pore Pathway 118
5.2.2 Accessibility to the Gating Pore Permeation Pathway 119
5.2.3 G331R and G331K Yield Delayed Rectifiers with Different Properties 121
5.2.4 Changing the Shape of the Gating Pore Pathway 121
5.2.5 The structure of *N.at-K$_v$3.2* is shaped to use the gating pore pathway 123
5.2.6 Conclusions 125
CHAPTER 6: DISCUSSION 138
6.1 Towards a General Model of Channel Function 138
6.2 Considerations for *In vivo* Applications 141
6.3 Future Directions 142
6.3.1 Structural Elements Affecting Voltage-Sensitivity 142
6.3.2 Assessing the Changing Shape of the Gating Pore 143
6.3.3 Future Studies within the Voltage-Sensing Domain 144

6.4 General Conclusions 145
CHAPTER 7: REFERENCES 147

LIST OF TABLES

TABLE 2-1: PCR PRIMERS USED FOR THE CLONING OF NOVEL CHANNELS INTO THE pXT7 EXPRESSION PLASMID AND FOR MUTAGENESIS EXPERIMENTS IN THE *jShak1* AND *N.at-K,3.2* CHANNELS.....48

TABLE 3-1: SUMMARIZED FIT PARAMETERS FOR *jShak1* S2/S4 MUTANTS INCLUDING GIBBS FREE ENERGY CALCULATIONS.....76

TABLE 3-2: DOUBLE MUTANT CYCLE ANALYSIS: $\Delta\Delta G_0$ FOR SINGLE AND DOUBLE MUTATIONS IN *jShak1* 77

TABLE 5-1: SUMMARY TABLE OF THE OBSERVED PHENOTYPES AND CONDUCTANCE PROPERTIES OF THE *N.at-K,3.2* SINGLE AND DOUBLE S4 MUTANTS EXPRESSED IN *X. laevis* OOCYTES 126

LIST OF FIGURES

FIGURE 1-1: CRYSTAL STRUCTURES OF TWO BACTERIAL POTASSIUM CHANNELS IN THE CLOSED AND OPEN CONFORMATION. 29

FIGURE 1-2: THE CRYSTAL STRUCTURE OF *RATK$_V$1.2* LACKS RESOLUTION OF THE LINKERS AND THE S1 AND S3 HELICES..... 30

FIGURE 1-3: DENDROGRAM SHOWING THE PREDOMINANCE OF MAMMALIAN CHANNELS AND K$_V$1 CHANNELS IN THE COMPARATIVE STRUCTURE/FUNCTION DATASET..... 31

FIGURE 1-4: MODEL OF OPEN AND CLOSED STATES OF *RATK$_V$1.2*, BASED ON ROSETTA MODELS..... 32

FIGURE 1-5: THE *jShak1* CHANNEL LACKS ONE ACIDIC RESIDUE IN S2 AND ONE BASIC TRIPLET MOTIF IN S4..... 33

FIGURE 1-6: THE *N.at-K$_V$3.2* CHANNEL LACKS TWO BASIC RESIDUES IN S4, THAT ALLOWS THE PASSAGE OF IONS THROUGH AN ALTERNATIVE PERMEATION PATHWAY. 34

FIGURE 1-7: A CARTOON OF THE STRUCTURAL BASIS FOR THE OMEGA CURRENT FLOW THROUGH THE GATING PORE PATHWAY COMPARED TO THE *SHAKER* MUTANT CHANNEL..... 35

FIGURE 2-1: CONSTRUCT MAP OF THE FULL LENGTH *jShak1* PXT7 EXPRESSION PLASMID. 51

FIGURE 2-2: CONSTRUCT MAP OF THE FULL LENGTH *N.at-K$_V$3.1* PXT7 EXPRESSION PLASMID. 52

FIGURE 2-3: CONSTRUCT MAP OF THE FULL LENGTH *N.at-K$_V$3.2* PXT7 EXPRESSION PLASMID. 53

FIGURE 2-4: Δ23 N-TRUNCATED *jShak1* CHANNELS LACK N-TYPE INACTIVATION BUT EXHIBIT SLOW C-TYPE INACTIVATION. 54

FIGURE 2-5: EXEMPLAR TRACES FOR N-TRUNCATED *WILD-TYPE jShak1*, S2 SINGLE MUTANTS AND THE S4 INSERTION MUTANTS SHOWING MEASURABLE OUTWARD TAIL CURRENTS..... 55

FIGURE 2-6: THE CONDUCTANCE/VOLTAGE RELATIONSHIPS FOR THE INWARDLY RECTIFYING *N.at-K$_V$3.2* SINGLE AND DOUBLE MUTANTS CAN BE DIVIDED INTO FIVE CONDUCTANCE GROUPS..... 56

FIGURE 3-1 SINGLE MUTATIONS IN THE S2 AND S4 HELICES MODIFY STEADY-STATE PROPERTIES OF THE CHANNEL. 78

FIGURE 3-2: DOUBLE MUTANTS CHANGING CHARGE CONTENT IN THE S4 ARE DIFFERENT THAN THE TRIPLET INSERTION MUTANTS. 79

FIGURE 3-3: THE CLOSED TO OPEN EQUILIBRIUM IS SHIFTED TOWARDS THE OPEN STATE IN THE QIF DOUBLE MUTANTS..... 80

FIGURE 3-4: THE ADDITION OF AN ACIDIC RESIDUE IN THE IFR MUTANT SHIFTS THE CLOSED TO OPEN EQUILIBRIUM TO FAVOR THE OPEN STATE. 81

FIGURE 3-5: THE CLOSED TO OPEN EQUILIBRIUM OF ALL RIF CONTAINING MUTANTS IS SHIFTED TO THE CLOSED CONFORMATION. 82

FIGURE 3-6: THE ADDITION OF AN ACIDIC RESIDUE IN S2 FORMS A FAVORABLE ELECTROSTATIC INTERACTION IN THE K294R MUTANT CHANNEL. 83

FIGURE 3-7: THE CLOSED TO OPEN EQUILIBRIUM IS SHIFTED TOWARDS THE OPEN CONFORMATION IN K294Q MUTANT CHANNELS WITH AN ACIDIC RESIDUE IN S2. 84

FIGURE 3-8: HOMOLOGY MODEL OF *jShak1* BASED ON THE STRUCTURE OF *RATK$_V$1.2*. 85

FIGURE 3-9: HOMOLOGY MODELS OF THE STRUCTURAL CONSTRAINTS IN *jShak1* BASED ON THE STRUCTURE OF *RATK$_V$1.2*. 86

FIGURE 3-10: STRUCTURAL ELEMENTS IN THE S2 AND S4 OF *JSHAK1* PREVENT FAVOURABLE ELECTROSTATIC INTERACTIONS IN THE OPEN STATE. 87

FIGURE 3-11: CARTOON OF INTERACTIONS OCCURRING BETWEEN THE S2 AND S4 HELICES IN THE OPEN STATE IN THE *JSHAK1* MUTANT CHANNELS AS DETERMINED FROM DOUBLE MUTANT CYCLE ANALYSIS. 88

FIGURE 4-1: ALIGNMENT OF *N.at-K$_V$3.1* AND *N.at-K$_V$3.2* PROTEIN SEQUENCES AGAINST *RATK$_V$1.2* AND *SHAKER*. 100

FIGURE 4-2: *N.at-K$_V$3.1* AND *3.2* ARE *SHAW/SHAB* TYPE CHANNELS. 101

FIGURE 4-3: PHYLOGENETIC ANALYSIS PLACED THE *N.at-K$_V$3* SEQUENCES WITH *SHAW* HOMOLOGUES. 102

FIGURE 4-4: CURRENTS MEDIATED BY THE *N.at-K$_V$3.1* CHANNEL, EXPRESSED IN *X. laevis* OOCYTES. 103

FIGURE 4-5: CURVE FIT ANALYSIS OF THE OPENING KINETICS OF *N.at-K$_V$3.1* CHANNEL. 104

FIGURE 4-6: ACTIVATION KINETICS OF THE *N.at-K$_V$3.1* CHANNEL. 105

FIGURE 4-7: CURRENTS MEDIATED BY THE *N.at-K$_V$3.2* CHANNEL EXPRESSED IN *X. LAEVIS* OOCYTES. 106

FIGURE 4-8: INACTIVATION OF THE *N.at-K$_V$3.2* CHANNEL. 107

FIGURE 4-9: *N.at-K$_V$3.2* IS PERMEANT TO MULTIPLE CATIONS. 108

FIGURE 4-10: A COMPARATIVE ALIGNMENT OF THE S4 VOLTAGE SENSOR AND PORE REGIONS OF *N.at-K$_V$3.2* WITH OTHER K$_V$ CHANNELS. 109

FIGURE 5-1: MUTATION OF H325 MODIFIES ACCESSIBILITY TO THE GATING PORE PATHWAY. 127

FIGURE 5-2: MUTATIONS OF G331 CREATE TYPICAL DELAYED RECTIFIERS WITH DIFFERENT VOLTAGE-SENSITIVITIES. 128

FIGURE 5-3: DOUBLE MUTANTS IN THE PROLINE BACKBONE ARE ALL INWARD RECTIFIERS. 129

FIGURE 5-4 DOUBLE MUTANTS IN THE ALANINE BACKBONE ARE PASS OMEGA CURRENT. 130

FIGURE 5-5: THE ADDITION OF ARGININE AT A CENTRAL POSITION IS NOT SUFFICIENT TO MAINTAIN A DELAYED RECTIFIER PHENOTYPE WHEN PAIRED WITH SMALL RESIDUES IN R1. 131

FIGURE 5-6: THE COMBINATION OF G331K WITH SMALL H325 MUTATIONS CREATED A CHANNEL THAT USES THE GATING PORE AT HYPERPOLARIZED POTENTIALS AND THE CANONICAL PORE AT DEPOLARIZED POTENTIALS 132

FIGURE 5-7: MUTATIONS AT R1 OR R3 CHANGE THE PERMEATION PROFILE OF *N.at-K_v3.2* 133

FIGURE 5-8 MUTATIONS AT R1 AND R3 IN *N.at-K_v3.2* CHANGE BOTH ACCESSIBILITY TO THE PERMEATION PATH AND THE SHAPE OF THE GATING PORE PATHWAY. 134

FIGURE 5-9: 4-AMINOPYRIDINE BLOCKS THE ALTERNATIVE PERMEATION PATHWAY IN *N.at-K_v3.2*. 135

FIGURE 5-10: CARTOON DEPICTING OUR CURRENT HYPOTHESIS OF HOW THE OMEGA CURRENT FLOWING THROUGH THE GATING PORE IN BOTH THE OPEN AND CLOSED CONFORMATIONS. 136

FIGURE 5-11: LOCATION OF RESIDUES IN *RATK$_v$1.2* THAT FORM THE GATING PORE IN *N.at-K_v3.2*. 137

LIST OF ABBREVIATIONS

4-AP – 4-aminopyridine

2TM – two transmembrane

4TM – four transmembrane

6TM – six transmembrane

24TM – twenty four transmembrane

Ba^{2+} - barium

Ca^{2+} - calcium

Ca_V – voltage-gated calcium channel

cDNA – complimentary deoxyribonucleic acid

Cl^- - chloride

CHO – chinese hamster ovary cells

CNS – central nervous system

Cs^+ - cesium

Kir – potassium inward rectifier channel

Eag – ether-a –go-go channel

Elk – ether–a-go-go like potassium channel

Gu^+ - guanidinium

hERG – human-ether-a-go-go channel

HEK293 – human embryonic kidney cell line 293

IK – intermediate conductance calcium activated potassium channel

K^+ - potassium

KchIP – potassium channel interacting protein

KcsA –bacterial potassium channel

VGC – voltage-gated channel

K_v – voltage-gated potassium channel

mRNA – messenger ribonucleic acid

MthK – calcium activated potassium channel

MTS - Methanethiosulfonate

MTSEA – (2-aminoethyl) methane thiosulfonate hydrobromide

MTSES – sodium (2-sulfonatoethyl) methane thiosulfonate

MTSET – (2-(triethylammonium) ethyl) methane thiosulfonate hydrobromide

Na^+ - sodium

Na_V – voltage-gated sodium channel

ND96 – physiological saline for frogs

NH^{4+} - ammonium

PCR – polymerase chain reaction

Rb^+ - rubidium

SK – small conductance calcium activated potassium channel

TEA – tetraethylammonium

CHAPTER 1: INTRODUCTION

1.1 Ion Channels and Membrane Potential

Membrane channels are integral membrane proteins that respond to a stimulus, by opening and closing the gate on a transmembrane pore, thus regulating the diffusion of ions down their electrochemical gradient across the lipid bilayer. Channels regulate the flux of cations such as potassium (K^+), sodium (Na^+) and calcium (Ca^{2+}) and anions such as chloride (Cl^-). Precise control of channel activity is critical for setting and altering the cellular membrane potential. Channel activity can be regulated by various stimuli including changes in membrane voltage, membrane stretch, G-proteins, intracellular ligands like cyclic nucleotides, free calcium and protons, and extracellular ligands, like glutamate, glycine and other neurotransmitters.

1.2 Cation Channel Relationships

1.2.1 Diversity, Structure and Evolution

Cation channels provide an essential function in a number of organisms including those that lack highly organized cellular structures. These channels are classified based on structure, function and ion selectivity. These include inward rectifier potassium channels (Kir), leak channels, voltage-gated potassium channels (K_v), Ca^{2+} activated potassium channels (K_{Ca}), and voltage-gated calcium (Ca_V) and sodium (Na_V) channels. Despite this functional diversity, several conserved architectural elements of these integral membrane proteins can be used to elucidate evolutionary relationships. (Anderson and Greenberg 2001; Derst and Karschin 1998; Kerschbaum et al. 2002; Miller 2000; Strong et al. 1993).

1.2.2 2TM Single Pore Potassium Channels

Two transmembrane (2TM) channels have the most ubiquitously found channel architecture, apparently present in every cellular organism (Jan and Jan 1992; Jan and Jan 1997).This tetrameric channel has both the amino (N) and carboxy (C) termini in the cytosol, and is comprised of two membrane-spanning domains that are linked by an ion

selective pore loop (Jiang et al. 2002, 2002). This 2TM architecture has strong structural homology with the S5-pore loop-S6 structure of the larger six transmembrane (6TM) channel proteins that contain both the selectivity filter and activation gate (Doyle et al. 1998; Jiang et al. 2002; Jiang and MacKinnon 2000; MacKinnon et al. 1998).

1.2.3 4TM Two Pore Potassium Channels

The four transmembrane (4TM) two pore potassium channels are composed of four transmembrane helices and two pore loops, having a topology like two 2TM channels spliced together. These channels associate as dimers to yield the fourfold symmetry in the functional pore (Goldstein et al. 1999).

1.2.4 6TM Single Pore Potassium Channels

1.2.4.1 General Structure

The 6TM voltage-gated potassium channel superfamily members share a common architecture but vary greatly in function, ion selectivity and regulation. Single alpha subunits are composed of six transmembrane helices, known as S1 to S6 respectively, with both N and C termini located cytosolically. Within the N-terminus, the T1 or tetramerization domain functions in assembly of four alpha subunits within the ER, and contributes to channel function through protein-protein interactions with the cytosolic face of the channel (Deutsch 2002; Kosolapov and Deutsch 2003; Strang et al. 2001; Varshney and Mathew 2002).

The highly conserved S5-pore loop-S6 contains the ion-selective pore, and shows significant structural similarity with the 2TM channels. The remaining helices, S1-S4, are known as the voltage-sensing domain. The S4 helix is the voltage-sensor, which has conserved basic residues occurring at every third position. This charged helix confers the ability to sense, and respond with structural rearrangements, to changes in transmembrane voltage on the channel.

1.2.4.2 KCNH – *erg, elk, eag*

The KCNH family of channels has the conserved 6TM architecture, but varies greatly in the C-terminus after the S6 helix, having a cyclic nucleotide-binding domain

(Gutman et al. 2003). Notably, these channels have a selectivity sequence of GFG, which differs from other K^+ channel pore sequence of GYG. This channel family has a characteristic S4 helix containing four basic residues at every third position, and an additional acidic or basic residue within the motif between R3 and R4 (corresponding to R4 and R5 in *Shaker*) (Titus et al. 1997).

1.2.4.3 Calcium Activated Potassium Channels -K_{CA}

Calcium activated potassium channels (K_{Ca}) are divided functionally, based on the amount of potassium conductance through the channels. Small conductance (*SK*) $K_{Ca}2$ and intermediate conductance (*IK*) $K_{Ca}3$, are activated by intracellular calcium and are voltage independent (Gutman et al. 2003). The tight association of calmodulin with the C-terminus of these channels confers calcium sensitivity (Fanger et al. 1999).

1.2.4.4 KCNQ

The KCNQ family is also known as K_v7 channels because of their strong structural similarity to the *Shaker superfamily* of voltage-gated potassium channels. Unlike *Shaker* channels, KCNQ channels require co-expression with a single transmembrane domain beta subunit (*MirP1*, *MirP2* or *MinK*) to have physiologically significant current (Abbott et al. 2001; Abbott and Goldstein 1998; Gutman et al. 2003).

1.2.4.5 *Shaker*

The voltage-gated potassium channel (K_v) *Shaker superfamily* has the highly conserved 6TM architecture and a potassium selective pore. These channels are activated solely by changes in transmembrane voltages (Jan and Jan 1997). The *Shaker superfamily* is composed of four distinct and functionally different subfamilies; *Shak, Shab, Shaw* and *Shal* (K_v1-*4* or *KCNA-D* respectively) (Gutman et al. 2003).Functional channels are either homotetrameric or heterotetrameric and are found primarily in neuron and muscle. K_v channels can be fast activating, and fast inactivating A-type potassium channels, or classical delayed rectifiers. The extreme functional diversity of K_v channels is accomplished through heterotetramerization, cystosolic beta subunit co-assembly, phosphorylation and alternative splicing of gene products, as well as the large number of sequence variants within the genome (Abbott et al. 2001; Abbott et al. 2006; Abbott and

Goldstein 1998; Covarrubias et al. 1991; Covarrubias et al. 1994; Kerr et al. 2001; Nitabach et al. 2002)

Even with only four genes, one for each channel subfamily, the K_v channels represent the majority of potassium channels in the *D. melanogaster* genome (Covarrubias et al. 1991; Moulton et al. 2003). This is also true of mammals with 27 K_v genes, and *C. elegans* with 9 K_v genes. Only the diversity of the two-pore leak channels surpasses the K_v channel content within the genome (Moulton et al. 2003).

In mammals, the K_v1, *Shak* family has the largest number of representatives, resulting from gene duplication and divergence during evolution, giving rise to eight distinct mammalian homologues for the singular *D. melanogaster* gene. This subfamily is characterized by fast activation kinetics, and for some channels N-type fast inactivation, which in mammalian excitable cells underlies the A-type current (Kerschbaum et al. 2002).

The K_v2, *Shab* genes encode delayed rectifier channels with a diversity of functions depending on alpha subunit composition. In mammals a number of genes encode K_v2-related subunits (K_v5, K_v6, K_v8, K_v9), which, when expressed as homotetramers, form non-functional channels (Gutman et al. 2003; Ottschytsch et al. 2005). However, these subunits, when expressed as heterotetramers with K_v2 subunits, form functional channels with distinctive kinetics, localization, levels of expression, and modify channel conductance (Kerschensteiner et al. 2003).

The K_v3, *Shaw* subfamily is comprised of members requiring a large depolarisation for activation in all organisms. This is compared to other subfamilies where mammalian channels show a leftward shift in their voltage dependence of activation when compared to the invertebrate paralogues (Klassen et al. 2006).

The K_v4, *Shal,* channels have a specialized beta subunit, *KchIP*, associated with the tetramer. Co-expression modifies inactivation kinetics, increases current density, and shifts inactivation to more depolarized potentials (Jegla and Salkoff 1997; Lin et al. 2004; Salvador-Recatala et al. 2006). K_v4 channels, like the *K_v1* subfamily, mediate fast activating, fast inactivating A-type currents (Huang et al. 2006).

All four K_v subfamilies can be found in all metazoans, including diploblastic jellyfish, suggesting the evolution of this gene family occurred over 500 million years

ago in the common animal ancestor (Jegla et al. 1995; Jegla and Salkoff 1995; Salkoff et al. 1992; Strong et al. 1993). The pattern of evolution hypothesized for the *Shaker superfamily* based on sequence similarities and functional properties in the subfamilies, involves the duplication of the original gene, giving rise to paralogous genes, the precursor to the *Shak/Shal* lineage and the precursor to the *Shab/Shaw* lineage (Moulton et al. 2003; Strong et al. 1993). These precursor genes were then duplicated again, giving rise to four functional subfamilies. With the full complement of K_v genes from the common ancestor, independent evolution, including the duplication and loss of the genes in common ancestors, or within phyla, gave rise to the current distribution of genes within extant organisms; thus there is independent origin of paralogues in different phyla.

1.2.5 24TM Single Pore Calcium and Sodium Channels

The alpha subunit of the twenty-four transmembrane (24TM) single pore voltage-gated channels is composed of four similar internal repeats that have the 6TM architecture. Voltage-gated calcium and sodium channels are monomeric where voltage-gated potassium channels are tetrameric, but the overall architecture is similar (Catterall 1992; Catterall 1991; Strong et al. 1993). It is believed that these 24TM channels evolved through two rounds of tandem duplication, in a similar fashion to that observed in *Shaker* channels, but where the duplicates are connected via functional intracellular loops. These intracellular loops, which connect these 6TM domains (named I, II, III, and IV) vary in length, and greatly affect channel function via phosphorylation and interaction with cytosolic factors, including accessory subunits. The pore loops in each domain also vary in length and sequence, but the selectivity filter has the conserved architecture where changes in residues confer different ion selectivity. Notably, the change of three amino acids in the pore loops of domains I, III and IV of a sodium channel will convert the selectivity filter to that of a calcium channel (Ahern et al. 2006).

1.3 Potassium Channel Structure

1.3.1 Structural Components and Mechanisms

The 6TM architecture of voltage-gated potassium channels is divided into two functional regions; 1) the selectivity filter and pore (S5-pore loop-S6) and 2) the voltage

sensing domain (S1-S4). These functional regions facilitate the activation of the channel through a number of voltage sensitive transitions from the closed to open state. These transitions involve conformation changes of the activation gate and are stabilized by inter and intra-subunit interactions. This is followed by a final voltage insensitive transition from an intermediate state to the open state, dependent on interactions of the permeant ion on the pore. Through voltage sensitive and voltage insensitive transitions, channels return to the closed state or enter an inactivated conformation of the channel (Bao et al. 1999).

1.3.1.1 Selectivity Filter and the Pore

The selectivity filter and pore structure defined by the highly conserved S5-pore loop-S6 has strong similarity among all potassium selective channels, including *MthK*, *KcsA*, *KirBac*, *Kir* and the 6TM channels *KvAP* and members of the Shaker superfamily (Jiang et al. 2002, 2002; Lu et al. 2001; Zhou and MacKinnon 2003). Potassium channels minimize the activation energy necessary for a potassium ion to traverse the lipid bilayer, allowing for fast physiologically significant ion flux, (10^8 ions-sec^{-1}) while having unfavorable energetics for other monovalent cations, like Na^+ to pass, ensuring selectivity of K^+ (Berneche and Roux 2001, 2003; Grabe et al. 2006; Roux and Berneche 2002).

The pore of the potassium channel can be divided into two distinct regions; the selectivity filter which is roughly 12 Å in length, and the pore cavity or vestibule, an aqueous cavern approximately 18 Å in length and 8-10 Å in diameter (Doyle et al. 1998; Treptow and Tarek 2006, 2006). The aqueous vestibule is lined by hydrophobic residues acting as an inert surface by minimizing the electrostatic interactions between protein and water providing no competition for the hydrated ions (Doyle et al. 1998; Grabe et al. 2006). Charge mutations, particularly to acidic residues, within the vestibule can cause the ionic selectivity of the channel to change (Grabe et al. 2006).

The selectivity filter sequence is a conserved TxxTxGYG motif on the non-helical portion of the pore-loop in which the carbonyl oxygens of the peptide bond act to stabilize the dehydrated potassium ions (Doyle et al. 1998; Yool and Schwarz 1991). In mutagenesis experiments, where the pore motif is mutated to GFG in *Kir2.1* or *KcsA* or GVG in *Shaker*, the resulting channels show selectivity and conduction properties

identical to *wild-type* channels (Heginbotham et al. 1994; Splitt et al. 2000). Chimeric channels formed by swapping the *KcsA* pore into *Shaker* were highly potassium selective, and gated by voltage but with different biophysical properties from *Shaker* presumably through the limited electrostatic interactions between the voltage sensor and turret residues in the *KcsA* pore (Lu et al. 2001). Similarly, when the voltage-sensing domain from *Shaker* was fused to the *KcsA* channel, the resulting recombinant channel was gated by changes in transmembrane voltages, and showed identical permeability to the *KcsA* channel (Lu et al. 2001).

This pore motif defines three distinct carbonyl bounded binding sites (S1-S3) for K^+ ions from all four subunits, layered 3-4 Å apart through the selectivity filter that stabilize the dehydrated K^+ ion (Berneche and Roux 2003; Doyle et al. 1998; Zhou and MacKinnon 2003). The entrance to the selectivity filter is formed by a cuff of aromatic tryptophan residues near the vestibule which acts to stabilize the partially dehydrated potassium ion, repulse anions and may be considered as a fourth occupied site (S4) (Doyle et al. 1998; Jiang et al. 2003; Morais Cabral et al. 2001; Zhou et al. 2001). Because of the steric interactions between the carbonyl groups and the ion, hydrated ions cannot pass through the selectivity filter. Small ions like sodium also have limited permeability, as the small atomic size is not stabilized by the cage of carbonyls, resulting in a lower energy difference between sodium in the aqueous environment. Sodium and cesium can pass through the selectivity filter with reduced flux rates under large driving forces like high voltage, (Domene and Sansom 2003; French and Shoukimas 1985).

Conversely, larger cations like barium (Ba^{2+}) can pass into the selectivity filter, but become bound in either the shallower extracellular binding site, roughly 5 Å from the extracellular solution or the deeper "lock in" site S3, allowing a single barium ion to block the potassium channel conduction path (Aiyar et al. 1996; Hurst et al. 1995; Jiang and MacKinnon 2000; Ranganathan et al. 1996). Block of potassium channels by external barium is modulated by extracellular cations; specifically, cesium (Cs^+) or ammonium (NH^{4+}) allow barium to bind more readily, while potassium and rubidium (Rb^+) will out-compete barium for access to the channel (Hurst et al. 1995).

When entering the conduction path, the eight-fold symmetrical hydration sphere of the potassium ions is displaced by carbonyls of the selectivity filter, where half of the

ion is stabilized within the binding site S4 (Zhou et al. 2001). Once in the filter, potassium ions rely on electrostatic repulsion to move ions through the passage. During potassium efflux, the high affinity binding site near the extracellular face will retain the bound potassium ion until an additional potassium ion from the cytosol is introduced (Berneche and Roux 2001; Zhou and MacKinnon 2003). Because of the electrostatic repulsion, the occupancy of the selectivity filter binding sites alternates during conductivity such that S1 and S3 are occupied, or S2 and S4 are occupied (Morais Cabral et al. 2001; Zhou and MacKinnon 2003). Any alterations in structure, via mutagenesis, can affect the occupancy of neighboring sites (Ogielska and Aldrich 1999). The functional conformation of the selectivity filter requires potassium in both the cytosolic and extracellular solution (Loboda and Armstrong 2001; Loboda et al. 2001; Melishchuk et al. 1998; Zhou et al. 2001). In absence of potassium, the channel permeation pathway collapses into a non-conductive hour-glass which is accessible only to the cytosol (Loboda et al. 2001; Zhou et al. 2001).

During long depolarisations the single activated conducting state moves into an inactive minimally conducting state involving a constriction of the outer pore (Olcese et al. 2001). This C-type type inactivation does not collapse the pore, but causes structural rearrangements in the selectivity filter such that extracellular access to the deep binding site, S3, is blocked (Harris et al. 1998; Kiss et al. 1999). Structural changes in the selectivity filter reduce potassium conductance, but can allow limited sodium conductance prior to entering the non-conducting state (Kiss et al. 1999). C-type inactivation can be slowed or inhibited by increases in extracellular potassium (Fedida et al. 1999; Kiss et al. 1999; Rasmusson et al. 1995). The high affinity external binding site in the selectivity filter, S1, is also known as the C-type site, and when occupied by potassium or rubidium it blocks the conformational change of the selectivity filter (Ogielska and Aldrich 1999; Yellen 1998).

1.3.1.2 Voltage Sensor

The S4 voltage sensor is highly conserved in all voltage-gated channels because voltage sensing is primarily a function of the relative movement of the S4 in response to changes in transmembrane voltage (Bezanilla 2000; Bezanilla et al. 1994; Durell et al.

2004; Gandhi et al. 2003; Jiang et al. 2003; Noda and Numa 1987; Noda et al. 1984; Perozo et al. 1994; Starace and Bezanilla 2001; Stuhmer et al. 1989; Stuhmer et al. 1989). The S4 contains a recognizable repeating basic acid motif, RXX or KXX which is repeated 4-7 times through the length of the helix (Bezanilla et al. 1994; Liman et al. 1991; Noda et al. 1984; Starace and Bezanilla 2001). These basic residues are positively charged at physiological pH and are labeled R/K1-R/K7 corresponding to their location in alignment. In *Shaker* each subunit contributes equally, with roughly 3 equivalent gating charges per subunit, to a total gating charge of 12-14 equivalent charges per channel protein (Aggarwal and MacKinnon 1996; Schoppa et al. 1992; Seoh et al. 1996; Smith-Maxwell et al. 1998, 1998). Charge neutralization experiments in *Shaker* have identified the first four basic residues as contributing most to gating, where different basic resides have differential response to the electric field (Liman et al. 1991; Logothetis et al. 1993; Logothetis et al. 1992; Perozo et al. 1994). Serial reductions in charge content results in a reduction in gating valence (Liman et al. 1991; Logothetis et al. 1992). Voltage insensitive channels can be created by introducing multiple charge neutralizations, R1, 2, 4 and R1,2,4,7 in the voltage sensor (Bao et al. 1999), while an inward rectifier phenotype can be generated by triple mutations involving R2 and R3 and a non-basic residue between them (Miller and Aldrich 1996). Changes in gating valence affect both the rate of channel activation, introducing rate limiting conformational transitions, as well as voltage sensitivity of the channel, requiring larger changes in transmembrane voltage to provide the energy for channel activation (Ledwell and Aldrich 1999; Miller and Aldrich 1996; Schoppa and Sigworth 1998, 1998, 1998; Smith-Maxwell et al. 1998, 1998; Zagotta et al. 1994). The non-basic residues within the conserved basic charge triplet motif have also been shown to affect gating, either through stabilizing side chain interactions or through steric hindrance limiting the S4 translocation (Logothetis et al. 1992; Miller and Aldrich 1996; Smith-Maxwell et al. 1998). Co-operative transitions between subunits are facilitated by the close proximity of the voltage sensor to the pore of the adjacent subunit allows co-operative and stabilizing interactions between the S4 basic residues and the turret residues (Laine et al. 2003; Mannuzzu and Isacoff 2000; Smith-Maxwell et al. 1998, 1998).

The role of the S4 in voltage sensing and channel activation has been demonstrated using mutagenesis, fluorescence tags, molecular dynamics simulations, and cysteine accessibility studies. However, where the voltage sensor is located within the channel protein, whether it is adjacent to the pore, or lying on the periphery near the lipid bilayer is debated. Interactions between the voltage-sensing domain (S1-S4 helices) and the ion selective pore region is still debated, such that the mechanism by which the translocation of the voltage sensor causes channel activation is not fully understood.

Currently, three mechanisms by which the S4 translocates through the membrane field have been proposed, based on crystal structure, modeling and experimental data. First, the long standing sliding helical screw model suggests a mechanism where the voltage sensor moves exposing three basic residues to the extracellular environment through three distinct activation steps (Zagotta et al. 1990; Zagotta et al. 1994; Zagotta et al. 1994; Catterall et al. 1986; Keynes and Elinder 1999; Baker et al. 1998; Tiwari-Woodruff et al. 2000; Elinder et al. 2001). In this model, the S4 lies within a protein lined crevasse formed by S1-S3 with a single side exposed to lipid (Elinder et al. 2001).The translocation of the 3 gating charges across the lipid bilayer involves a 180° rotation and vertical movement of 12-13.5 Å (Ahern and Horn 2005; Glauner et al. 1999; Lecar et al. 2003).

The most controversial of the proposed models originated with the crystal structure of *KvAP*, where a paddle near the boundary of the protein was formed by the S3b-S4 helices (Jiang et al. 2003; Jiang et al. 2003). In this model, the paddle moves 20 Å through the lipid bilayer (Jiang et al. 2003). Not only did the paddle model conflict with the results of previous experimental studies, but additional studies performed using fluorescence resonance protein tagging, co-variant analysis and molecular dynamic modeling suggested the paddle model did not represent gating (Chanda et al. 2005; Ahern and Horn 2005; Durell et al. 2004; Fleishman et al. 2004; Treptow et al. 2004). Notably, the more recently published *RatK_v1.2* structure places the voltage sensor within the bulk of the channel, and not on the periphery (Long et al. 2005). However, the abundance of data produced to test the paddle model also called into question the conventional model because of the small translocations of the voltage sensor causing channel activation.

In the transport model the S4 is located within the gating pore, an aqueous canal that is continuous with the intracellular solution, located at the interface of the pore and voltage sensing domains (Chanda et al. 2005; Asamoah et al. 2003; Gandhi et al. 2003; Goldstein 1996; Larsson et al. 1996). Water cavities within large proteins have been shown to focus the local electric field, which can then be modified by temperature, pH and asymmetric ionic content (Islas and Sigworth 2001; Klapper et al. 1986; Rashin et al. 1986). Islas and Sigworth (2001) suggest that an intracellular cavity approximately 20 Å deep, with a 10 Å opening dimension exists within K_v channel proteins. The ~3 Å septum between the intracellular and extracellular environments is maintained by proteinaceous interactions between S4 and the rest of the voltage sensing domain (Islas and Sigworth 2001; Starace and Bezanilla 2001; Starace et al. 1997; Sokolov et al. 2005; Tombola et al. 2005). Mutations of the R1 (R362) position in *Shaker* to alanine, cysteine, serine, and valine formed a new conductive path, allowing current to flow through the gating pore (Tombola et al. 2005). This Omega current is non-selective, allowing a variety of monovalent cations to pass, including lithium, guanadinium, and sodium (Tombola et al. 2005). The Omega current was observed only when the channel was at rest, and disappeared as the channel reached threshold voltage, when the normal outward potassium current was observed. The Omega current was also observed when the non-conducting W434F pore mutation was introduced, as well as in the presence of TEA (Tombola et al. 2005). The highly conserved E283 position on S2 is known to form a salt bridge with S4 residues in both the open and closed conformation of the channel (Papazian et al. 1991; Tiwari-Woodruff et al. 2000). When E283 was replaced with the shorter aspartic acid residue, the amount of Omega current doubled, implying that the gating pore is bounded by S2 (Tombola et al. 2005). Similarly, histidine scanning revealed that a proton pore allowing a "piquito" current along the length of S4 is created by a mutation of R1 (R362H) in *Shaker* (Starace et al. 1997). Further elucidation of the aqueous crevasse revealed that R2 (R365 in *Shaker*) lies at the top of an internal aqueous cavity in the closed state, but in the open conformation R3 (R368 in *Shaker*) lies at the base of an externally facing crevasse (Starace and Bezanilla 2004). Translocation of R2 and R3 across the septum can account for 66% of total gating charge in the *Shaker* channel (Starace and Bezanilla 2004). The electric field is focused across this

proteinaceous gasket, so small conformational changes accomplish the movement of charges across the entire electric field, resulting in large electrical charge displacement (Islas and Sigworth 2001, 1999; Larsson et al. 1996; Tombola et al. 2006). Recently, it has been shown that the voltage sensing arginines may traverse the majority of the focused electric field predominantly by reorienting side-chains rather than a translocation of the voltage sensor backbone (Chanda et al. 2005). This is accomplished by a slight 2 Å vertical translation in combination a 45° tilt of the voltage sensor, such that the charges relocated from the internal aqueous crevasse to the external crevasse causing the movement of 3 equivalent charges (Chanda et al. 2005).

The structural rearrangements required for the function of voltage-gated potassium channels are stabilized by electrostatic interactions with the S1-S3 helices. Two highly conserved acidic residues in S2 (E283 and E293 in *Shaker*) and a single acidic residue in S3 (D316 in *Shaker*) form electrostatic interactions within the voltage sensing domain, acting to stabilize both the open and closed conformations (Keynes and Elinder 1999; Silverman et al. 2003). During gating, the relative movement of the S4 helix causes the interactions with acidic residues in the S1-S3 helices to break and reform with different residues in the voltage sensor (Gandhi et al. 2003). Specifically, the first acidic (E1) residue in S2 (E283) has been shown interact with R368 (R3) in the closed conformation while it interacts with R371 (R4) in the open state (Tiwari-Woodruff et al. 2000; Tiwari-Woodruff et al. 1997). K374 (K5) in S4 interacts with the second acidic (E2) residue in S2 (E293) and the conserved acidic (D1) residue in S3 (D313) in the closed state. After the channel activates via movment of S4, R377 (R6) moves into position to form stabilizing salt bridges with these same residues (Papazian et al. 1995). Similar results have been observed in *eag* channels, where the interaction between R3 (R365) and E1 (E283) occurs in the first voltage dependent gating step while the channel is closed, and where the interaction between E1 (E283) and R4 (R371) stabilizes the open conformation (Silverman et al. 2003). In *eag*, a magnesium ion stabilizes the interaction between helices by binding in the extracellular facing crevasse of the gating pore (Silverman et al. 2003).

1.3.1.3 Activation Gate

Channel conductance can be modified external to the selectivity filter through the intracellular constriction of the activation gate, which provides both a physical and energetic barrier to diffusion (Webster et al. 2004). The structural differences between the crystal structure of *MthK* (open conformation) and that of *KcsA* (closed conformation) (Figure 1-1) reveal that S6 helices are a component of the activation gate (Blunck et al. 2006; Jiang et al. 2002, 2002). In the closed conformation the cytosolic ends of the S6 helices in *KcsA* are in close association, blocking the intracellular side of the selectivity filter (Del Camino et al. 2005; Del Camino and Yellen 2001; Jiang et al. 2002, 2002). The pore in the deactivated or closed conformation is accessible only to extracellular ions (Armstrong 1992; Cordero-Morales et al. 2006).

In *Shaker*, the voltage sensor transduces the change in transmembrane energy, exerting force on the intracellular activation gate causing the S6 helices to hinge on conserved glycine residues and the bundle to splay open creating a 12 Å wide path allowing access to the selectivity filter (Jiang et al. 2002; Yifrach and MacKinnon 2002). The bundle crossing and mechanism of activation are conserved in both 2TM and 6TM channels, however in other channels, activation energy required for conformational changes in the channel protein are provided by the interaction with cytosolic ligands (Grottesi et al. 2005).

In *Shaker*, the S6 bundle crossing mechanism involves a conserved PXP (PVP or PIP) motif midway along the length of S6 causing a 20° kink in the helix (Ding et al. 2005; Labro et al. 2003). During activation the kinked helix pivots on an upstream glycine residue, G466, hinging the activation gate out of the permeation path (Ding et al. 2005; Tieleman et al. 2001). Bacterial channels, *MthK*, *KcsA*, and *KirBac* lack the proline kinks, but a conserved glycine hinge functions similarly allowing a 30° kink in the open conformation (Ding et al. 2005; Domene et al. 2005; Shrivastava and Baher 2006; Yifrach and MacKinnon 2002). Recently, a valine (V478) in *RatK$_v$1.2* directly below the PVP motif was identified as forming a hydrophobic constriction in both the open and closed conformation of the channel, forming a gate to the intracellular pore cavity of the channel (Treptow and Tarek 2006). Mutations of the highly conserved motif can cause constitutively open channels, as in P475D mutant channels, where the conformation of

the closed activation gate is destabilized (Sukhareva et al. 2003). Conversely, mutations P473D, V474D and V474W cause improper folding and channels fail to transit from the endoplasmic reticulum, while P473A, P473W and P475A mutants are non-conducting (Hackos et al. 2002).

The activation gate has been identified, and the mechanism by which it permits or prevents ionic accessibility to the selectivity filter has been elucidated, yet the mechanism by which the translocation of the voltage sensor opens the activation gate is not fully understood. It has been shown that proximal residues in the S4-S5 linker (L45) in *Shaker* (LGRTLKAS) and the C-terminus of S6 (NFNYFY) interact and distal residues in L45 (MRELGLL) and the gating hinge S6 sequence (PVPVIVS) interact to connect the movement of the S4 to the intracellular activation gate, specifically L389 and P393 in the S6 PVP motif (Durell et al. 2004; Lu et al. 2002; Ohlenschlager et al. 2002). Other mutations in the leucine heptad repeat in the *Shaker* L45 linker (L375V and L382V) impair the closed to open transition requiring larger energetic movements of S4 to open the activation gates (McCormack et al. 1991). By modeling the structure of *KcsA* and *KvAP* on the crystal structure of *Rat*K_v*1.2*, Long et al. (2005) showed that the C-terminal end of S6 runs underneath the L45 alpha helix. In this model, compression of the L45 linker in turn compresses the S6 inner helix closing the activation gate and closing the pore (Long et al. 2005, 2005). Chimeric channels made by combining the S4 voltage sensor from *Shaker* with the *KcsA* pore are not gated by voltage unless both the L45 sequence LGRTLKASMRELGLL and the C-terminus of S6 PVPVIVSNFNYFY from *Shaker* are both present in the channel (Lu et al. 2002). It is believed that conformational changes resulting from gating charge movements are transduced through L45 leucine interactions with S6 residues (Long et al. 2005; McCormack et al. 1991).

1.3.1.4 N-terminal Inactivation Peptide

Channels can exist in three obvious conformations, the activated or open state, the deactivated or closed state, and the inactivated non-conducting state. Once the channel has entered the activated state, it can either deactivate via closure of the activation gate by repolarisation of the membrane, or inactivate by entering a stable state with reduced conductivity. Channels in the inactive state are not available to re-enter the activated

conducting state until they are held at hyperpolarized potentials for a period of time, often entering the deactivation state.

Fast N-type inactivation occurs within milliseconds of channel opening causing the fast inactivation, which is characteristic of A-type potassium currents (Hoshi et al. 1990; Rasmusson et al. 1995). The mechanism of N-type inactivation is commonly known as "ball and chain" inactivation. In this instance, the ball is the N-inactivation peptide located on the N-terminus of the alpha subunit or on accessory beta subunits (Accili et al. 1998; Morales et al. 1995). During channel activation, the physical nature of the inactivation ball causes it to enter and occlude the intracellular pore. The sequence of the N-inactivation ball is not conserved among channels, but the physical structure is conserved (Murrell-Lagnado and Aldrich 1993). Typically ten hydrophobic residues are surrounded by a series of positive charges. The hydrophobic residues are hypothesized to interact with the hydrophobic vestibule residues while the charged residues are attracted to and facilitate entry into the pore (Murrell-Lagnado and Aldrich 1993). To obtain correct conductance measurements from tail-current data, the inactivation ball must be removed (Hopkins et al. 1994). This ensures that the conductance measurement reflects the percent of channels that have the activation gate opened at a set voltage.

1.4 Structure-Function Studies: Applications, Advantages and Limitations

1.4.1 Structure-function studies on K_v channels

Recent scientific advances have provided a set of tools and techniques, which provide the ability to assess the structural basis for the function of ion channels. These tools include 1) patch-clamp electrophysiology, 2) highly selective neurotoxins, 3) isolation, cloning and sequencing of ion channels from cDNA, 4) bioinformatic and computational tools and 5) protein crystal structures.

The use of potassium channels to identify the structural components important for channel function, particularly the use of K_v channels to elucidate the structure/function interactions giving rise to voltage sensitivity have several distinct advantages over larger and more complex ion channels like Na_V or Ca_V. Because K_v channels can function as homotetramers with physiologically significant current levels without the co-expression

of accessory subunits, and readily express in multiple cell lines (HEK293, CHO, oocytes), it possible to assess the function of channels directly through electrophysiological experiments. Unlike many other proteins, it is possible to assess the intermediate conformational changes involved with functional changes at sub-millisecond resolution by using specifically designed protocols. The use of patch clamp or cut open oocyte techniques enables the modification of both intracellular and extracellular environments, including ionic composition, and the application of pharmacological agents.

K_v channels are relatively small proteins, which are readily modified using molecular biological techniques. The recent publication of the protein crystal structure of *RatK_v1.2* provides a 3-dimensional map that can be used in conjunction with experimental data to identify structural elements essential to function. Because of their important roles in both excitable and non-excitable cells *in vivo*, a number of disease states or channelopathies caused by natural functional mutants have been identified. Potassium channels are found in all organisms, with a highly conserved architecture, thus elucidation of structure/function relationships in K_v channels can be widely applicable to a variety of channels.

Traditional structure/function studies have many limitations because of the tools used, and the context in which the experimental data were interpreted. Specifically, the number of channels selected for structure/function analysis is extremely limited, and the bias towards isolation and characterization of channels from "model organisms" or medically interesting organisms fails to provide a general model of voltage-gated channel function.

1.4.2 MUTAGENESIS

Before a three dimensional model of the channel protein was available, structural models depended on hydropathy plots and predictions of secondary structure from mutagenesis experiments. The sequential replacement of amino acids in the channel protein with either the alanine (Ala) with its small methyl side-chain or tryptophan (Trp) with a bulky aromatic side-chain have been used to determine the secondary structure of the functional regions of K_v channels, specifically the pore (Yifrach and MacKinnon

2002) and the voltage-sensing domain (S1-S4) (Li-Smerin et al. 2000). By comparing the stability and functional activity, shifts in Boltzmann slope or half activation voltage (V_{50}) of the multiple single mutants to *wild-type* channels, a functional scan of the channel protein is performed, identifying functionally important residues.

Similarly, cysteine accessibility and proximity studies provide information about the location and relative positions of residues within the functional protein. Application of MTS sulfhydral modifying agents, on either the extracellular or intracellular surface of the protein, covalently attaches an ethylamine ($MTSEA^+$), ethyltrimenthyammonium ($MTSET^+$) or ethylsulfonate ($MSES^-$) residues to the exposed thiol side-chain of the cysteine, modifying channel function. With the exception of $MTSEA^+$, the large modifying agents cannot penetrate the membrane; thus any modification of channel activity by application of the MTS reagent indicates the residue is exposed to the aqueous environment. The neutralization of exposed residues provides information as to their function, and the introduction of cysteines at other sites can elucidate helical packing and accessibility to the bulk solution. For example, the accessibility of cysteine mutations of basic residues in S4 provided evidence for the translocation of the sensor through the gating pore of *Shaker* (Wang et al. 1999). Cysteine residues can also be introduced to positions within the protein that are believed to be in close proximity. The application of an oxidizing reagent, like hydrogen peroxide, will cause the thiol side-chains to crosslink forming a disulphide bond. Specifically this can be used to assess conformational changes during channel activation such that disulphide bridges between adjacent residues in the closed state will shift the open-closed probability to favor the closed state, while application of oxidizing reagents during channel activation can lock the channel in the open conformation (Broomand et al. 2003; Gandhi et al. 2003).

Many site-directed mutagenesis experiments intended to elucidate structure and function of K_v channels based on hypotheses formulated for a specific property of the channel family, based on a current structural model. These hypotheses are tested through specific mutagenesis experiments. These experiments can be very informative about obvious functional elements, like the basic residue repeats within the voltage sensor, or the conserved acidic residues within S2 and S3 and other conserved motifs (Papazian et al. 1995; Papazian et al. 1991; Seoh et al. 1996; Tiwari-Woodruff et al. 2000; Tiwari-

Woodruff et al. 1997). However, depending upon the mutation introduced, the impact on channel function can be different (Bao et al. 1999; Miller and Aldrich 1996). Moreover, site-directed mutagenesis based on *a priori* assumptions regarding channel function may miss important structural interactions that contribute greatly to channel function. This was observed in the conversion of voltage sensitivity of *Shaker* to that of *Shaw*, where mutations of the basic residues failed to reproduce the voltage sensitivity of *Shaw*, while the mutation of adjacent non-basic residues did shift the voltage sensitivity (Smith-Maxwell et al. 1998, 1998). However, even in this instance, the change in channel phenotype required the replacement of three residues, not simply a single site mutation. Similarly, the formation of chimeric channels by domain swapping fails to account for steric interactions between domains that have evolved independently in separate channels (Lu et al. 2002; Smith-Maxwell et al. 1998, 1998). Thus, the limited number of channels employed in these structure/function studies may have led to functional models specific to these channels. These models may fail to encompass the full scope of the structure/function relationships in voltage-gated potassium channels specifically, and channel function in general.

1.4.3 Energetic Perturbation Analysis

Energetic perturbation analysis or double mutant cycle analysis employs specific sets of mutations, to formulate structure-function models within a single channel, but determines the relative energetics of the independent and pair-wise mutations in the channel protein (Perozo 2000). By comparing the effect the specific mutations have on two channel properties, half activation voltage (V_{50}) and effective charge (z), inferences on relative stability of the open vs. closed conformations of the channel or the relative stability of the bound vs. unbound state of a channel blocking molecule (Gross and MacKinnon 1996; Tiwari-Woodruff et al. 1997). By calculating free energy values for the mutation from the equivalent charge (from the Boltzmann slope for the channel) and half-activation voltage (V_{50}), periodicity in alpha helices, location of loops and role of electrostatic interactions can be deduced, providing valuable secondary structure information (Li-Smerin et al. 2000). While the relative proximity of residues, and by

association helices, can be assessed using measures of free energy, the exact positions of residues within the channel cannot be determined without *a priori* models.

Double mutant cycle analyses can directly test the stabilizing interactions between residues based on introducing specific mutations at suspected sites of interaction. In this analysis, the shifts in free energy of two single mutants are quantified, and compared to the shift in free energy observed for the double mutant (Horovitz 1996). If the Gibbs free energy of the double mutant is equal to that of the sum of the single mutations, it is assumed that the effects of the mutations are independent. However, mutational pairs that act to stabilize one channel conformation to a greater extent than the sum of the individual mutations are said to be synergistically interacting, while negative interactions that destabilize the channel protein are inferred when the sum of the free energy change caused by the single mutations is less than that observed in the double mutant. In *Shaker* salt-bridge formation, the perturbation by single charge neutralizations (E293Q) and single charge reversals, (E293K) was greater compared to double neutralizations (E293Q+K374Q) or double reversals (E293K +K374E) (Papazian et al. 1995; Tiwari-Woodruff et al. 1997).

1.4.4 Crystal Structure

A number of potassium channel proteins have been crystallized, the 2TM *KcsA* channel from the eubacterium *Streptomyces lividans*, the 2TM *MthK* channel from the archeabacterium *Methanobacterium thermoautotrophicum*, the 6TM *KvAP* channel from archaebacterium *Aeropyrum pernix*, and the 6TM $K_v1.2$ channel from *Rattus norvegicus*. These structural models provide a framework on which other analyses can be organized, and mechanisms of channel function can be interpreted.

Protein crystal structures are based on crystalline protein samples, and the conformations of protein regions may have substantial differences from those in solution (Acharya and Lloyd 2005). This presents a particular difficulty for crystallization of integral membrane proteins like ion channels, as the crystalline protein is often formed in the absence of the stabilizing interactions provided by the lipid bilayer. The crystal structures for many potassium channel proteins (*MthK, KcsA, KvAP)* have used a Fab antibody to stabilize the protein allowing for crystallization, but have since been

crystallized in the presence of lipids to stabilize their structure (Darman et al. 2006; Jiang et al. 2002; Jiang et al. 2003; Ruta et al. 2005; Zhou et al. 2001). While the structure of the highly selective potassium pore is conserved in these crystal structures, the artificial constraint on channel structure caused by the Fab complex, has resulted in the peripheral voltage sensing structures (specifically the S1-S4 regions), in *KvAP* exhibiting inconsistencies between the crystal structure and experimental data, resulting in the highly controversial, "paddle model" of channel gating (Jiang et al. 2003; Ruta et al. 2005; Tombola et al. 2006). When *KvAP* was re-crystallized in the presence of lipids, and in the absence of the antibody, the voltage sensor remained on the periphery of the channel at the protein-lipid interface, but was oriented vertically through the membrane (Lee et al. 2005).

The crystal structure of *RatK_v1.2* more realistically depicts the open conformation of the channel, including a more consistent position of the voltage-sensing domain. The relative locations of the transmembrane helices, and the position of the alpha-subunits is generally consistent with the experimental structure-function data (Long et al. 2005). However, the crystal structure lacks any intracellular and extracellular loops with the exception of the S4-S5 linker and the S5-pore loop –S6 indicating that they are highly flexible even in a whole molecule crystal. The crystal structure of the *RatK_v1.2* protein also depicts the S1 and S3 helices as poly-alanine helices (Figure 1-2)(Long et al. 2005). Because crystal structures are representative of statistical averages of the molecules within the protein, the lack of resolution of the S1 and S3 helices, specifically that of the side chains suggests that these regions exhibit conformational flexibility such that small changes within protein structure of these helices do not involve significant energetic changes even as they are crystallized (Acharya and Lloyd 2005; Long et al. 2005). Thus, this structure fails to provide an accurate description of side-chain interactions between these helices. Although crystal structures are useful for building models and evaluating experimental data, many questions remain unaddressed.

1.4.5 Bioinformatic Comparative Analysis

Genetic sequences, encoding the protein structure of the channel, are readily available for a number of model organisms through whole genome sequencing projects

and large-scale cDNA sequencing efforts. Using a bioinformatics approach, it is possible to identify the highly conserved sequences of K_v channels within the genome (Li and Gallin 2005, 2004). However, without cloning and functional expression, we are incapable of making all but the vaguest predictions as to the physical properties of the channel. Specifically, the invertebrate channels characterized to date, including those from model organisms like *Caenorhabditis elegans* and *Aplysia californica*, have the conserved K_v channel structure, but have manifested quantitatively large variation in electrophysiological properties compared to the intensively studied vertebrate channels.

A limited number of channels have been characterized, representing the medically interesting phylum, Chordata, and the majority of these channels are members of the K_v1 subfamily (Figure 1-3) (Li and Gallin 2004). Thus, to date, only a relatively small region of total sequence-space for voltage-gated potassium channels has been sampled, and only a limited part of the total possible range of electrophysiological activities for these channels has been characterized. For models to have more general validity, and for structure/function relationships to be set in context, it is important to examine potassium channels from more diverse taxa. Additional channels from invertebrates, with increased representation from multiple phyla, with all channel subfamilies represented, increases the ability of machine learning algorithms to distinguish non-conserved, functionally important residues from random mutations during evolution. The highly conserved invariant residues, like the basic residue repeats in the voltage sensor, are essential to the function of K_v channels. However, non-conserved residues are known to contribute to channel function, and allowing a quantitative gradation of protein function within the conserved structure (Smith-Maxwell et al. 1998, 1998).

1.4.6 Homology Models and Molecular Dynamics

By utilizing known crystal structures of K_v channels in homology models, it is possible to create models of structures of channels or components of channels that have not yet been crystallized. Prior to the crystallization of a 6TM K_v channel, a number of homology models were built on *MthK* and *KcsA* channel crystal structures (Laine et al. 2003; Laine et al. 2004). The highly conserved pore architecture of these channels was the focus of these studies, which attempted to determine the structural basis for ion

channel selectivity and the mechanism by which potassium passed through the pore (Ranatunga et al. 2001; Shrivastava et al. 2000). Similarly, molecular dynamics studies attempt to reconcile experimental data, crystal structure data and biochemical realities to form accurate models. However, this approach fails to reach a generally applicable structure/function model because of the highly specialized data set that represents a small number of channels, from a limited number of organisms (Berneche and Roux 2001; Durell et al. 1998; Durell et al. 2004). Also, the conformational changes occurring on a millisecond timescale are computationally intractable, and thus limit dynamics simulations. These molecular models do provide a framework upon which new hypotheses of channel function can be developed and tested, and then the model can be revised in an iterative hypothesis/results/experimental cycle. Application of these hypotheses to under-represented phyla, and newly characterized channels may also broaden the applicability of the model, moving towards a general model of channel function.

Homology models are limited by a multitude of factors including the accuracy of the crystal structure used as a template. Accurate amino acid alignments and threading of channel sequence on the crystal structure backbone can influence the accuracy of the mapped interactions. Moreover, for interactions of the channel in the closed (resting) conformation, homology models are limited by the lack of a closed state crystal structure of a 6TM channel. This is best demonstrated by Yarov-Yarovy (2006) who used ROSETTA to model the complete structure, including loops and side-chain residues of S1 and S3 of *RatK$_v$1.2* on the backbone of the *RatK$_v$1.2* crystal structure, and create a structural model of the open and closed state of the channel. The ROSETTA model threaded the sequence as to provide residue and side chain detail on the S1 and S3 helices as well as including loops. However, the ROSETTA model was mis-threaded prior to the S3 helix, such that the sequence modeled as helices was not the same as the regions identified in by multiple alignments (Figure 1-4). This caused inaccurate models of channel structure. Despite the problems in the modeling, this analysis provides a framework for creating additional structural hypothesis on a closed state channel.

1.5 Objectives of Thesis

The objective of my thesis is to use information about invertebrate channels to inform a more general model of the voltage-gated potassium channel structure/function relationships. Because the pore architecture is so highly conserved, I focus my attention on the voltage-sensing domain (S1-S4). Here I perform an integrative structure/function analysis explore how interactions within the voltage-sensing domain effect the function channel protein.

First, I elucidated the structural interactions within the channel protein that change the relative conformational stabilities of the open vs. closed state, and how these interactions may affect local protein packing in a jellyfish channel *jShak1* through mutational analysis. These results were interpreted using Double Mutant Cycle Analysis and presented in the context of a homology model based on the *Rat*K_v*1.2* crystal structure.

Second, I characterized two *Shaw* potassium channels from the free living marine flatworm *Notoplana atomata* which have novel channel properties, despite conservation of channel structure. Here I used specifically designed protocols to explore the slow, early opening transitions of the *N.at-*K_v*3.1* delayed rectifier, determining that sub-threshold conformational changes delay channel opening. Furthermore, I showed that *N.at-*K_v*3.2* is an inward rectifier that is permeable to multiple cations, despite a conserved pore structure, and here I proposed that structural differences within the S4 voltage sensor allows ion conductance through an alternative permeation pathway.

Finally, I performed a number of site-directed mutagenesis experiments within the S4 voltage sensor of *N.at-*K_v*3.2*, focusing on the structural packing with the voltage-sensing domain, and how this contributed to the accessibility and shape of the alternative permeation pathway. This work demonstrated the flexibility and tolerance of the channel protein to structural modification and suggested that a general model of how voltage-gated channel structure contributes to function has yet to be determined.

1.5.1 Intramolecular Interactions Determine Voltage-sensitivity in a Cnidarian Voltage-gated Potassium Channel, *jShak1*[1]

Many voltage-gated channels isolated from invertebrates show rightward shifted voltage-conductance relationships, compared with those from vertebrates. The flatworm channels, *N.at-K_v3.1* from *Notoplana atomata* and *SK$_v$1.1* from *Schistosoma mansonii*, have half activation voltages (V_{50}) of +9.3 mV and +20 mV respectively (Kim et al. 1995; Klassen et al. 2006). A *Shab* channel from the mollusc *Aplysia californica* has a V_{50} of +17 mV (Quattrocki et al. 1994), while a *Shaw* channel K_v3 (egl-36) from *Caenorhabditis elegans* has the most rightward shifted V_{50} reported to date, +63 mV (Johnstone et al. 1997). The V_{50} values of both *Polyorchis* channels are markedly more positive than those of homologous vertebrate K_v1 channels (Grigoriev et al. 1997; Jegla et al. 1995). In comparison most other K_v1 channels, including *jShak2*, *jShak1* has one fewer positively charged motif in the S4 region, with a charged residue being absent at the position equivalent to R362 in *Shaker* (Figure 1-5).

Both of the K_v1 potassium channels (*jShak1* and *jShak2*) from the jellyfish, *Polyorchis penicillatus*, differ from all other, non-cnidarian, K_v channels in that one of the conserved acidic residues in S2, corresponding to E283 in the Shaker channel, is a neutral asparagine (N227 in *jShak1*). The recently cloned K_v1 channel from the Portuguese-Man-o-War *Physalia physalias* also lacks the 1st acidic residue in S2 (S231 in *PpK_v1)* and has a shortened S4 (Bouchard et al. 2006) suggesting that these two structural differences may reflect a conserved variant of channel architecture in the hydrozoans. Previous mutagenesis analysis in *jShak1* (Grigoriev et al. 1997) demonstrated that the addition of length and charge in the S4 voltage sensor, to either side of the conserved K294 residue (K374 in Shaker) had complex effects on channel properties, but did not simply shift the voltage sensitivity of *jShak1* to the range observed for vertebrate K_v1 channels.

In this study we utilized *jShak1* to investigate the effects of mutating the neutral N227 residue to an acidic residue, either N227E or N227D. We changed the identity of

[1] A version of this chapter is being prepared for submission to the Journal of General Physiology.

charged residues in S4 to evaluate their role in setting voltage sensitivity. Finally, using double mutant cycle analysis to evaluate energetic changes in the equilibrium between open and closed states, we examined the effects of combining the S2 mutations with the S4 mutations that alter both the length and charge of S4, to identify interactions involved in stabilizing the major conformational states of the channel.

1.5.2 Atypical Phenotypes from Flatworm K_v3 channels[2]

The few potassium channels from basal phyla that have been described provide a rich source of structural and functional novelty. Potassium currents from jellyfish and flatworms have been characterized (Blair and Anderson 1993; Buckingham and Spencer 2000; Day et al. 1995; Holman and Anderson 1991; Keenan and Koopowitz 1984; Meech and Mackie 1993; Przysiezniak and Spencer 1994), and four functional potassium channel proteins have been cloned from cnidarians (Bouchard et al. 2006; Jegla et al. 1995; Jegla and Salkoff 1997), and one from *Schistosoma mansonii* (Kim et al. 1995), a parasitic trematode. What little is known of the K^+ channels from these two phyla indicates that they differ in several respects from many of their homologues in vertebrates, insects, and molluscs. The potassium channels of flatworms and jellyfish tend to be shifted in their voltage/conductance curves in a more depolarized direction (Blair and Anderson 1993; Buckingham and Spencer 2000; Day et al. 1995; Grigoriev et al. 1997; Jegla et al. 1995; Jegla and Salkoff 1997), and one flatworm potassium current in central neurons activates very rapidly allowing for high-frequency firing (Buckingham and Spencer 2002). The potassium channels of "basal" phyla, those that diverged earliest within the metazoan clade, are more likely to exhibit novel properties because of their long divergence times from commonly studied channels in phyla such as the nematodes, arthropods, and vertebrates.

To date, no potassium channels have been cloned from non-derived, free-living, flatworms. We therefore applied a degenerate PCR approach to characterize voltage-gated potassium channels from *Notoplana atomata*, a marine, polyclad flatworm, that is representative of early bilaterians. We cloned and characterized two *Shaw*-type voltage-

[2] A version of this chapter has been published. Klassen et al. 2006. Journal of Neurophysiology. 95: 3035-3046.

gated channels with disparate and unusual properties for this channel family. When expressed in oocytes, *N.at-K$_v$3.1* exhibited a non-inactivating, outward current with slow opening kinetics due to a number of voltage-dependent, pre-opening intermediate events. In contrast, a second channel, *N.at-K$_v$3.2*, was constitutively open in the range of normal resting potentials but showed weak inward rectification at potentials more positive than -40 mV. Both of these flatworm *Shaw*-type channels express currents with properties that are not normally seen in other members of the *Shaw* subfamily (Rudy and McBain 2001). Evolutionarily early natural selection in a basal metazoan has produced two *Shaw* channels with diverse electrical phenotypes that are convergent with phenotypes produced by distantly related families of K^+ channels in "higher' metazoans.

1.5.3 A Natural Alternative Permeation Pathway in *N.at-K$_v$3.2*[3]

In the previous section, we reported that the expression of the flatworm channel *N.at-K$_v$3.2* yielded a weak inward rectifier that is open at hyperpolarized potentials (Klassen et al. 2006). This channel, *N.at-K$_v$3.2*, preferentially passes potassium, but is also permeable to a number of cations, including cesium, lithium, guanidinium, sodium, and to a limited extent barium (Klassen et al. 2006). Structurally, *N.at-K$_v$3.2* resembles other Shaker superfamily channels. It is a 6TM channel with the characteristic S4 voltage-sensing domain and highly conserved reentrant pore loop and selectivity filter (Figure 1-6) (Klassen et al. 2006). Because the pore domain of *N.atK$_v$3.2* is highly conserved among potassium channels (Figure 1-6), we proposed that the pore of *N.at-K$_v$3.2* is uncoupled from the voltage sensor, and that this channel utilizes the gating pore as a permeation pathway, (Islas and Sigworth 2001; Starace and Bezanilla 2001; Starace et al. 1997) allowing the natural equivalent of a cation selective Omega current to pass along the S4 voltage sensor (Tombola et al. 2005).

The voltage sensor S4 helix in *N.at-K$_v$3.2* differs from other K_v channels in that the first (R1) and third (R3) basic residue positions are not arginine or lysine (Figure 1-6). In *N.at-K$_v$3.2* a histidine (H325) is present in the first position and a glycine (G331) is at the third position. In K_v channels, histidine substitution for a basic residue is less

[3] A version of this chapter is being prepared for submission to the Journal of Biological Chemistry.

disruptive than other mutations because the positive charge in that position is maintained at physiological pH (Starace et al. 1997). The presence of glycine residues confers flexibility on a protein as well as allowing for close helical packing (Bright and Sansom 2004; Chou and Fasman 1974, 1974; Javadpour et al. 1999; Li and Deber 1992; Russ and Engleman 2000). It is well established that in Shaker superfamily channels, glycine residues form flexible functional hinges. Specifically, glycine residues in the S6 helix are believed to hinge the kinked alpha helical bundle crossing, allowing opening of the activation gate in response to membrane depolarisations (Ding et al. 2005; Jiang et al. 2002). Specifically, a single glycine residue is conserved (G466 in Shaker) in over 468 potassium selective and cyclic nucleotide gated channels and is thought to be critical in gating of the S6 hinge (Schealy et al. 2003). This structural conservation suggests that glycine residues would only occur at positions requiring an essential and functional hinge. The presence of a glycine hinge at a central position in the S4 voltage sensor, suggests a critical structural motif that is required for proper function of the channel protein.

To elucidate the relative contributions of these unique residues to the biophysical properties of *N.at-K$_v$3.2*, we created a number of single S4 mutants. In *Shaker*, mutations of R1 (R362) to alanine, valine, serine, and cysteine produced the artificial Omega current mutants (Tombola et al. 2005). Here we reproduce those mutations creating H325A, H325C, H325S, H325V mutants, as well as reintroducing the arginine found at this position in all other channels, H325R. In addition, the charge was reversed by replacement with a glutamate (H325E).

Because of its central position in the helix, the mutations at G331, were designed to determine: 1) if at rest the glycine kinks the S4 allowing current to flow, 2) if recovery of an alpha helical conformation is sufficient to reconnect the sensor to the canonical pore, and 3) if the addition of basic charges of differing side chain lengths can result in typical delayed rectifier channels. To this end, we created four mutants. The first mutant introduces a proline, G331P, which is known to disrupt the secondary structure of the helix, causing an ~30 degree kink (Barlow and Thornton 1988; Bright et al. 2002; Teitelman et al. 1987; Tieleman et al. 2001; von Heinje 1991). The second mutant introduces an alanine, G331A, which, when compared to glycine should have the most

pronounced stabilization of the alpha helix (Chakrabartty et al. 1991; O'Neil and Degrado 1990; Serrano et al. 1992). The last two mutants introduce the arginine and lysine (G331R, G331K), which are found in other K_v channels at this postion, contributing to the equivalent charge movement that gates the channel (Perozo et al. 1994; Starace and Bezanilla 2001). Finally, we created double S4 mutants, which combine all 24 pair-wise combinations of the H325 and G331 mutants to determine the shape and nature of the Omega current path.

Here we demonstrate that the inwardly rectifying *N.at-K_v3.2* channel uses an alternative permeation path, rather than the canonical pore to allow an influx of cations. We propose a structural model of the alternative permeation pathway in *N.at-K_v3.2*, where the accessibility of the pathway is permitted by the histidine (H325) in position R1, and the glycine hinge (G331) in position R3 allows the shape of the gating pore to change in response to changes in transmembrane voltage (Figure 1-7). Mutations to either residue in the S4 can produce a gating pore pathway with different ionic selectivity whose selectivity varies from the *wild-type* channel. Some mutations (H325S, H325A, H325C, H325R, G331R, G331K) can produce a delayed rectifier, while some pair-wise combinations of mutations appear to use the alternative path when the S4 is at rest, but allow potassium efflux through the canonical pore upon reaching threshold voltage.

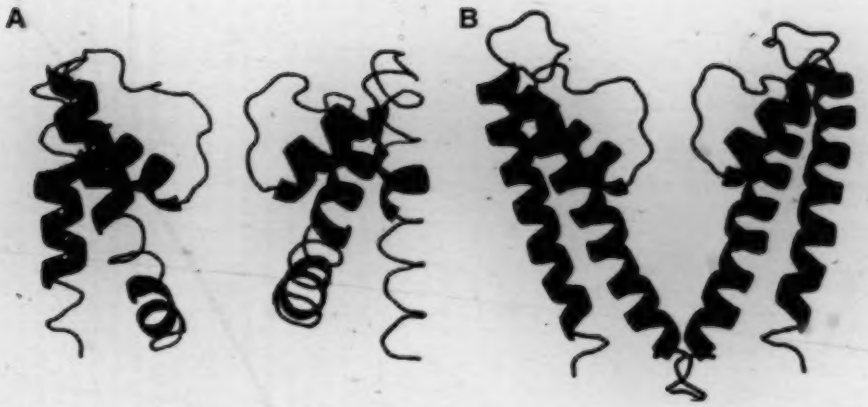

Figure 1-1: Crystal structures of two bacterial potassium channels in the closed and open conformation.
A. The open conformation of the *MthK* channel shown in magenta.
B. The closed structure of *KcsA* in blue. The accessibility of ions to the pore can be limted by the bundle crossing of the M2 domains (equivalent to S6 in 6TM channels).

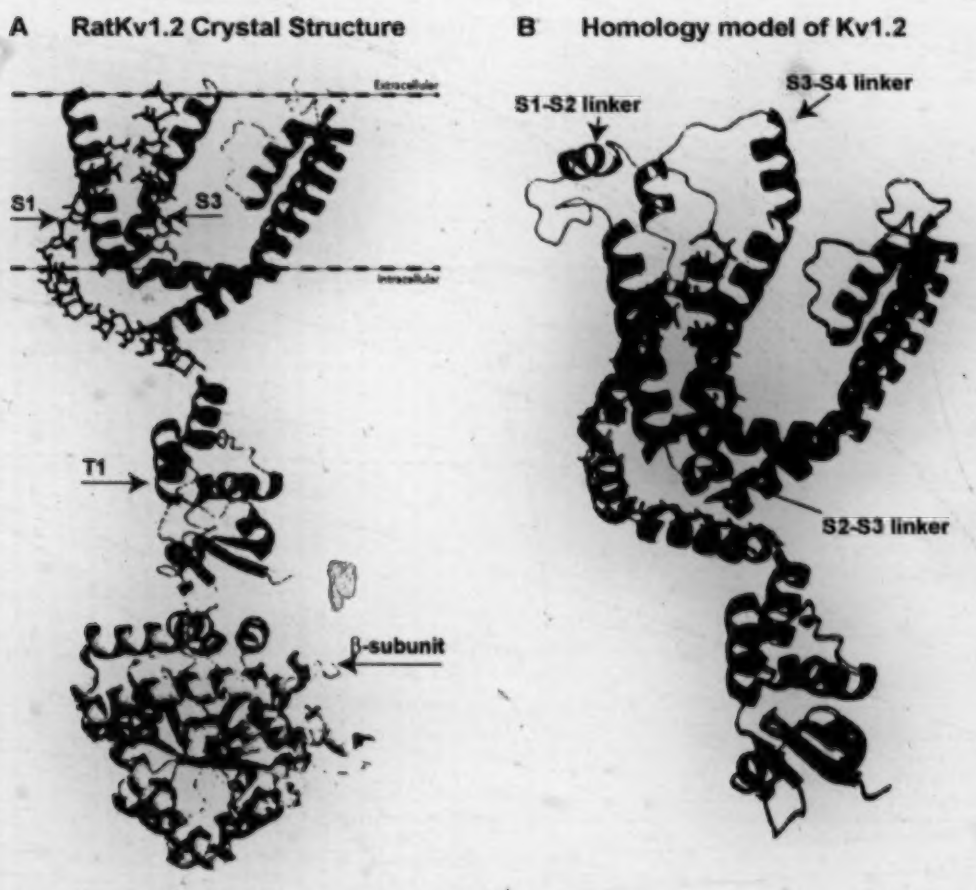

Figure 1-2: The crystal structure of *RatK$_v$1.2* lacks resolution of the linkers and the S1 and S3 helices.

A. The *Rat K$_v$1.2* crystal structure (PDB Accession 2A79) with the well-defined regions in magenta and the poorly defined structures shown as blue poly-alanine helices. Note there are no intercellular or extracellular loops shown joining the transmembrane helices and S1 and S3 are only resolved sufficiently to determine the presence of the helix but not the sidechains.

B. Homology model of the *RatK$_v$1.2* sequence (in green) on the backbone of the 2A79 structure (same colors as in A) prepared by Megan O'Mara of the Tieleman lab. Note that the intracellular and extracellular loops have been modelled and the positions of the residues in S1 and S3 have now been assigned based on a multiple alignment of 140 Kv1 family sequences and on interactions defined by published mutagenesis experiments. Note that the energy minimization was limited, using the SWISS-MODEL web server.

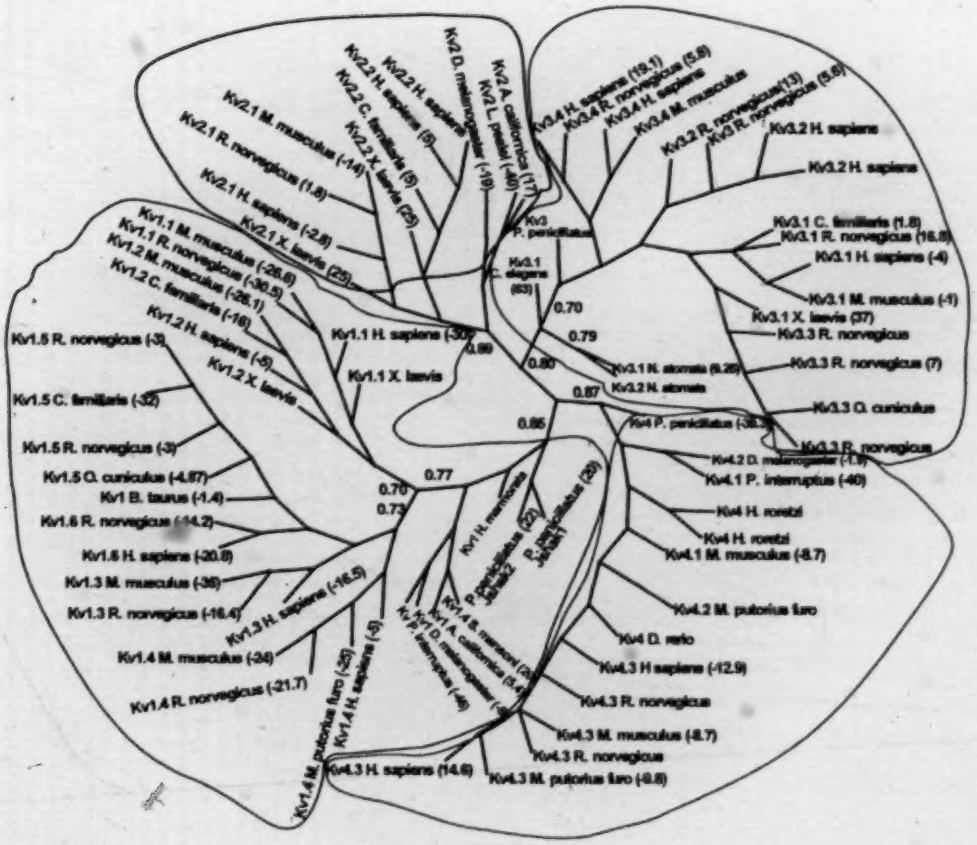

Figure 1-3: Dendrogram showing the predominance of mammalian channels and K_v1 channels in the comparative structure/function dataset.
In this tree, prepared December 2004, the channel subfamilies *Shak* (bounded by red), *Shab* (bounded by blue), *Shaw* (bounded by purple) and *Shal* (bounded by brown), are shown. All mammalian channels are black, non-mammalian chordate channels (frog and fish) are in green, and invertebrate channels from all other phyla are in blue.

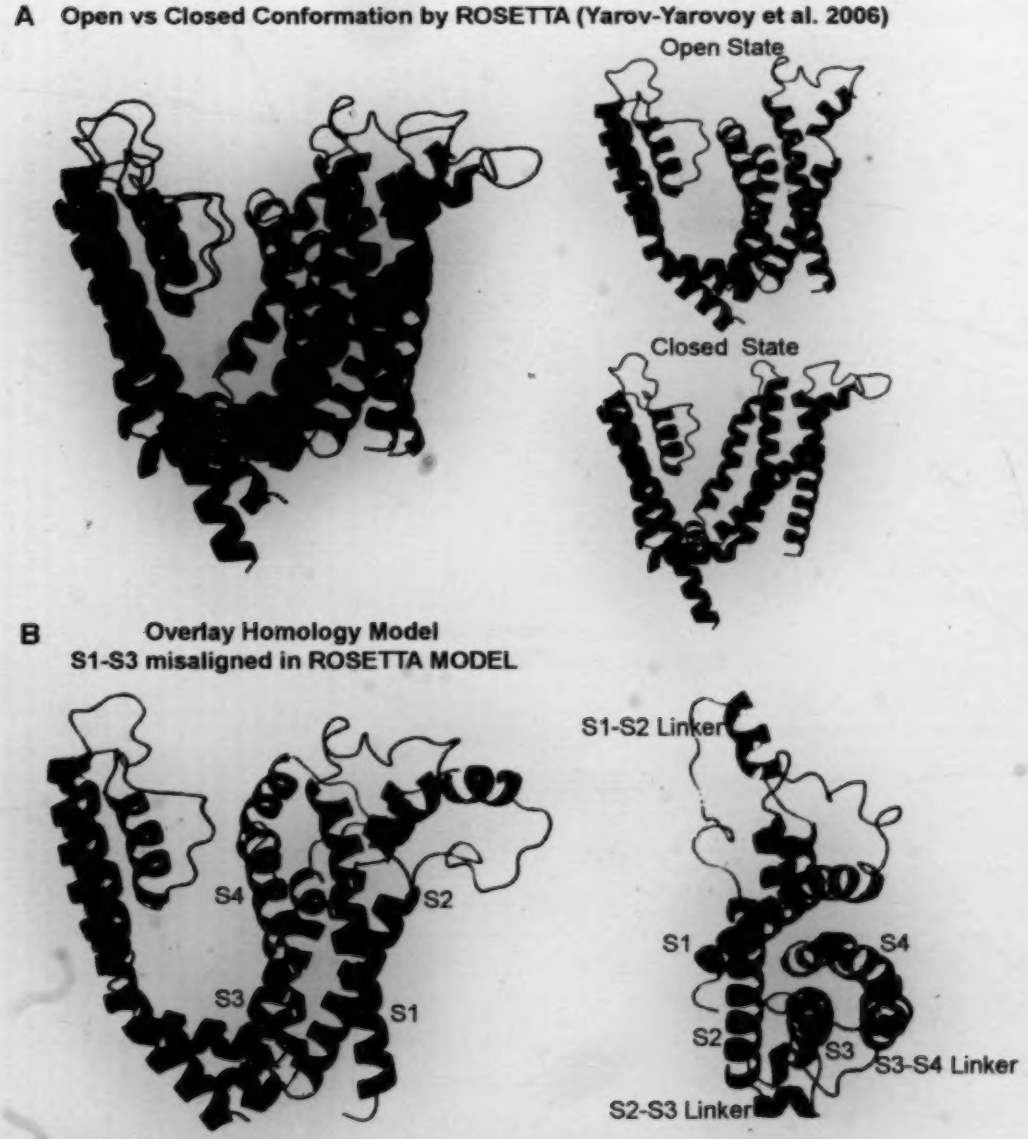

Figure 1-4: Model of open and closed states of *RatK$_v$1.2*, based on ROSETTA models.

A. Models of the open conformation (red) and closed conformation (blue) of the mis-threaded ROSETTA models from Yarov-Yarovoy et al. (2006).

B. Overlay of the *RatK$_v$1.2* model from Figure 1-2 (green) over open state model from Yarov-Yarovoy et al. (2006) (red). Note that the S1-S2 and S3-S4 loops differ due to different sequence alignments.

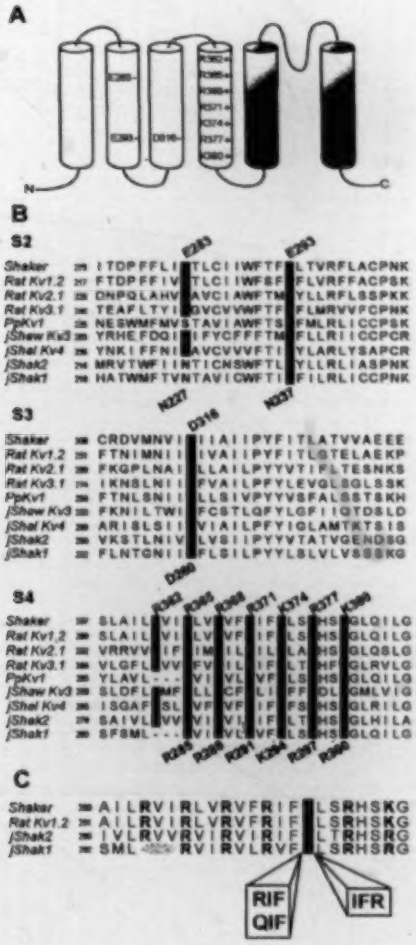

Figure 1-5: The *jShak1* channel lacks one acidic residue in S2 and one basic triplet motif in S4.

A. A schematic of a single 6TM alpha subunit of the *Shaker* voltage-gated potassium channel. The S5-pore, S5-S6 loop and S6 domain are shown in grey while the S1-S4 transmembrane helices are white.

B. Alignments of the transmembrane helices S2, S3 and S4. Residues in *Shaker* are labelled in black while corresponding positions in *jShak1* are labelled in blue. *jShak1* lacks an acidic residue in S2 (N227) but contains the stabilizing acidic residue in S3 (D260). The S4 voltage sensor of *jShak1* is shorter than the other K_v1 channels by one basic motif. The highly conserved acidic residues in S2 (E283 and E293) and the conserved acidic residue in S3 (D316) are shown in blue while the basic residues in the S4 voltage sensor are shown in red.

C. Alignment of S4 helix of *jShak1* with three other channels' S4 helices, indicating the sites of insertion of the S4 mutants on either side of position K294 in *jShak1*.

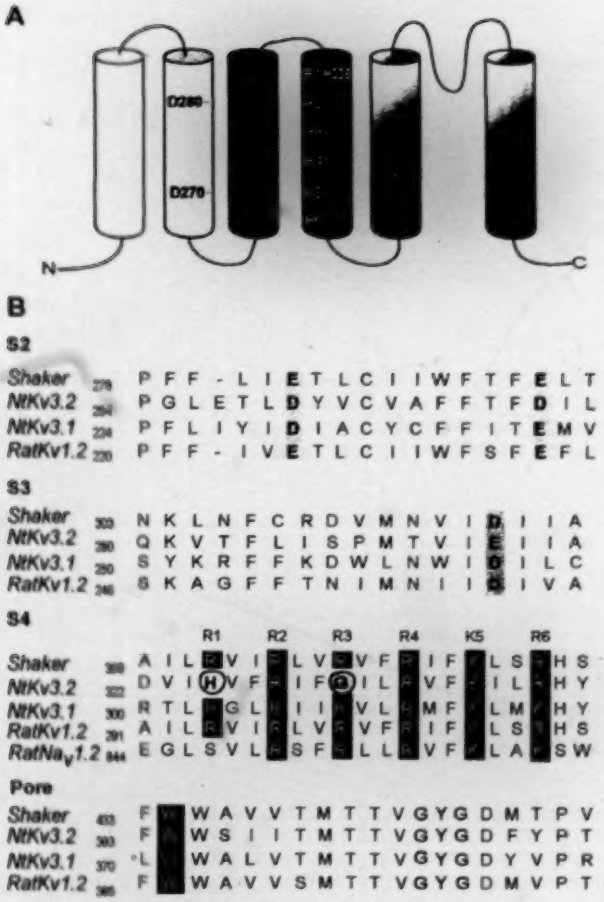
A
D280
D270
N
C
B
S2
Shaker
NtKv3.2
NtKv3.1
RatKv1.2
P F F - L I E T L C I I W F T F E L T
P G L E T L D Y V C V A F F T F D I L
P F L I Y I D I A C Y C F F I T E M V
P F F - I V E T L C I I W F S F E F L
S3
N K L N F C R D V M N V I D I I A
Q K V T F L I S P M T V I E I I A
S Y K R F F K D W L N W I D I L C
S K A G F F T N I M N I I D I V A
S4
R1 R2 R3 R4 K5 R6
A I L R V I R L V R V F R I F R L S R H S
D V I H V F R I F R I L R V F R I L R H Y
R T L R G L R I I R V L R M F R L M R H Y
A I L R V I R L V R V F R I F R L S R H S
E G L S V L R S F R L L R V F R L A R S W
Pore
F W W A V V T M T T V G Y G D M T P V
F W W S I I T M T T V G Y G D F Y P T
L W W A L V T M T T V G Y G D Y V P R
F W W A V V S M T T V G Y G D M V P T

Figure 1-6: The *N.at-K$_v$3.2* channel lacks two basic residues in S4, that allows the passage of ions through an alternative permeation pathway.

A. A schematic of a single 6TM alpha subunit in the *Shaker* voltage-gated potassium channel. The colored conserved S5-pore loop –S6 is shown in grey while the S4 voltage sensor is blue. The S2 and S3 helices that stabilize the voltage sensor during conformation changes are shown in pale grey and blue grey respectively.

B. Alignments of the S2, S3, and S4 transmembrane helices where charged residues are highlighted. The S4 voltage sensor of *N.at-K$_v$3.2* aligns well with other channels, but has a histidine at position R1(yellow) and a glycine in the central R3 position (orange). An aligment of the pore indicates that the ion selective sequence (GYG) is present in the *N.at-K$_v$3.2 channel.*

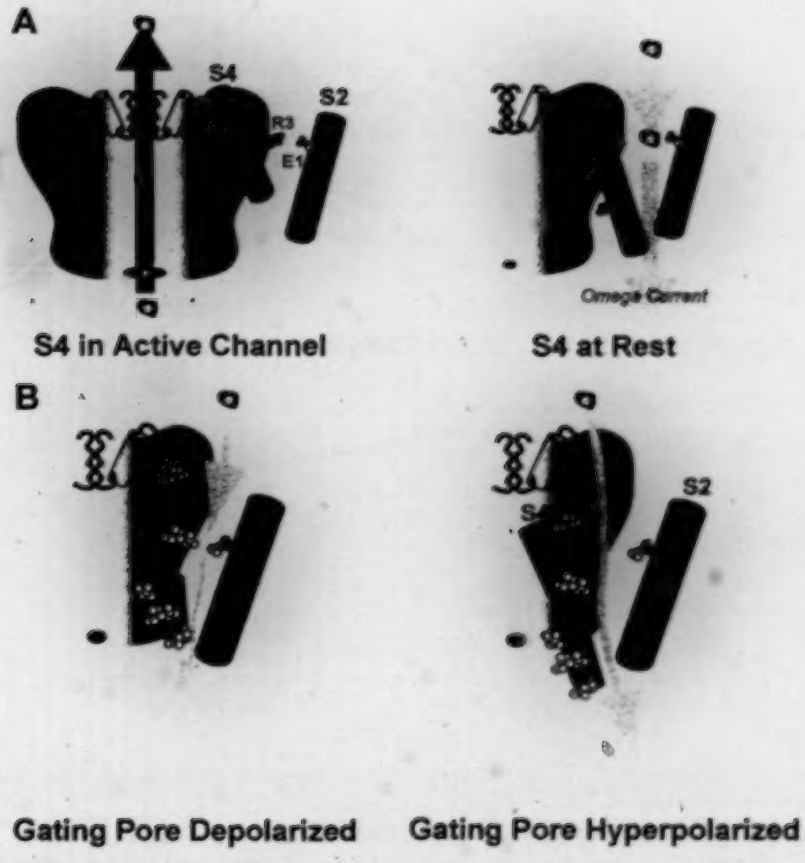

Figure 1-7: A cartoon of the structural basis for the Omega current flow through the gating pore pathway compared to the *Shaker* mutant channel.
A. The structural model for the Omega current mutant in *Shaker* created by reducing the side-chain length of the arginine in R1 (eg. R362C). The alternative permeation pathway is closed when the voltage-sensor translocates through the membrane, opening the canonical pore. When the voltage sensor is at rest, the small side chain of the R1 residue, permits a non-selective influx of cations.
B. Model of permeation in *N.at-K_V3.2* where even at depolarized potentials the flexible glycine hinge allows a small ionic flow. In our model, H325 (at R1) allows access to the pore, and G331 (at R3) provides flexibility in protein packing, and untethers the voltage-sensing domain from the pore.

CHAPTER 2: MATERIALS AND METHODS:

2.1 CREATION OF AN N-INACTIVE FORM OF *jShak1* IN pXT7

The *wild-type jShak1* coding region contained in BlueScript Plasmid (Jegla et al. 1995) was amplified using primers WJG1182 and WJG1173 (Table 2-1). The PCR fragment was cut using unique XhoI and SpeI sites and was inserted into the pXT7 plasmid and sequenced to confirm that no PCR-induced errors were present. Translational efficiency of transcribed mRNA is enhanced by using pXT7 as the expression vector because the inserted coding region is flanked by 5'UTR and 3'UTR sequences from *X. laevis* globin mRNA (Figure 2-1).

The full-length *jShak1* channel in pXT7 was used as a template for PCR amplification with primers WJG 2037 and WJG 1246 (Table 2-1). The PCR fragment and the *wild-type* containing expression plasmid were cut with unique XhoI and HpaI restriction sites. The PCR product was then ligated into the *wild-type* plasmid, and cut with XhoI and HpaI (NEB) to create a Δ23 N-truncated channel without the N-type inactivation ball, as described previously (Jegla et al. 1995). By removing fast inactivation (Hoshi et al. 1990) the steady-state conductance of the channels can be more accurately measured from tail currents. This channel is designated as *wild-type* for all subsequent experiments.

2.2 ISOLATION OF NOTOPLANA CHANNELS[4]

2.2.1 COLLECTION AND ISOLATION OF DNA AND RNA

Specimens of *Notoplana atomata* were collected from the mid-intertidal zone on cobble beaches at Bamfield Inlet, BC, Canada. Animals were held in running seawater and starved for four days prior to isolation of DNA. Genomic DNA was prepared either by SDS/proteinase K lysis followed by phenol extraction (Strauss 1998) or by the Carlson lysis method (Carlson et al. 1991) followed by methylene chloride extraction (Maureen Krause, Department of Biology, Hofstra University, Hempstead NY, personal

[4] Isolation of *Shaw* channels from *Notoplana atomata* was performed by D.A. Atherton.

communication).Total RNA was isolated from whole organisms using the Totally RNA Kit (Ambion).

2.2.2 Cloning and Sequencing

Initial PCR fragments of voltage-gated potassium channels were obtained using degenerate primers (Table 2-1, Jegla et al. 1995) and cloned into pGEM-T (Promega). Individual plasmids were then sequenced and the translated sequence was used to search the NCBI non-redundant protein sequence database using BLASTP (Altschul et al. 1997) to identify potassium channel fragments. Complete nucleotide sequences for the two channel mRNAs were determined using a combination of inverse PCR on genomic DNA and RACE-PCR on cDNA (Invitrogen GeneRacer kit). Sequences were determined from both strands of uncloned PCR product from at least two independent reactions to avoid unintended PCR errors. Open reading frames for each channel were amplified using appropriately designed primers (Table 2-1), cloned into pXT7 expression plasmid (Dominguez et al. 1995), and fully sequenced to confirm that no errors had been introduced (Figure 2-2, Figure 2-3).

2.2.3 Phylogenetic Analysis of Notoplana channels[5]

Amino acid sequences were aligned using the XALIGN algorithm (Wishart et al. 1994) as implemented in Peptool v1.0 (www.biotool.com), and hand adjusted. Four distinct phylogenetic analyses were performed to address four different questions. First, to test if the Notoplana sequences were more related to ERG or Shaker superfamily proteins, an alignment of 43 taxa and 327 positions was assembled. Second, resolution within the Shaker superfamily was sought from a dataset of 38 taxa and 292 positions. Third, a data set of 31 taxa and 324 positions, was used to resolve the position of the Notoplana sequences in the Shaw/Shab clade. Fourth, a dataset, using *N.at-K,3.1* as a surrogate for both N. atomata channels, was assembled with 46 taxa and 324 positions.

Optimal tree topologies of the 46, 43 and 38 taxon datasets were determined from distance matrices calculated by Tree-Puzzle 4.0.2 (Schmidt et al. 2002) with 8 plus 1 rate categories estimated from a starting Neighbor Joining tree (Saitou and Nei 1987). Trees

[5] Phylogenetic analysis was performed by J.B. Dacks and W.J. Gallin.

were constructed from these matrices using the Fitch program, which implements the Fitch-Margoliash algorithm (Fitch and Margoliash 1967) with global rearrangements and jumbling implemented. This analysis also yielded Quartet Puzzling support values. Additional confidence estimates for the 38 taxon dataset were obtained using ProtML 2.2 (Adachi and Hasegawa 1996) with 10,000 replicates. For the 31 taxon dataset, the optimal tree topology and Bayesian posterior values were obtained using MrBayes v3.0b4 (Ronquist and Huelsenbeck 2003) with the default parameters for amino acid sequences.

For maximum likelihood (ML) distance bootstrapping, Seqboot (from the PHYLIP 3.6 package) was used to produce 100 pseudoreplicate datasets. These were analyzed using Tree-Puzzle to produce distance matrices with parameters estimated from the original dataset in coordination with Puzzleboot (www.tree-puzzle.de). These distance matrices were then analyzed using Fitch (for the smaller datasets) or Neighbor (for the larger datasets). Analyses with Neighbor incorporated the Jumbling option, while Fitch analyses were done with 10 times jumbling and global re-arrangements. Seqboot, Fitch and Neighbor are all programs from the PHYLIP v3.6 (Felsenstein 1995) suite of phylogenetic analysis programs.

2.3 MUTAGENESIS

In presenting and discussing my results, all mutations are named as per Larsson and Elinder (2000). For example, the mutation K294R, the *wild-type* residue is K294, where the amino acid is 294, and the mutant channel is K294R (Larsson and Elinder 2000).

2.3.1 SITE-DIRECTED MUTAGENESIS

2.3.1.1 *jShak1 Mutants*

The single K294Q, K294R, R291K and R291Q mutants, as well as the double mutants R291K+K294R, K294Q+R297K and K294R+R297K were created by pairing a single antisense primer containing the desired mutations with WJG2037 (Table 2-1). The resulting PCR products were digested with XhoI and BglII and ligated into the cut N-truncated *wild-type* plasmid to create the S4 mutants. The sequence of all mutants was

confirmed by sequencing the cloned plasmid with two flanking primers in the pXT7 plasmid.

2.3.1.2 *N.at-K,3.2 Mutants*

The full-length *N.at-K,3.2* channel in pXT7 was used as a template for two rounds of PCR site-directed mutagenesis. To create the H325 mutants, the 5' construct primer WJG 1497 was paired with the antisense mutagenesis primers WJG2054-2059 containing the desired mutation and a unique BspEI restriction site (Table 2-1). The resulting PCR fragment and the wild-type containing expression plasmid were cut with unique BglII and BspEI restriction sites (NEB). The PCR product was then ligated into the wild-type plasmid to create the H325 mutants. To create the G331 mutants, the 3' construct primer WJG1494 was paired with the sense mutagenesis primers WJG1950, 1951, 1952 and 1961 containing the desired mutation and the unique BspEI restriction site (Table 2-1). The resulting PCR fragment and the wild-type containing expression plasmid were cut with BspEI and EagI (NEB). The PCR product was ligated into the wild-type plasmid to create the G331 mutants. All mutant plasmids were fully sequenced to confirm the desired mutation and the absence of PCR induced mutations.

2.3.2 Overlapping Extension

In the *jShak1* channel, the triplet mutations of the S4 sensor, whereby either RIF or QIF was inserted on the N-terminal side of K294, or IFR was inserted on the C-terminal side of K294 (Figure 1-5C), were constructed in this plasmid using overlapping PCR extension as described previously (Grigoriev et al. 1997).

The S2 mutations at asparagine residue 227 were created by overlapping PCR mutagenesis. Primers used to create the N227E mutation were WJG1062 and WJG1063 and construction of N227D used primers WJG1064 and WJG1065. In both instances the flanking primers were WJG1149 and WJG1181. The resulting PCR products were digested with HpaI and ClaI and ligated into the *wild-type* or S4 mutant plasmids to create single (S2) and double (S2/S4) mutations respectively.

2.3.3 *N.at-K,3.2* Double Mutant Cut and Paste

To create the S4 double mutants, we employed a classic cut and paste approach where the G331 mutant plasmids were designated to be vector, and H325 mutants were designated as inserts. In this procedure, the six H325 mutant expression plasmids and the four G331 mutant expression plasmids were cut with BglII and BspEI restriction enzymes, and the restriction digest was run on a 0.8% agarose gel. The resulting 500 base pair fragment containing the H325 mutation and the ~4000 base pair linear vectors containing the G331 mutants were excised from the gel and purified using the Qia-quick Gel Extraction Kit (Qiagen). The purified H325 containing fragments were ligated into the G331 containing vectors, resulting in the production of twenty-four S4 double mutants. These plasmids were fully sequenced to confirm the presence of both H325 and G331 mutations.

2.4 Electrophysiological Methods

2.4.1 Channel Expression

2.4.1.1 mRNA Creation

Purified plasmids were prepared from 10 ml overnight cultures (Terrific Broth (Ausubel et al. 1987) with 100 μg/ml ampicillin using a Wizard Miniprep Kit (Promega). Plasmids were linearized with XbaI a unique restiction enzyme, and gel purified using the Qia-quick Gel Extraction Kit (Qiagen). Capped mRNAs were prepared by *in vitro* transcription using a mMessage mMachine (Ambion) T7 polymerase kit, and stored at -80°C.

2.4.1.2 Oocyte Preparation

2.4.1.2.1 Oocyte Extraction

Two year old female *X. laevis* (Biological Sciences Animal Services) were reversibly anaesthetised in 0.17% MS-222 (Sigma) and a single lateral incision made in the abdomen 1 cm from the midline, 1 cm caudal to the pelvic girdle (Animal Care Protocol # 400503). A single ovary was removed, and two sutures were used to close the

incision. Frogs were left to recover from surgery for 4-8 hours before they were returned to the aquatics facility.

2.4.1.2.2 Biochemical Oocyte Preparation for Mutagenesis Experiments

The ovarian lobe was manually separated into half centimetre clumps. Ovarian pieces were rinsed three times in MBM (in mM: NaCl 88, KCl 1, $Ca(NO_3)_2$ 0.33, $CaCl_2$ 0.41, $MgSO_4$ 0.82, NaHCO3 2.4, HEPES 10 (Tris Base to pH 7.5), sodium pyruvate 2.5 supplemented with penicillin G 0.1g/L and gentamycin sulfate 0.05 g/L (Huang et al. 1993) and incubated on a rotating shaker for 2h in 2mg/ml collagenase 1A (Sigma) in MBM at room temperature. Eggs were removed from the collagenase solution, rinsed in MBM and incubated, ~200 eggs/glass scintillation vial, at 17°C overnight in fresh MBM. Eggs were de-folliculated by immersion in a hypo-osmotic phosphate buffer (in mM: K_2PO_4 100 (pH 6.5 with HCl)) for 1h. Following treatment, eggs were left for 2 h in fresh MBM to recover prior to manipulation.

2.4.1.2.3 Manual Oocyte Preparation for N.at-K_v3.1 and N.at-K_v3.2 Channel Characterization

Ovarian lobes were separated into clumps of about 50 oocytes. These were then washed in low-calcium oocyte saline (ND96, in mM NaCl 96; KCl 2; $CaCl_2$ 1; $MgCl_2$ 1; HEPES 5; pH 7.6) and incubated in 2 mg/ml collagenase (Sigma type IV) in calcium-free ND96 for about 1h. Selected stages V to VI oocytes were then manually de-folliculated using Dumont #5 forceps (Fisher Scientific). De-folliculated oocytes were rinsed in fresh ND96 (in mM NaCl 96; KCl 2; $CaCl_2$ 1.8; $MgCl_2$ 1; HEPES 5; pH 7.6) before mRNA injection.

2.4.1.3 Channel Injection and Incubation

2.4.1.3.1 jShak1 Mutant Channels

Mature oocytes (stage V-VII) were injected with 48.6 nl mRNA (200-600 ng/nl) and incubated in MBM at 17°C with daily changes of incubation medium.

2.4.1.3.2 Wild-type Flatworm K_v3 Channels

Mature oocytes (stage V-VII) were injected with 50 nl of mRNA (1 ng/nl) and held at room temperature with daily changes of incubation medium (ND96 supplemented with sodium pyruvate at a final concentration of 2.5 mM).

2.4.1.3.3 N.at-K_v3.2 Mutant Channels

Mature oocytes (stage V-VII) were injected with 40.6 nl mRNA (200-600 ng/nl) and incubated in SOS+ (in mM: NaCl 96, KCl 2, $CaCl_2$ 1.8, $MgCl_2$ 1, HEPES 5, sodium pyruvate 2.5 (adjusted to pH 7.4), supplemented with 3% horse serum (Sigma) and gentamycin sulfate 0.01 g/ml) at 17°C.

2.4.2 ACQUISITION OF DATA

2.4.2.1 General Methods

Electrophysiological experiments were performed 1 to 2 days after injection. Recordings were made in an RZ-17 perfusion chamber (Warner Instruments) and oocytes were perfused with ND96. Oocytes were impaled with glass microelectrodes fabricated from borosilicate glass, filled with 3 M KCl and having a resistance of 0.5 to 1 MΩ. Experiments were driven by a GeneClamp 550B amplifier (Axon Instruments) controlled by pClamp 9.0 software (Axon Instruments). Data were acquired through an Axon Instruments 1322A analogue/digital converter at a sampling rate of 100 μs with no on-line filtering. Data was analysed using Clampfit 9.0 (Axon Instruments). Measurements were performed with leak subtraction (P/N = 4) for delayed rectifiers, but not for *N.at-K_v3.2* and *N.at-K_v3.2* mutants showing inward rectification as these channels conducted over the range of command membrane potentials used. For combination delayed/inward rectifier channels recordings were made first with leak subtraction (P/N=4), and analyzed to determine that the small influx of current was real and not an ohmic leak current. When non-ohmic currents were subtracted, outward inflections in current traces at hyperpolarized potentials were observed. Thus, subsequent recordings on combination delayed/inward rectifier channels were performed without leak subtraction.

2.4.2.2 *jShak1* N-truncated Mutant Characterization

The N-truncated *jShak1 wild-type* channel had identical activation properties to the full-length channel, but lacked fast N-type activation (Figure 2-4A, 2-4B). The N-truncated *jShak1* channels expressed in pXT7 had higher rates of translation compared to mRNA prepared from BlueScript (Grigoriev et al. 1997; Jegla et al. 1995), but had identical electrophysiological properties. The N-truncated channels manifested variable C-type inactivation, with IFR-E having the most inactivation at 150 ms, however, all channels opened quickly allowing for peak currents to be obtained by 50 ms. Therefore, all electrophysiological protocols were designed to elicit current measurements prior to significant C-type inactivation (Figure 2-4C, 2-4D).

Steady-state conductance was measured using standard tail current protocols where the membrane is held at -90 mV for 10 ms followed by a series of 50 ms depolarisations from -140 mV to +90 mV in 10 mV steps followed by a 20 ms step to -90 or -70 mV for inward tails or -50, -40, or -30 mV for outward tails, followed by a 200 ms return to a -90 mV holding potential. Steady-state voltage-conductance curves were obtained by measuring the tail current 1-3 ms after the capacitative transient (Figure 2-5).

2.4.2.3 *N.at-K$_n$3.2* Current/Voltage Protocols

2.4.2.3.1 Inward Rectifier and Combination Delayed/Inward Rectifier Channels

Steady-state currents for inward rectifier channels were elicited using standard current/voltage protocol, where the membrane is held at -90 mV for 50 ms followed by a series of 400 ms depolarisations from -140 mV to +90 mV in 10 mV steps followed by a return to a -90 mV holding potential.

2.4.2.3.2 Delayed Rectifier Channels

Steady-state currents for delayed rectifier channels were elicited using standard current/voltage protocol, where the membrane is held at -90 mV for 50 ms followed by a series of 200 ms depolarisations from -140 mV to +90 mV in 10 mV steps followed by a return to a -90 mV holding potential. Current/voltage measurements were taken 10 ms before the end of the activation step, before the capacitative transient. Currents were

normalized for each mutant independently. The mean and standard error of the mean for the normalized current for each voltage step was plotted to create I/V curves.

2.4.2.4 Inward Rectifier Permeability

Perfusion experiments in which $[K]_{out}$ was varied from 2 mM, 10 mM, 50 mM and 98 mM were performed in ND96 and ND96 with choline replacing NaCl, with increasing $[K]_{out}$ compensated for by decreasing either Na^+ or choline concentration (ND96, in mM NaCl or ChoCl 96-X; KCl 2+X; $CaCl_2$ 1; $MgCl_2$ 1; HEPES 5; pH 7.6). For ion substitution experiments done in modified saline, the bath solution was either a control saline (Control, in mM NaCl 78; KCl 2; $CaCl_2$ 1; $MgCl_2$ 1; ChoCl 18; HEPES 5; pH 7.4) or a solution (High K^+, Low Na^+, Low Cl^- and High Ca^{2+}) where the ion concentrations were modified by substituting with 20 mM KCl (replacing ChoCl), 88 mM ChoCl (replacing 70 mM NaCl), 38.5 mM Na_2SO_4 (replacing 78 mM NaCl) or 10 mM $CaCl_2$ (replacing ChoCl) respectively.

In ion substitution experiments performed to test permeability, the bath contained a 100 mM solution of a single cationic salt, guanidinium chloride (GuCl), LiCl, CsCl, NaCl, KCl, or $BaCl_2$, and, in mM; HEPES 10; EDTA 1; pH 7.6.

The dose responses curve for pharmacological blockers were created by dissolving 4-AP or TEA in ND96 creating a 100mM stock, and serial dilutions of this stock were used at the concentrations specified.

2.5 Data Analysis

2.5.1.1 Gibb's Free Energy Analysis

Voltage-conductance curves obtained for the *jShak1* mutants were fitted with a four-parameter Boltzmann curve:

$$I / I_{max} = y0 + \left[\frac{G_{max}}{\left(1 + e\left(\frac{-(V - V_{50})}{b}\right)\right)} \right] \qquad \text{(Eq. 2-1)}$$

Where y0 is an offset, G_{max} is maximal conductance, V_{50} is the voltage at which half of the channels are activated, and b is the Boltzmann slope factor. Charge (z), the number of elementary charges responsive to V was calculated as:

$$z = \frac{RT}{bF} \qquad \text{(Eq. 2-2)}$$

Where R is the gas constant (8314 J/kmol*K), T is temperature (25°C) in degrees Kelvin (298°K), and F is Faraday's Constant (96.4846 C/kmol).

Gibbs Free Energy at 0mV was calculated for each mutant by:

$$\Delta G_0 = 0.2389(zFV_{50}) \qquad \text{(Eq. 2-3)}$$

For double mutant cycle analysis Gibbs free energy was compared to the *wild-type* channel:

$$\Delta\Delta G_0 = \Delta G_{0mut} - \Delta G_{0wt} \qquad \text{(Eq. 2-4)}$$

Negative values indicate that the equilibrium is shifted towards the open state through a combination of leftward shift in voltage sensitivity and/or a change in z value for the mutant channel. Positive $\Delta\Delta G_0$ values are caused by a combination of rightward shift in half activation voltage and/or a decreased z value of the mutant channel compared to the *wild-type*, indicating an increased stabilization of the closed state compared to the open state of the channel.

2.5.1.2 Calculated Conductance for *N.at-K$_v$3.2* mutants

To obtain a measure of ionic conductance (G) through the alternative permeation path in *N.at-K$_v$3.2* mutant channels the current for each voltage step was divided by the voltage step used to elicit the response minus the reversal potential (E_{rev}) for the experiment:

$$G_{(Vm)} = \left[I_{Vm}/(Vm - E_{rev})\right] \qquad \text{(Eq. 2-5)}$$

The E_{rev} for the experiment was taken as the x-intercept from the slope of the line connecting the two data points marking the transition from influx to efflux (crossing 0 μA) in the I/V plot for individual experiments.

All mutants with similar conductance profiles were grouped together, resulting in five Conductance Groups (Figure 2-6) to allow comparisons between the data sets. In defining the conductance groups, the G/V curves were divided into three regions; 1) below the E_{rev} (~ -60 mV), 2) between E_{rev} and the plateau phase (~ -60 mV to 0mV) and 3) the plateau phase (+ 0 mV), and examined for the shape of the conductance curve (eg. falling conductance, ohmic conductance, rising conductance) in these regions.

Conductance/voltage relationships for the delayed rectifiers and combination delayed/inward rectifiers were fit with a four parameter sigmoidal Boltzmann curve and normalized to G/Gmax, to compare the biophysical properties (V_{50} and slope factor) of the mutants.

2.6 MOLECULAR MODELING[6]

The crystal structure of the $K_v1.2$ potassium channel in the open state (2A79.pdb) (Long et al. 2005) was used as the primary modeling template for homology modeling of *jShak1* in the closed state. The crystal structure maps the coordinates for residues Cys32 to Gly131, Thr219 to Ala243 and Met288 to Thr421. The two unresolved chains, represented in the crystal structure as by polyglycines and polyalanines, are Chains C and D. Chain C represents the T1-S1 linker and S1 helix, while Chain D represents the S3 helix. Chains C and D are 52 and 21 residues long, respectively. The identity of the residues comprising Chains C and D was determined using the known structural elements and secondary structure predictions from PredictProtein (Rost et al. 2004), on the complete primary sequence of $K_v1.2$ (NCBI# P63142). The corresponding regions of the primary sequence were threaded onto the polyglycine or polyalanine backbones and the side-chains were rebuilt using SwissPDBViewer (Guex and Peitsch 1997; Peitsch et al. 1995; Peitsch et al. 1997). The missing inter-helical loop regions of the voltage sensor were rebuilt using SwissPDB loop databases (Guex and Peitsch 1997).

The pair-wise sequence alignment of *jShak1* and *Rat$K_v1.2$* and the corresponding secondary structure predictions (Rost et al. 2003) were used to identify the T1-S1 linker region, S1 and S3 helices of *jShak1*. These regions were threaded onto the polyglycine and polyalanine backbones of the corresponding regions of the $K_v1.2$ crystal structure

[6] Molecular modeling was performed by M. O'Mara and M. Renstone.

and the side-chains were rebuilt using SwissPDBViewer (Guex and Peitsch 1997; Schwede et al. 2003). A homology model of *jShak1* was constructed in SwissModel using the resolved residues of the $K_v1.2$ channel structure as a modeling template. The threaded T1-S1 region, S1 and S3 helices were incorporated into the homology model and the missing inter-helix loops were rebuilt using SwissModel and SwissPBDViewer loop databases (Guex and Peitsch 1997; Schwede et al. 2003). The resulting subunit model was energy minimized and refined to remove any steric clashes. The symmetry information from the $K_v1.2$ crystal structure was used to derive the coordinates of the other three identical *jShak1* subunits to give the complete channel. The *jShak1* channel model was tetramerized and loop and interface regions were refined. Finally, the model was energy minimized again to remove any residue clashes or irregularities at the subunit interfaces. The completed *jShak1* homology model was checked using WHATIF (Vriend 1990) and found to be of comparable quality to the $K_v1.2$ channel. The root-mean squared deviation (RMSD) between the $K_v1.2$ crystal structure and the *jShak1* homology model was 0.13Å.

Table 2-1: PCR Primers used for the cloning of novel channels into the pXT7 expression plasmid, and for mutagenesis experiments in the *jShak1* and *N.at-K,3.2* channels.

Primer	Template	Function	Direction	Sequence 5'-3'
Multiuse Primers				
WJG1118	K_v channel	degenerate primer in	sense	TCGGAATTCTATGACTACTGTTGGNTAYGGNGA
WJG1119	K_v channel	degenerate primer in	antisense	ACTTCTAGAGGTAGTGCTATTRYNAGNACNCC
WJG1174	pXT7	external sequencing	sense	TGCTTGTTCTTTTTGCAGAAG
WJG1175	pXT7	external sequencing	antisense	GCTTAGAGACTCCATTCGGG
WJG1218	pXT7	T7 sequencing primer	sense	TAATACGACTCACTATAGGG
WJG1402	K_v channel	nested degenerate	antisense	TCNCCRTANCCAACAGTAGTCAT
WJG1403	K_v channel	nested degenerate	sense	GGNGTNCTNRYAATAGCACT
WJG1404	5' RACE Primer	outside Invitrogen	sense	CGACTGGAGCACGAGGACACTGA
WJG1405	5' Nested RACE	nested Invitrogen	sense	GGACACTGACATGGACTGAAGGAGTA
WJG1406	3' RACE Primer	outside Invitrogen	antisense	GCTGTCAACGATACGCTACGTAACG
WJG1407	3' Nested RACE	nested Invitrogen	antisense	CGCTACGTAACGGCATGACAGTG
WJG1427	pXT7	SP6 sequencing primer	antisense	TATTTAGGTGACACTATAG
jShak1 Structure/Function Study				
WJG1062	jShak1	N227E overlap	sense	CTGTGGAGACGGCTGTAATATGCTGGTTTAC
WJG1063	jShak1	N227E overlap	antisense	GCCGTCTCCACAGTAAACATCCACGTC
WJG1064	jShak1	N227D overlap	sense	CTGTGGACACGGCTGTAATATGCTGGTTTAC
WJG1065	jShak1	N227D overlap	antisense	GCCGTGTCCACAGTAAACATCCACGTC
WJG1149	jShak1	outside flanking	sense	GCCCGTATTTGCCCCAAAAG
WJG1150	jShak1	outside flanking	antisense	GCCATTGAACCAACAATTTGACCC
WJG1152	jShak1	inside flanking primer	antisense	GAACGATCCTTTACTGCTACTTAC
WJG1173	jShak1	pXT7 cloning wt	antisense	GG**ACTAGT**TTTAAAGGATAAGTACACGAGCCGTTT
WJG1176	jShak1	internal primer	sense	CCATAGACCAACTTTTGAATCCAT
WJG1177	jShak1	internal primer	sense	GACATTCCCGTGGTTTACAGA
WJG1178	jShak1	internal primer	sense	CAATAGCTTTGCCAGTGCCT
WJG1179	jShak1	internal primer	antisense	AATATAAAATGGATTCAAAAGTTGGTCTA
WJG1180	jShak1	internal primer	antisense	AAAGACACTACGATAATGACTACGGA
WJG1181	jShak1	internal primer	antisense	CGTAACATGCTGAACGATCC
WJG1182	jShak1	pXT7 cloning wt	sense	GG**CTCGAG**CCACCATGATGTTTGTAGCCACTAA

Table 2-1 (Cont.): PCR Primers used for the cloning of novel channels into the pXT7 expression plasmid, and for mutagenesis experiments in the *jShak1* and *N.at-K,3.2* channels.

Primer	Template	Function	Direction	Sequence 5'-3'
WJG2037	jShak1	Δ23 n-truncation	sense	GG**CTCGAG**CCACCATGGAAGACAATGCAGA
WJG2111	jShak1	K294Q	antisense	CCTA**AGATCT**GTAAACCACGGGAATGTCTCGATAGTTGAAACAC
WJG2112	jShak1	K294R	antisense	CCTA**AGATCT**GTAAACCACGGGAATGTCTCGATAGTCGAAACAC
WJG2147	jShak1	R291K+K294R	antisense	CCTA**AGATCT**GTAAACCACGGGAATGTCTCGATAGTCGAAACACCTTTAAAACC
WJG2149	jShak1	R291K	antisense	CCTA**AGATCT**GTAAACCACGGGAATGTCTCGATAGTTTAAACACCTTTAAAACC
WJG2150	jShak1	R291Q	antisense	CCTA**AGATCT**GTAAACCACGGGAATGTCTCGATAGTTTAAACACCTGTAAAACC
WJG2151	jShak1	K294Q+R297K	antisense	CCTA**AGATCT**GTAAACCACGGGAATGCTTCGATAGTTGAAACAC
WJG2152	jShak1	K294R+R297K	antisense	CCTA**AGATCT**GTAAACCACGGGAATGCTTCGATAGTCGAAACAC
Novel Channels from Notoplana atomata				
WJG1394	N.at-K,3.2	1st GeneRacer primer	sense	CCGTCCATGGGGCTACCTCGTC
WJG1395	N.at-K,3.2	2nd GeneRacer primer	sense	GTCGGGTCTGCCTGTGCGCTCAT
WJG1396	N.at-K,3.2	1st GeneRacer primer	antisense	GAGCGCACAGGCAGACCCGACGA
WJG1397	N.at-K,3.2	2nd GeneRacer primer	antisense	CGACGAGGTAGCCCCATGGACGG
WJG1398	N.at-K,3.1	1st GeneRacer primer	sense	GCTCAACTGGATCGATATTCTCTGTAA
WJG1399	N.at-K,3.1	2nd GeneRacer primer	sense	CGCCTTCCGCATTCTCCTCTATTCT
WJG1400	N.at-K,3.1	1st GeneRacer primer	antisense	GGCCGTAGGGAATTGATGTGAAGTT
WJG1401	N.at-K,3.1	2nd GeneRacer primer	antisense	AGACGATGGAGCCGAATAGGATGGA
WJG1414	N.at-K,3.2	5' RACE primer	antisense	CGAAGGTGAAAAAGGCGACA
WJG1415	N.at-K,3.2	3' RACE primer	antisense	CGGCCGTGATATCTGCTCAA
WJG1419	N.at-K,3.2	internal primer	sense	AATCGAGAAGTGCTGCTGGGTGAG
WJG1420	N.at-K,3.2	internal primer	antisense	CTCACCCAGCAGCACTTCTCGATT
WJG1421	N.at-K,3.2	internal primer	sense	CGCTAGATTACGTGTGTGTCGCCTTT
WJG1422	N.at-K,3.1	internal primer	antisense	CACTGAGGAGGCTGAAATGAACATC
WJG1423	N.at-K,3.1	internal primer	antisense	TAGAATAGAGGAGAATGCGGAAGGCG
WJG1424	N.at-K,3.1	internal primer	antisense	GGCGGTATCGCATTCGACCTCCAC
WJG1425	N.at-K,3.1	internal primer	antisense	GTTTGGCCTGGCACGCGTTTCTTG
WJG1431	N.at-K,3.2	internal primer	antisense	CTGCATGTGGCGGCGAATCT
WJG1475	N.at-K,3.2	internal primer	sense	CGGCGTCCTCGTTGTGGCTTTC
WJG1476	N.at-K,3.2	internal primer	sense	CGATATGGATGGTTGCGGCAGTG

Table 2-1 (Cont.): PCR Primers used for the cloning of novel channels into the pXT7 expression plasmid, and for mutagenesis experiments in the *jShak1* and *N.at-K,3.2* channels.

Primer	Template	Function	Direction	Sequence 5'-3'
WJG1491	N.at-K,3.2	internal primer	antisense	CCCTGCATGTGGCCGGCGAATCTC
WJG 1492	N.at-K,3.2	internal primer	sense	CCGCTACGCTCTGGATCTGCACCTTCTGTC
WJG1493	N.at-K,3.2	internal primer	antisense	CCGCAATGCTCCTCACATAGACAAAAGGTGCAGATC
WJG1494	N.at-K,3.2	pXT7 cloning	antisense	GG**ACTAGT**CGCAGCGGTGCTCCTCACAC
WJG1495	N.at-K,3.1	pXT7 cloning	sense	GGG**TGATCA**CCGCCATGATGGCCGAAAGAGTCGT
WJG1496	N.at-K,3.1	pXT7 cloning	antisense	GGG**TCTAGA**TTTTCTTTCTTAAGCAATTATCAGATGTTCTCC
WJG1497	N.at-K,3.2	pXT7 cloning	sense	GGG**TGATCA**CCATGACGTCCCGCCTCGCCTTC
WJG1590	N.at-K,3.1	internal primer	antisense	CGGCATGGCGGTCGAA
Notopleura Voltage Sensor Mutations				
WJG1950	N.at-K,3.2	G331P	sense	GTGATCCACGTG**TTCCGGA**TTTTCCCTATCCTGCGTGTC
WJG1951	N.at-K,3.2	G331A	sense	GTGATCCACGTG**TTCCGGA**TTTTCGCTATCCTGCGTGTC
WJG1952	N.at-K,3.2	G331K	sense	GTGATCCACGTG**TTCCGGA**TTTTCAAAATCCTGCGTGTC
WJG1961	N.at-K,3.2	G331R	sense	GTGATCCACGTG**TTCCGGA**TTTTCAGGATCCTGCGTGTC
WJG2054	N.at-K,3.2	H325R	antisense	**TCCGGAA**CACCCGGATCACATCGAGG
WJG2055	N.at-K,3.2	H325A	antisense	**TCCGGAA**CACTGCGATCACATCGAGG
WJG2056	N.at-K,3.2	H325V	antisense	**TCCGGAA**CACTACGATCACATCGAGG
WJG2057	N.at-K,3.2	H325C	antisense	**TCCGGAA**CACACAGATCACATCGAGG
WJG2058	N.at-K,3.2	H325S	antisense	**TCCGGAA**CACGGAGATCACATCGAGG
WJG2059	N.at-K,3.2	H325E	antisense	**TCCGGAA**CACCTCGATCACATCGAGG

* underlined basepairs indicate codon mutation resulting in amino acid change
# bolded basepairs indicate restriction enzyme recognition site used for cloning

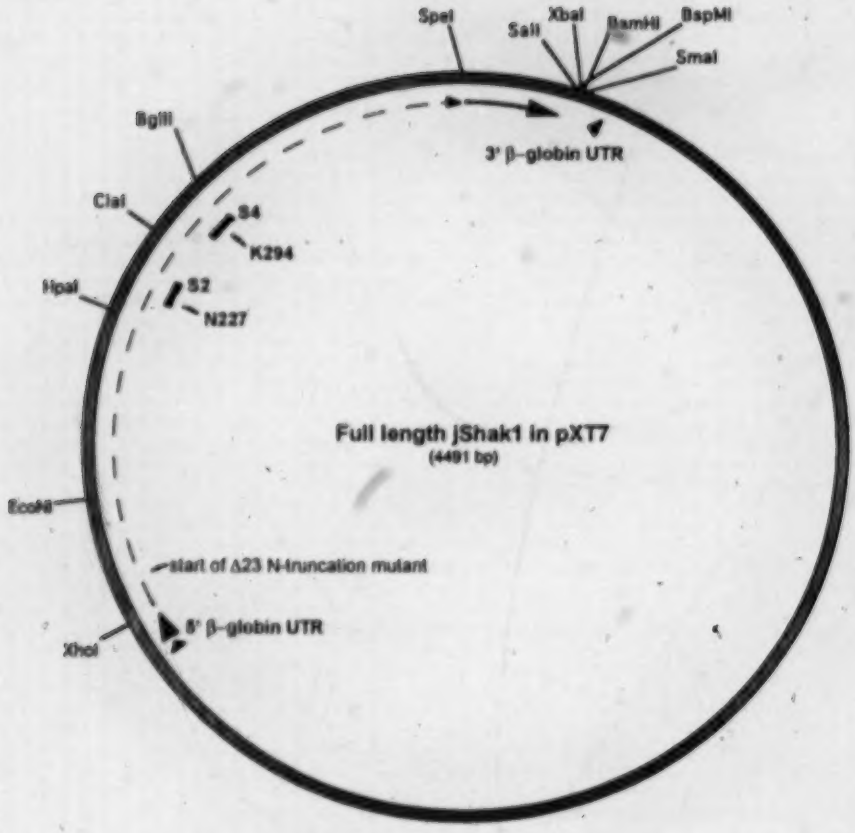

Figure 2-1: Construct map of the full length *jShak1* pXT7 expression plasmid. The open reading frame of the channel is denoted by the dashed arrow. The residues of interest (N227 and K294) are labeled within the marked S2 and S4 sequences. The location of the beginning of the N-truncated Δ23 mutant is also marked. Restriction enzymes used in mutant preparation are labeled.

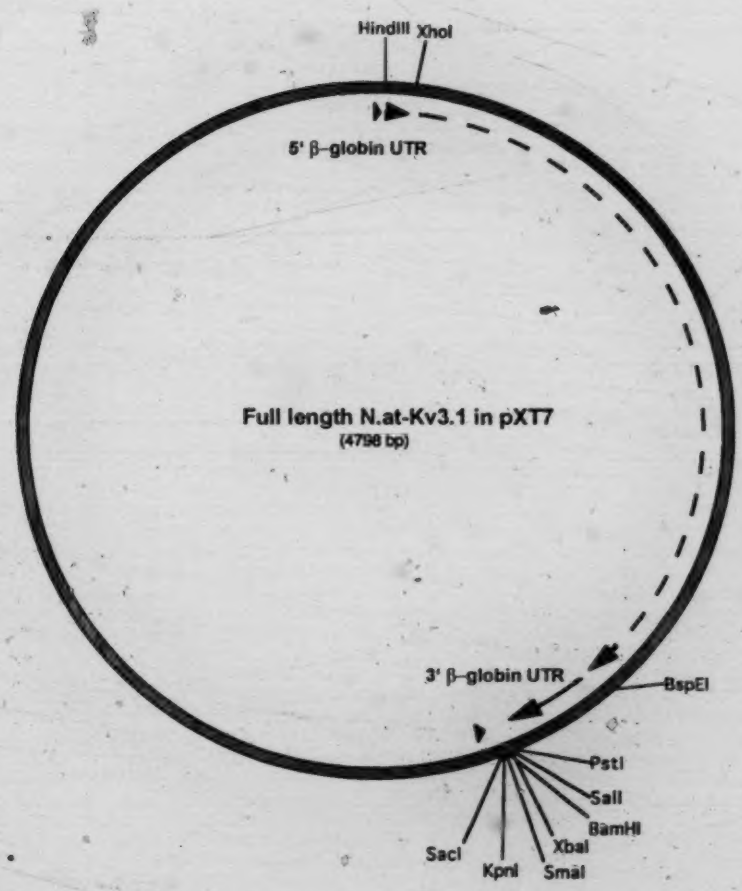

Figure 2-2: Construct map of the full length *N.at-K,3.1* pXT7 expression plasmid. To clone the *wild-type* channel into pXT7, the PCR fragment was digested, and purified, and ligated into the corresponding cut-sites in pXT7. The open reading frame of the channel is denoted by the dashed arrow. The restriction enzymes used for cloning are marked.

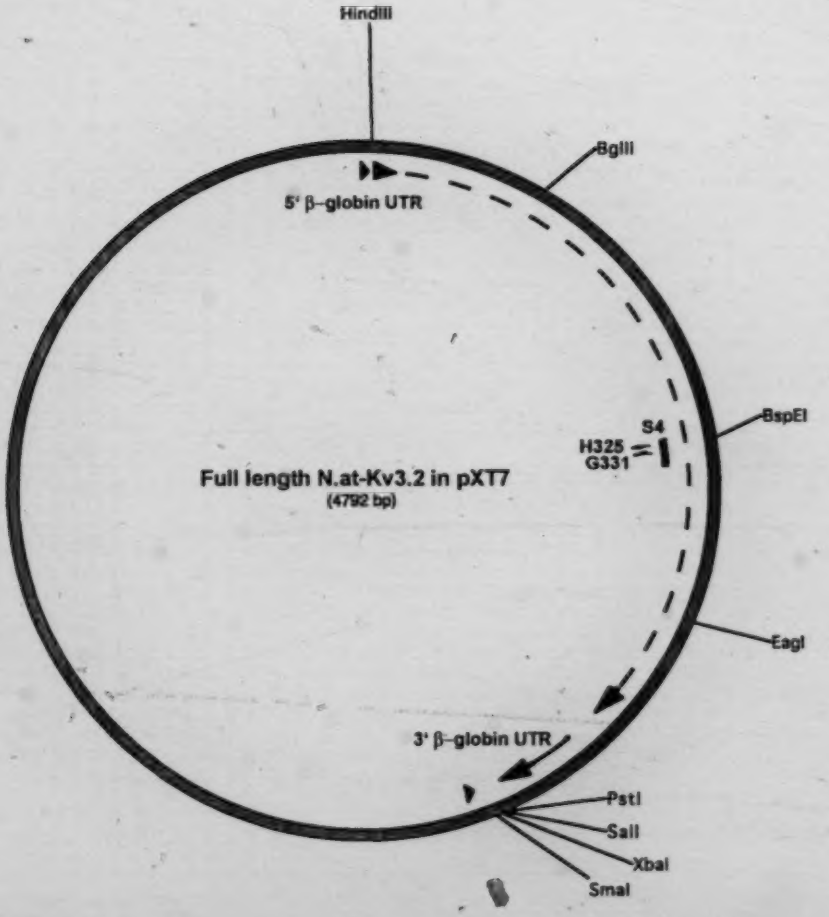

Figure 2-3: Construct map of the full length *N.at-K,3.2* pXT7 expression plasmid. The open reading frame of the channel is denoted by the dashed arrow. The residues of interest (H325 and G331) are labeled within the marked S4 sequence. The location to create double mutant channels the unique BspEI site was used to isolate a short fragment of plasmid containing the H325 mutations. This fragment was cleaned and ligated into the corresponding sites of the large G331 containing vector during cut and paste mutagenesis.

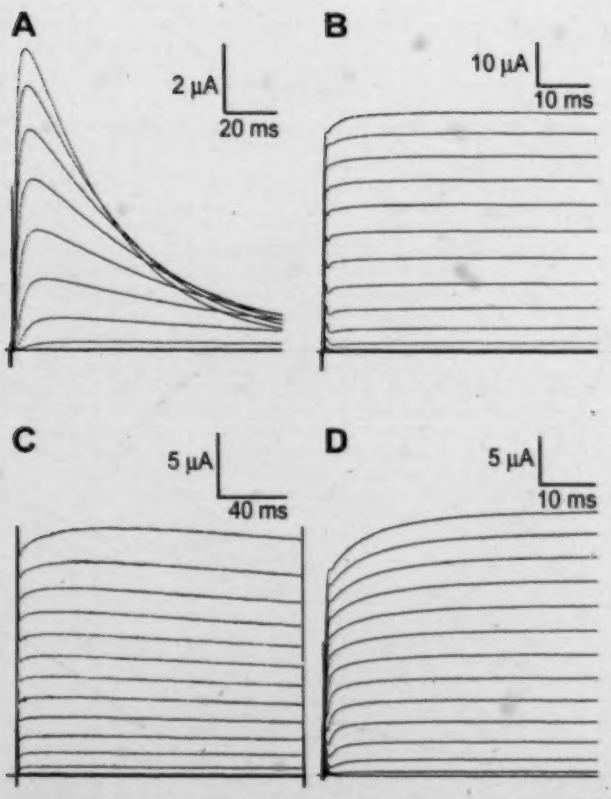

Figure 2-4: Δ23 N-truncated *jShak1* channels lack N-type inactivation but exhibit slow C-type inactivation.

A. Current traces of the full-length wild type *jShak1* channel show fast opening and fast N-type inactivation. Outwardly-directed currents evoked by 100 ms step depolarisations from a holding potential of -90 mV to a range of potentials from -90 to + 90 mV in 10 mV increments followed by a return to -90 mV.

B. The Δ23 N-truncated wild-type *jShak1* channel lacks N-type inactivation. Currents elicited as in A.

C. C-type inactivation was observed in some N-truncated S2/S4 mutant *jShak1* channels. Currents of the IFR-E double mutant showed the most C-type inactivation as shown here. Currents evoked as in A.

D. Shortened acquisition protocols allowed channels to open fully but limited the amount of slow inactivation. Outwardly-directed currents from IFR-E evoked by 50 ms step depolarisations from a holding potential of -90 mV to a range of potentials from -90 to + 90 mV in 10 mV increments followed by a return to -90 mV to induce inward tail currents.

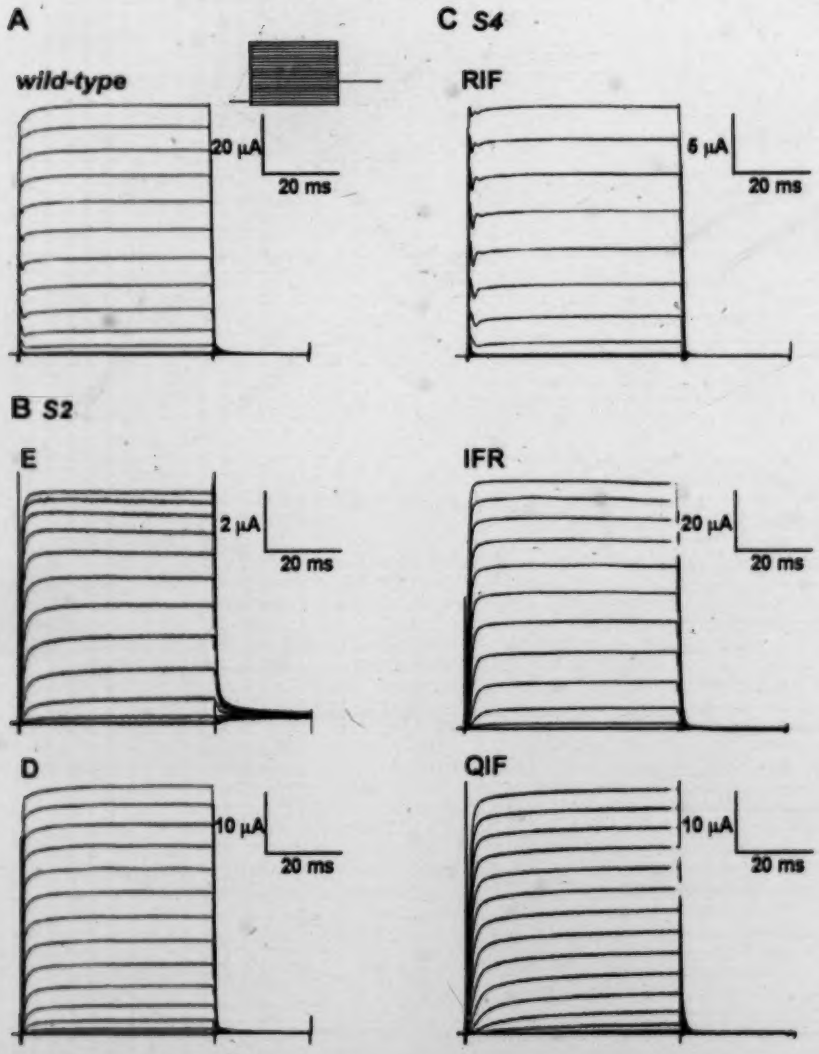

Figure 2-5: Exemplar traces for N-truncated *wild-type jShak1*, S2 single mutants and the S4 insertion mutants showing measurable outward tail currents.
A. N-truncated *wild-type jShak1* channels exhibit measurable outward tail currents evoked by a 20 ms -30 tail step after a range of 50 ms step depolarisations -90 to + 90 mV in 10 mV from a holding potential of -90 mV. GV measurements were obtained 1-3 ms after the capacitative transient.
B. Measurable tail currents obtained for the N227E and N227D S2 mutants obtained as in A.
C. Measurable tail currents obtained for the RIF, QIF and IFR S4 insertion mutants obtained as in A.

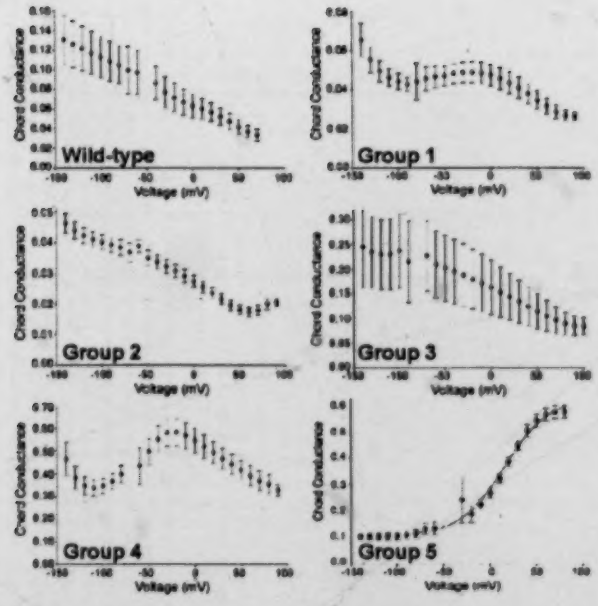

Figure 2-6: The conductance/voltage relationships for the inwardly rectifying *N.at-K$_v$3.2* single and double mutants can be divided into five conductance groups. These conductance profiles were assigned based on the shape of the curve through three voltage ranges: below E_{rev}, above E_{rev} below the plateau phase of the current/voltage relationships, and through the shallow slope phase (typically greater than 0 mV). Because conductance was calculated using an extrapolated reversal potential in Eq. 2-5, the largest error was at or near the E_{rev} point, and therefore was not plotted.

CHAPTER 3: INTRAMOLECULAR INTERACTIONS DETERMINE VOLTAGE-SENSITIVITY IN A CNIDARIAN VOLTAGE-GATED POTASSIUM CHANNEL, *jShak1*[7]

3.1 RESULTS

3.1.1 RELATIONSHIP BETWEEN V_{50} AND EQUIVALENT CHARGE

This study was designed to determine how specific interactions between residues within the voltage-sensing domain (S1 to S4) of a K_v1-type channel, *jShak1*, affect voltage sensitivity. We focused on two features of structure that, based on previous reports, would be expected to be involved in setting the voltage sensitivity. These features were, the nature of the residue at position 227 in the S2 transmembrane segment, and the number of charges and length of the segment carrying positively charged residues in the S4 transmembrane segment with particular reference to position K294, which is known to play an important role in folding in the *D. melanogaster Shaker* channel (Papazian et al. 1995; Perozo et al. 1994). For perturbation analysis, half-activation voltages (V_{50}) and equivalent gating charge (z) were obtained using the non-inactivating N-truncated S2 and S4 single and double mutants. Gibbs free energy differences were calculated to determine the impact of the single mutations independently and their combined effect in the double mutants.

There was no significant correlation between V_{50} values and slope factors in this set of channel proteins (r^2=0.0552 for linear regression). V_{50} values reflect the transmembrane potential required to hold half of the channel protein tetramers open and half closed, whereas the slope factor is a function of the number of charges that pass through the voltage field during the conformational changes associated with channel activation. It is important to note that this translocation can be due to a combination of voltage sensor movement relative to the membrane and movement of the voltage gradient relative to the membrane. The energy required for channel opening is a function of the product of the V_{50} and the number of charges that move during the opening transition.

---

[7] A version of this chapter is being prepared for submission to the Journal of General Physiology.

Thus, the mutations that are described here cause changes in the energy required for opening through two distinct effects; changing the amount of charge translocated through the membrane potential field and changing the internal energy difference between the open and closed state.

3.1.2 S2 Mutants

As has been observed for other K_v channels, *jShak1* can be stabilized in the open state through formation of a salt bridge between an acidic residue at position 227 in S2 and positively charged residues in S4. Replacing the neutral asparagine at position 227 with aspartate, N227D, had small effects on the V_{50} of activation (15.8 mV vs 18.8 mV) and on the Boltzmann slope factor (17.86 vs 16.14) compared to the *wild-type* channel (Figure 3-1A, Table 3-1). The Gibb's free energy difference indicates that the N227D mutation stabilized the open state to a small extent ($\Delta\Delta G_{0N227D}$ = -0.21, Table 3-1). However, the number of charges that moved through the field was essentially unchanged.

The glutamate mutant (N227E) that differs from the N227D mutant by having an additional methylene group in the side-chain of amino acid 227, caused the most significant shift of all of the single mutations examined. We observed a hyperpolarizing shift (by -41 mV) of the V_{50} of activation to -22.56 +/- 1.8 (Figure 3-1A, Table 3-1). This mutation also affected the Boltzmann slope factor, increasing the steepness, by decreasing the slope factor, to 10.74 from 16.14, indicating that one more charge was translocated through the field during channel opening compared to the *wild-type*. The N227E mutation substantially stabilized the open state compared to the *wild-type* channel ($\Delta\Delta G_{0N227E}$= -2.12, Table 3-1).

3.1.3 S4 Mutants

3.1.3.1 Triplet Insertions

Although the effect of individual 3-residue S4 insertion mutations in the full-length channel were reported in an earlier study (Grigoriev et al. 1997), we have now characterized these mutations in the N-truncated forms to provide more accurate measures of V_{50} and slope factor that are comparable to the values measured for other channel mutants. While the slope values were similar to the previously published values,

the V_{50} values differed noticeably from those previously reported for the N-inactivating channel (Figure 3-1B, Table 3-1). The differences can be attributed to the errors arising from calculating conductance from peak current using an estimated E_k as compared to directly measuring conductance from tail currents, as in this study.

The QIF mutation favors the open state relative to the *wild-type* channel ($\Delta\Delta G_{0QIF}$= -0.84). This mutant translocates more charge through the field than the *wild-type* channel (2.38±0.11 vs. 1.65±0.11), in spite of the fact that the third arginine in S4 has been converted to an uncharged glutamine residue. Both the IFR and RIF insertion mutants shift the channel equilibrium towards the closed state relative to the *wild-type* channel (Figure 3-1B, Table 3-1). Interestingly, the IFR mutation increases the translocated charge to 2.26±0.10 while the RIF mutation translocates virtually the same charge (1.72±0.12) as the *wild-type* channel (Table 3-1).

3.1.3.2 S4 Single Mutants

The single amino acid mutations at K294 had similar V_{50} of activation (K294R = 49.95 +/- 2.11 mV; K294Q = 48.18+/- 1.49), and equivalent charge (K294R = 1.67 +/- 0.03; K294Q = 1.68 +/- 0.05). In both channels, channel equilibrium favored the closed state relative to the *wild-type* channel (Figure 3-1C, Table 3-1). While the K294R mutation showed similar opening kinetics to the *wild-type* channel and all other mutants, the K294Q showed distinctly slower opening kinetics (data not shown) indicating that the activation mechanism is altered but not the relative stability of the open and closed states.

The single amino acid mutation, R291Q destabilized the membrane causing increased leak current and prevented stable clamping. This mutation was generally lethal to oocytes resulting in 100% oocyte death two days post-injection. The few reliable recordings from this channel obtained from low concentration mRNA injection showed a large rightward shift in half-activation voltage (R291Q = 93.68 +/- 14.58 mV), with a very large slope factor, indicating a significant reduction in charge (1.19). The R291Q channel favored the closed state relative to the *wild-type* channel with the largest observed Gibb's free energy value (ΔG_{0R291Q}= 2.51+/-0.25, Table 3-1). In contrast, the R291K had a similar Gibb's free energy to the *wild-type* (ΔG_{0R291K}= 0.81 vs $\Delta G_{0jShak1}$= 0.71). The R291K mutant had a similar V_{50} of activation to the IFR insert (26.07+/-1.54

mV vs 29.36+/-1.19 mV). However, the R291K mutant, like the R291Q mutant, had less equivalent charge passing through the field (1.16+/-0.03 vs 1.19 =/- 0.09, Table 3-1).

3.1.3.3 S4 Double Mutants

In an attempt to assess the effect of changing the charge content in the S4 without increasing the length of this segment through triplet insertions, a series of substitution mutants were created. The R291K+K294R double mutant caused oocyte death when expressed at high concentrations, and limited recordings indicated a very rightward shifted V_{50} (80.36 +/- 4.97 mV, Table 3-1), with the smallest valence recorded (1.06 +/- 0.13) for any mutant channel. This channel favored the closed state compared to the *wild-type* channel and had a similar $\Delta\Delta G$ value to the single K294R mutant ($\Delta\Delta G_{0R291K+K294R}$=1.22 vs $\Delta\Delta G_{0K294R}$= 1.17, Figure 3-2, Table 3-1).

The double mutants K294R+R297K and K294Q+R297K both showed a rightward shifted V_{50} of activation (K294R+R297K= 38.79+/- 3.93mV; K294Q+R297K= 45.02 +/- 1.44mV, Table 3-1) that were similar to the single K294R and K294Q mutants (Figure 3-2B,C). The K294Q+R297K mutant had a similar equivalent charge to both the *wild-type* and K294Q channel (1.51+/- 0.06 vs 1.65+/-0.11 vs 1.68+/- 0.03), but not to the QIF channel (2.55 +/- 0.17, Figure 3-2). The K294R+R297K mutant translocated less charge through the electric field to open the channel compared to the K294R or RIF channel (1.23+/- 0.09 vs 1.67+/-0.05 vs 1.72=/-0.12) but this movement required a lower potential across the membrane (Figure 3-2C). Both channels favored the closed conformation compared to the *wild-type* channel. ($\Delta\Delta G_{0K294R+R297K}$= 0.34 vs $\Delta\Delta G_{0K294Q+R297K}$= 0.86, Table 3-1).

3.1.4 Double Mutant Cycle Analysis

3.1.4.1 QIF Mutations

The addition of QIF in the S4 voltage sensor of *jShak1* shifted the V_{50} of activation in a hyperpolarizing direction by approximately -21 mV relative to the *wild-type* channel and increased the translocated charge to 2.38±0.11 (Figure 3-3A, Table 3-1). When the N227D mutation was combined with the QIF addition then this double mutant, QIF-D, showed a further -17 mV leftward shift (V_{50} of -19.92 +/- 1.38 mV, Table 3-1)

while maintaining a similar slope to the QIF mutant alone (10.6 compared to 11.1) implying a charge of 2.48 compared to 2.38 (Table 3-1). The QIF-D double mutation stabilized the open state significantly more than the sum of the effects of the QIF or N227D mutations individually ($\Delta\Delta G_{0QIF\text{-}D}$ = -1.87 compared to $\Delta\Delta G_{0QIF} + \Delta\Delta G_{0N227D}$ = -1.05,Table 3-2). This large negative $\Delta\Delta G_0$ for the double mutant indicates that the N227D mutation in S2 and the QIF mutation in S4 interact synergistically to stabilize the open state.

The double mutant QIF + N227E (QIF-E) also shifted the V_{50} of activation in a hyperpolarizing direction, by approximately -23 mV, compared with the QIF mutation alone, but the translocated charge for this mutant protein was similar to that for the *wild-type* channel, 1.72±0.11 (Figure 3-3B, Table 3-1). Gibbs free energy calculations show that QIF-E favored the open state compared to the *wild-type* channel ($\Delta\Delta G_{0QIF\text{-}E}$ = -1.81). However, the sum of Gibb's energies for the single mutants ($\Delta\Delta G_{0QIF} + \Delta\Delta G_{0N227E}$ = -2.57) was greater than that observed in the double mutant ($\Delta\Delta G_{0QIF\text{-}E}$=-1.81), indicating that the combined QIF and the N227E mutations antagonized their independent abilities to stabilize the open state.

3.1.4.2 IFR Mutations

The addition of an IFR motif to the C-terminal side of K294 in the S4 voltage sensor of *jShak1* shifted the V_{50} of activation by approximately +11 mV in the depolarizing direction when compared to the *wild-type* channel, increased the translocated charge to 2.26±0.10 (Figure 3-4A, Table 3-1) and stabilized the closed state ($\Delta\Delta G_{0IFR}$ = 0.81). In contrast, the double mutant combining IFR + N227D (IFR-D) shifted the V_{50} of activation in the hyperpolarizing direction, by approximately -11 mV relative to the *wild-type* without causing a significant change in the translocated charge, thus favoring the open state of the channel ($\Delta\Delta G_{0IFR\text{-}D}$= -0.40). Importantly, this shift favoring the stabilization of the open state was opposite to the summed effect of the single mutations ($\Delta\Delta G_{0IFR} + \Delta\Delta G_{0N227D}$ = 0.6, Table 3-2), indicating a synergistic interaction between these mutation sites in S2 and S4.

The V_{50} of activation for the double mutant IFR + N227E (IFR-E) was shifted in the hyperpolarized direction by approximately -46 mV compared to the IFR mutant alone

(Figure 3-4B). This mutant had the same number of translocated charges as the *wild-type* channel (Table 3-1). The Gibbs' free energy value for the IFR-E double mutation was approximately the same as for the sum of the free-energy values for independent IFR and N227E mutations ($\Delta\Delta G_{0IFR\text{-}E}$ = -1.27 compared to $\Delta\Delta G_{0IFR}$ + $\Delta\Delta G_{0N227E}$ = -1.31, Table 3-2) indicating that the mutations in S2 and S4 acted independently in the double mutant.

3.1.4.3 RIF Mutations

The addition of the RIF motif to the N-terminal side of K294 shifted the V_{50} of activation in the depolarizing direction by +32 mV compared to the *wild-type* channel without affecting the number of translocated charges, while the double mutant RIF + N227D (RIF-D) showed a hyperpolarizing shift of -12 mV compared to the single RIF mutant (Figure 3-5A). Additionally, the slope factor was decreased when compared to the RIF single mutant (from 16 to 12.3), corresponding to an increase of the translocated charges to 2.10. Combining the RIF and N227D mutations in a single channel stabilized the closed conformation of the channel to a greater extent than the sum of the independent single mutations ($\Delta\Delta G_{0RIF\text{-}D}$ = 1.16 compared to $\Delta\Delta G_{0RIF}$ + $\Delta\Delta G_{0N227D}$ = 1.05, Table 3-2), but this difference was small.

In comparison, the RIF + N227E (RIF-E) mutant had a similar voltage sensitivity to the RIF mutant alone (app. 51 mV in both cases, Figure 3-5B) and did not appreciably change the slope factor (16.78 vs. 15.97, Table 3-1). Introduction of the N227E mutation in the RIF backbone did not have the same stabilizing interaction as was observed in the RIF-D mutant. Double mutant cycle analysis indicated that the addition of a long glutamate side-chain in S2 stabilized the closed state in the double mutant ($\Delta\Delta G_{0RIF\text{-}E}$ = 1.10 compared to $\Delta\Delta G_{0RIF}$ + $\Delta\Delta G_{0N227E}$ = -0.89, Table 3-2).

3.1.4.4 K294R Mutations

The single mutation of lysine to arginine shifted the V_{50} of activation a similar amount to the insertion of the RIF motif (49.95+/- 2.11 mV vs 50.92+/-1.04 mV) with a nearly identical equivalent charge (1.67+/-0.05 vs 1.72+/-0.12). The double mutant K294R+N227D (K294R-D) failed to shift the voltage sensitivity of half-activation (45.22+/-3.18 mV) relative to K294R but decreased the number of charges (1.30+/-0.10)

translocated through the field during activation, compared to the *wild-type* and K294R (Figure 3-6A, Table 3-1). The combination of the K294R and N227D mutations in a single channel has favourable interactions to stabilize the open channel state compared to the sum of the independent single mutations ($\Delta\Delta G_{0K294\text{-}D} = 0.63$ compared to $\Delta\Delta G_{0K294R} + \Delta\Delta G_{0N227D} = 0.96$, Table 3-2).

In comparison, the K294R + N227E (K294R-E) mutant had a leftward shifted voltage sensitivity compared to K294R alone (38.10 +/- 3.46 mV, Figure 3-6B) as well as a slightly shifted slope factor (17.34 vs. 15.78, Table 3-1). Gibbs free energy calculations showed that K294R-E favored the closed state compared to the *wild-type* channel ($\Delta\Delta G_{0K294\text{-}E} = 0.91$). The sum of Gibb's energies for the single mutants ($\Delta\Delta G_{0K294R} + \Delta\Delta G_{0N227E} = -0.95$, Table 3-2) favored the open conformation indicating that the channel conformation of K294R-E inhibits the stabilizing interaction of S4 with N227E.

3.1.4.5 K294Q Mutations

Like the K294R mutant, the K294Q mutation shifted the V_{50} of activation in the depolarizing direction by +30 mV compared to the *wild-type* channel while decreasing the slope factor (15.34 vs. 16.14). The double mutant K294Q + N227D (K294Q-D) shifted the V_{50} of activation in the hyperpolarized direction (22.81 +/- 2.63) relative to K294Q but did not affect the equivalent charge (Figure 3-7A, Table 3-1). The interactions between K294Q and N227D in the double mutant acted to stabilize the open channel conformation compared to the effects of the single mutations alone ($\Delta\Delta G_{0K294Q\text{-}D} = 0.13$ compared to $\Delta\Delta G_{0K294Q} + \Delta\Delta G_{0N227D} = 0.94$, Table 3-2).

The K294Q+N227E (K294Q-E) mutant favored the open conformation compared to the single K294Q mutant and the *wild-type* channel shifting the half activation voltage to 13.04 mV (Table 3-1). Gibbs free energy calculations show that K294Q-E favors the open state compared to the *wild-type* channel ($\Delta\Delta G_{0K294Q\text{-}E} = -0.32$). However, the sum of Gibb's energies for the single mutants ($\Delta\Delta G_{0K294Q} + \Delta\Delta G_{0N227E} = -0.96$, Table 3-2) is greater than that observed in the double mutant ($\Delta\Delta G_{0K294Q\text{-}E} = -0.32$), indicating that the protein conformation of the double mutant antagonizes the effects of the single mutants alone.

3.1.5 HOMOLOGY MODELING OF *jShak1* ON THE *RatK$_v$1.2* TEMPLATE

The open-state *jShak1* homology model and closed-state ROSETTA model give a continuous representation of the intracellular domain and transmembrane domain of the channel, minus the N-terminus and C-terminus. Loop regions missing from the original *K$_v$1.2* crystal structure have been rebuilt from loop databases to give a continuous model of the transmembrane domain, from the start of the T1-S1 linker to the end of the S6 helix. Analysis of the Ramachandran plot for the hybrid K$_v$1.2 structure shows that 99.0% of residues were in favourable regions of the plot, while the VK139 and VK140 models contained 94.0% of residues in favourable regions of the Ramachandran plot, respectively. PROCHECK and WHAT IF protein structure checks were performed on the open-state homology model and the original K$_v$1.2 crystal structure. The results showed the models were of comparable to the quality of the template crystal structure. The backbone root mean squared deviation (RMSD) between the *jShak1* open-state homology model and the K$_v$1.2 crystal structure was 0.13 Å.

The quality of the initial sequence alignment is a crucial for the development of an accurate homology model. Here, the *jShak1* sequence was robustly aligned with a set of 140 voltage-gated potassium channel sequences using MUSLCE v3.6 (Edgar 2004, 2004) and the pair-wise alignment of *jShak1* and *RatK$_v$1.2* was extracted and used as input to the SWISS MODEL program (Schwede et al. 2003), which performs an energy minimization on side-chain conformation but does not do a global conformational minimization (Figure 3-8). The structural template for modeling was derived from the published crystal structure of *RatK$_v$1.2*, PDB file 2A79 (Long et al. 2005). The S1 and S3 helices and in the K$_v$1.2 structure are not sufficiently well resolved to identify the placement of the individual residues and are represented as polyalanine and polyglycine helices in the PDB file. The interhelical linkers are not resolved in the crystal structure and so are absent from the PDB file. The placement of residues in the S1 and S3 helices was determined by comparing PredictProtein secondary structure predictions (Rost et al. 2003) on K$_v$1.2 to the corresponding structural motifs in the crystal structure. The PredictPrtotein method pinpoints the location of transmembrane helices to approximately 80% accuracy. Here, we found the predicted location of the resolved pore and voltage sensor transmembrane helices matched the experimentally determined location of each

transmembrane helix within one or two residues, lending confidence to the predicted range of the unresolved T1-S1 region and the S3 helix. Reassuringly, the predicted span S1 and S3 helices were viably placed within the resolved secondary structurale motifs and the predicted span of the unresolved transmembrane helices matched the length of the polyalanine and polyglycine chains.

The interhelical linkers were modeled purely from loop databases. In each case, a loop conformation accepted from the database was the lowest energy tertiary structure for a given sequence that matched the secondary structure predictions for that region. The modeling of these structures was informed with information from electrophysiological and perturbation studies on a number of channels. It is important to note that the $K_v1.2$ channel was crystallized in the absence of an intact membrane (i.e. equivalent to a 0 mV transmembrane potential), and so it represents the open conformation of the channel since the V_{50} for *RatK_v1.2* has been reported to be -17 mV (Scholle et al. 2000) or -35 mV (Stuhmer et al. 1989).

Figure 3-9A shows the alignment of the S3-linker-S4 portion of the two structures. The *RatK_v1.2* linker is large and flexible and includes a helical region, as predicted from the mutagenesis analysis of Mathur et al. (1997). The *jShak1* linker is short, near the length of a fully extended polypeptide, and thus should act to anchor the C-terminal end of S3 and the N-terminal end of S4 in close proximity during channel transitions between the open and closed state. The strong similarity between the S4 and L45 linker in the open state of the channel is illustrated in Figure 3-9B. When the membrane is depolarized the translocation of the S4 helix is coupled to lateral movement of the L45 segment that pulls the intracellular ends of the S5 and S6 helices apart, opening the activation gate, allowing K^+ flow through the pore. Because of this essential function, it is expected that the three mutations that insert a tripeptide into the S4 helix will likely to distort the conformation of the channel by displacing the N-terminus of the S4 helix in an outward (extracellular) direction. However, the length, shape and conformation of the S3-S4 linker has been shown to affect voltage sensitivity suggesting that modifications to the length of the S4 may independently affect voltage sensitivity regardless of charge content of the S4 (Gonzalez et al. 2001; Mathur et al. 1997).

The alignment of the S2 helices (Figure 3-10A) illustrates a clear positional equivalence of $K_v1.2$ E226 and *jShak1* N227 and of $K_v1.2$ E236 and *jShak1* E237, as shown in the alignment in Figure 1-5B. The alignment of the S4 helices shows that the alignment of the S4 helices of $K_v1.2$ and *jShak1* are consistent with the alignment shown in Figure 1-5B, with the exception that the SML tripeptide at the N-terminal end of the *jShak1* S4 is part of the helix, not part of the connecting linker (Figure 3-10B).

The model of the S2 and S4 helices (Figure 3-10C) illustrates the basis for the difference between the *wild-type* and N227E mutant of *jShak1*. In the *wild-type* channel (Figure 3-10C) the N227 residue is not in close proximity with any of the basic residues of S4, whereas in the $K_v1.2$ model (Figure 3-10C) the glutamate residue at the position homologous to E227 in *jShak1* is very close to one of the arginine residues in the S4 helix; this reaction would be expected to stabilize the open configuration of the channel and thus yield a V_{50} value considerably more hyperpolarized than that for a channel without an acidic residue in that position. In the homology model, the channel is in the open conformation, and the residues that are thought to stabilize the closed state by forming salt bridges are not in close proximity. It is clear that the process of channel closing will require rotation and translocation of all three helices to form the predicted interaction network between residues E237, D260, and positive residues in S4.

3.2 Discussion

Perturbation analysis compares the difference in free energy between the open and closed states of the *wild-type* channel with that of the mutant channels (Hong and Miller 2000; Li-Smerin et al. 2000; Monks et al. 1999; Perozo 2000). Mutations may stabilize or destabilize either of these conformations relative to the other. In double mutant cycle analysis the $\Delta\Delta G_0$ values for two single mutations are compared with the observed $\Delta\Delta G_0$ value for the double mutant channel. If the difference between the double mutant and the summed $\Delta\Delta G_0$ for the single mutants is zero ($\Delta\Delta G_{0double} - (\Delta\Delta G_{0mut1} + \Delta\Delta G_{0mut2}) = 0$) then the single mutations are acting independently in the double mutant channel (Horovitz 1996). Conversely, if there is a difference between the double mutant and the sum of the single mutations ($\Delta\Delta G_{0double} - (\Delta\Delta G_{0mut1} + \Delta\Delta G_{0mut2}) \neq 0$), then the residues at the two positions are energetically coupled, either through direct

or indirect interactions. Differences in $\Delta\Delta G_0$ provide a quantitative measure of the strength of pair-wise interactions between sites of mutations (Horovitz 1996). In our study, if the difference between $\Delta\Delta G_{0double}$ and $\Delta\Delta G_{0mut1} + \Delta\Delta G_{0mut2}$ was greater than zero then an opposing interaction between the two residues was said to stabilize the closed conformation while a difference less than zero stabilized the open conformation through a synergistic interaction.

For voltage-gated potassium channels the Gibbs' free energy difference between the opened and closed conformations is a function of both V_{50} and the equivalent number of charges that must move through the electrical field of the membrane during conformational changes in the channel, calculated from the Boltzmann slope factor (Zagotta et al. 1994). Recent studies have shown that the depth and position of the membrane electrical field can be influenced by the protein structure near the S4 voltage sensor (Chanda et al. 2005).

The channel, *jShak1*, has a number of structural elements that make it useful for probing structural interactions involved in stabilizing the open and closed conformational states of the channel. First, the S2 transmembrane helix contains a single acidic residue (E237) that is conserved in other K_v1 channels, but lacks a second acidic residue that is present in most other K_v1 channels but which is an asparagine in *jShak1* (E237/N227; Figure 1-5B). Secondly, the S4 voltage sensor is shorter by a single triplet motif than other K_v1 channels, containing 6 basic residues corresponding to R365-R380 in Shaker (Figure 1-5B). This provides a naturally occurring, physiologically functional channel with a simpler voltage sensor than most other K_v1 channels. Modeling shows that the length of the S4 is similar to other K_v1 channels, but the Ser-Met-Val (SML) amino acid sequence replaces the N-terminal basic motif. Finally, the S3-S4 linker in the *wild-type jShak1* channel is the shortest reported in any Shaker channel being composed of only 3 amino acids. All of the *jShak1* mutants, including those with the tripeptide insert, activate in response to voltage, suggesting that both the voltage sensor and linker move minimally during activation. However, changes in the S3-S4 linker's length, shape and conformation have been shown to affect voltage sensitivity in *Shaker* (Mathur et al. 1997).

This study was designed to test the effect of mutating the N227 residue to acidic residues N227E or N227D on the voltage sensitivity of the channel, and to determine how these mutations interact with the charged content of S4, by altering the charge of residues on either side of K294, as well as determining the effect the insertion of length vs. charge has on the ordered structure of the voltage sensor.

3.2.1 SINGLE MUTATIONS IN S2 STABILIZE THE OPEN STATE

In the *wild-type jShak1* channel, the neutral asparagine at position N227 in S2 is not capable of forming the stabilizing salt bridges with S4 residues R288 and R291 (homologous to R368 and R371 in *Shaker*) when the channel enters the open conformation (Silverman et al. 2003; Tiwari-Woodruff et al. 1997). Neutralization of the S2 residue in *Shaker*, E283Q, causes a rightward shift of +78 mV, while double charge reversals E283R with R371E yield the normal, more hyperpolarized shift (Papazian et al. 1995). In *jShak1*, the N227E and N227D mutations both moved V_{50} in a hyperpolarized direction, consistent with this residue forming electrostatic interactions with the basic residues in S4, although the -41 mV shift in N227E is much smaller than the shift observed in *Shaker*, implying that the short S3-S4 linker constrains channel packing in *jShak1*. The greater side-chain length of glutamate permits a much greater stabilization of the open state, as indicated by the magnitude of the shift in half activation voltage compared to that caused by the mutation to aspartate. This suggests that packing of the channel in this region is highly constrained, to the extent that the carboxylate group of the aspartate side-chain is unable to move towards the interacting positive charge(s) on the S4 helix to produce a more stable salt bridge. The equivalent charge movement during channel activation was also increased by the N227E mutation but not by the N227D mutation. Because the acidic residues in S2 have been shown not to contribute to gating charge (Seoh et al. 1996), we suggest that the longer side-chain of the glutamate mutant modifies the shape of the electric field across the membrane allowing more equivalent charge movement with the same translocation of the voltage sensor.

3.2.2 DOUBLE MUTANTS CHANGING CHARGE CONTENT IN THE S4 ARE DIFFERENT THAN THE TRIPLET INSERTION MUTANTS

The original mutagenesis studies in *jShak1*, were designed to determine whether the lack of one triplet charged motif in S4 was the basis for the depolarized V_{50} of activation (Grigoriev et al. 1997). Double mutation of S282R and M283V to replace charge content at the N terminal end of S4 produced a channel that did not differ noticeably from the *wild-type*, indicating that increasing charge on S4 alone could not recover the voltage sensitivity observed in other K_v channels (Grigoriev et al. 1997). The triplet motifs inserted into the S4 helix in *jShak1*, had diverse effects depending on the location of the insertion and the charge content of the motif. While QIF and RIF inserted into the N-terminal side of K294, and IFR inserted into the C-terminal side expressed mature functional channels, IFQ insertions on the C-terminal side failed to express (Grigoriev et al. 1997) . The secondary structure and length of the S3-S4 linker and composition and packing of the highly conserved S4-S5 linker have been shown to affect significantly both activation properties and voltage sensitivity of the channel (Gonzalez et al. 2001; Ohlenschlager et al. 2002). The structure of *jShak1*, with the short S3-S4 linker and shortened S4, constrains large-scale movements caused by length insertion. While K294 is a highly conserved residue in all K_v channels, insertions of triplet motifs to either side of this position will affect helical packing, such that K294 may be relocated. This repositioning of the lysine would modify the stabilizing electrostatic interactions with S2 and S3, presumably shifting the open to closed equilibrium.

In an attempt to isolate the charge effects on this channel, a series of mutants were created to assess conformational stability when the relative positions of basic (Arg or Lys) and neutral residues (Gln) were modified individually or in pairs in the voltage sensor at or near position K294. The R291Q and R291K+K294R mutants showed extremely rightward shifted V_{50} values (93.7 mV and 80.4 mV respectively). Both of these mutations favored the closed state, having large free energy values ($\Delta\Delta G_{0R291K+K294R} = 1.22$, $\Delta\Delta G_{0R291K} = 1.81$). Comparatively, the *jShak1* R291K mutant expressed robustly and was rightward shifted compared to *wild-type* (26.1 mV vs 18.8 mV). The V_{50} of activation for R291K (26.1 mV) was similar to the IFR triplet motif insert (29.4 mV). However, the slope factor of R291K was substantially larger than the

IFR mutant (22.4 vs 11.6), indicating that approximately half the equivalent charge moves during channel activation, compared to IFR, suggesting that the addition of the longer basic side-chain is modifying the location or shape of the transmembrane electric field.

Double S4 mutants designed to modify the conserved lysine and arginine (K294R or Q+ R297K) had half-activation voltages that were slightly leftward shifted compared to the K294R or Q single mutants alone. The free energy values for the double S4 mutants were more similar to the *wild-type* ($\Delta\Delta G_{0K294Q+R297K}$=0.86, $\Delta\Delta G_{0K294R+R297K}$= 0.34). Based on *Shaker* mutagenesis, we believe the addition of the lysine residue at the C-terminal end of the S4 acts to stabilize the open conformation of the channel by interacting preferentially with E237 (E293 in *Shaker*) and D260 (D316 in *Shaker*), forming stabilizing salt bridges during channel activation (Papazian et al. 1995).

In our experiments, the isolated charge effects were insufficient to describe the results observed with the insertion of the triplet motifs. We believe that there are confounding length effects in the S4 triplet motif mutants which act in concert with the charge effects of these mutants. The instability in channel structure, which occurs with excessive charge neutralization or localized packing changes due to side-chain interactions, affects protein structure during gating transitions (Bao et al. 1999; Miller and Aldrich 1996). The addition of length in the constrained S4 is tolerated because of the limited shifts in relative residue position, but the modifications in non-basic residue position may have a greater effect than modification of charge as demonstrated by our charge effect mutants. The *Shaker* ILT (V369I+I372L+S377T) mutation, mimicking non-basic residue content of *Shaw*, reproduced the kinetic and voltage sensitivity of *Shaw* in the *Shaker* backbone (Smith-Maxwell et al. 1998, 1998). These non-basic residues are implicated in co-operative interactions in the activation process suggesting additional mechanisms, external to salt-bridge formation, by which a channel may favor the closed state vs. the open conformation.

3.2.3 ACIDIC RESIDUE MUTATIONS AT POSITION N227 STABILIZE INTERACTIONS WITH A LONGER S4

Double mutants, containing either N227D or N227E and an S4 triplet motif insert, all caused a shift of the equilibrium towards the open state relative to the single triplet mutant. For the most leftward shifted channels QIF-E and QIF-D, the $\Delta\Delta G_0$ values were very similar suggesting that the N227E or N227D mutants had comparable interactions with the S4 basic residues. However, the sum of the single QIF and N227E mutations predicted a greater stabilization of the open state ($\Delta\Delta G_{0QIF} + \Delta G_{0N227E} = -2.85$) than was observed in the double mutant channel ($\Delta\Delta G_{0QIF\text{-}E} = -1.84$) suggesting an interfering interaction between the two mutations, while a synergistic interaction was observed for the QIF-D double mutant ($\Delta\Delta G_{0QIF} + \Delta G_{0N227D} = -1.05$ vs $\Delta\Delta G_{0QIF\text{-}D} = -1.87$). Since the difference between the QIF-D and QIF-E double mutants is that the side-chain of the acidic residue at position 227 has one more methylene group in the glutamate than in the aspartate, this may indicate that the QIF mutation can alter the conformation of the protein such that in the open state the S4 helix is closer to the S2 helix than in the *wild-type*. This would yield higher interaction energy between aspartate and the two arginine residues in the open state by moving the positive and negative charges closer together, while leading to a lower interaction energy between glutamate and the two arginine residues because of steric crowding.

In the IFR double mutants, the presence of acidic S2 residues also favored the open conformation of the channel. The IFR-E mutation, with the longer glutamate side-chain shifted the half activation voltage leftward by 38 mV as compared to the IFR-D mutation that only shifted leftward 10mV. Double mutant cycle analysis showed that in the IFR-D mutant a positive interaction between N227D and the S4 mutation acts to stabilize the open conformation of the channel ($\Delta\Delta G_{0IFR} + \Delta\Delta G_{0N227D} = 0.6$ vs $\Delta\Delta G_{0IFR\text{-}D} = -0.4$), while in the IFR-E mutant the stabilization of the open state comes from two independent non-synergistic additive contributions from the IFR and N227E mutations ($\Delta\Delta G_{0IFR} + \Delta\Delta G_{0N227E} = -1.31$ vs $\Delta\Delta G_{0IFR\text{-}E} = -1.27$) (Horovitz 1996).

While the RIF insert in S4 shifted the closed to open equilibrium to favor the closed state, the double mutants with the acidic residue shifted the energetics slightly towards the open state compared to the RIF single mutant alone ($\Delta G_{0RIF} = 1.94$, $\Delta G_{0RIF\text{-}D}$

= 1.87, $\Delta G_{0RIF\text{-}E}$ =1.80). The $\Delta\Delta G_0$ values for both double mutants are also very similar ($\Delta\Delta G_{0RIF\text{-}E}$=1.10, $\Delta\Delta G_{0RIF\text{-}D}$ = 1.16), however the energetics of interaction with the acidic S2 residues are different. In RIF-E, the longer side-chain of N227E has a disruptive interaction with the additional argenine, while in RIF-D mutants the effects of N227D and RIF appear to be non-synergistic, acting in an additive fashion only. Because the RIF and QIF insertions both occur on the N-terminal side of K294, the protein structure in this region, and the interactions with S2 residues should be similar, particularly as it is the first 2 argenines which form the electrostatic interactions. The QIF-E and RIF-E mutants showed similar interference between the long glutamate side-chain and the S4 voltage sensor. However, the QIF-D and RIF-D mutants showed very different interactions, where the QIF containing S4 had a synergistic stabilizing interaction with the acidic N227D while the RIF mutant had independent additive interaction. This suggests that protein packing caused by the addition of a basic residue is different from that of a neutral residue and that the interactions and packing in *jShak1* favor a less charged voltage sensor.

The closed conformation of the *Shaker* channel is the more stable state at membrane potentials below V_{50}, so mutations that shift the equilibrium towards the open state can be either destabilizing the closed state or stabilizing the open state (Hackos et al. 2002; Yifrach and MacKinnon 2002). If the insertion of the triplet QIF motif to the N-terminal side of K294 (K374 *Shaker*) in *jShak1* displaces the surrounding residues that stabilize the closed state by forming electrostatic interactions with E237 (E293 *Shaker*) in S2 and D260 (D316 *Shaker*) in S3, the neutral glutamine would replace the basic lysine at position 294. This replacement would prevent salt bridge formation between the basic K294 residue in S4 and the acidic E237 and D260 residues (Papazian et al. 1995; Tiwari-Woodruff et al. 1997). In *Shaker* the direct substitution of glutamine for lysine (K374Q) fails to form an active channel and remains in the endoplasmic reticulum (Papazian et al. 1991), but double mutants K374Q with E293Q shifts the V_{50} of the channel in a hyperpolarized direction, presumably by destabilizing the closed state conformation (Papazian et al. 1995). To test this hypothesis, the K294Q mutation was designed to remove the stabilizing interactions between the highly conserved lysine and the acidic residues in S2 and S3. However, this channel had a rightward shifted half-activation

voltage with slow activation kinetics, clearly favoring the closed conformation of the channel. This is the first functional single mutant channel containing a charge neutralization at this highly conserved position. Because the K374Q mutant in *Shaker* failed to export from the endoplasmic reticulum, presumably due to improper folding, we believe that protein packing in the mature *jShak1* channel does not represent the best packing for comparison to the unmodified channel.

3.2.4 ACIDIC MUTATIONS AT POSITION N227 STABILIZE PROTEIN STRUCTURE IN SINGLE K294 MUTANTS

Mutation of the highly conserved lysine K294 (K374 in *Shaker*) to either the basic residue, arginine (K294R), or the neutral residue, glutamine (K294Q), substantially shifted the V_{50} of activation in the depolarized direction, by +30 mV. In *Shaker* the K374Q mutant channels remain in the endoplasmic reticulum, failing to express functional channels in the cell membrane (Papazian et al. 1995; Papazian et al. 1991; Perozo et al. 1994), however, double mutants containing the K374Q mutation with E293Q or D316N mutations express functional channels with leftward shifted half-activation voltages (Papazian et al. 1995). The functional expression of the K294Q *jShak1* mutant suggests that the additional structural constraint by the short S3-S4 linker aids functional protein packing during synthesis.

The most favourable energetic interactions for both K294R and K294Q were observed with the N227D containing S2 mutations. Despite the depolarized V_{50} activation value (45.2mV) for the K294R-D double mutant, double mutant cycle analysis showed that a stabilizing synergistic interaction is occurring between S2 and S4 ($\Delta\Delta G_{0K294R} + \Delta\Delta G_{0N227D} = 0.96$ compared to $\Delta G_{0K294R\text{-}D} = 0.63$). Similarly, the K294Q-D double mutant has stabilizing S2 and S4 interactions ($\Delta\Delta G_{0K294Q} + \Delta\Delta G_{0N227D} = 0.94$ compared to $\Delta G_{0K294Q\text{-}D} = 0.13$). In the K294Q-D double mutant, this favourable interaction was reflected in the -25 mV shift in half activation voltage relative to the K294 single mutant channel.

The N227E containing K294R double mutant had a slight (~11 mV) leftward shift in half-activation voltage relative to the K294R single mutant. However, the $\Delta\Delta G0$ value ($\Delta\Delta G_{0K294R\text{-}E} = 0.91$) suggests that the double mutant favors the closed state compared to

the *wild-type*. Double mutant cycle analysis suggests the addition of N227E mutation causes an interfering interaction ($\Delta\Delta G_{0K294R} + \Delta\Delta G_{0N227E} = -0.95$ compared to $\Delta\Delta G_{0K294R\text{-}E} = 0.91$) similar to that observed in the RIF-E mutant ($\Delta\Delta G_{0RIF\text{-}E} = 1.10$). The K294Q-E double mutant had a noticeable leftward shift in V_{50} (13.04 mV) compared to the K294Q mutant (48.2 mV). The $\Delta\Delta G_{0K294Q\text{-}E}$ favors the open conformation (-0.32) compared to the *wild-type* channel. Like the QIF-E mutant the K294Q-E double mutant cycle analyis shows an interfering interaction between S2 and S4 because of steric crowding related to the longer side-chain of glutamate ($\Delta\Delta G_{0K294Q} + \Delta\Delta G_{0N227E} = -0.96$ vs $\Delta\Delta G_{0K294Q\text{-}E} = -0.32$). However, the negative $\Delta\Delta G_0$ value indicates that the presence of K294Q and N227E in the same channel still stabilizes the protein more than the *wild-type*, to the same extent as the N227E mutant alone does.

3.2.5 Homology Modeling

In the absence of high-resolution structures of the ion channel of interest, homology models provide a three-dimensional map of a protein. They are structural predictors, which are highly dependant on the accuracy of the underlying sequence alignment and as such, require progressive refinement as new results become available. In the case of the *jShak1* open-state homology model, secondary structure predictions and loop database searches were used to bridge the gaps in the $K_v1.2$ template structure, allowing the development of a more complete homology model. A homology model, like a crystal structure, represents a single, state-dependant snapshot of *jShak1*. While the open-state *jShak1* model described here is a true homology model, no physiologically viable crystal structure exists for the closed-state of a potassium channel with voltage sensors attached. Here we have threaded the *jShak1* primary sequence onto a predicted ROSETTA model of the closed state to give a closed state conformation of the *jShak1* pore and voltage sensors. While ROSETTA models give tremendous insights into unresolved structures, ROSETTA is a structure-prediction tool, not a crystal structure. Homology and ROSETTA models, when interpreted in conjunction with experimental results, are enormously powerful visualization tools which can help provide a general overview of the mechanism of channel gating (Yarov-Yarovoy et al. 2006).

3.2.6 CONCLUSIONS

With the crystallization of *KvAP* and *RatK$_v$1.2* new models of channel gating and resulting conformational changes have been identified (Chanda et al. 2005; Jiang et al. 2002; Jiang et al. 2003; Jiang et al. 2003; Long et al. 2005; Ruta et al. 2005; Ruta and MacKinnon 2004). In this context, homology modeling provides a greater understanding of residue interactions, particularly when a channel like *jShak1* is used. By utilizing this natural structurally constrained channel, it is possible to determine the effects that varying mutations have on stabilizing the different conformational changes observed during channel activation. Our results suggest that the mutations of S2 and S4 have distinct effects on protein packing and interactions in this channel (Figure 3-11). In this study we have shown that the open state is stabilized by the S2 acidic mutations, N227E and N227D, and that in a longer S4 backbone, the additional methylene group in N227E causes steric interference, while a synergistic stabilization of the open state is achieved by the shorter N227D mutation (Figure 3-11). We have also shown that the modification of charge content in S4 fails to produce the same results as the introduction of length and/or charge in the triplet motif insertions. This indicates that the relative positions of non-basic residues and the interactions between charged residues have an effect on protein packing around the S4 that effect voltage sensitivity in this channel.

Table 3-1: Summarized Fit Parameters for *jShak1* S2/S4 Mutants including Gibb's Free Energy Calculations

Channel	n	V_{50}		Boltzmann Slope		z		ΔG_0		$\Delta\Delta G_0$
Jsk1wt	10	18.80	+/- 1.14	16.14	+/- 0.82	1.65	+/- 0.11	0.71	+/- 0.08	
N227D	14	15.80	+/- 3.19	17.86	+/- 1.07	1.52	+/- 0.11	0.50	+/- 0.09	-0.21
N227E	8	-22.56	+/- 1.80	10.74	+/- 0.85	2.55	+/- 0.17	-1.41	+/- 0.17	-2.12
QIF	7	-2.47	+/- 1.20	11.11	+/- 0.57	2.38	+/- 0.11	-0.13	+/- 0.07	-0.84
QIF-D	10	-19.92	+/- 1.38	10.69	+/- 0.54	2.48	+/- 0.12	-1.16	+/- 0.12	-1.87
QIF-E	6	-25.89	+/- 2.72	15.61	+/- 0.92	1.72	+/- 0.11	-1.10	+/- 0.19	-1.81
IFR	8	29.36	+/- 1.19	11.60	+/- 0.45	2.26	+/- 0.10	1.52	+/- 0.07	0.81
IFR-D	9	8.24	+/- 3.99	15.50	+/- 0.99	1.74	+/- 0.11	0.30	+/- 0.15	-0.40
IFR-E	8	-17.15	+/- 2.05	18.10	+/- 0.78	1.45	+/- 0.06	-0.57	+/- 0.06	-1.27
RIF	9	50.92	+/- 1.04	15.97	+/- 1.23	1.72	+/- 0.12	1.94	+/- 0.14	1.23
RIF-D	5	38.49	+/- 0.85	12.29	+/- 0.30	2.10	+/- 0.05	1.87	+/- 0.08	1.16
RIF-E	8	51.18	+/- 2.99	16.78	+/- 0.54	1.55	+/- 0.05	1.80	+/- 0.08	1.10
K294R	7	49.95	+/- 2.11	15.78	+/- 0.53	1.67	+/- 0.05	1.88	+/- 0.10	1.17
K294R-D	13	45.22	+/- 3.18	21.11	+/- 1.41	1.30	+/- 0.10	1.34	+/- 0.15	0.63
K294R-E	21	38.10	+/- 3.46	17.34	+/- 0.73	1.54	+/- 0.07	1.62	+/- 0.13	0.91
K294Q*	4	48.18	+/- 1.49	15.34	+/- 0.28	1.68	+/- 0.03	1.86	+/- 0.10	1.16
K294Q-D	5	22.81	+/- 2.63	15.76	+/- 1.20	1.68	+/- 0.15	0.85	+/- 0.05	0.14
K294Q-E*	2	13.04	+/- 5.35	19.01	+/- 1.99	1.38	+/- 0.14	0.39	+/- 0.13	-0.32
R291Q*	2	93.68	+/- 14.58	21.81	+/- 1.65	1.19	+/- 0.09	2.51	+/- 0.25	1.81
R291K	11	26.07	+/- 1.54	22.36	+/- 0.63	1.16	+/- 0.03	0.81	+/- 0.10	0.10
R291K+K294R*	3	80.36	+/- 4.97	25.65	+/- 3.64	1.06	+/- 0.13	1.92	+/- 0.16	1.22
K294R+R297K	8	38.79	+/- 3.93	21.66	+/- 1.50	1.23	+/- 0.09	1.05	+/- 0.08	0.34
K294Q+R297K	7	45.02	+/- 1.44	17.17	+/- 0.71	1.51	+/- 0.06	1.57	+/- 0.10	0.86

* expressed mutation disrupts the cell membrane causing an unsteady voltage-clamp and is ultimately lethal

Table 3-2: Double Mutant Cycle Analysis: $\Delta\Delta G_0$ for single mutations and double mutations in *jShak1*

S2 mutants / *S4 mutants*	$\Delta\Delta G_0$	*N227E* Single Mutant	*N227E* Sum Single Mutations	*N227E* Double Mutant	*N227E* Dif*	*N227D* Single Mutant	*N227D* Sum Single Mutations	*N227D* Double Mutant	*N227D* Dif*
		-2.12				-0.21			
QIF	-0.84		-2.95	-1.81	1.14		-1.05	-1.87	-0.82
IFR	0.81		-1.31	-1.27	0.04		0.6	-0.40	-1
RIF	1.23		-0.89	1.10	1.99		1.05	1.16	0.11
K294R	1.17		-0.95	0.91	1.86		0.96	0.63	-0.33
K294Q	1.16		-0.96	-0.32	0.63		0.94	0.13	-0.81

* Difference was calculated: Dif = $\Delta\Delta G_{0\text{double}} - (\Delta\Delta G_{0\text{single S2}} + \Delta\Delta G_{0\text{single S4}})$

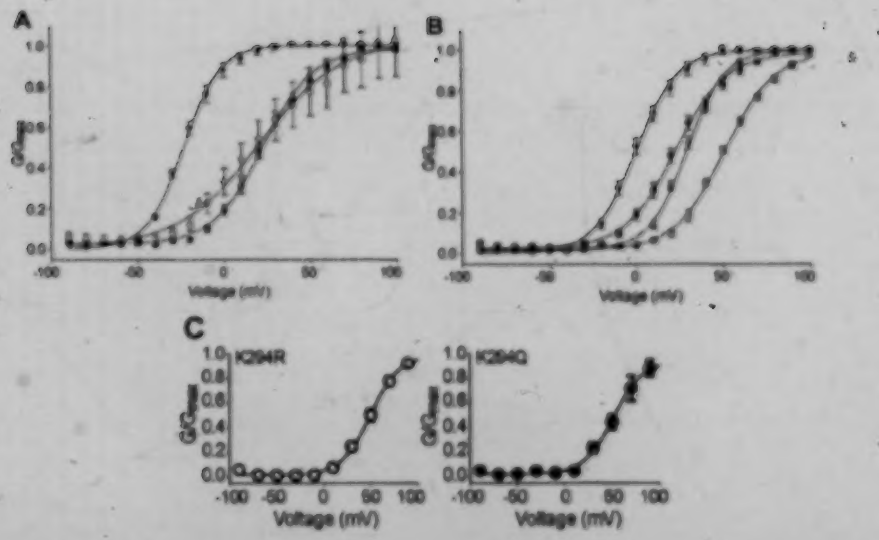

Figure 3-1 Single mutations in the S2 and S4 helices modify steady-state properties of the channel.

A. The steady-state activation curve for *jShak1* S2 mutants reveals that the N227E (inverted triangles) channels are activated at far more hyperpolarized potentials than N227D (open circles) and wild-type channels (filled circles). In this analysis the amplitudes of the tail currents were measured 1-3 ms after the disappearance of the stimulus artefact and then normalized to the maximal tail current. The solid curve represents the fit to a Boltzmann function giving V_{50} and slope parameters (b) for each channel (error bars = S.E.M); wild-type (filled circles) V_{50} = 18.8 +/- 1.1 mV, b = 16.1 +/- 0.8 mV/e (n=10), N227D (open circles) V_{50} = 15.8 +/- 3.2 mV, b = 17.9 +/- 1.1 mV/e (n=14), N227E (inverted triangles) V_{50} = -22.6 +/- 1.8 mV, b = 10.7 +/- 0.85 mV/e (n=8).

B. The steady-state activation curve for *jShak1* S4 insertion mutants reveals that the insertion of the QIF motif to the N-terminal side of K294 shifts the activation curve in the hyperpolarized direction while the IFR and RIF insertions shift the activation curve in the depolarized direction compared to wild-type channels. The solid curve represents the fit to a Boltzmann function giving V_{50} and slope parameters (b) for each channel (error bars = S.E.M); wild-type (filled circles) V_{50} = 18.8 +/- 1.1 mV, b = 16.1 +/- 0.8 mV/e (n=10), QIF (inverted triangles) V_{50} = -2.5 +/- 1.2 mV, b = 11.1 +/- 0.6 mV/e (n=7), IFR (open triangles) V_{50} = 29.4 +/- 1.2 mV, b = 11.6 +/- 0.5 mV/e (n=8), RIF (open circles) V_{50} = 50.9 +/- 1.0 mV, b = 16.0 +/- 1.2 mV/e (n=9).

C. The steady-state activation curves for the *jShak1* S4 single amino acid mutants K294R and K294Q revealing that the mutation of the highly conserved lysine shifts the activation curve in a depolarized direction. Measurements were performed as in A. The solid curve represents the fit to a Boltzmann function giving V_{50} and slope parameters (b) for each channel (error bars = S.E.M). Curves are separate graphs to show the striking similarity in behavior of K294R and K294Q; K294R (open circles) V_{50} = 49.9 +/- 2.1 mV, b = 15.8 +/- 0.5 mV/e (n=7), K294Q (filled circles) V50= 48.2 +/- 1.5, b = 15.3 +/- 0.3 mV/e (n=4).

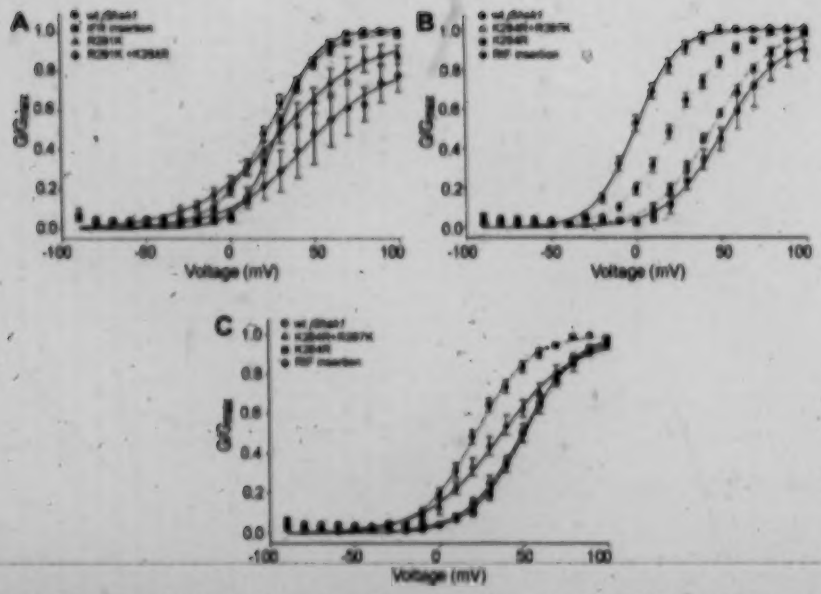

Figure 3-2: Double mutants changing charge content in the S4 are different than the triplet insertion mutants.

A. The steady-state activation curve for the R291K+K294R double mutant is extremely shifted in the depolarized direction with the shallowest slope of all mutants. R291K alone has a similar half-activation voltage as the IFR mutant, but has a much shallower slope. The solid curve represents the fit to a Boltzmann function giving V_{50} and slope parameters (b) for each channel (error bars = S.E.M); wild-type (red circles) V_{50} = 18.8 +/- 1.1 mV, b = 16.1 +/- 0.8 mV/e (n=10), IFR (green squares) V_{50} = 29.4 +/- 1.2 mV, b = 11.6 +/- 0.5 mV/e (n=8), R291K (grey triangles) V_{50} = 26.1 +/- 1.5 mV, b = 22.4 +/- 0.6 mV/e (n=11), R291K+K294R (emerald diamonds) V_{50} = 80.4 +/- 4.9 mV, b = 25.6 +/- 3.6 mV/e (n=3).

B. The steady-state activation curve for the K294Q+R297K double mutant is similar to the rightward shifted K294Q single mutant and substantially rightward shifted compared to both QIF and wild-type channels. The solid curve represents the fit to a Boltzmann function giving V_{50} and slope parameters (b) for each channel (error bars = S.E.M); wild-type (red circles) V_{50} = 18.8 +/- 1.1 mV, b = 16.1 +/- 0.8 mV/e (n=10), K294Q (pale green squares) V_{50} = 48.2 +/- 1.5 mV, b = 15.3 +/- .3 mV/e (n=4), K294Q+R297K (pink triangles) V_{50} = 45.0 +/- 1.4 mV, b = 17.2 +/- 0.7 mV/e (n=7), QIF (navy diamonds) V_{50} = -2.5 +/- 1.2 mV, b = 11.1 +/- 0.6 mV/e (n=7).

C. The steady-state activation curve for the K294R+R297K double mutant is slightly rightward shifted compared to the K294R and RIF mutant channels, but has a much shallower slope. The solid curve represents the fit to a Boltzmann function giving V_{50} and slope parameters (b) for each channel (error bars = S.E.M); wild-type (red circles) V_{50} = 18.8 +/- 1.1 mV, b = 16.1 +/- 0.8 mV/e (n=10), K294R (dark green squares) V_{50} = 49.9 +/- 2.1 mV, b = 15.8 +/- 0.5 mV/e (n=7), K294R+R297K (purple triangles) V_{50} = 38.8 +/- 3.9 mV, b = 21.7 +/- 1.5 mV/e (n=8), RIF (blue diamonds) V_{50} = 50.9 +/- 1.0 mV, b = 16.0 +/- 1.2 mV/e (n=9).

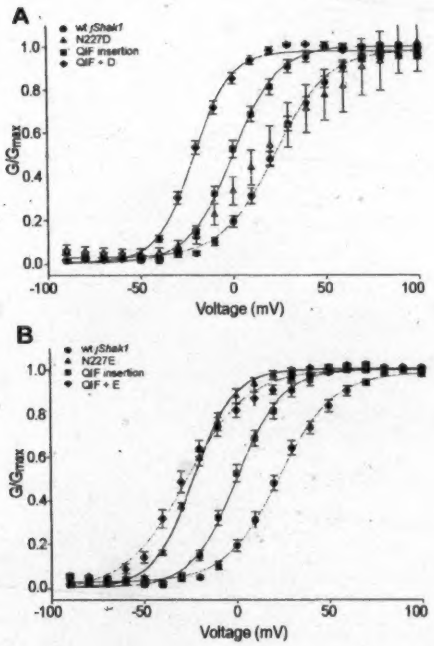

Figure 3-3: The closed to open equilibrium is shifted towards the open state in the QIF double mutants.

A. The steady-state activation curve for the QIF-D double mutant is shifted in a hyperpolarized direction compared to the single mutant and wild-type channels. The solid curve represents the fit to a Boltzmann function giving V_{50} and slope parameters (b) for each channel (error bars = S.E.M); wild-type (red circles) V_{50} = 18.8 +/- 1.1 mV, b = 16.1 +/- 0.8 mV/e (n=10), QIF (green squares) V_{50} = -2.5 +/- 1.2 mV, b = 11.1 +/- 0.6 mV/e (n=7), N227D (orange triangles) V_{50} = 15.8 +/- 3.2 mV, b = 17.9 +/- 1.1 mV/e (n=14), QIF-D (aqua diamonds) V_{50} = -19.9 +/- 1.4 mV, b = 10.8 +/- 0.5 mV/e (n=10).

B. The steady-state activation curve for the QIF-E double mutant is shifted in a hyperpolarized direction compared to the single mutant and wild-type channels but has a shallower slope than the QIF mutant alone. The solid curve represents the fit to a Boltzmann function giving V_{50} and slope parameters (b) for each channel (error bars = S.E.M); wild-type (red circles) V_{50} = 18.8 +/- 1.1 mV, b = 16.1 +/- 0.8 mV/e (n=10), QIF (green squares) V_{50} = -2.5 +/- 1.2 mV, b = 11.1 +/- 0.6 mV/e (n=7), N227E (blue triangles) V_{50} = -22.6 +/- 1.8 mV, b = 10.7 +/- 0.85 mV/e (n=8). QIF-E (pink diamonds) V_{50} = -25.9 +/- 2.7 mV, b = 15.6 +/- 0.9 mV/e (n=6).

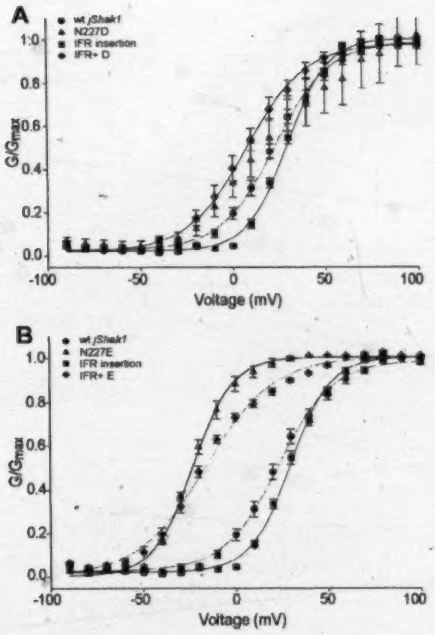

Figure 3-4: The addition of an acidic residue in the IFR mutant shifts the closed to open equilibrium to favor the open state.

A. The steady-state activation curve for the IFR-D double mutant is shifted in a hyperpolarized direction compared to the single mutant and wild-type channels. The solid curve represents the fit to a Boltzmann function giving V_{50} and slope parameters (b) for each channel (error bars = S.E.M); wild-type (red circles) V_{50} = 18.8 +/- 1.1 mV, b = 16.1 +/- 0.8 mV/e (n=10), IFR (green squares) V_{50} = 29.4 +/- 1.2 mV, b = 11.6 +/- 0.5 mV/e (n=8), N227D (orange triangles) V_{50} = 15.8 +/- 3.2 mV, b = 17.9 +/- 1.1 mV/e (n=14), IFR-D (aqua diamonds) V_{50} = 8.2 +/- 4.0 mV, b = 15.5 +/- 1.0 mV/e (n=9).

B. The steady-state activation curve for the IFR-E double mutant is shifted in a hyperpolarized similar to that of the N227E single mutant, but has a much shallower slope. The solid curve represents the fit to a Boltzmann function giving V_{50} and slope parameters (b) for each channel (error bars = S.E.M); wild-type (red circles) V_{50} = 18.8 +/- 1.1 mV, b = 16.1 +/- 0.8 mV/e (n=10), IFR (green squares) V_{50} = 29.4 +/- 1.2 mV, b = 11.6 +/- 0.5 mV/e (n=8), N227E (blue triangles) V_{50} = -22.6 +/- 1.8 mV, b = 10.7 +/- 0.85 mV/e (n=8), IFR-E (pink diamonds) V_{50} = -17.5 +/- 2.0 mV, b = 18.1 +/- 0.8 mV/e (n=8).

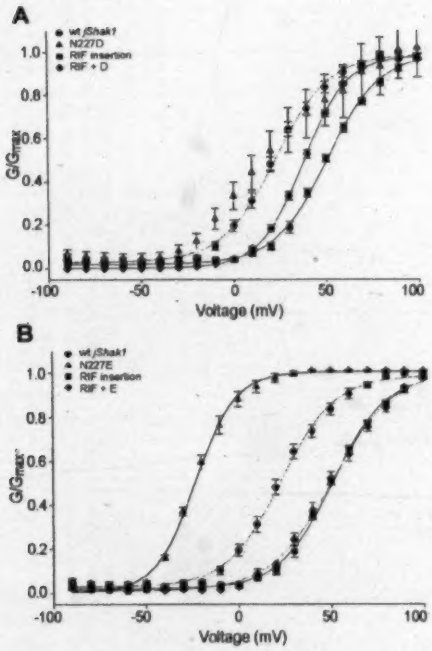

Figure 3-5: The closed to open equilibrium of all RIF containing mutants is shifted to the closed conformation.

A. The steady-state activation curve for the RIF-D double mutant is shifted in a depolarized direction and has a much steeper slope compared to the N227D and wild-type channels. The solid curve represents the fit to a Boltzmann function giving V_{50} and slope parameters (b) for each channel (error bars = S.E.M); wild-type (red circles) V_{50} = 18.8 +/- 1.1 mV, b = 16.1 +/- 0.8 mV/e (n=10), RIF (green squares) V_{50} = 50.9 +/- 1.0 mV, b = 16.0 +/- 1.2 mV/e (n=9), N227D (orange triangles) V_{50} = 15.8 +/- 3.2 mV, b = 17.9 +/- 1.1 mV/e (n=14), RIF-D (aqua diamonds) V_{50} = 38.5 +/- 0.9 mV, b = 12.3 +/- 0.3 mV/e (n=5).

B. The steady-state activation curve for the RIF-E double mutant is shifted in a depolarized direction opposite to that of the N227E single mutant, and has a much shallower slope. The solid curve represents the fit to a Boltzmann function giving V_{50} and slope parameters (b) for each channel (error bars = S.E.M); wild-type (red circles) V_{50} = 18.8 +/- 1.1 mV, b = 16.1 +/- 0.8 mV/e (n=10), RIF (green squares) V_{50} = 50.9 +/- 1.0 mV, b = 16.0 +/- 1.2 mV/e (n=9), N227E (blue triangles) V_{50} = -22.6 +/- 1.8 mV, b = 10.7 +/- 0.85 mV/e (n=8), RIF-E (pink diamonds) V_{50} = 51.8 +/- 3.0 mV, b = 16.8 +/- 0.5 mV/e (n=8).

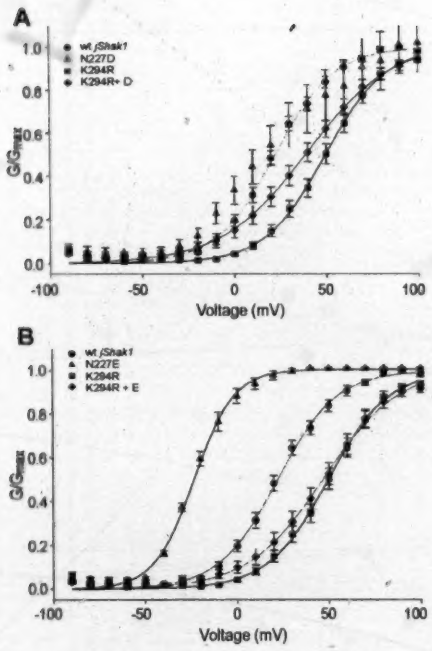

Figure 3-6: The addition of an acidic residue in S2 forms a favorable electrostatic interaction in the K294R mutant channel.

A. The steady-state activation curve for the K294R-D double mutant has similar voltage sensitivity to the K294R single mutant, but with a much shallower slope than either compared to the N227D and wild-type channels. The solid curve represents the fit to a Boltzmann function giving V_{50} and slope parameters (b) for each channel (error bars = S.E.M); wild-type (red circles) V_{50} = 18.8 +/- 1.1 mV, b = 16.1 +/- 0.8 mV/e (n=10), K294R (green squares) V_{50} = 49.9 +/- 2.1 mV, b = 15.8 +/- 0.5 mV/e (n=7), N227D (orange triangles) V_{50} = 15.8 +/- 3.2 mV, b = 17.9 +/- 1.1 mV/e (n=14), K294R-D (aqua diamonds) V_{50} = 45.2 +/- 3.2 mV, b = 21.1 +/- 1.4 mV/e (n=13).

B. The steady-state activation curve for the K294R-E double mutant is shifted leftward compared to the single K294R mutation alone, but still favors the closed conformation. The solid curve represents the fit to a Boltzmann function giving V_{50} and slope parameters (b) for each channel (error bars = S.E.M); wild-type (red circles) V_{50} = 18.8 +/- 1.1 mV, b = 16.1 +/- 0.8 mV/e (n=10), K294R (green squares) V_{50} = 49.9 +/- 2.1 mV, b = 15.8 +/- 0.5 mV/e (n=7), N227E (blue triangles) V_{50} = -22.6 +/- 1.8 mV, b = 10.7 +/- 0.85 mV/e (n=8), K294R-E (pink diamonds) V_{50} = 38.1 +/- 3.5 mV, b = 17.3 +/- 0.7 mV/e (n=21).

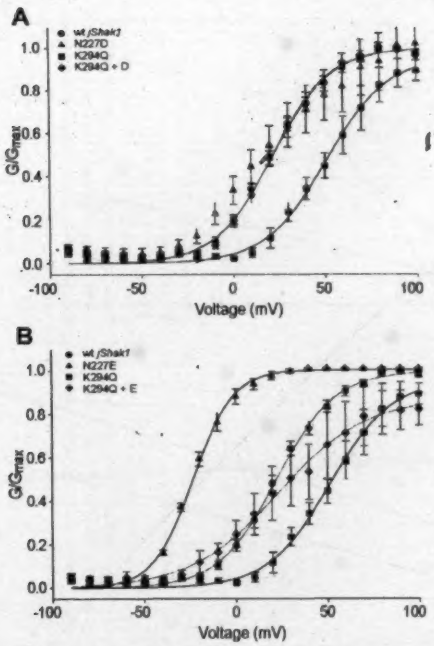

Figure 3-7: The closed to open equilibrium is shifted towards the open conformation in K294Q mutant channels with an acidic residue in S2.

A. The steady-state activation curve for the K294Q-D double mutant is shifted in a hyperpolarized direction compared to K294Q alone, with a steeper slope compared to the N227D and wild-type channels. The solid curve represents the fit to a Boltzmann function giving V_{50} and slope parameters (b) for each channel (error bars = S.E.M); wild-type (red circles) V_{50} = 18.8 +/- 1.1 mV, b = 16.1 +/- 0.8 mV/e (n=10), K294Q (green squares) V_{50} = 48.2 +/- 1.5 mV, b = 15.3 +/- .3 mV/e (n=4), N227D (orange triangles) V_{50} = 15.8 +/- 3.2 mV, b = 17.9 +/- 1.1 mV/e (n=14), K294Q-D (aqua diamonds) V_{50} = 22.8 +/- 2.6 mV, b = 15.8 +/- 1.2 mV/e (n=5).

B. The steady-state activation curve for the K294Q-E double mutant is shifted in a hyperpolarized direction relative to the wild-type or the K294Q single mutant, but has a shallower slope. The solid curve represents the fit to a Boltzmann function giving V_{50} and slope parameters (b) for each channel (error bars = S.E.M); wild-type (red circles) V_{50} = 18.8 +/- 1.1 mV, b = 16.1 +/- 0.8 mV/e (n=10), K294Q (green squares) V_{50} = 48.2 +/- 1.5 mV, b = 15.3 +/- .3 mV/e (n=4), N227E (blue triangles) V_{50} = -22.6 +/- 1.8 mV, b = 10.7 +/- 0.85 mV/e (n=8), K294Q-E (pink diamonds) V_{50} = 13.0 +/- 5.4 mV, b = 19.0 +/- 1.9 mV/e (n=2).

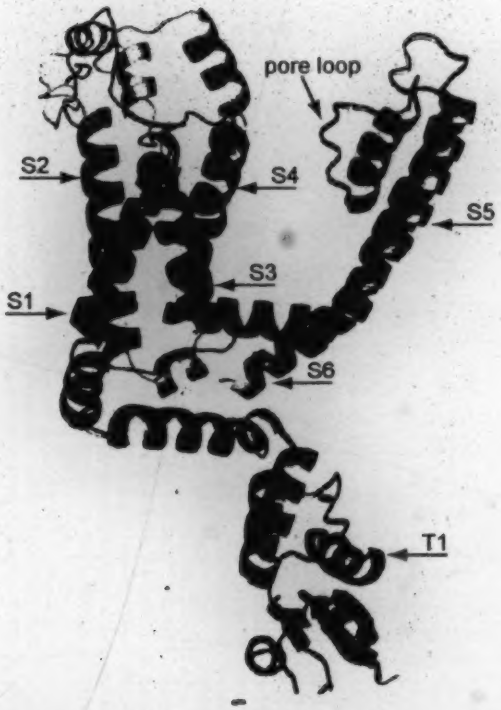

Figure 3-8: Homology model of *jShak1* based on the structure of *RatK$_v$1.2*.
Full alpha subunit complete with T1 domain and modeled loops *RatK$_v$1.2* (orange) and *jShak1* (blue). The placement of residues in the S1 and S3 helices was determined by comparing PredictProtein secondary structure predictions on K$_v$1.2 to the corresponding structural motifs in the crystal structure. The PredictProtein method pinpoints the location transmembrane helices to approximately 80% accuracy. The interhelical linkers were modeled purely from loop databases where the conformation selected gave the lowest energy tertiary structure for a given sequence that matched the secondary structure predictions for that region. The modeling of these structures was informed with information from electrophysiological and perturbation studies on a number of channels.

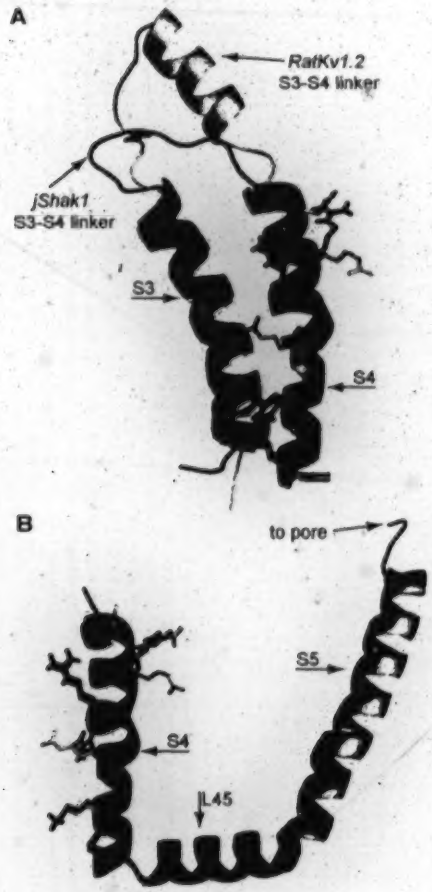

Figure 3-9: Homology models of the structural constraints in *jShak1* based on the structure of *RatK$_v$1.2*.

A. Overlay of S3 and S4 showing the extremely short 3 amino acid S3-S4 linker which anchors the C-terminal end of S3 and N-terminal end of S4 in *jShak1* in close proximity during gating transitions. The homology model of *jShak1* (blue) is placed over the model of *RatK$_v$1.2* (orange). The basic residues in S4 are illustrated as side-chain sticks, and transmembrane helices are labelled.

B. Overlay of the highly conserved S4-S5 linker (L45) that is conserved in both *RatK$_v$1.2* (orange) and *jShak1* (blue). The L45 couples the translocation of the voltage sensor to the opening of activation gate. This conserved mechanism suggests that length insertions in the short S4 of *jShak1* should move residues extracellularly rather than modify the amphipathic packing of L45.

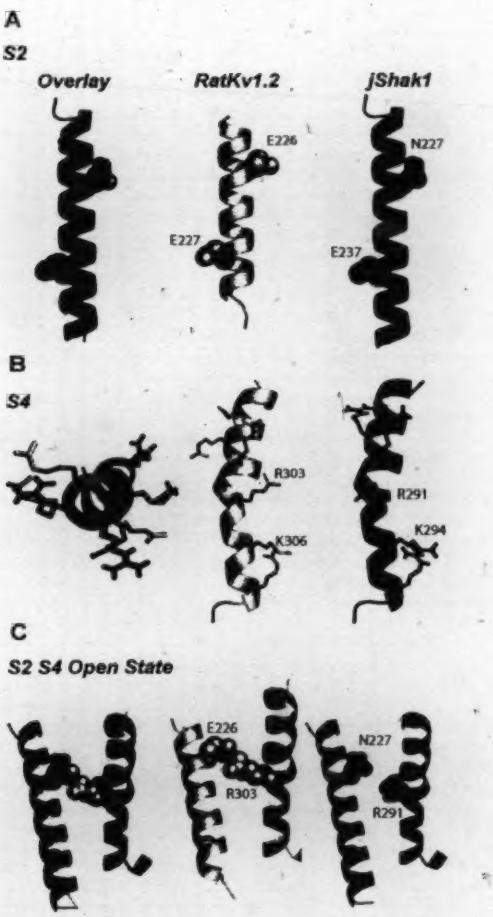

Figure 3-10: Structural elements in the S2 and S4 of *jShak1* prevent favourable electrostatic interactions in the open state.

A. A structural overlay of S2 transmembrane domains of *RatK$_v$1.2* (orange) and *jShak1* (blue) showing the homologous positions of E226 to N227 and E236 to E237 (respectively). The short non-charged side-chain of N227 prevents favorable electrostatic interactions with S4 residues in the open conformation that can be recovered with mutations to either glutamate (N227E) or aspartate (N227D).

B. A structural overlay of S4 showing relative location of the S4 basic residue side-chains in *RatK$_v$1.2* (orange) and the shortened S4 of *jShak1* (blue). The periodicity and side - chain location of the arginine residues between the channels is preserved the C-terminal end of the helix. Specifically, positions K306/R309 in *RatK$_v$1.2* overlay K274/R377 in *jShak1*.

C. Homology model of the interactions between S2 and S4 residues in the open conformation of the channel illustrating the favourable salt bridge interactions between E226 and R303. The N227 residue in *jShak1* (blue) does not form a salt bridge with R291, while E226 shows a strong interaction with R303 in *RatK$_v$1.2* (orange).

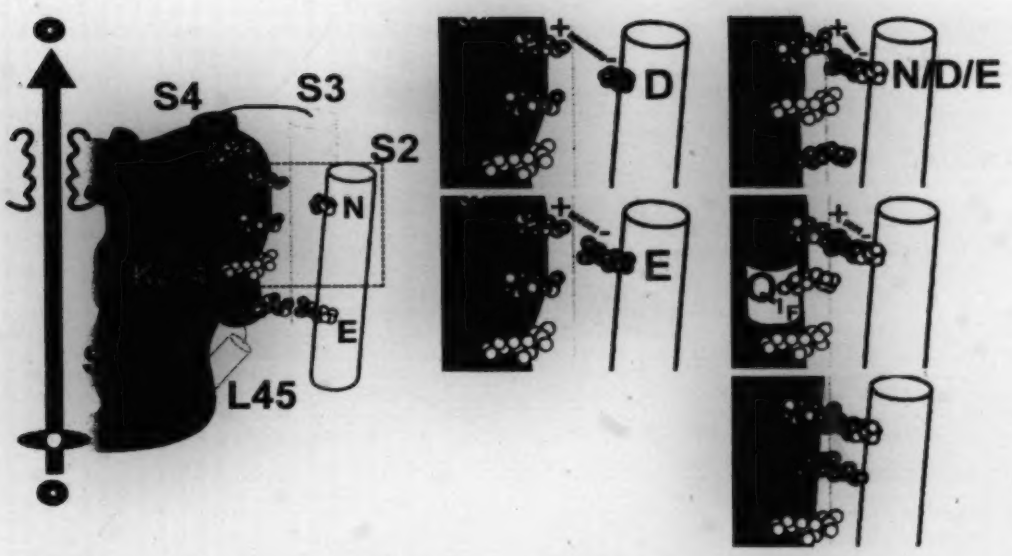

Figure 3-11: Cartoon of interactions occurring between the S2 and S4 helices in the open state in the *jShak1* mutant channels as determined from Double Mutant Cycle Analysis.

The cartoon of the *wild-type jShak1* channel shows the proximity of the S2 (yellow) and S4 (blue) helices in the open conformation of the channel. The basic residue motif (red) is indicated on the S4 helix, and the position of the K294 residue is indicated in orange. The N227 residue is shown on the S2 as having a short side chain that is uncharged (pink). The outlined black box indicates where the inter-helical interactions within the voltage-sensing domain occur in the mutant channels. The addition of a negative charge in the N227D (blue) and N227E (purple) mutant channels formed a stabilizing electrostatic interaction with R288 in S4, however the longer side-chain of N227E allowed a more stabilizing interaction. The insertion of IFR (brown) to the C-terminal side of K294 provided increased length and charge in the voltage sensor. The S4 insertion alone shifted the open to closed equilibrium to the closed state, while double S2/S4 mutants shift the equilibrium to the open state. The insertion of QIF (pink) to the N-terminal side of K294 added only length to the S4, and shifted the open to closed equilibrium towards the open state, with larger leftward shifts occurring in the double mutants containing the S2 acidic residues. Unfavorable steric interactions were observed in the RIF (red) S4 length and charge mutant, both in the presence and absence of the S2 acidic residues. In all cases, the open to closed equilibrium of the double S2/S4 mutants channel was shifted to favor the open conformation with the addition of N227D to a greater extent than the N227E mutation indicating that the longer glutamate side-chain had negative steric interactions with the S4 helix when either length or charge was added to the voltage-sensor.

CHAPTER 4: ATYPICAL PHENOTYPES FROM FLATWORM K_V3 CHANNELS[8]

4.1 RESULTS

4.1.1 *N.at-K_v3.1* AND *N.at-K_v3.2* ARE SHAW-TYPE CHANNELS

PCR with degenerate primers applied to genomic DNA of *Notoplana atomata* yielded several small fragments whose sequences were characteristic of the pore and S6 regions of potassium channels. New primers, whose design was based on the unique sequences obtained from these clones, were used for inverse PCR of genomic DNA and 5'-RACE and 3'-RACE reactions using cDNA to obtain full-length cDNA sequences, *N.at-K_v3.1* and *N.at-K_v3.2* (GenBank accession numbers AY186793.1 and AY186794.1 respectively), that encode proteins with strong similarities to characterized potassium channels in the Shaker superfamily (Figure 4-1). BLASTP searches of the non-redundant NCBI protein database using *N.at-K_v3.1* and *N.at-K_v3.2* sequences retrieved members of the *Shaw* subfamily of 6 transmembrane domain K^+ channels as the best scoring match (e-values of 6e-75 and 8e-70 respectively). However, K^+ channels from other Shaker subfamilies were also retrieved at near equivalent scores (8e-55 and 8e-69 e-values respectively) for the next most significant, non-*Shaw*, match.

To confirm that these channel proteins are members of the Shaker superfamily, and not of the ERG-type with which *N.at-K_v3.2* shares inward rectifying properties (see below), *N.at-K_v3.1* and *N.at-K_v3.2* were aligned with 36 taxonomically diverse sequences from the four Shaker sub-families, and with five ERG-type channels (a total of 43 channel sequences). Analysis of this dataset clearly separated the ERG channels from the clade of Shaker family channels, in which the *N. atomata* sequences were embedded by 100% Resampling of Estimated Log Likelihood (RELL) and bootstrap support in ML and ML distance analyses (not shown). In analyses of the Shaker superfamily proteins, both *N.at-K_v3.1* and *N.at-K_v3.2* were clearly positioned within the *Shaw/Shab* clade, with 97% RELL and 85% bootstrap support (Fig. 4-2, Node D). Strongly supported nodes

[8] A version of this chapter has been published. Klassen et al. 2006. Journal of Neurophysiology. 95: 3035-3046.

excluded them from the *Shab (100/100%), Shal* (100/100%) and *Shak* (100/95%) groups (Fig. 4-2, nodes E, F and A respectively). To further clarify this placement, a dataset of 38 sequences containing diverse *Shaw* and *Shab* homologues, rooted by *Shal* sequences, was investigated by Bayesian and ML distance methods (Fig. 4-3). Below we show that *N.at-K$_v$3.2* shares a distinct electrophysiological trait with the nematode *C. elegans Shab* 3 channel (EXP-2), namely inward rectification. However, three strongly supported nodes separate these two sequences (Fig. 4-3). Therefore the inward rectifying properties of N.*at-K$_v$3.2* and *C. elegans Shab* 3 must have evolved separately.

In all analyses, the two *N. atomata* sequences strongly group together in ML and Bayesian analyses despite lower support from ML distance methods. It is therefore likely that they represent the product of lineage-specific gene duplication. When *N.at-K$_v$3.1* is used as a surrogate for the two sequences, it strongly groups with *Shaw*-type channels (99/77%) by ML and ML distance methods. This grouping along with the exclusion of the two *Notoplana* channels from the *Shal* clade (Fig. 4-2 and Fig. 4-3), further confirms the *Shaw* affiliation of both sequences.

The clade consisting of the two channels from *N. atomata* branches basal to the K$_v$3 type channel from the cnidarian, *Polyorchis penicillatus*, in Figure 4-3. Thus, there is an alternative interpretation, that the two *N. atomata* channels form a clade representing a novel K$_v$ channel family. Given the fact that all the channels within the K$_v$ group evolved in common ancestor of metazoans, this would mean that there existed another channel family that was lost in all other phyla for which the K$_v$ channels have been studied. However, if only *N.at.-K$_v$3.1* is included in the phylogenetic analysis it groups robustly within the K$_v$3 clade and weakly as a sister group to the *P. penicllatus* K$_v$3 channel. Given the long branch lengths of the *N. atomata* channel clade and the relatively weak support for placing this clade basal to the *P. penicillatus* K$_v$3 channel, we think that this formal possibility is unlikely to be true. Both *N.at-K$_v$3.1* and *N.at-K$_v$3.2* sequences exhibit relatively long branches when compared to other *Shaw*-type proteins (Fig. 4-2), consistent with the differences in electrophysiological properties exhibited by these flatworm channels.

4.1.2 *N.at-K$_v$3.1* EXPRESSES A NON-INACTIVATING K+ CURRENT WITH SLOW, EARLY OPENING TRANSITIONS

4.1.2.1 Voltage-sensitivity

For *N.at-K$_v$3.1* currents, the I-V relationship was determined by applying 100 ms step depolarisations from a holding potential of -90 mV to a range of potentials from -140 to +70 mV in 10 mV increments followed by a return to -90 mV. Maximal current was measured 95 ms after the initial stimulus artefact. The steady-state activation properties were determined from the amplitude of tail currents measured immediately after the stimulus artefact and plotted against the voltage used to elicit the current. The amplitudes of the tail currents were normalized and fitted to a standard, first-order Boltzmann Function using Clampfit 9.2.

X. laevis oocytes injected with *N.at-K$_v$3.1* mRNA expressed currents with delayed rectifier properties. Voltage-clamped oocytes expressing this channel responded to step depolarisations to potentials greater than approx. – 30 mV with a slowly activating outward current (Fig.4-4*A,B*). Steady-state activation was characterized by a V_{50} of + 9.3 ± 1.2 mV, with a Boltzmann slope parameter of +14.5 ± 1.01 mV/e (n = 9) (Fig. 4-4*C*).

4.1.2.2 Activation Kinetics

The kinetics of activation was determined by performing a two component, pre-depolarisation protocol. Clamp currents were measured while holding the oocyte at the holding potential (-60mV) for 15 ms followed by a 50 ms step to -90 mV then applying a range of 800 ms pre-depolarisation steps from -90 mV to +50 mV in 10 mV increments immediately followed by a 200 ms step to +50 mV to fully open all channels. The kinetics of channel opening was analyzed by fitting the current traces to formulae representing different models using the model comparison function in Clampfit 9.2 (Axon Instruments).

Unlike currents characteristic of the *Shaw* subfamily of potassium channels, the *N.at-K$_v$3.1*-mediated currents have a slow rate of activation, with a 10 to 90% rise time of 150 ms, compared with 3 to 7 ms for mammalian K$_v$3.1 and K$_v$3.2 (Rudy and McBain 2001). The opening kinetics include an unusually long, late rising phase after the initial opening phases (Fig. 4-5*A* and 4-6*A*). Single exponential functions and single sigmoidal functions failed to fit the opening kinetics observed in *N.at-K$_v$3.1* because of the combination of the sigmoidal shape early in the time course of the opening transitions and the long, late phase of activation. Increasing the number of terms yielded an improved fit with the sum of two sigmoidal terms (Eq. 4-1) or the sum of three exponential terms (Eq. 4-2) (Fig. 4-5*A* and 4-5*B*).

$$I(t) = \left[\frac{A}{\left(1 + \exp^{(-(t/\tau 1))}\right)}\right] + \left[\frac{B}{\left(1 + \exp^{(-(t/\tau 2))}\right)}\right] + C \qquad \text{(Eq. 4-1)}$$

$$I(t) = \left[A * \left(1 - \exp^{(-(t/\tau 1))}\right)\right] + \left[B * \left(1 - \exp^{(-(t/\tau 2))}\right)\right] + \left[C * \left(1 - \exp^{(-(t/\tau 3))}\right)\right] + D \quad \text{(Eq. 4-2)}$$

However, neither of these forms fitted the early phase of the kinetics well (Fig. 4-5*B*). A better fit was obtained with Eq. 4-3. that is the sum of two terms, each the product of a co-operative exponential term (n=4, Figure 4-5*C*) and a non-co-operative exponential term all with different time constants (Fig. 4-5*C* and Fig. 4-6*A*).

$$I(t) = \left[A * \left(1 - \exp^{(-(t/\tau fast1))}\right)^n \left(1 - \exp^{(-(t/\tau fast2))}\right)\right] + \left[B * \left(1 - \exp^{(-(t/\tau slow1))}\right)^n \left(1 - \exp^{(-(t/\tau slow2))}\right)\right] \quad \text{(Eq. 4-3)}$$

The steepness of the activation curve increased as the holding potential became more positive (Fig. 4-6*B*), suggesting that the kinetic parameters vary not only as a function of the depolarizing potential, but also as a function of holding potential. However the form of the curves did not vary with the holding potential, i.e. Eq. 4-3 provided a good fit for activation curves elicited from different holding potentials.

In currents elicited from a holding potential of -90 mV to a range of potentials (-20 mV to +50 mV) the contributions of the fast (A) and slow (B) components in Eq. 4-3 were invariant (A = 0.315+/- 0.017, B = 0.685 +/- 0.017)(n = 6). For these currents the time constants of activation τ_{fast1} and τ_{slow1} showed linear dependence on stimulation voltage (Fig. 4-6*C*). Similarly, τ_{slow2} showed linear voltage dependence, decreasing

markedly with membrane depolarisation. However, τ_{fast2} was independent of depolarisation voltage over the range tested (Fig. 4-6*D*).

The shape of the opening curve is a function of the holding potential, manifesting much faster opening with less delay when the holding potential is more positive (Fig. 4-6*B*). Little or no inactivation was observed, even when depolarisation was extended to 1 s. When currents were elicited from a range of holding potentials (-20 mV to +40 mV) to a final potential of +50 mV, the ratio of A to B was independent of the holding potential (A = 0.425 +/- 0.039, B = 0.575 +/- 0.039) (n = 6). Both τ_{fast1} and τ_{slow1} were sensitive to the holding potential: τ_{fast1} showed a sigmoidal dependence on holding potential (inflection point at -22 mV) while τ_{slow1} showed an exponential dependence (Fig. 4-6*E*). Both τ_{fast2} and τ_{slow2} showed an exponential dependence on holding potential (Fig. 4-6*F*).

4.1.3 *N.at-K_v3.2* EXPRESSES AN INWARD RECTIFYING K^+ CURRENT

4.1.3.1 Current-Voltage Relationships

For *N.at-K_v3.2* currents, the I-V relationship was determined from oocytes held at -60 mV by applying a 50 ms step to –90 mV prior to a 500 ms step to a range of potentials from -140 mV to +80 mV in 10 mV steps followed by a 50 ms step back to -90 mV. Current amplitudes were measured after inactivation had occurred and constant current was obtained. The resulting currents were normalized and plotted against the voltage used to elicit the current.

Voltage-clamped oocytes injected with *N.at-K_v3.2* mRNA responded to step depolarisations from a holding potential of -90 mV with currents that show inward rectification (Fig. 4-7*A*). At membrane potentials more negative than -40 mV the channel exhibited inward currents that were approximately proportional to the test potential. At extremely hyperpolarized potentials (-140 to –110 mV) the current was slow to reach peak steady-state current. This delay might arise from poor voltage clamp at hyperpolarized potentials. When the membrane was depolarized beyond -40 mV, the incremental increase in peak steady-state current became less with each successive voltage step. At the more depolarized potentials (greater than +10 mV) peak current was observed immediately after the voltage step but within 20 ms a reduction to the steady-state current level was observed (Fig. 4-7*A*). The current/voltage relationships shown in

Figure 4-7*B* are based on measurements taken after steady-state current levels had been reached.

4.1.3.2 Inactivation Kinetics

A "relaxation" of the peak outward current in response to test pulses more positive than -40 mV was observed (Fig. 4-8*A*). This relaxation to the steady-state current level was best fitted by the sum of three exponential functions providing three separate time constants of inactivation (Fig. 4-*8B,C,D*). The relative contribution of the exponential term A (slow term) remains constant over the voltage range while the contribution of exponential term B (intermediate term) increases with increasing voltage. Exponential term C (fast term) decreases with increasingly depolarized potentials. Thus, the increased steepness of the relaxation at more positive voltages is due to the decrease of tau 1 and tau 3 (Fig. 4-8*B*) and not a shift in relative contributions of the faster terms.

4.1.3.3 Channel Permeability

Oocytes expressing *N.at-K_v3.2* had markedly hyperpolarized resting potentials (-68 +/- 12.7 mV, n = 11) when compared with both control oocytes injected with nuclease-free water (- 39 +/- 3.8 mV, n = 15) and with oocytes injected with the delayed rectifier channel, *N.at-K_v3.1*, (- 38 +/- 4.1 mV, n = 8) described above. Current-voltage curves (Fig. 4-7*B*) suggested that *N.at-K_v3.2* channels were constitutively open over the voltage range of test protocols, accounting for the relatively hyperpolarized resting potentials. The Goldman equation was used to calculate the relative permeabilities for Na^+ and K^+, assuming that *X. laevis* oocytes have $[K^+]_{internal}$ = 150 mM and $[Na^+]_{internal}$ = 20 mM (Kusano et al. 1982) For uninjected and *N.at-K_v3.1* injected eggs, the ratio of Na^+ permeability to K^+ permeability for the leak current is 0.34 and 0.33 respectively. Expression of constitutively open *N.at-K_v3.2* channels hyperpolarize the membrane, as would be expected for a potassium-selective channel, but the resting potential (-69 mV) is substantially more positive than the equilibrium potential for K^+ (-110 mV) as shown in Figure 4-9C. The calculated ratio of Na^+ permeability to K^+ permeability for cells expressing the *N.at-K_v3.2* channel is 0.08.

Perfusion experiments in which $[K^+]_{out}$ was varied from 2 mM, 10 mM, 50 mM and 98 mM also showed that the major permeant ion was K^+ (Fig. 4-7*B*). However, the E_{rev}

values measured when K^+ replaced Na^+ in solution are significantly different from the theoretical calculation for E_{rev} if K^+ was the sole permeant ion (Fig. 4-7C). When choline was substituted for Na^+ in the bath solution, the extrapolated E_{rev} was even more positive than predicted if it is assumed that the channels are only permeant to potassium. Thus there must be other significantly permeant ions (Fig 4-7C). Ion substitution experiments were performed in modified saline solutions in which the concentration of a single ion of interest was modified. The inward currents of *N.at-K_v3.2* are shown to be affected most by changes in potassium and sodium and this channel has limited permeability to calcium (Fig. 4-9A). This limited ionic selectivity accounts for the reversal potentials not following the expected Nernst relationship for potassium ions. A second set of ion substitution experiments were performed in which a single cation was present in the bath solution. *N.at-K_v3.2* is shown to preferentially pass potassium ions but this channel also passed other cations (Fig. 4-9B). Potassium inward currents were greater than those for any other cations tested, but a significant inward current was observed for all ions tested (Fig. 4-9B). While *N.at-K_v3.2* is permeable to two cationic K-channel blockers, CsCl and $BaCl_2$, the channel's permeability to potassium ions was insensitive to 10 mM extracellular TEA.

4.2 Discussion

Although these two *N. atomata* channel sequences are members of the *Shaw* family of potassium channels their long branch-lengths on the phylogenetic tree suggest that their electrophysiological characteristics should differ substantially from the other *Shaw* type channels. In the case of *N.at-K_v3.1,* the large number of differences in sequence were reflected in a phenotype with far slower opening kinetics when compared with other *Shaw* channels, whereas a distinctive inward-rectifying phenotype was seen when *N.at-K_v 3.2* was expressed.

4.2.1 *N.at-K_v3.1* Activation Kinetics

Although we evaluated simpler kinetic schemes for fitting the channel opening data for *N.at-K_v3.1*, Eq. 4-3 was the simplest formula to give an accurate fit over the full time course of activation. Sigmoidal channel opening kinetic behaviour is thought to be due to a requirement for two or more voltage-dependent first-order transitions between closed

states prior to the opening transition (Zagotta et al. 1994; Zagotta et al. 1994).The fact that this channel has such a complex kinetic behaviour that is affected by the pre-depolarisation holding potential suggests that the voltage-dependent transitions in the channel-opening process have different voltage sensitivities. It is important to note that this behavior is different from the Cole-Moore effect (Cole and Moore 1960), in which the onset of channel opening varies with the holding potential but the shapes of the activation curve are superimposable by simple translation along the time axis. The shape of the *N.at.-K_v3.1* channel activation curve, but not its position on the time axis, varies with holding potential.

Although a number of different activation schemes would be consistent with the kinetics of *N.at-K_v3.1*-mediated currents, it appears that there are two independent activation mechanisms and that both include slow transitions that are activated at relatively negative voltages and fast transitions that are activated at more depolarizing voltages. Thus, this channel is a natural substrate for studying the kinetic intermediates of the activation process using single channel recording methods, since pre-opening and opening transitions (Zagotta et al. 1994; Zagotta et al. 1994) can be separated by an appropriately designed excitation protocol. Separation of the early transitions in the closed state from the final opening transition has also been achieved by the application of a naturally occurring snail toxin (BrMT) to N-terminally deleted *Shaker B* that dramatically slows early activation transitions by stabilizing the voltage sensor (Sack et al. 2004).

4.2.2 *N.at-K_v3.2* IS AN INWARD RECTIFIER

Currents mediated by *N.at-K_v3.2* were evident at all physiologically significant potentials. The characteristic decrease in conductance in the upper right quadrant of current/voltage curves is a weak inward rectification that is incomplete. Inward rectification is found in a number of channels from different families, e.g. *erg, Kir, C.elegans Shab3* (EXP-2), and *KATI-1*. However, a number of different mechanisms appear to be at play in producing inward rectification.

One possible mechanism of inward rectification in *N.at-K_v3.2* might be that channels were constitutively open (at potentials between - 140 mV and - 40 mV), but are

inactivated with membrane depolarisation above – 40 mV. Miller and Aldrich were able to convert *Shaker B* channels to inward rectifiers by a triple mutation of the S4 voltage sensor (Miller and Aldrich 1996). Unlike *N.at-K$_v$3.2*, this *Shaker B* mutant is not constitutively open at rest since channels are mostly inactivated at rest.

Hyperpolarization-induced "activation" of the *Shaker B* mutant is by recovery from N-type inactivation occurring through the open state. This is the mechanism suggested for intrinsic, voltage-dependent activation of other 6 transmembrane (TM) inward rectifiers such as *KAT1* and *hERG* (Muller-Rober et al. 1995; Sanguinetti et al. 1995). Secondly, inward rectification might result from relatively slow activation and ultra-fast, N-type inactivation as was seen in another 6TM channel, the *EXP-2* channel (*Shab3*) of *Caenorhabditis elegans* (Fleischhauer et al. 2000). In *N.at-K$_v$3.2,* at the most positive test potentials (above + 30 mV), the rectification may also be due to inactivation having both an initial fast phase and a slower phase (Fig. 4-8). The slow development of inward current that was only apparent at the most hyperpolarized command potentials used might be caused by a relatively slow removal of inactivation at very hyperpolarized potentials. However, inactivation cannot account for all of the rectification observed in *N.at-K$_v$3.2*. A steady-state reduction in current was observed at potentials (- 40 mV) before any inactivation was apparent. Rectification without inactivation first appeared at potentials more positive than app. - 10 mV (Fig 4-7*A*).

It is also possible that the voltage sensor of *N.at-K$_v$3.2* is modified such that the mechanics of activation is altered significantly. In *Shaker* channels the transmembrane electric field is focused across aqueous crevices in the membrane (Starace and Bezanilla 2004) implying that the S4 segment moves a short distance, (Cha et al. 1999) between crevices and specific acidic residues in S2 and S3 segments (Laine et al. 2003; Silverman et al. 2003; Swartz 2004). Substitution of a proline with hydrophilic residues at a specific site in the S6 activation gate of some *Shaker* channels can destabilize the closed state of the channel making it constitutively open and uncoupling the gate from the voltage sensor (Sukhareva et al. 2003). In this case, inward rectification may be caused by intracellular block by other cations. Partial block by intracellular Na^+ and Mg^{2+} occurs at very positive potentials in *H. sapiens K$_v$ 2.1* causing weak inward rectification of what is in other respects a typical delayed rectifier (Lopatin and Nichols 1994). Polyamine or

Mg^{2++} block is seen in the 2TM, strongly inward-rectifying potassium channels such as *IRK1* (Lopatin and Nichols 1994; Stanfield et al. 1994).

Finally, mutation of the S4 transmembrane domain can allow an alternative permeation pathway through the channel (Starace and Bezanilla 2004). For example, mutation of the first arginine in *Shaker B* removes a side -chain that blocks an alternate, parallel ionic pathway to the pore. This Omega current has been shown to be a cation-selective permeation pathway along the length of S4 which is only present when S4 is in the resting state (Tombola et al. 2005). As shown in Figure 4-9, the *N.at.-K_v3.2* channel is permeable to many cations, although K^+ is the most permeant ion. The canonical pore sequence in *N.at.-K_v3.2* shows no sequence differences that would indicate that this channel should show such a low specificity (see Figure 4-10). Thus, the unusual permeability properties of this channel would be consistent with its manifesting a naturally occurring Omega current. It is also worth noting that *N.at.-K_v3.2* has a tyrosine residue at a position three residues C-terminal to the GYG selectivity sequence. In *Shaker* a mutation, T449Y, at the homologous position has been strongly correlated with the sensitivity of that channel to TEA inhibition (Taglialatela et al. 1994). *N.at.-K_v3.2* current is not affected by TEA up to a concentration of 10 mM, indicating that the ion conductance path may not involve the canonical pore region, but rather the conductance pathway characteristic of the Omega current.

The relatively non-selective cationic Omega current in the *D. melanogaster* ShakerB channel is caused by mutation of the first Arg residue in the S4 domain to one of Ala, Cys, Ser or Val (Tombola et al. 2005). The S4 helix of the *N.at.-K_v3.2* channel differs from the normal S4 sequence in that the first residue is His, not Arg, and the third Arg residue is replaced with Gly (See Figure 4-10). Thus, the S4 region of *N.at.-K_v3.2* contains amino acid substitutions that might be expected to create an Omega current conductance pathway and uncouple S4 from the canonical channel gate.

If this is an example of a naturally occurring Omega current, then the canonical ion conductance pathway must be uncoupled from the normal activation mechanism, since depolarisation is not associated with the appearance of a more K^+-specific current, as is seen in the case of the synthetic Omega current mutants (Tombola et al. 2005). The inward rectification in this channel thus could be due to the S4 voltage-sensing helix

moving from the resting state to the open conformation, effectively occluding the permeation pathway but not opening the canonical pathway.

4.2.3 CONCLUSIONS

Here we have demonstrated that isolation of voltage-gated K^+ channels from organisms that diverged basal to the deuterostome/protostome split yield fertile material for new structure-function studies. As increasing selection pressure during early metazoan radiations produced striking phenotypic variants within single Shaker sub-families, these same phenotypes of slow activation and inward rectification were convergently evolved in other 6TM-channel families in "higher" metazoans. The surprising divergence from "standard" Shaker phenotypes shown by these two flatworm channels would not have been predicted from phylogenetic or bio-informatic characterization alone, underscoring the value of comparative functional studies when interpreting genomic or proteomic data. This comparative data can be complemented by mutagenesis studies focused upon the S2, S3, S4 and pore regions that will determine the structural basis for these unusual activation properties. Although macroscopic current recordings demonstrate that the two *N. atomata* channels have unusual kinetic properties, a detailed structure-function analysis will require detailed single channel recordings. As the scope of genetic and genomic studies expands to encompass a wider evolutionary diversity of organisms than the intensively studied model organisms, this general approach to sampling functional sequence space should prove fruitful in the analysis of other examples of protein machinery.

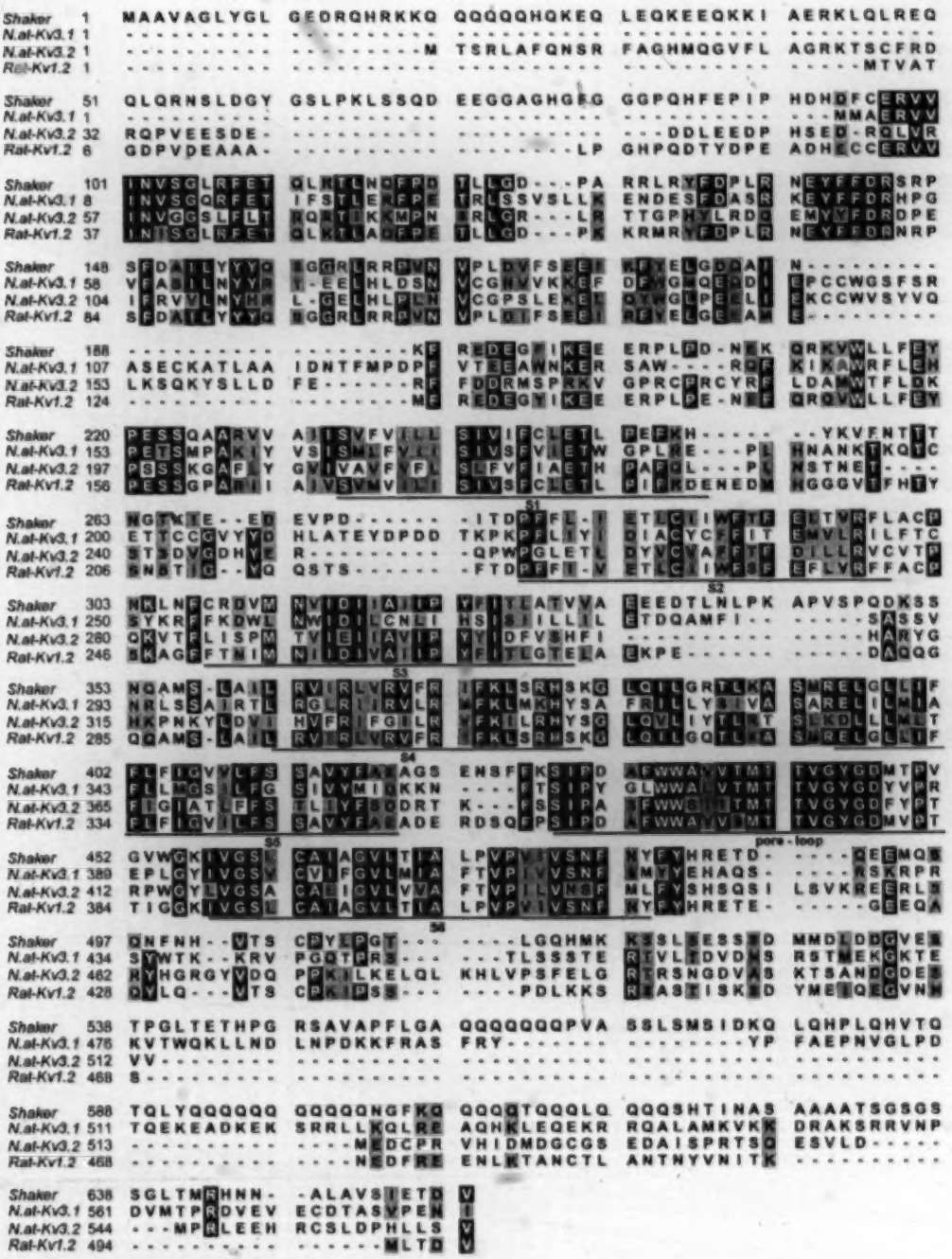

Figure 4-1: Alignment of *N.at-K,3.1* and *N.at-K,3.2* protein sequences against *RatK,1.2* and *Shaker*.

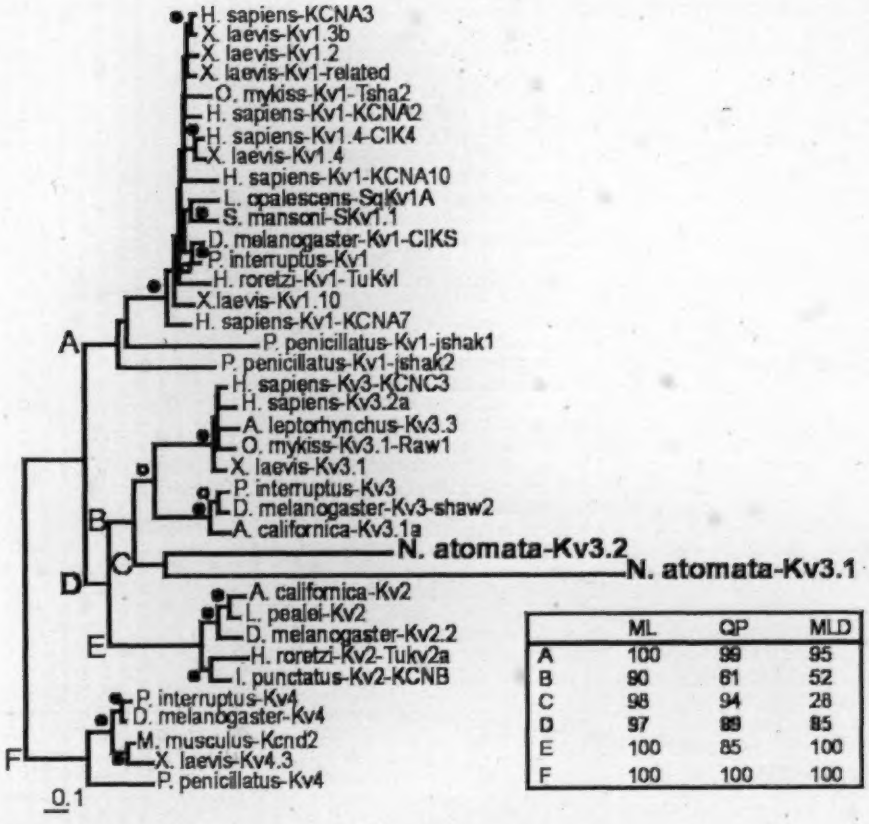

	ML	QP	MLD
A	100	99	95
B	90	81	52
C	98	94	28
D	97	89	85
E	100	85	100
F	100	100	100

Figure 4-2: *N.at-K$_v$3.1* and *3.2* are *Shaw/Shab* type channels.
Notoplana atomata sequences (bolded) resolved as part of the *Shab/Shaw* clade (Node D), but are more likely to be members of the *Shaw* sub-family (Node B). *N.at-K$_v$3.1* and *3.2* were more closely related to each other than to any other channels (Node C). Monophyly of the *Shab* (Node E), *Shak* (Node A) and *Shal* (Node F) sub-families excludes the *N.atomata* sequences. The best ML distance topology is shown as an unrooted tree of 38 K^+ channel protein sequences. The inset table shows support values for labeled nodes as follows: ML = ProtML RELL, QP = Quartet Puzzling, MLD = ML distance. All other nodes are labeled with a closed circle (indicating 95% plus support in both ML and ML distance methods), a solid circle (71-94%) or an open circle (50-70%). In all cases of discrepancy between methods, the lower value was taken.

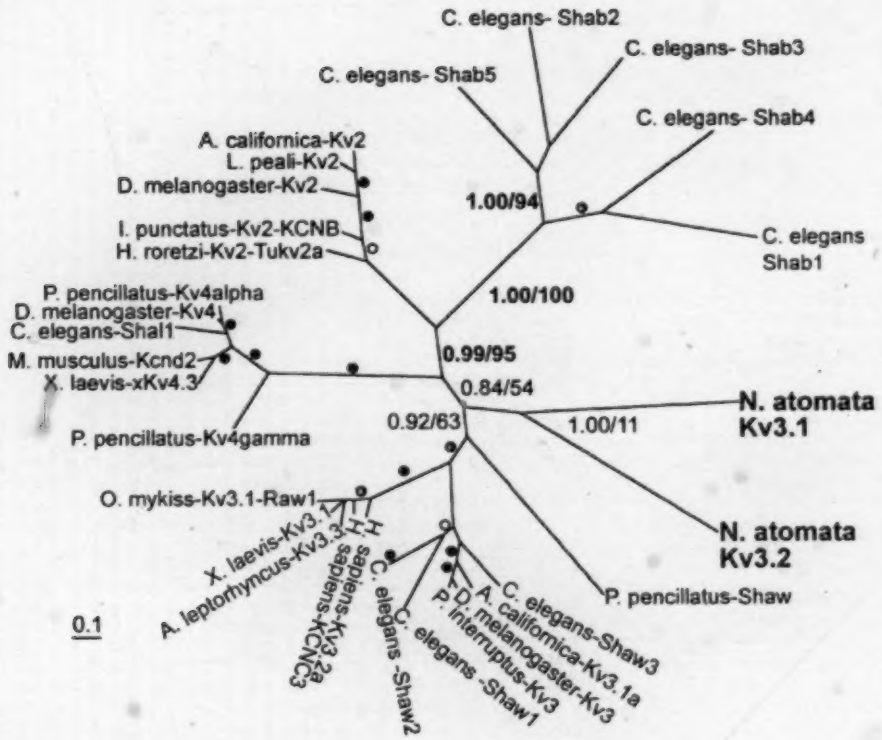

Figure 4-3: Phylogenetic analysis placed the *N.at-K$_v$3* sequences with *Shaw* homologues.

Analysis of a *Shab/Shaw/Shal* dataset excluded the *N.at-K$_v$3* sequences as *Shab* or *Shal* homologues. The *N.at-K$_v$3* sequences are bolded, as are support values for three robust nodes separating the inward rectifying (*Caenorhabditis elegans-Shab3* and *Notoplana atomata-K$_v$3.2*) channels. The taxon label for the *C. elegans –Shaw2 alt 5* sequence is not shown for space considerations but was tightly clustered with the *C. elegans-Shaw2* sequence. This is the best tree topology obtained by Bayesian analysis; the clade of Shal (K$_v$4) sequences defines the root of this tree. Bayesian posterior probabilities and MLD bootstrap values are given at relevant nodes. All other nodes are labelled with closed circle (95% plus support for both methods), a shaded circle (71-94%) or open circle (50-70%). In all cases of discrepancy between methods, the lower value was taken.

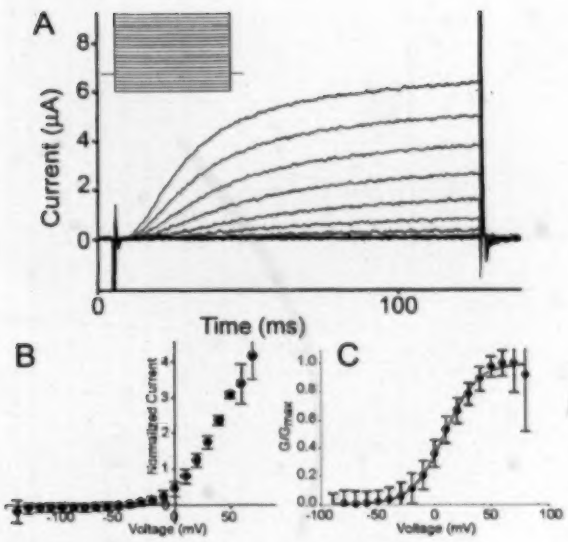

Figure 4-4: Currents mediated by the *N.at-K$_v$3.1* channel, expressed in *X. laevis* oocytes.

A. Outwardly-directed currents evoked by 100 ms step depolarisations from a holding potential of -90 mV to a range of potentials from -140 to + 70 mV in 10 mV increments followed by a return to -90 mV that produced inward tail currents. The stimulus protocol is inset on the right.

B. Current/voltage plot showing an activation threshold between - 40 and - 20 mV.

C. Steady-state activation curve for *N.at-K$_v$3.1* -mediated currents. The solid curve represents the best fit to a Boltzmann function.

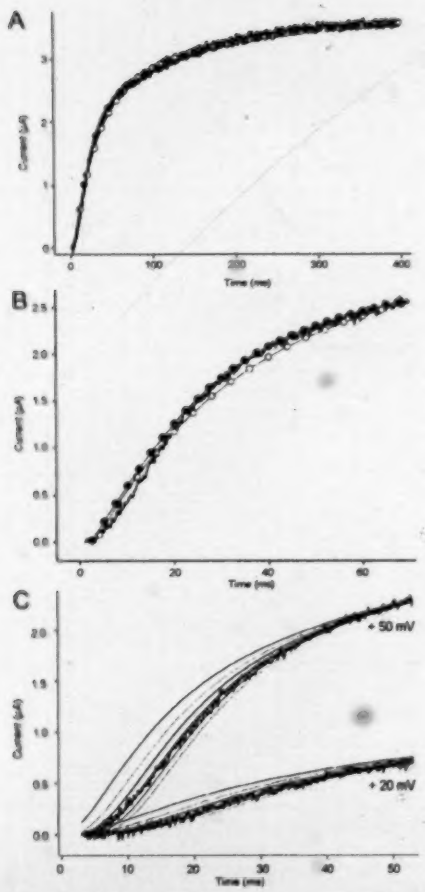

Figure 4-5: Curve fit analysis of the opening kinetics of *N.at-K$_v$3.1* channel.
A. Curve fit analysis of the first 400 ms of channel opening in response to a step to + 50 mV from a holding potential of – 90 mV. The combination of a sigmoidal shape early in the time course of the opening transitions and the long, late phase of activation prevented fitting of a single exponent or single sigmoid curve. The double sigmoidal curve of Eq. 4-1 (orange circles) and the triple exponential curve of Eq. 4-2 (blue circles) both fitted well to the later portion of the curve.
B. Curve fit analysis from A showing the first 70 ms of channel opening. Neither the double sigmoidal curve (Eq. 4-1, orange circles) or the triple exponential curve (Eq. 4-2, blue circles) fitted the slow early transitions well.
C. Kinetic analysis of activation demonstrated that the opening transitions require 4 subunits. Current traces for the initial 80 ms of current development is shown for depolarisations to either + 50 mV or + 20 mV from a holding potential of - 90 mV (as in Fig. 3A). Curves were fitted to Eq. 4-3 with different values of n (where n = 1, green; 2, pink; 3, blue; 4, red; 5, aqua; 6, grey). The best fit was obtained for n = 4 (heavy red line).

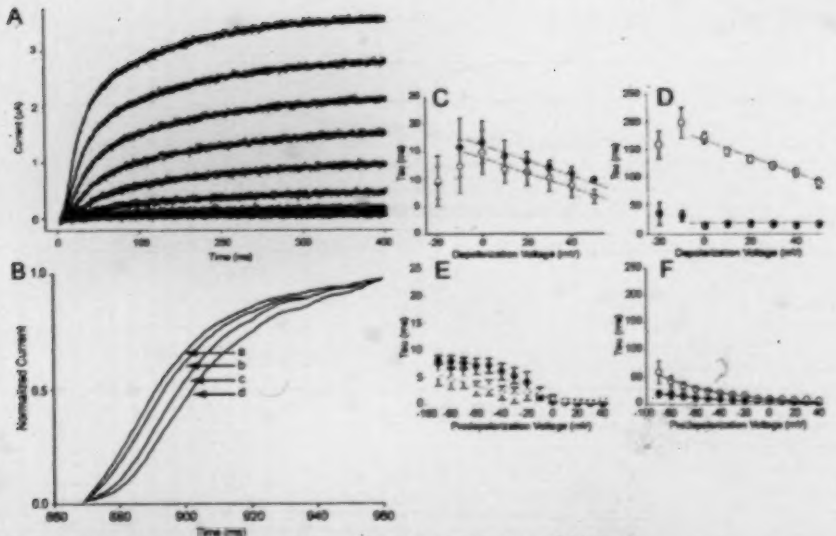

Figure 4-6: Activation kinetics of the *N.at-K$_v$3.1* channel.

A. Current traces for the N.at-Kv3.1 channel showing the first 400 ms of channel opening from a holding potential of -90 mV to a range of potentials from -140 mV to + 50 mV in 10 mV steps. The best fit for kinetic analysis was obtained by fitting with Eq. 4-3 where n = 4 (red lines).

B. Scaled, smoothed superimposed current traces showing that pre-depolarisation of the membrane reduced the initial delay in channel opening and increased the rate at which equilibrium was achieved. An 800 ms pre-depolarisation step was followed by a 100 ms step to + 50 mV to fully open the channels. The sigmoidal shape of the current trace varied in response to the pre-depolarisation voltage. Pre-depolarisation voltages (holding potentials) were a = + 30 mV, b = 0 mV, c = - 40 mV and d = - 90 mV.

C and D. Kinetic analysis of activation of currents from a constant holding potential to a range of supra-threshold potentials. All parameters were generated using Eq. 4-3 where n =4. The total contributions of the fast components (A for τ_{fast1} and τ_{fast2}) and slow components (B for τ_{slow1} and τ_{slow2}) remained constant for the potentials tested (0.315 +/- 0.017 and 0.685 +/- 0.017 respectively). C: Both τ_{fast1} (filled circles) and τ_{slow1} (open circles) of activation decreased in a linear, voltage-dependent manner. D: τ_{fast2} (filled circle) did not show any voltage dependence while τ_{slow2} (open circle) decreased linearly in a voltage-dependent manner. E and F: Kinetic analysis of activation of currents following prolonged sub-maximal depolarisation. The relative contributions of the fast components (A for τ_{fast1} and τ_{fast2}) and slow components (B for τ_{slow1} and τ_{slow2}) remained constant over the range of pre-depolarisation voltages tested (0.425 +/- 0.039 and 0.575 +/- 0.039 respectively). E: Both τ_{fast1} (filled circles) and τ_{slow1} (open circles) of activation decreased as the conditioning pre-pulse became more depolarized. τ_{fast1} exhibited a sigmoidal dependence on holding potential with the inflection point occurring near threshold while τslow1 showed an exponential decrease. F: Both τ_{fast2} (filled circles) τ_{slow2} (open circles) showed an exponential decrease with increasing holding potential.

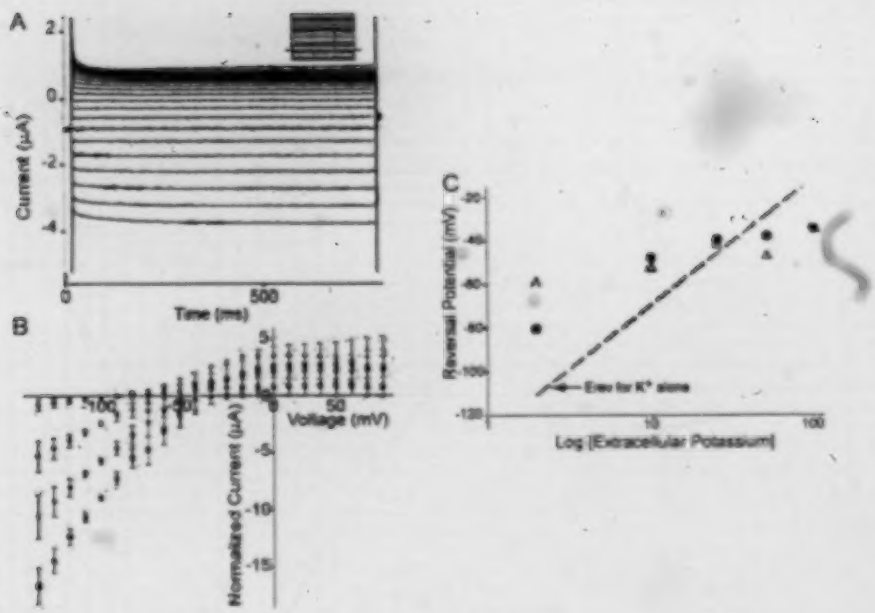

Figure 4-7: Currents mediated by the *N.at-K$_v$3.2* channel expressed in *X. laevis* oocytes.

A. Currents evoked by 500 ms step depolarisations from a 50 ms pre-pulse at - 90 mV to a range of potentials from - 140 to + 80 mV in 10 mV increments followed by a 50 ms step back to – 90 mV. The holding potential was – 60 mV. Currents were activated very rapidly throughout this range, though currents evoked by hyperpolarizing steps also expressed a slowly activating component, and currents produced by strong depolarisations showed evidence of rapid and slow partial inactivation.

B. Current-voltage relationships for the *N.at-K$_v$3.2* channel at different $[K^+]_{out}$. The reversal potential of *N.at-K$_v$3.2*-mediated currents depended upon the external concentration of potassium ions. The reversal potentials were measured by the same protocol as illustrated in *A*:, first in normal ND96 (2 mM K^+, filled circles) then in saline in which a proportion of the sodium ions had been replaced with potassium ions (10 mM K^+, open circles; 50 mM K^+, filled triangles; 98 mM K^+, filled squares).

C. The reversal potentials measured for different values of $[K_{out}]$ deviate from the theoretical Nernst potential for potassium ions ($[K^+]_{internal}$ = 150 mM as reported in Kusano et al. 1982. Reversal potentials were extrapolated from the experiment in *B* in which a proportion of the sodium ions in the saline were replaced with potassium ions (filled circles), as well as the same experiment in which choline chloride was used instead of sodium (open triangles). This deviation from the expected relationship for potassium ions suggests that *N.at-K$_v$3.2* is permeable to ions other than potassium.

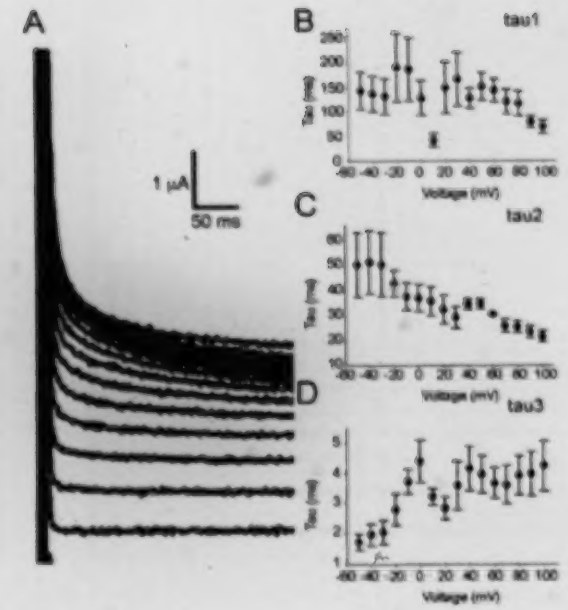

Figure 4-8: Inactivation of the *N.at-K$_v$3.2* channel.
A. Outwardly directed currents of *N.at-K$_v$3.2*. elicited from the protocol described in 6*A*. Inactivation of the channel was best fitted with a triple exponent.
B. C. and D: The relative contribution of the exponential term A (slow term) remained constant over the voltage range while the contribution of exponential term B (intermediate term) increased with increasing voltage. The exponential term C (fast term) decreased linearly with increasingly depolarized potentials. B. Tau1, the slow time constant of inactivation, was sensitive to voltage, becoming noticeably faster at more depolarized potentials. C. Tau2, the intermediate time constant of inactivation, was not voltage sensitive. D. Tau3, the fast time constant of inactivation, appeared to be slightly voltage sensitive, becoming somewhat faster at more depolarized potentials.

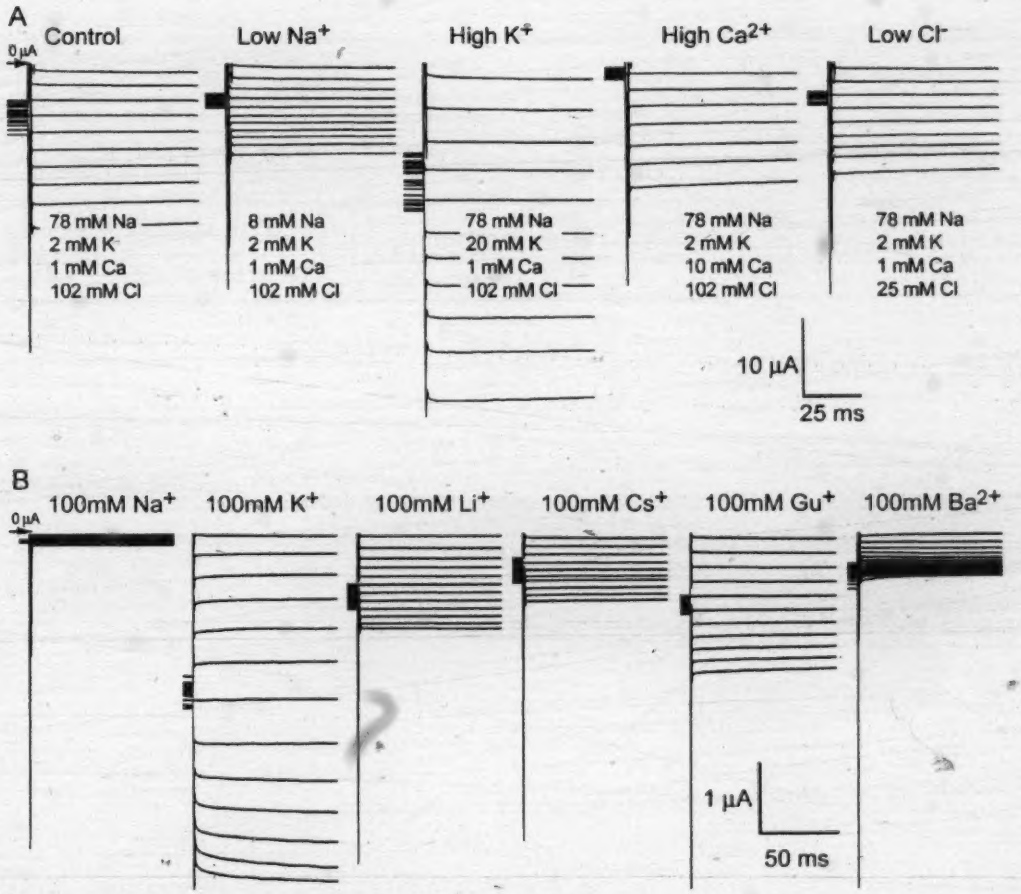

Figure 4-9: *N.at-K,3.2* is permeant to multiple cations.
A. A permeability experiment showing only inward currents for the first 250 ms of channel opening using the protocol described in 6A. The inward currents were obtained using either a control saline (Control, in mM NaCl 78; KCl 2; $CaCl_2$ 1; $MgCl_2$ 1; ChoCl 18; HEPES 5; pH 7.4) or a solution in which the ion concentrations were modified by substituting with 20 mM KCl, 88 mM ChoCl, 38.5 mM Na_2SO_4 or 10 mM $CaCl_2$ (High K^+, Low Na^+, Low Cl^- and High Ca^{2+} respectively) to give the ionic concentrations shown. A noticeable difference in inward currents was observed in the high K^+ and low Na^+ bath solutions and to a lesser extent in the high Ca^{2+} bath solution.
B. A single permeability experiment showing only the inward currents for the first 40 ms of channel opening using the protocol described in 6A. A perfusion experiment was performed changing the single cation (x= monovalent cations; K^+, Li^+, Cs^+, Gu^+ (guandinium), Na^+, or Ba^{2+}) present in the bath (in mM, xCl 100; HEPES 10, EDTA 1). A noticeable inward current was observed for all cations tested, including the known K-channel blockers Cs^+ and Ba^{2+}.

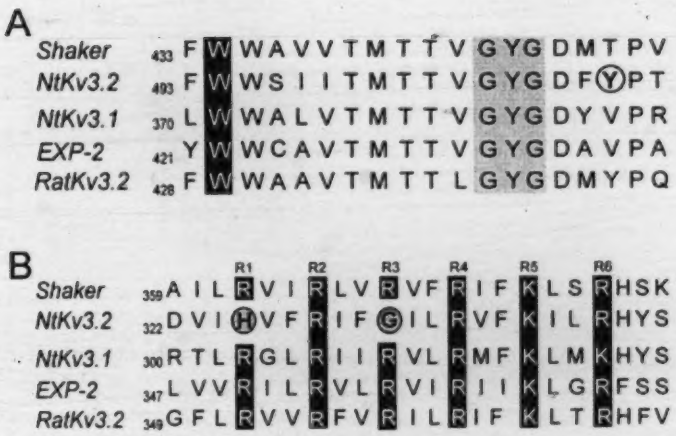
A
Shaker 433 F W W A V V T M T T V G Y G D M T P V
NtKv3.2 493 F W W S I I T M T T V G Y G D F Y P T
NtKv3.1 370 L W W A L V T M T T V G Y G D Y V P R
EXP-2 421 Y W W C A V T M T T V G Y G D A V P A
RatKv3.2 428 F W W A A V T M T T L G Y G D M Y P Q
B
R1 R2 R3 R4 R5 R6
Shaker 359 A I L R V I R L V R V F R I F K L S R H S K
NtKv3.2 322 D V I H V F R I F G I L R V F K I L R H Y S
NtKv3.1 300 R T L R G L R I I R V L R M F K L M K H Y S
EXP-2 347 L V V R I L R V L R V I R I I K L G R F S S
RatKv3.2 349 G F L R V V R F V R I L R I F K L T R H F V

Figure 4-10: A comparative alignment of the S4 voltage sensor and pore regions of *N.at-K$_v$3.2* with other K$_v$ channels.

A. Alignment of the highly conserved pore region. The characteristic GYG selectivity sequence is highlighted in grey. The location of the non-conducting *Shaker* mutation W434F is indicated in black. Sequence analysis of the pore suggests *N.atK$_v$3.2* should be TEA sensitive due to a tyrosine position after the pore (circled) as the homologous site T449 in *Shaker* when mutated to tyrosine gave increased TEA sensitivity in that channel. B. Alignment of the S4 voltage sensor in selected channels. The characteristic positive arginine lysine repeats (R1-R7) are shaded in grey. The Omega current is caused by mutating R1 in *Shaker* to R362A, R362C, R362S, or R362V. *N.atK$_v$3.2* has a histidine (H325) at position R1 and a glycine (G331) at position R3. The combination of the hinging action of the glycine in the middle of the helix coupled with the presence of the planar side chain at R1 may create a native Omega current.

CHAPTER 5: A NATURAL ALTERNATIVE PERMEATION PATHWAY IN *N.at-K$_v$3.2*[9]

5.1 RESULTS

5.1.1 SINGLE S4 MUTATIONS

5.1.1.1 H325A/C/S/R/V/E Mutants

The mutation of the histidine at position R1 to either a hydrophobic valine (H325V) or negatively charged glutamate (H325E) produced weakly inwardly rectifying channels (Figure 5-1). H325V appeared similar to the wild-type *N.at-K$_v$3.2,* with large inward currents below -90mV, which begin to rectify near -10mV giving rise to a linear plateau to +40mV (Figure 5-1). The conductance of H325V was highest at hyperpolarized potentials, which dropped to a steady conducting state from -130mV to -100mV (Group 1, Figure 5-1). This was followed by a step to a lower constant conductance state near the reversal potential. The conductance then decreased in a linear fashion through the remainder of the voltage range (-40 mV to +80 mV).

The addition of a negative charge at position R1 did not substantially change the IV properties, compared to the neutral valine. H325E had a reversal potential of -75 mV, showing limited rectification, with a current that did not reach a steady plateau at positive potentials (Figure 5-1). H325E showed a consistent linear decrease through the voltage range until +50mV where a constant conductance state was reached (Group1, Figure 5-1).

All other single mutations of the first histidine (H325A, H325S, H325C, H325R) created a delayed rectifier phenotype more commonly associated with *Shaw* type voltage gated potassium channels (Figure 5-1). The conductance changes in response to changes in membrane potential of these channels followed a sigmoidal Boltzmann curve and had similar properties (Figure 5-1). The most leftward shifted H325 single mutant channel was H325A with a half activation voltage (V_{50}) of 51.9 +/- 3.4 mV and a slope factor of 21.8 +/- 1.6 (Table 2). The remaining delayed rectifier mutants had V_{50} values greater than +60 mV (Figure 5-1, Table 5-1). Surprisingly, the shallowest slope factor was

---

[9] A version of this chapter is being prepared for submission to the Journal of Biological Chemistry.

observed in the only channel with the addition of a basic residue, H325R (27.3+/- 2.7). Both the H325S and H325C mutants had similar conductance properties, with V_{50} values of 60.6 +/- 4.5 mV vs. 62.5+/- 5.8 mV and slopes of 19.2+/-1.9 vs. 22.9 +/- 2.1, respectively (Table 2). The right-shifted voltage sensitivities of all the H325 delayed rectifier channels suggests that R1 does not contribute substantially to the gating charge in this S4 voltage sensor.

5.1.1.2 G331P/A/R/K Mutants

Mutations of the flexible glycine residue at position R3 in the S4 voltage produced both inward rectifiers and delayed rectifiers (Figure 5-2). The replacement of glycine with a proline residue was expected to induce a constitutive kink within the voltage sensor, permitting the flow of cations through the gating pore. The G331P mutant was a weak inward rectifier with a reversal potential of -100mV. The outward current began to rectify at -40mV, reached a plateau at +10mV and remains constant through the voltage range tested. The conductance/voltage relationship of G331P is similar to H325E (Group 2) where there was a linear decrease through the entire voltage range until +60mV where a minimally conducting state was reached (Figure 5-2).

The replacement of glycine with alanine at position R3 (G331A) was expected to confer helical stability on the voltage sensor. Unexpectedly, the G331A mutant was also a weak inward rectifier (Figure 5-2). This channel appeared to pass current linearly with voltage from -140mV to -70mV with a reversal potential of -89mV. The outward current plateaued at +20mV and remains constant. Unlike the H325E, H325Vand G331P channels, G331A has an initially constant conductance through to the reversal potential (-140mV to -80 mV) that is followed by a linear decrease in conductance until a minimally conducting state is reached at +50mV (Figure 5-2, Group 3).

The recovery of a typical voltage sensor, by replacing glycine with basic positively charged arginine (G331R) or lysine (G331K) converted *N.at-*K_v*3.2* into a delayed rectifier (Figure 5-2). Both channels have a threshold voltage of -20 mV. However, voltage conductance relationships for the two mutants differ substantially. The G331R channel was similar to the H325R delayed rectifier mutant, with a V_{50} of 73.8 +/- 9.7 mV and a slope of 23.8 +/- 2.8 mV/e (Figure 5-2, Table 5-1). In comparison,

the G331K mutant was more left shifted with a V_{50} of 36.0 +/- 1.0 mV, with a substantially steeper slope factor of 15.2 +/- 0.5 mV/e (Figure 5-2, Table5-1).

5.1.2 Double S4 Mutants

5.1.2.1 G331P with H325 Mutants

The addition of either a hydrophobic side uncharged residue (H325A or H325V) or an acidic residue (H325E) within the proline containing S4 (G331P) produced similar current and conductance profiles (Figure 5-3). Mutant channels with double G331P+H325A (G331P+A) substitutions appeared to have a linear current/voltage relationship between -140mV and -70mV with a reversal potential of -83 mV. The outward currents peaked at -10mV, and remain at a steady plateau through the voltages tested (Figure 5-3). The conductance profile for this channel was similar to that of G331A, changing from a constant conductance state to a linear decreasing conductance at -70mV (Figure 5-3, Group 1). The G331P+H325V (G331P+V) double mutant had I/V relationships to -50mV (through the reversal potential, -67mV) and gradually decreased until the plateau at +10mV. Similarly, the G331P+H325E (G331P+E) mutant had a linear I/V curve through a reversal potential of -80mV to +20mV, where weak rectification occurred (Figure 5-3). The G331P+H325C (G331P+C) double mutant had current and conduction properties similar to the other G331P containing mutants. This channel had a linear I/V curve through the reversal point at -83mV until -70 mV when the current decreased until the outward plateau at +10mV (Figure 5-3). Like G331P+A, the G331P+V, G331P+E and G331P+C channels all had an initial constant conducting state at hyperpolarized potentials (Figure 5-3, Group 3).

The addition of a polar, uncharged side-chain at the entrance to the gating pore, G331P+H325S (G331P+S), produced a weak inward rectifier, which had a linear I/V curve to -50mV, through the -73mV reversal potential. The slope of the I/V curve then gradually decreased as voltage increased until +10mV where the I/V curve became linear again (Figure 5-3). The conductance/voltage profile for this channel was similar to the other G331P containing mutants, but the horizontal steady conductive state occurred from -140mV to -80mV (Figure 5-3, Group 3).

The G331P+H325R (G331P+R) mutant containing arginine in the first position in the S4 also exhibited inward rectification (Figure 5-3). This channel showed a strong inward current between -140mV and -100mV, which is followed by a linear I/V curve through the -80mV reversal potential to a peak at +40mV where it then plateaued. Like H325V, the conductance/voltage relationship for G331P+R shows an initial high conductance at hyperpolarized potentials that decreased with increasing voltage (-140mV to -70 mV), followed by a drop to a steady conducting state (-60mV to +10mV). The conductance then decreased in a linear fashion through to +90 mV (Figure 5-3, Group 1). These results suggest that the proline kink induced by the substitution of the R3 glycine with proline (G331P) disrupts the voltage sensor helix to such an extent that the double mutants are all inward rectifiers (Figure 5-3).

5.1.2.2 G331A with H325 Mutants

The addition of alanine at position R3 (G331A) was designed to stabilize a non-kinked conformation of the S4 voltage sensor, but inward rectification persisted. The double S4 mutants, where R1 (H325) is also replaced, exhibit notable inward currents (Figure 5-4). The G331A+H325A (G331A+A) and G331A+H325C (G331A+C) channels were identical to the G331P mutant channel in both current and conductance profiles. The G331A+A channel had a linear I/V curve from -140mV to -50mV through a -70mV reversal potential, while G331A+C channels show similar current but pass through a -84mV reversal potential. In both channels the I/V curve plateaued around +10mV and remained constant to +50mV (Figure 5-4). The conductance profile for both channels showed a linear reduction in conductance from -140 mV to +50 mV (Figure 5-4, Group 2).

The addition of a negatively charged glutamate (H325E) on the G331A backbone is functionally similar to the H325E single mutant. Current produced by the G331A+H325E (G331A+E) channel had a reversal potential of -89mV, and the I/V curve plateaued at +10mV (Figure 5-4). The conductance profile reduced steadily in a linear fashion from -140mV to +50mV where a stable minimal conductance state was achieved (Figure 5-4, Group 2).

The G331A+H325V (G331A+V) double mutant showed a similar current and conductance profile to the H325V single mutant (Figure 5-4). This channel appeared to have a linear I/V curve from -110mV to -30mV, reversing at -70mV (Figure 5-4). The slope of the I/V curve gradually reduced, reaching a nearing a near horizontal slope at +30mV. The conductance profile for this channel showed a high initial conductance state at hyperpolarized potentials that reduced gradually to a stable conducting state from -80 mV to 0 mV, followed by a linear reduction in conductance until a minimally conducting state was reached at +70 mV (Figure 5-4, Group 1).

However, not all double S4 mutants in this backbone show true rectification (Figure 5-4). The replacement of R1 with either serine (G331A+H325S) or arginine (G331A+H325R) appeared to create a biphasic inward rectifier, which had two distinct components to current flow a small inward current and a large outward current (Figure 5-4). The I/V curve below the reversal potential, in both channels had a shallow slope, and the outward I/V curve is not linear, with increasingly shallow slope at depolarized potentials (Figure 5-4). The conductance profiles for these channels exhibit a W-shape (Figure 5-4, Group 4), with a low initial conductance rising to a maximum and followed by a return to a low conductance state. The G331A+S channel had a maximum conductance at -80 mV, and returned to a low conductance state at +20mV, followed by an increase in conductance to +70 mV. In comparison, G331A+R had maximal conductance at -70mV, and returned to a low conductance state at +70mV (Figure 5-4, Group 4).

5.1.2.3 G331R with H325 Mutants

Mutation to a "typical" S4 voltage sensing back-bone by the replacement of glycine with arginine at position R3 (G331R) yielded a delayed rectifier in the single mutant. However, the double mutants all yielded weak inward rectifiers, leak channels or biphasic inward rectifiers (Figure 5-5). The addition of a negative glutamate residue (G331R+H325E) to the arginine rich S4 voltage sensor created a weak inward rectifier (Figure 5-5). The G331R+E channel had large non-linear I/V curve from -140mV to -100mV, which became linear from -100 mV to +10 mV (through the reversal potential of -72mV) (Figure 5-5). The I/V curve plateaued at +10mV and remained constant to

+70mV. This channel shows a high initial conductance, which dropped to a lower conductance state between -40mV and -10mV, followed by a linear reduction in conductance +70mV (Figure 5-5, Group 1).

The G331R+H325C (G331R+C) channel exhibits a phenotype, which is similar to "leak" channels. This channel had a linear current across all voltages tested, passing through the -51mV reversal potential (Figure 5-5). This channel had a nearly constant conductance through the entire voltage range (-140mV to +90 mV) with inflections at the reversal potential and 0 mV (Figure 5-5, Group 1). These inflections suggest the shape of the permeation path is changing such that the resistance to ion passage increases.

The other S4 double mutants in the G331R backbone all exhibit a biphasic I/V curve (Figure 5-5). The G331R+H325A (G331R+A) and G331R+H325V (G331R+V) had large inward currents at more hyperpolarized potentials. The slope of the I/V curve became shallower as it approached the reversal potential of -62mV in both channels. The slope then became steeper reflecting large ionic efflux (Figure 5-5). These channels exhibited weak rectification at potentials more depolarized than +40 mV. The conductance profile for these channels resembled the G331A+R double mutant (Figure 5-5, Group 4). The G331R+A channel had a skewed W-shape conductance with a peak at -20mV and a slow decline in conductance through the more depolarized potentials. Similarly, the G331R+V channel had a peak conductance at -20mV, which declined steeply to a minimally conducing state at +80 mV (Figure 5-5). The S4 double mutant that mimics the voltage sensor found in all other K_v channels, G331R+H325R (G331R+R) was also a biphasic inward rectifier (Figure 5-5). This channel had a shallow I/V curve below the reversal potential of -52mV, which is followed by a steep slope in the I/V curve to +10 mV (Figure 5-5). At the most depolarized potentials the slope of the I/V curve becomes exceptionally shallow, reflecting the weak rectification in this channel. The maximum conductance in this channel occurred at 0mV however a minimally conducting state is not reached at depolarized potentials (Figure 5-5, Group 4).

5.1.2.4 G331K with H325 Mutants

By replacing the flexible glycine hinge with the basic, positively charged lysine (G331K) a delayed rectifier phenotype was created (Figure 5-6). When double mutants

were created in the lysine-containing S4 voltage sensor, the delayed rectifier phenotype was also observed (Figure 5-6). The S4 double mutant G331K+H325R (G331K+R) is the only double mutant that showed purely delayed rectification, with a threshold voltage of -40mV (Figure 5-6). That the conductance profile was similar to the G331K single mutant alone, with a similar slope factor (16.5 +/- 1.0 mV/e) but with a more left shifted half activation voltage (25.6 +/ -1.2 mV), implying that the introduction of an additional charge in the voltage sensor shifts the voltage sensitivity of the channel leftward compared to the G331K single mutant alone.

All of the other G331K-containing S4 double mutants have non-ohmic inward currents below the reversal potential and exhibit outward currents at more depolarized potentials. The G331K+H325S (G331K+S), G331K+H325C (G331K+C), G331K+H325V (G331K+V), G331K+H325A (G331K+A) and G331K+H325E (G331K+E) channels all passed measurable inward currents and at depolarized potentials exhibited typical potassium efflux (Figure 5-6). The reversal potential in these channels varies from -50mV in the G331K+C channel to -70mV in the G331K+S channel. The conductance profile for these channels fits a Boltzmann sigmoid curve, where the mutants have different biophysical properties (Figure 5-6, Group 5). The G331K+A mutant has similar properties to the G331+R channel, with a V_{50} of 22.5 +/- 1.8 mV and a slope of 15.7+/- 1.5 mV/e, while G331K+C, G331K+V and G331K+S are comparatively left shifted by 7, 10 and 15 mV respectively (Table 5-1). The most pronounced hyperpolarized shift was observed when a glutamate residue was added to the voltage sensor. The G331K+E mutant had a V_{50} of -27.5 +/- 2.1 mV (Table 5-1).

5.1.3 Channel Permeability

5.1.3.1 H325E and H325V Permeation Profiles

Mutation of the histidine at position R1 should change the accessibility of extracellular ions to the gating pore, but permeation through the path should be similar once an ion had gained access. The addition of the large acidic side-chain of glutamate (H325E) should attract cations to the extracellular face of the gating pore, but limit access to larger ions. A large potassium influx is observed in this channel (Figure 5-7). At -140mV cesium and guanidinium pass the same amount of current (I_{Cs}/I_K=72.2+/-14.1%,

I_{Gua}/I_K=76.9+/-13.7%). H325V channels have large inward potassium currents, and intermediate cesium and guanidinium currents (I_{Cs}/I_K=45.2+/-8.7%, I_{Gua}/I_K=38.3+/-6.9%), while the influx of lithium, sodium and barium is low (less than 20% K^+ current at -140mV) (Figure 5-7).

5.1.3.2 G331P and G331A Permeation Profiles

The shape of the gating pore pathway was expected to be drastically changed by the addition of proline kink in the S4 helix, or by replacing the flexible glycine hinge with a rigid alanine. Both G331P and G331A were permeant to multiple cation species, but differed in permeation profiles, indicating a different shape of gating pore. In G331P, potassium had the largest influx, while the other cations exhibited similar current conduction at hyperpolarized potentials (I_{Na}/I_K= 30.4+/-6.1%, I_{Cs}/I_K=50.5+/-14.5%, I_{Gua}/I_K=45.2+/-13.5%, I_{Li}/I_K=33.1+/-10.0%, I_{Ba}/I_K=26.1+/-10.0% (Figure 5-7). The straight helix of the G331A mutant allows a large non-linear potassium influx. The other cations all have a minimal influx at hyperpolarized potentials (less than 9% K^+ current at -140mV; Figure 5-7).

5.1.3.3 H325R with G331P/A/R Permeation Profiles

The H325R and G331R single mutants both yielded a typical K_v delayed rectifier phenotype. However, when these mutations are combined in the S4 voltage sensor, a biphasic inward rectifier was observed. Thus, it appears that localized packing in the gating pore can be perturbed by the combination of mutations at R1 (H325) and R3 (G331) changing the shape of the permeation path. The three S4 double mutants; G331P+R, G331A+R and G331R+R all had high potassium influx at hyperpolarized potentials. In the G331A+R and G331R+R channels the influx of cesium is comparable to that of guanidinium, though G331A+R appears more permeant to these cations (G331A+R=I_{Cs}/I_K=53.5+/-5.2%, I_{Gua}/I_K=52.4+/-7.5% vs. G331R+R I_{Cs}/I_K=29.8+/-7.5%, I_{Gua}/I_K=33.8+/-6.6%, Figure 5-8). In G331P+R channels the guanidinium influx was larger than cesium (I_{Cs}/I_K=52.3+/-3.0%, I_{Gua}/I_K=34.9+/-3.9%, Figure 5-8). Small inward currents were carried by barium and sodium in these channels.

5.1.3.4 4-AP Block of the Omega Path

The *N.at-K$_v$3.2* channel is capable of passing a number of monovalent and divalent ions, including the known channel blockers cesium and barium. Guandinium ions also pass through the alternative permeation path in this channel, suggesting a large accessible pore on the extracellular face. To test the accessibility of the alternative permeation path to larger ions, we selected 4-aminopyridine (4-AP) because the compound is twice the size of guanidinium alone, and has a planar ring structure and is a known K^+ channel blocker (Figure 5-9). Using 10-fold increases in 4-AP concentration (10μM to 10mM), a dose-response curve was created for *N.at-K$_v$3.2* channels using the standard I/V protocol as described in the Methods section. The observed inward current was larger than saline alone at 10uM concentrations, indicating either a stabilization of the gating pore by 4-AP, allowing for increased current, or that at low concentrations, 4-AP is permeable through the gating pore. However, at larger concentrations, the observed inward current diminished in a linear fashion with increasing 4-AP concentration (Figure 5-9). Block of the channel was instantaneous with no visible modification to opening kinetics or rectification, suggesting the 4-AP was able to gain access to the gating pore, becoming stuck in the path, and prevented current flow in a small population of channels.

5.2 DISCUSSION

5.2.1 Proposed Structural Model of the Gating Pore Pathway

A comparative sequence analysis of *N.at-K$_v$3.2* against other Shaker superfamily channels suggested that the unusual inward rectifier phenotype exhibited by this channel is based on the unique composition of the S4 voltage sensor (Figure1-7) (Klassen et al. 2006). We believe that the presence of a histidine residue (H325), rather than a basic residue at position R1 in the voltage sensor, permits access of extracellular cations to the gating pore pathway when the voltage sensor is in the resting conformation. This occurs when the proteinaceous gasket across the gating pore, between the S2 and S4 helices is not formed by the association of an acidic S2 residue (D1) with R1. We suggest that the large planar ring of histidine limits the accessibility of cations to the alternative permeation pathway, such that the *wild-type N.at-K$_v$3.2* appears to be potassium selective.

We also believe that the central glycine residue (G331), with its small side-chain permits the Omega current to flow along the voltage sensor at hyperpolarized potentials, but has little contribution to the ion selectivity of the alternative permeation pathway.

Because the voltage sensor in *N.at-K$_v$3.2* has a number of basic residues, it should move in response to transmembrane voltage. However, in our model of channel function, the limited movement of voltage sensor fails to open the ion selective pore because the flexible glycine hinge kinks, preventing the conformational change that otherwise would pull on the S4-S5 linker to open the activation gate. Membrane depolarisations still cause the voltage sensor to move locally, resulting in a changing the shape of the gating pore pathway. These changes in protein conformation increase the resistance of the pathway to ion flow, decreasing the conductance through the gating pore to a minimally conducting state. Here we evaluate our proposed model of *N.at-K$_v$3.2* channel function based on the results from our mutagenesis experiments.

5.2.2 Accessibility to the Gating Pore Permeation Pathway

In voltage-gated potassium channels, the voltage sensor is thought to reside in an aqueous crevasse that acts to focus the transmembrane electric field across a small region of the channel protein (Gandhi et al. 2003; Goldstein 1996; Larsson et al. 1996). In *Shaker* the division between intracellular and extracellular vestibules is thought to be formed by a proteinaceous septum created by the residue side-chains of E283 in S2 and R362 (R1) in S4 at hyperpolarized potentials, and by E283 and R371 (R4) at depolarized potentials (Islas and Sigworth 2001; Sokolov et al. 2005; Starace and Bezanilla 2004; Starace et al. 1997; Tombola et al. 2005). Mutation of R362 to smaller uncharged residues caused a measurable influx of a TEA insensitive non-selective cation current, the Omega current, along the length of S4 (Tombola et al. 2005). In *N.at-K$_v$3.2*, R1 is a charged non-basic histidine residue (H325), and the replacement of H325 with the arginine residue found at that position in other K_v channels, creates a non-inactivating delayed rectifier, typical of *Shaw*-type channels, The long positively charged side-chain likely blocks access to the gating pore, presumably through reestablishing the protein bridge between S2 and S4 (Papazian et al. 1995; Tombola et al. 2005). These results directly support our model, where H325 allows access of extracellular ions to the gating

pore. This further suggests that the introduction of an additional charge in the S4 voltage sensor increases the movement of the S4 voltage sensor in response to membrane depolarisations to such an extent that the flexibility in the glycine hinge is overwhelmed, and the S4-S5 linker moves, opening the activation gate (Figure 5-10).

Unlike the case with *Shaker*, replacing H325 of *N.at-K$_v$3.2* with serine, cysteine or alanine at the entrance to the gating pore creates a delayed rectifier. This also supports our model of channel behavior as the access to the gating pore in *N.at-K$_v$3.2* appears to be blocked even with the addition of small side chains. The differences in function between *Shaker* and *N.at-K$_v$3.2* may be based on the structural basis for the *wild-type* channels. Specifically, *Shaker* has evolved to mediate the efflux of potassium in response to depolarisations of the membrane, while *N.at-K$_v$3.2* has evolved to utilize the alternative gating pore pathway, instead of the canonical pore.

The addition of an acidic residue at the entrance to the gating pore, (H325E) resulted in an inward rectifier, with the most pronounced influx of cations of all mutant channels. Specifically, cesium and guanidinium had ~75% the amount of potassium current through the gating pore at hyperpolarized potentials. We believe that side-chain repulsion between H325E and D260 (the first acidic residue in S2) opens the aperture at the gating pore, in addition to attracting cations with negatively charged carboxyl groups (Figure 5-10).

The H325V mutant unexpectedly showed inward rectification, indicating that side-chain packing, and local protein interactions affect accessibility through modification of the "gasket" at the interface of the extracellular and intracellular canals. The permeability of cations through the gating pore in H325V channels is less than that observed in H325E, but is greater than the wildtype channel (H325V, I_{Cs}/I_K=45.2+/-8.7%, H325E, I_{Cs}/I_K=72.2+/-14.1%, *N.at-K$_v$3.2*, I_{Cs}/I_K=27.0+/-9.0%). Our model of channel function, suggests that ions accessing the gating pore are permitted through the disrupted septum between S2 and S4, were the relative ionic permeabilities are dictated by the steric interactions between residue side-chains. Again, our model of channel function is corroborated by these results where the smaller non-polar valine residue allows greater accessibility to all cations, compared to the planar histidine ring in the *wild-type* channel which limits access to the gating pore, providing limited selectivity for potassium.

5.2.3 G331R and G331K Yield Delayed Rectifiers with Different Properties

The wild-type channel fails to open the canonical potassium selective pore even under large (+50mV) depolarisations. Our model suggests that the glycine residue (G331) hinges, fail to transmit the gating movement to the S4-S5 linker, which in turn fails to open the activation gate (Mathur et al. 1997). The replacement of the glycine with basic residues, arginine and lysine, create a delayed rectifier phenotype (Figure 5-10). Notably, the G331R mutant has a similar half activation voltage to the H325R delayed rectifier mutants (73.8 mV vs 69.9 mV), but the G331R mutant has a steeper slope (b=23.8 mV/e vs 27.3 mV/e) suggesting that while the addition of charge at R1 or R3 does not change the voltage sensitivity of the channel, but substitution of charge at R3 increases the equivalent charge that translocates the electric field. The G331K channel had a substantially left-shifted half activation voltage (36.0 mV vs 73.8 mV) and steeper slope (b=15.2 mV/e vs. 23.8 mV/e) compared to G331R. This shift is likely due to stabilizing electrostatic interactions, facilitated by the longer basic side chain, between S2 and S4 at both the hyperpolarized and depolarized positions of the voltage sensor, similar to the case in *Shaker*, where R3 (R368) forms stabilizing salt-bridges with E293 in the resting state, and in E283 in the open conformation (Papazian et al. 1995; Tiwari-Woodruff et al. 2000). However, in *N.at-K$_v$3.2* the acidic residues in S2 are both aspartic acid, thus the longer side-chain of lysine compared to arginine may be required to form the electrostatic interaction. The combination of the basic residue at R1 (H325R) and the stabilizing interaction of lysine (G331K) in the voltage sensor shifts the voltage sensitivity of the resulting delayed rectifier in the leftward direction by 10mV, compared to the G331K mutation alone.

5.2.4 Changing the Shape of the Gating Pore Pathway

The aqueous path of the gating pore in *Shaker* made accessible by R1 mutation, lies along the straight S4 voltage sensor. This channel preferentially passes guanidinium, and cesium before potassium (Tombola et al. 2005). We have provided evidence that H325 in at position R1 is responsible for the ionic selectivity of the wild-type *N.at-K$_v$3.2*. However, if the shape of the conductance path changes during voltage sensor activation,

and if our model is correct, and the basis of that changing conductance path is facilitate by the central glycine residue (G331), then substitutions modifying protein packing below R3 in the voltage sensor should greatly modify the conductance properties of the channel. By substituting proline (G331P) at a central position in the voltage sensor of *N.at-K_v3.2*, the helix should kink by ~30°, and allow increase ion conductance through the gating pore (Tieleman et al. 2001). Conversely, the addition of alanine (G331A) is expected to straighten the helix, and should reduce the ability of cations to pass through the gating pore at more depolarized potentials (Chakrabartty et al. 1991; O'Neil and Degrado 1990; Serrano et al. 1992). Unlike the alternative path in *Shaker,* both the G331A and G331P mutants allow large K+ influx, however G331A mutants show the limited permeability to all other cations (less than 10% K+ at -140mV), while the G331P channel shows significant sodium influx (30%).

In the sodium channel, *Na_v1.2a*, a TTX insensitive potassium influx was observed in double charge neutralization mutants in Domain II but not in the single mutations alone (Sokolov 2005). At hyperpolarized potentials, double R2 (R850Q) R3 (R853Q) mutants showed linear inward currents that disappeared with depolarisation, and activation of the sodium selective pore (Sokolov et al. 2005). Similarly, double neutralizations, R3 (R853Q) and R4 (R856Q) show a linear efflux of current at depolarized potentials when the canonical pore is blocked by TTX (Sokolov et al. 2005). Because the *N.at-K_v3.2* has non-basic residues at R1 and R3, our model proposes that the permeation pathway is open whether the voltage sensor is in the resting or activated conformation, but that the shape of the pathway changes during membrane depolarisations causing changes in relative ion permeability and conductance. Therefore, the shape of the alternative permeation pathway should be affected by substitutions at both positions. This is best demonstrated by the biphasic inward rectifiers produced by the double mutants G331A+S, and all of the G331R containing double mutants except G331R+C (Table 5-1), indicates that the shape of the gating pathway is changing as the voltage sensor translocates through the membrane. The W-shaped conductance profile for these channels corresponds to the shape changes in the current-voltage relationships, showing a voltage sensitive conformation changes in the gating pore.

By locking the conformation of the voltage sensor helix by the addition of a central alanine, arginine or proline, the permeability and conduction profiles of the gating pore pathway change. In combination with mutations of the N-terminal histidine located at the extracellular and intracellular interface of the gating pore vestibules, allows an influx of cations in these double mutant channels. The pair-wise mutations within the S4 voltage sensor disrupt the precise secondary structure of the voltage sensing domain that allow the blockade of the alternative permeation pathway by the single mutations alone.

G331R+R mutants recover a typical voltage sensor but have a notable influx of cations and fail to open the selective pore, while G331K+R mutants are left shifted delayed rectifiers. The addition of both charge and increased side-chain length has been demonstrated to cause local rearrangements in the voltage sensor affecting helical packing and electroctrostatic interactions in *jShak1* (here as Chapter 2). Other double mutants exhibit a typical delayed rectifier phenotype in addition to allowing current to flow the potassium selective pore. The combination of G331K with all histidine mutations, with the exception of G331K+R, all show a small influx of current at hyperpolarized potentials and activation of the pore at depolarized potentials allowing an efflux of potassium. This duality in function is observed in both the *Shaker* and *Na$_V$1.2a* gating pore mutants, where the Omega current ceases when the main pore is activated through membrane depolarisations. In the *Na$_V$1.2a* mutant the amount of current passing through the relative pathways differs substantially, with potassium influx through the gating pore being ~9% of the sodium influx through the selectivity filter (Sokolov et al. 2005). This difference in current flow between pathways is observed in the G331K containing double mutants, providing further evidence of the two permeation pathways in *N.at-K$_V$3.2*, where the gating pore pathway has evolved to allow the channel to act as a potassium selective inward rectifier.

5.2.5 THE STRUCTURE OF *N.at-K$_V$3.2* IS SHAPED TO USE THE GATING PORE PATHWAY

N.at-K$_V$3.2 has the conserved 6TM structure found in K$_V$ channels, including the highly conserved potassium selectivity filter, and characteristic S4 voltage sensor. However, the histidine residue in position R1 and the glycine residue in position R3 in the voltage sensor, instead of the basic arginine residues found in those positions in other

K_v channels, create an alternative permeation path through the gating pore that is preferentially used by this channel. In *N.at-K_v3.2* this pathway is shaped to allow cation influx at hyperpolarized and depolarized potentials, even as the voltage sensor translocates through the pore. At rest, H325 allows extracellular ions to access the aqueous gating pore canal, while the flexibility and reduced side-chain of G331 residue permits Omega current to pass in the activated voltage sensor (Figure 5-11). Here we have demonstrated that amino acid substitutions at H325 and G331 can yield a typical *Shaw*-type delayed rectifier, presumably through the stabilization of the channel protein by structural rearrangements and electrostatic interactions that are not utilized by the *wild-type N.at-K_v3.2* channel.

The use of this naturally occurring alternative pathway has evolved in *N.at-K_v3.2*, such that acidic residues in the S2 and S3 domains that contribute to channel stabilization during conformation transitions, have been modified to stabilize the alternative pathway in this channel instead. Specifically, in *Shaker* the substitution of E283 with aspartic acid, doubled the size of the Omega current by reducing the S2 contribution to proteinaceous septum blocking the gating pore (Tombola et al. 2005). In *N.at-K_v3.2* both residues in S2 (D260 and D270) have the shorter side-chain, allowing greater current flow through the gating pore bounded by S2 and S4. To date, the only K_v channel with an aspartic acid at the second position in S2 is *N.at-K_v3.2*; this position is occupied by a highly conserved glutamate in all other channels. The longer side-chain of the glutamic acid forms salt-bridges with basic residues in the voltage sensor in both the open (K374 in *Shaker*) and closed conformation (R377 in *Shaker*) (Tiwari-Woodruff et al. 2000; Tiwari-Woodruff et al. 1997). Because this stabilizing interaction is limited in *N.at-K_v3.2* by the shorter side-chain of D260 in S2, the stabilizing acidic residue in S3, which is an aspartic acid in all other K_v channels (D316 in *Shaker*), is a glutamic acid in this channel. Thus, the *N.at-K_v3.2* channel protein, maintains the stabilizing interactions within the voltage-sensing domain, but maximizes the cation flow through the gating pore even during voltage sensor movements.

5.2.6 CONCLUSIONS

The inwardly rectifying 6TM voltage-gated potassium channel, *N.at-K$_v$3.2*, has evolved to utilize an alternative permeation pathway along the length of the S4 voltage sensor, rather than the canonical pore. This unique mechanism evolved through changes in the electrostatic interactions between the voltage sensor and the surrounding domains, as well as having a glycine residue rather than a basic residue at a central position in S4. The proteinaceous septum between the S2 and S4 domains, at the interface of the extracellular and intracellular aqueous crevasse of the gating pore, is not present in *N.at-K$_v$3.2*, due H325 in position R1. Our model suggests that at rest, the path is accessible because of the shortened side-chain of the aspartic acid D260 in S2 and the planar ring of H325 in S4, while voltage sensor movement in response to changes in transmembrane voltage, moves the small G331 residue into a comparable position, allowing continued ionic flux, and prevents the opening of the canonical pore. Mutations of H325 can prevent Omega current influx and create a delayed rectifier (H325A/C/S/R), but can also change the permeability of the pathway to other cations (H325V/E). Substitution of stabilizing residues at a central position (G331P/A) simply alter the permeability and conduction properties of the gating pore pathway, while reconstruction of the hypothetical ancestral basic residue content (G331R/K) that is normally found in the voltage sensor produced delayed rectifiers with different biophysical properties. Finally, by creating double mutants (R1/R3) we demonstrated that the accessibility, shape and function of the gating pore could be modified. The selectivity of the gating pore pathway is related to ionic size and chemical properties as well as localized protein packing and side-chain interactions. It is possible that the Omega current flows in a hydrated, or partially hydrated fashion, and that the chemical properties of the ions may stabilize the structure of the gating pore as the ions pass through.

Table 5-1: Summary table of the observed phenotypes and conductance properties of the *N.at-K,3.2* single and double S4 mutants expressed in *X. laevis* oocytes.

Channel	n	Phenotype		Conductance Properties	
Wild-type	*	Inward rectifier		Wild-type	
H325A	5	Delayed rectifier		V_{50}=51.9 +/- 3.4	b= 21.8 +/- 1.6
H325C	5	Delayed rectifier		V_{50}=62.5 +/- 5.7	b= 22.9 +/- 2.1
H325S	4	Delayed rectifier		V_{50}=60.6 +/- 4.5	b= 19.2 +/- 1.9
H325R	7	Delayed rectifier		V_{50}=69.9 +/- 8.8	b= 27.3 +/- 2.7
H325E	18	Inward rectifier		Group 2	
H325V	12	Inward rectifier		Group 1	
G331P	6	Inward rectifier		Group 2	
G331A	14	Inward rectifier		Group 3	
G331R	7	Delayed rectifier		V_{50}=73.8 +/- 9.7	b= 23.8 +/- 2.8
G331K	12	Delayed rectifier		V_{50}=36.0 +/- 1.0	b= 15.2 +/- 0.8
H325A + G331P	8	Inward rectifier		Group 3	
H325C + G331P	6	Inward rectifier		Group 3	
H325S + G331P	6	Inward rectifier		Group 3	
H325R + G331P	11	Inward rectifier		Group 1	
H325E + G331P	6	Inward rectifier		Group 3	
H325V + G331P	8	Inward rectifier		Group 3	
H325A + G331A	9	Inward rectifier		Group 2	
H325C + G331A	7	Inward rectifier		Group 2	
H325S + G331A	7	Biphasic inward rectifier		Group 4	
H325R + G331A	8	Biphasic inward rectifier		Group 1	
H325E + G331A	8	Inward rectifier		Group 2	
H325V + G331A	9	Inward rectifier		Group 1	
H325A + G331R	8	Biphasic inward rectifier		Group 4	
H325C + G331R	7	Leak Channel		Group 1	
H325S + G331R	n/a	No detectable current		n/a	
H325R + G331R	7	Biphasic inward rectifier		Group 4	
H325E + G331R	10	Inward rectifier		Group 1	
H325V + G331R	10	Biphasic inward rectifier		Group 4	
H325A + G331K	12	Combined Inward/Delayed	Group 5	V_{50}= 22.5 +/- 1.8	b= 15.7 +/- 1.5
H325C + G331K	7	Combined Inward/Delayed	Group 5	V_{50}= 15.6 +/- 3.4	b= 23.7 +/- 2.8
H325S + G331K	6	Combined Inward/Delayed	Group 5	V_{50}= 7.6 +/- 0.4	b= 15.0 +/- 0.4
H325R + G331K	6	Delayed rectifier		V_{50}= 25.6 +/- 1.2	b= 16.5 +/- 1.0
H325E + G331K	7	Combined Inward/Delayed	Group 5	V_{50}= -27.5 +/- 2.1	b= 23.3 +/- 2.1
H325V + G331K	7	Combined Inward/Delayed	Group 5	V_{50}= 12.1 +/- 1.2	b= 10.2 +/- 1.1

* data from Klassen et al. 2006 except for pharmacology data

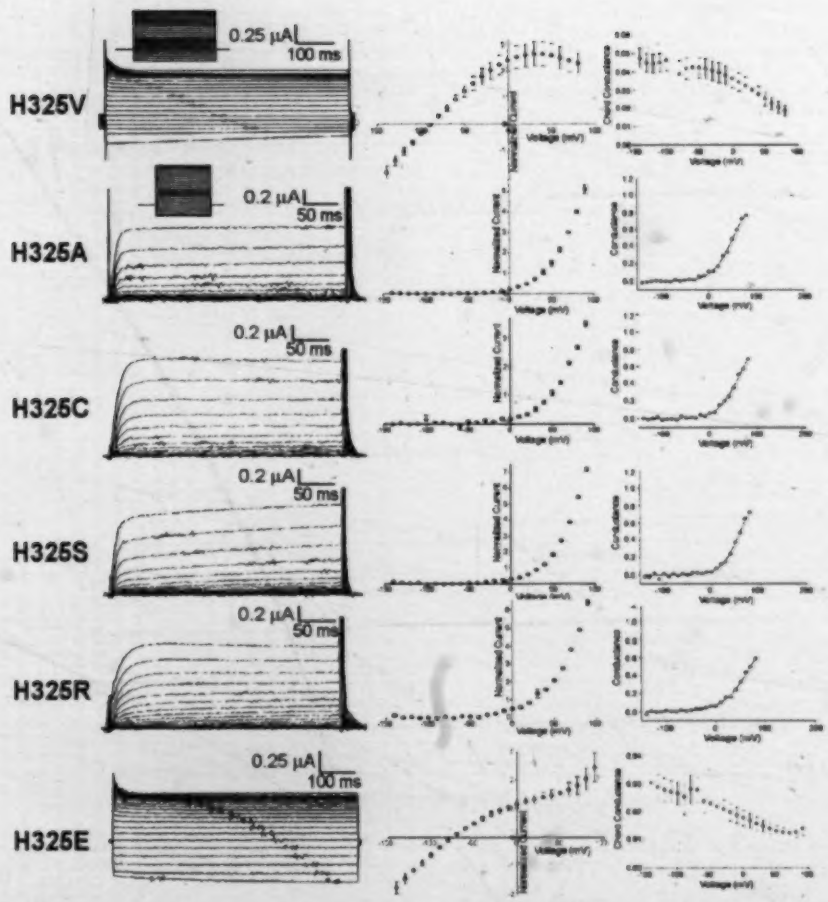

Figure 5-1: Mutation of H325 modifies accessibility to the gating pore pathway. Inward rectification persists in H325E and H325V single S4 mutants. These channels exhibit different current/voltage relationships (column 2), with changing slopes throughout the voltage range. The conductance/voltage relationships for H325V and H325E clearly demonstrate this difference where H325E has a linear decrease in conductance from -140mV to +60mV where it enters a minimally conducting state. H325V mutants have a constant conductance through to the reversal potential, and then show a decrease in conductance through depolarized potentials. The H325C/S/R/A mutants modified protein structure sufficiently to block the gating pore and open the canonical potassium poret. These channels are all right shifted delayed rectifiers with V_{50} values greater than +50 mV.

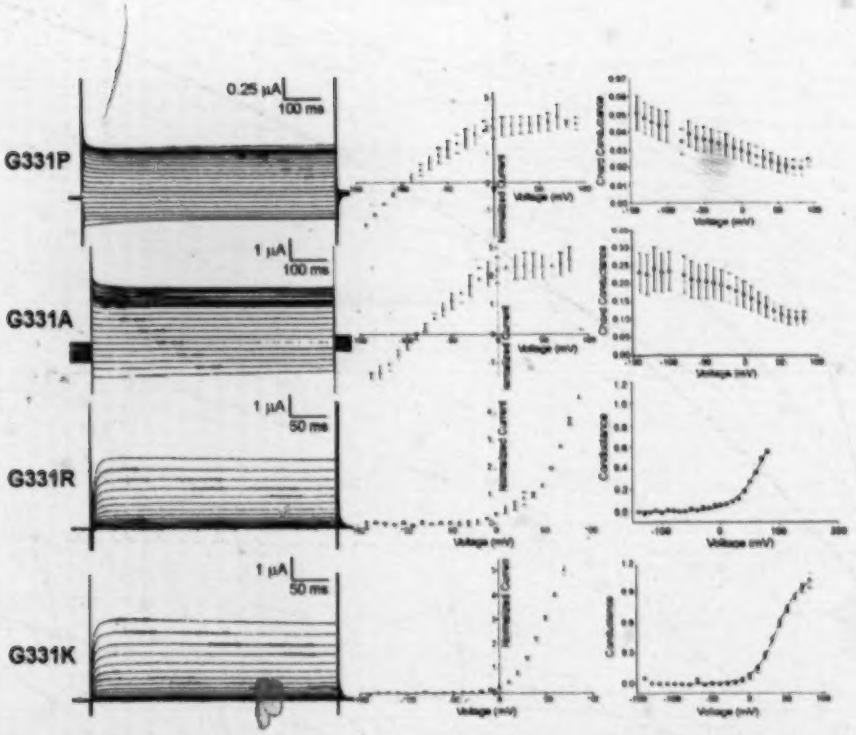

Figure 5-2: Mutations of G331 create typical delayed rectifiers with different voltage-sensitivities.
While inward rectification persists in G331P and G331A single S4 mutants, the impact of the longer guanidine group of lysine over that of arginine indicates the finite structural tolerances in the *N.at-K$_v$3.2* gating pore. B331R and G331 mutant channels are closed at hyperpolarizations and open in response to membrane depolarisation. G331K with the longer side chain appears to form stabilizing electrostatic interactions with the surrounding protein, such that the open conformation is favored.

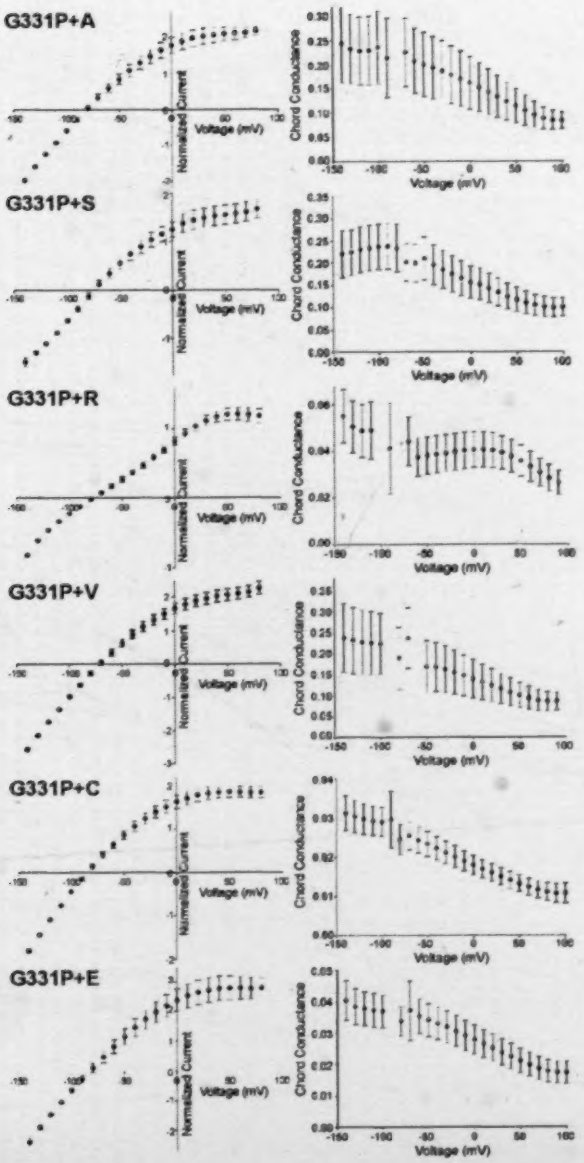

Figure 5-3: Double mutants in the proline backbone are all inward rectifiers. The large kink in the alpha helical structure created by the G331P mutation disrupts the favorable action of the H325 single mutants that create typical delayed rectifiers. The conductance/voltage relationships indicate there are changing conductance states within the double mutant channel, suggestive of shape changes within the gating pore pathway.

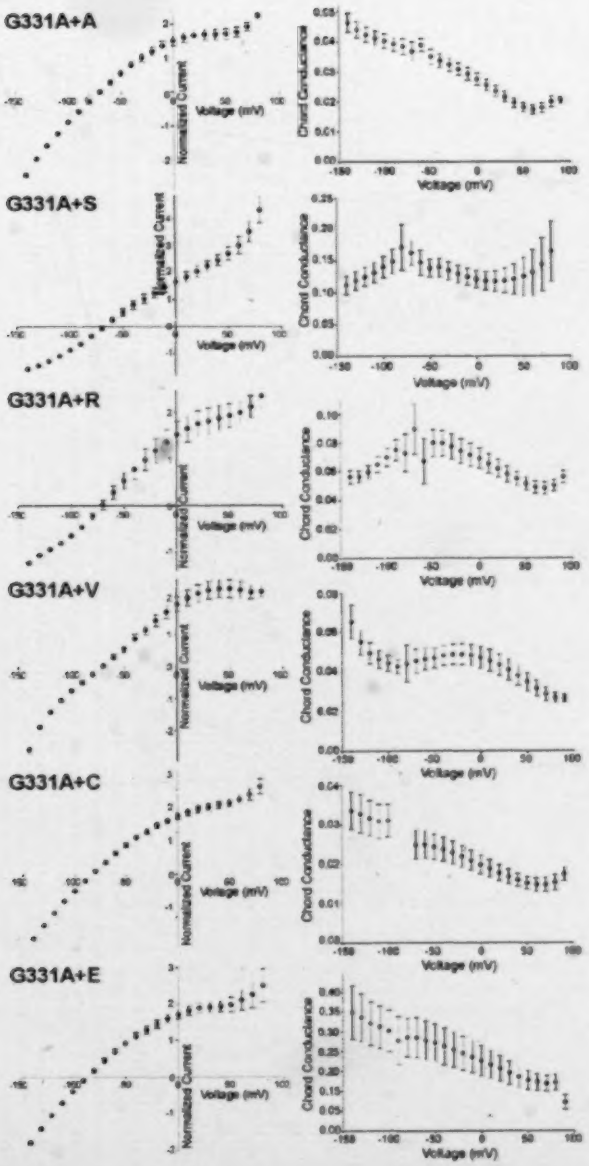

Figure 5-4 Double mutants in the alanine backbone are pass Omega current. By straightening the S4 alpha helix, it appears that the permeation pathway comes more restrictive to ion flow when it is combined with different residues at the R1 entrance to the gating pore. The appearance of a W-shaped conductance profile in the G331A+R and G331A+S channels indicates the path way becomes more conductive at intermediate voltages (-50mV to 0mV).

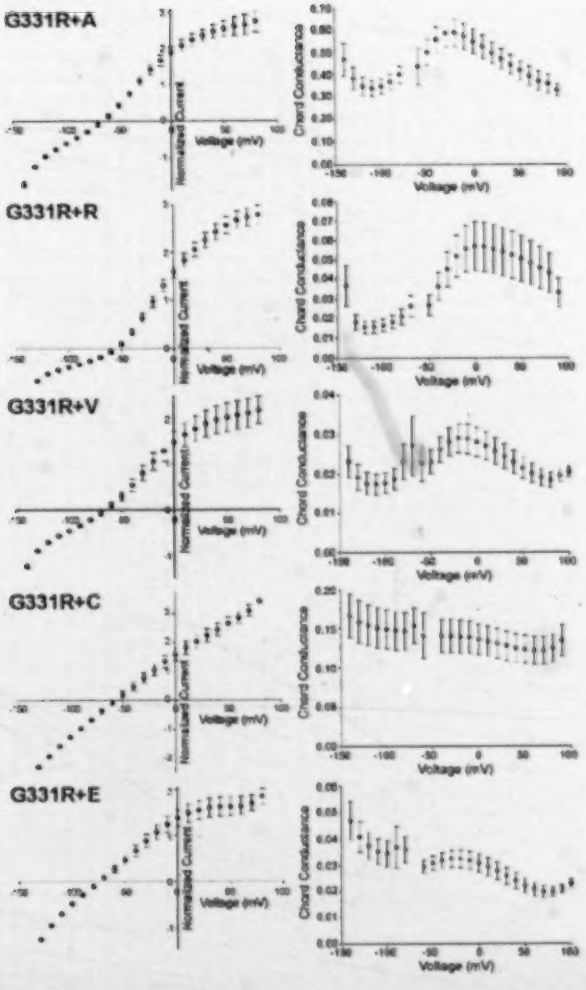

Figure 5-5: The addition of arginine at a central position is not sufficient to maintain a delayed rectifier phenotype when paired with small residues in R1.
The addition of a single basic residue at position G331 was sufficient to recover a delayed rectifier phenotype. However, when paired with residue changes at the N-terminal end of the S4, a new phenotype of channel behaviour is observed, a biphasic inward rectifier. These channels, G331R+V, G331R+R, G331R+A all have the W-shaped conductance profile that suggests that at hyperpolarized potentials there is less conductance than the peak conductance that occurs at a more moderate voltage.

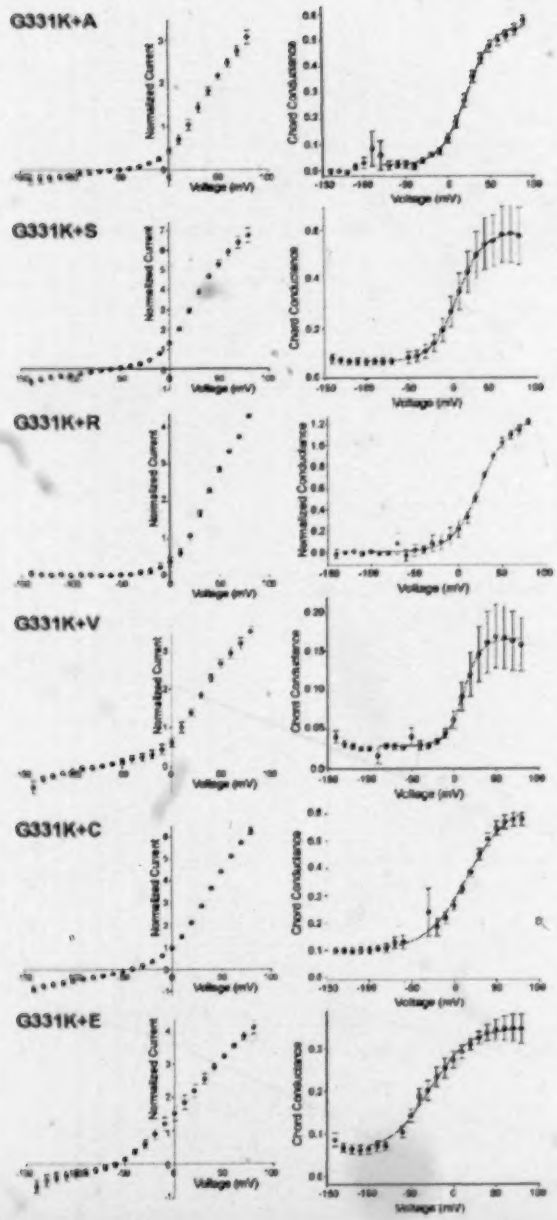

Figure 5-6: The combination of G331K with small H325 mutations created a channel that uses the gating pore at hyperpolarized potentials and the canonical pore at depolarized potentials.

The only double mutant channel that created a solely delayed rectifier was G331K+R that had left-shifted voltage sensitivity compared to the G331K single mutant alone. The proportion of the Omega current to the efflux of current through the pore was very small.

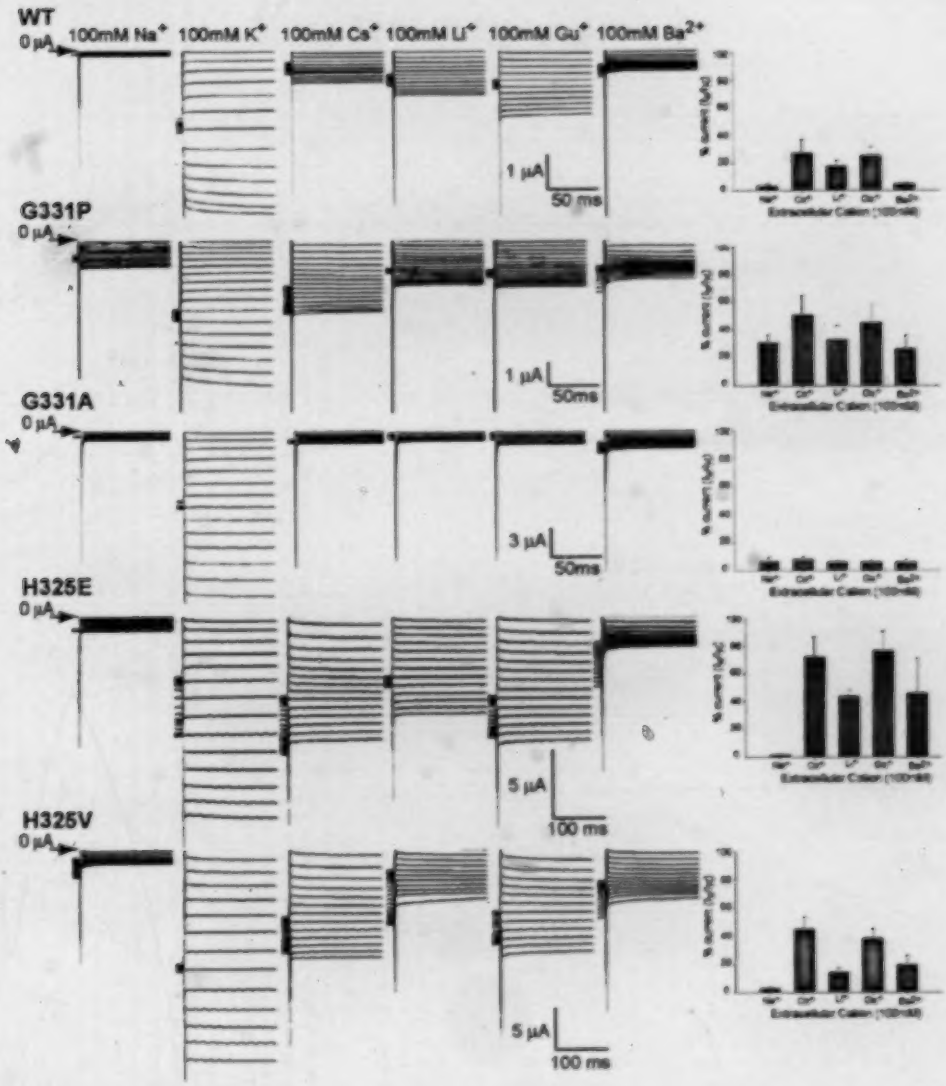

Figure 5-7: Mutations at R1 or R3 change the permeation profile of *N.ai-K$_v$3.2*
A single permeability experiment showing only the inward currents using the protocol described in Chapter 2. A perfusion experiment was performed changing the single cation (x= monovalent cations; K^+, Li^+, Cs^+, Gu^+ (guandinium), Na^+, or Ba^{2+}) present in the bath (in mM, xCl 100; HEPES 10, EDTA 1). A noticeable inward current was observed for all cations tested, including the known K-channel blockers Cs^+ and Ba^{2+}. The inset graph shows the percent cation current passing at -140mV compared to the large influx of potassium at the same voltage step (I_x/I_k *100).

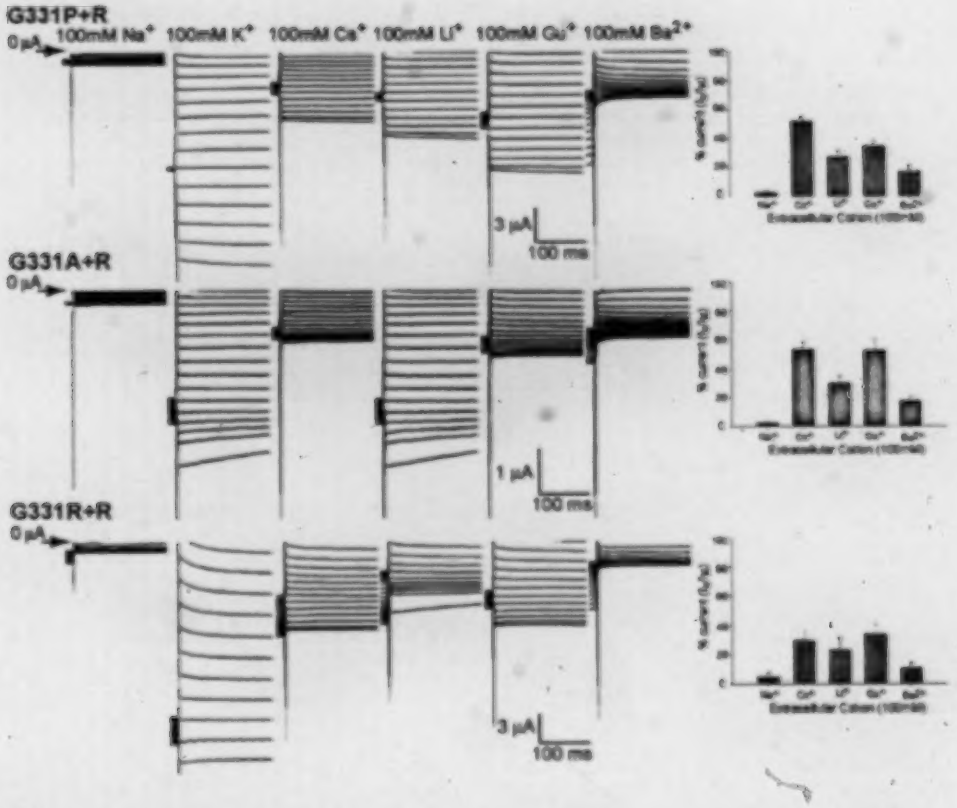

Figure 5-8 Mutations at R1 and R3 in *N.at-K$_v$3.2* change both accessibility to the permeation path and the shape of the gating pore pathway.
A single permeability experiment showing only the inward currents using the protocol described in Chapter 2. A perfusion experiment was performed changing the single cation (x= monovalent cations; K^+, Li^+, Cs^+, Gu^+ (guandinium), Na^+, or Ba^{2+}) present in the bath (in mM, xCl 100; HEPES 10, EDTA 1). A noticeable inward current was observed for all cations tested, including the known K-channel blockers Cs^+ and Ba^{2+}. The inset graph shows the percent cation current passing at -140mV compared to the large influx of potassium at the same voltage step (I_x/I_k *100).

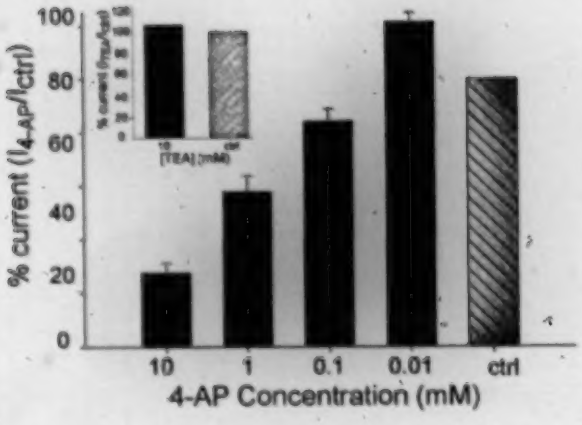

Figure 5-9: 4-aminopyridine blocks the alternative permeation pathway in *N.at-K*$_{\alpha}$*3.2*.
This graph represents the average of 5 individual dose-response perfusion experiments where 4-AP was perfused into the extracellular solution, and the channel was acclimated for 2 minutes before the standard protocol was run. Blockage of the permeation pathway by 4-AP was reversible. The inset is the average of 5 individual experiments where 10mM TEA was perfused into the extracellular bath. The channel was acclimated for 2 minutes prior to voltage protocols being performed. There was no observable change in current flow at hyperpolarized potentials in the presence or absence of TEA.

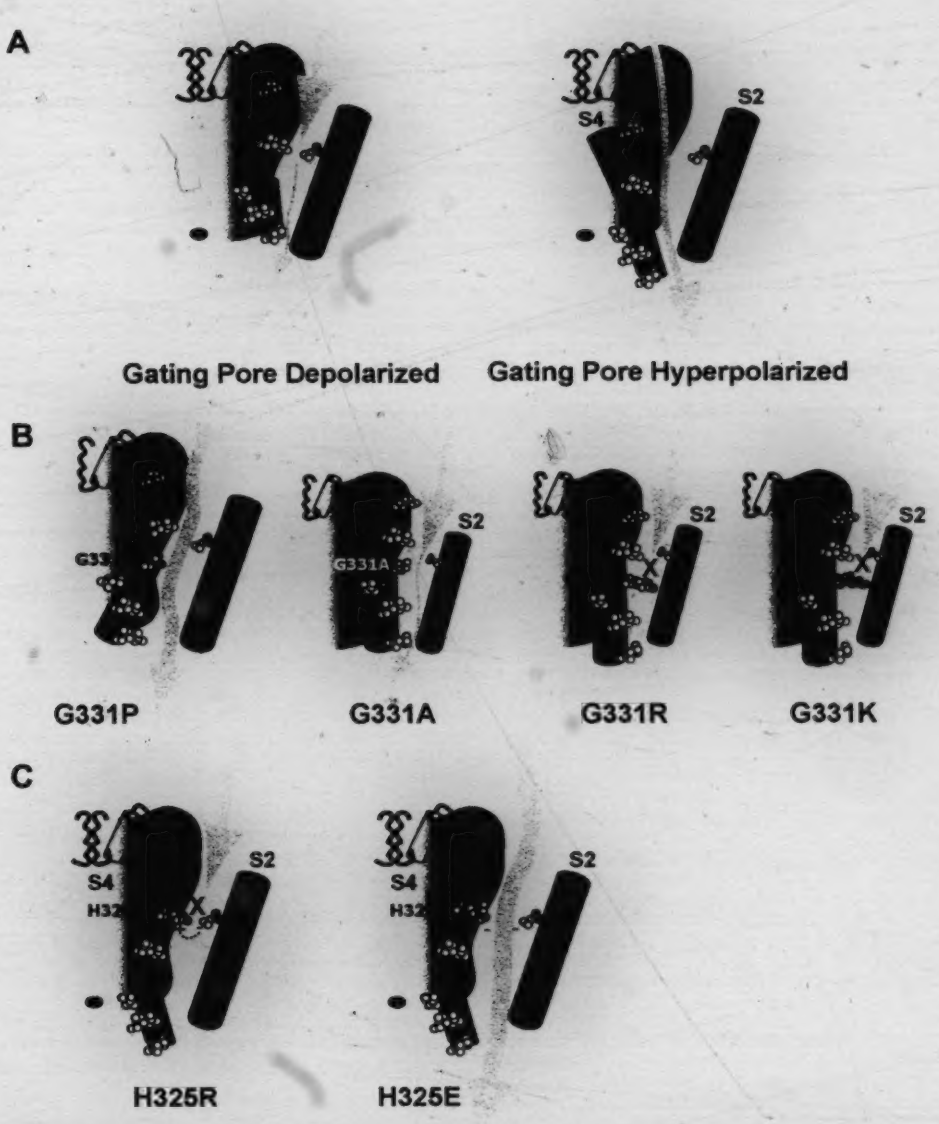

Figure 5-10: Cartoon depicting our current hypothesis of how the Omega current flowing through the gating pore in both the open and closed conformations.
A. The combination of two mutations in the S4 helix allow permeation of cations in both the voltage-dependent "open" and "closed" states of *N.at-K_v3.2.*
B. Mutations at G331 (G331P and G331A) change the shape and conductance of ions through the gating pore channel, or block the pore and create typical delayed rectifiers (G331R and G331K)
C. Mutations of H325 can create delayed rectifiers (H325R/A/S/C) or change the accessibility and permeation properties of the gating pore (H325E and V).

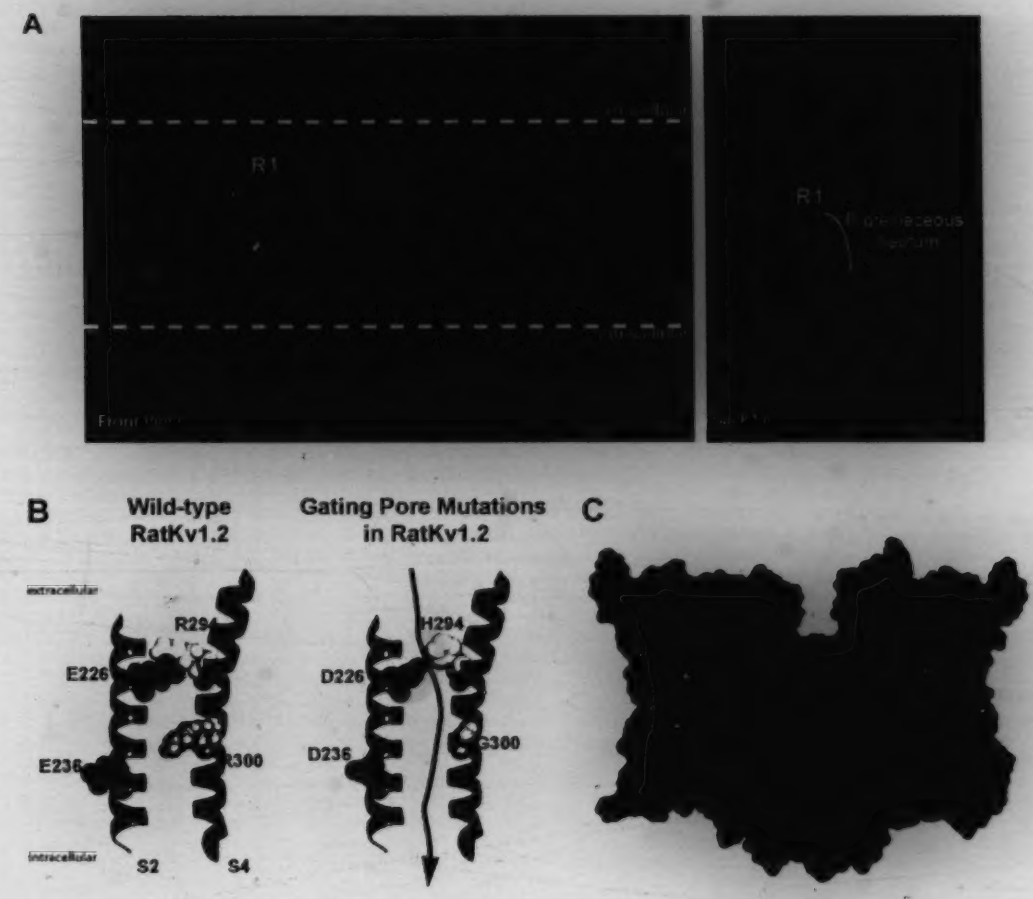

Figure 5-11: Location of residues in *RatK$_v$1.2* that form the gating pore in *N.at-K$_v$3.2*.

A. Structural location of the gating pore (red) in the closed state homology model of *RatK$_v$1.2* (Yarov-Yarovy et al. 2006). The individual panels show the tetrameric channel as observed from the front and back of a single subunit, with contributing residues from S2 (E226 green) and S4 (R1 yellow; R3 orange) highlighted.

B. The structural contributions of the S2 and S4 helices to the gating pore are shown to emphasize absence of interactions that block the gating pore in *N.at-K$_v$3.2*. Ribbon diagrams modeling the block of the gating pore in wild-type *RatK$_v$1.2* and modeled residues in *RatK$_v$1.2* that form the gating pore in *N.at-K$_v$3.2*.

C. Surface accessibility of the gating pore and contributions of S2 (purple) and S4 (teal) helices to the gating pore in the tetrameric channel as shown in ribbon form in B.

CHAPTER 6: DISCUSSION

6.1 TOWARDS A GENERAL MODEL OF CHANNEL FUNCTION

Members of the Shaker-superfamily of voltage-gated (K_v) ion channels are major determinants of the electrical phenotype of excitable cells such as neurons, myocytes, and some epithelial cells. These channels detect changes in transmembrane voltages and become activated through a conformational change that opens the activation gate, allowing ions to pass through a selective pore. The voltage sensitivities of activation and inactivation are critical to the role that these channels play in shaping action potentials and modifying the firing properties of neurons and other excitable cells (Connor and Stevens 1971; Przysiezniak and Spencer 1994). This superfamily has its origins in the early metazoans (Jegla et al. 1995) and their consequent functional radiation was presumably in response to selection for a variety of electrical phenotypes, especially within neuronal lineages. These phenotypes include: slow repetitive firing (Connor and Stevens 1971), high frequency firing (Erisir et al. 1999), rhythmical firing (Wu et al. 2001), oscillating membrane potentials (Huguenard and McCormick 1992), and action potential duration and shape changes (Spencer et al. 1989).

The essential physiological role of K_v channels ensures that regions of the channel required for function, like the S4 voltage sensor and the highly selective pore, are conserved, and are readily identifiable in comparative sequence analysis. However, the range of function observed for K_v channels cannot be explained solely by changes within these highly conserved regions. Thus, structure-function analysis can provide valuable insight into the roles of specific domains and function of residues within the channel protein, identifying those structures responsible for the biophysical properties of a specific channel.

With the plerethora of structure-function data currently available, there is movement towards a unified model of the mechanism of K_v channel function. However, it is difficult to reconcile all structure-function data into a single cohesive model of channel function because of conflicting experimental data. It is important to recognize that regardless of *a priori* assumptions, any structure-function analysis performed is channel specific, and is only truly informative of the structural basis of function within

that channel. It is the integration of these multiple experimental datasets, obtained using a range of techniques, that provides more accurate models of channel behavior. Thus, the accuracy of generalized models of channel behavior improves with increased structure/function studies, and the broad applicability of these models can be improved by extending the range of channel upon which the model is based. In my work, I have performed an integrative comparative structure/function analysis and have determined the applicability of the current models of the mechanism of K_v channel function to invertebrate channels. By contributing a large experimental dataset focusing on the interactions, spatial orientation, and protein packing in the voltage-sensing domain, the current model of channel function can be further refined to encompass the larger range of channel function apparent in invertebrate channels.

Here I have explored the underlying structural interactions within voltage-sensing domains (S1-S4) of two invertebrate channels, *jShak1* and *N.at-K_v3.2*. Comparative analysis of these channels shows a similarity in structure to model organisms, and the extensively studied medically interesting channels. Thus the generalized models of channel behavior based on the structure/function studies in the previously characterized channels, like *Shaker* and *RatK_v1.2*, should be applicable to the invertebrate channels. To test the ability of the current model of channel behavior to explain invertebrate channel function, I selected combined a number of structure/function tools; phylogenetic analysis, mutagenesis, Gibbs free energy analysis, permeability studies and homology modeling.

As demonstrated in *Shaker*, the relative stabilities of the open vs. closed conformation of the channel can be greatly modified with changes in the electrostatic interactions between the S2 and S4 helices. These interactions clearly described the structural basis of the right-shifted voltage sensitivity *jShak1*, where channel is more affected by the lack of an acidic residue within S2, than the lack of a triplet charged motif within S4. However, the current model of channel function failed to describe the modifications of *jShak1* voltage-sensitivity resulting from changes in the charge content and length of the S4 helix. I believe that disruption in the non-electrostatic interactions between the S4 voltage sensor and surrounding helices shifted the relative stability of the open state of the channel to a greater extent than new electrostatic salt-bridges between S2 and S4 stabilized it. In the absence of an additional charged motif in S4, the most

stabilization arose from the addition of a longer glutamate side chain (N227E) in S2, while in channels with increased length and charge in S4, steric hindrances between helices favored the increased stability of the open state by the addition of the shorter aspartate residue (N227D). These favorable interactions are based on protein packing and are extremely channel specific because of the co-evolution of the protein helices within the channel that co-varied to allow for gradations in channel function. These results support the current model of stabilizing electrostatic interaction between the S4 and surrounding protein which form, break and reform during voltage sensor movement and provide us with an indication of how close the packing tolerances are in the voltage-sensing domain.

While a conserved architecture of the pore domain is observed for 2TM, 6TM and 24TM channels, and a conservation of function exists, specifically the regulation of cation flow through a selective pore, the diversity of phenotypes observed for invertebrate channels suggests that although the architecture of the channel is a shared basic plan, variations on that plan can yield a spectrum of specialized functions. In our characterization of two novel invertebrate channels, *N.at-K_v3.1* and *N.at-K_v3.2*, we found a slow-delayed rectifier and a weak inward rectifier. Neither channel phenotype was obvious from a simple comparison of aligned sequences, where both channels have similar charge content in S2 and S3 compared to other K_v channels, and the voltage sensor in *N.at-K_v3.1*contained identical charge content as *Shaker*. The structural basis for weak inward rectification in *N.at-K_v3.2* is different from the only other inwardly rectifying K_v channel, *Exp2*, a *Shab* channel from *C. elegans*. The structure of the *N.at-K_v3.2* channel protein allows for an alternative permeation pathway in *N.at-K_v3.2* external to the highly conserved pore, which allows the non-selective Omega current to flow. This permeation pathway, is bounded by the S2 and S4 helices, where the non-basic residue in position R1 allows access to the aqueous gating pore when the voltage sensor is at rest, presumably through a lack of contribution to a proteinaceous septum dividing the intracellular and extracellular gating pore vestibules. However, the lack of a voltage-gated channel crystallized in the closed conformation limits our understanding of the structural interactions and proximity of the helices in the closed state, and homology modeling of non-K_v1 channels on *RatK_v1.2* present difficulties because of the substantial

sequence differences between subfamilies. Moreover, the structural flexibility of the glycine residue at a central position in the voltage sensor, G331, allows flexibility and may affect close helical packing of the voltage sensor during conformational changes within the pathway, requiring molecular dynamics studies to identify the position and packing of residues within the voltage sensor, and the arrangement of adjacent helices.

6.2 CONSIDERATIONS FOR *IN VIVO* APPLICATIONS

While generalized models of channel structure-function relationships can provide valuable insight into the interactions within the channel protein, the applicability of these studies to *in vivo* physiology are limited. Specifically, structure-function studies on K_v channels are performed on homomultimeric channels to minimize the confounding intersubunit interactions. In particular, the ability of channels to heteromultermize with differential stoichometry, and the interactions with beta-subunits *in vivo* creates a multitude of biophysical and pharmacological phenotypes (Abbott et al. 2001; Abbott et al. 2006; Christie et al. 1990; Ottschytsch et al. 2005). For example, homomeric *RabbitK_v1.5* channels expressed in HEK cells do not exhibit a voltage-sensitive shift in activation with the application of 4-AP, while *RabbitK_v1.2* do shift with drug treatment. However, heteromultimers of K_v1.5 with K_v1.2 have a shift in the voltage dependence of activation with application of 4-AP, which is similar to K_v1.2 alone (Kerr et al. 2001). Moreover, the endogenous potassium currents in the rabbit portal vein have identical sensitivity to the pharmacological blockers as the heterotetrameric channel protein (Kerr et al. 2001) . Co-immunoprecipitation assays performed on native vascular muscle tissue from both *Rattus norvegicus* (Rat) and *Oryctolagus cuniculus* (Rabbit) show that K_v1.2 and K_v1.5, and K_v1.2beta subunits co-express endogenously giving rise to the potassium current in vascular smooth muscle (Kerr et al. 2001; Plane et al. 2005; Thorneloe et al. 2001).

In addition, the ability to reconcile *in vivo* potassium currents with those of homomeric channels *in vitro* can be further confounded by the expression system used for *in vitro* studies. It has been demonstrated that *Xenopus* oocytes have endogenously expressed mRNA for the modulatory beta subunits, MiRP2, MiRP4.1, MiRP4.2 and MinK. Expression of *hERG* and *KCNQ* currents in oocytes in the presence of endogenous

beta subunits or during siRNA inhibition of the subunits, results in large changes in the biophysical properties of the channel (Anantharam et al. 2003). More recently, endogenous MiRP2 has been demonstrated to affect the expression level dependent changes in channel gating (Gordon et al. 2006).

Because ion channels are integral membrane proteins, they interact with and are stabilized by the surrounding lipid bilayer. Prior to the crystallization of *KvAP*, and the comparison of structural packing of prokaryotic and eukaryotic channels (Richardson et al. 2006), the lipid bilayer was believed to stabilize channel structure through hydrophobic-hydrophilic interactions with the channel protein (Williamson et al. 2003). However, a recent publication from the MacKinnon group (Schmidt et al. 2006), suggests that the composition of the phospholipid bilayer stabilizes the positively charge voltage sensor of *KvAP* through interactions with a counter ion in the membrane, specifically the negatively charged lipid phosphodiester group. These results indicate that in bacterial channels, the interactions between the charged basic repeats of the voltage-sensor and the lipid environment are significant factors in setting the voltage response (Williamson et al. 2003). Thus, the environment in which a channel is expressed and structural interactions external to the channel protein can have large effects on channel function *in vivo*.

6.3 Future Directions

6.3.1 Structural Elements Affecting Voltage-Sensitivity

In our study of the basis of voltage sensitivity in *jShak1* we identified the lack of an acidic S2 residue as the most important factor in shifting the voltage dependence of activation in the hyperpolarized direction. With the recent isolation and characterization of a similar K_v1 channel in the Portuguese Man O'War, *P. physalis*, it appears that the loss of the first acidic residue in S2 in K_v1 channels may be phylum-specific, where all cnidarian K_v1 channels may exhibit this loss (Bouchard et al. 2006). Therefore, isolation and characterization of additional K_v1 channels should elucidate an evolutionary trend in the subfamily, particularly since the K_v3 and K_vA channels from *P. penicillatus* both contain two acidic residues in S2, and the conserved aspartate in S3. Furthermore, by performing similar energetic perturbation analysis in *PpK$_v$1*, which has the most similarity in secondary structure to *jShak1*, including the lack of a triplet charge motif in

S4 and the extremely short S3-S4 linker, it may be possible to further elucidate the structural interactions between the S2 and S4 helices. It is expected that Double Mutant Cycle Analysis will show similar trends between the two channels, where the substitution of an acidic residue in S2 will shift the voltage-sensitivity of activation leftward, and that the longer glutamate side-chain will have favorable interactions with the unmodified S4. Likewise, the effects of the addition of charge and length will be confounded by the limitations to structural packing imposed byby the shortened S3-S4 linker.

6.3.2 Assessing the Changing Shape of the Gating Pore

The underlying structure of the alternative permeation pathway through the gating pore is not well understood. In *Shaker* access to the gating pore is allowed by mutating the first arginine (R1) to residues with smaller side-chains, while in *Na$_V$1.2* current flow through the gating pore requires a double mutation at adjacent basic residues (R2 and R3 or R3 and R4), suggesting that the proteinaceous septa between the extracellular and intracellular aqueous canals have a different shape in these channels. Here we demonstrated that *N.at-K$_V$3.2* has evolved a natural permeation pathway through the gating pore, where both residues at R1 and R3 contribute to the pathway. The size and changing shape of this pathway is difficult to elucidate because the S4 voltage sensor moves in response to changes in transmembrane voltage. Thus, the permeation pathway may reduce from a high conducting state at hyperpolarized potentials to a low conducting state at depolarized potentials, or because this pathway is permeable to a number of cations, the permeation and thus the charge carrying ion may also change with voltage. Thus, performing inside-out patch clamp perfusion experiments in bi-ionic conditions is necessary to accurately determine the conductance profile of a single cation through the channel. Comparisons of these conductance profiles for the different ions at different voltages should further elucidate the shape changes within the gating pore pathway, where changing conductance of a singular ion of a known size can be used as a molecular caliper to determine the size of the pathway. With the large number of structural mutants, both single and double mutants, within the S4, these experiments would provide a large experimental dataset that can form the basis for molecular dynamics studies, and protein

models can be formulated with specific attention to side chain distances as indicated by the changing permeabilities.

6.3.3 Future Studies within the Voltage-Sensing Domain

The structure-function studies performed here have demonstrated that a number of interactions within the voltage-sensing domain shape channel function. Our examination of invertebrate channels has demonstrated the structural flexibility within the K_v channel family that allows a large variation of function from a conserved general architecture. Specifically, we have identified that structural constraint within the channel, as in *jShak1*; with the short S3-S4 linker limits large structural changes in channel packing. We have shown that this structural constraint shifts the closed to open equilibrium with the addition of length and charge to the S4. However, it is also possible that the short S3-S4 linker may also stabilize the channel protein because the short linker requires S3 and S4 helices to be in close proximity such that the loss of a stabilizing electrostatic interaction between the domains (K294Q) does not prevent proper protein packing and export from the ER, as observed for the equivalent mutation in *Shaker* (K374Q). Modifications to the length of the extracellular S3-S4 linker in naturally constrained channels, may allow for the elucidation of the role of the linkers in channel function, specifically, it may be possible to assess the amount of movement of the voltage sensor, by limiting the flexibility of the linker through the reduction in length, or the introduction of a secondary structure like that observed in *Shaker*.

Comparative analysis can identify non-conserved residues between channels, but with current models of channel behavior, it is not obvious how these residues affect channel function. Protein packing that changes both the electrostatic and non-electrostatic interactions within K_v channels has large effects on channel function but cannot be inferred from sequence alone. This is most obvious in *N.at-K_v3.2* where the structural prediction based on sequence similarity would suggest a delayed rectifier with high potassium selectivity, where the reality is much more complex. Here we have demonstrated that channel function can be affected directly through side chain interactions with other helices, which modify protein packing both directly through steric hindrances. Thus, future studies should focus on sites opposite to the charged residue in

the helix and on non-basic residues adjacent to a charged motif. Exhaustive mutagenesis on these sites would be expected to shift the voltage sensitivity of the channel, indicating the extent to which these protein interactions affect channel function. By utilizing the three dimensional homology model it would then be possible to identify residues in the surrounding channel protein that may interact with these residues in S4 that would not have been identified by comparative sequence analysis alone. These residues in close proximity in the channel protein, could then be mutated and their contribution to or disruption of channel function can be assessed. Finally, by performing Double Mutant Cycle Analysis on pairwise mutations, it would be possible to determine if the effects of these mutations on channel function are additive, or it they have a combinatorial effect on channel function.

6.4 General Conclusions

Comparative analysis of the single and double S4 *N.at-K$_v$3.2* mutants with the structures of the Omega current mutants in *Shaker* and *Na$_v$1.2* and proton current mutants in *Shaker* demonstrates that conserved protein interactions between the voltage sensor and surrounding helices can be disrupted without destroying the function of the ion selective pore. This corroborates the results of the energetic perturbation analysis in *jShak1*. Effects of major modifications to the channel protein, via the introduction of additional length at a central helical position, were explainable by effects on packing, and modification of the conformational equilibrium. The flexibility within the channel protein suggests that the core function can be quantitatively modified to a minor or major extent by changes in protein packing and structural interactions within the functional domains, and between subunits. The work I have presented here shows that the current general models of the mechanism of voltage-gated channel function have limited applicability to invertebrate channels. The under-representation of non-chordate phyla in the general model and unequal sampling of Shaker channel subfamilies in structure/function studies, fails to accurately represent the range of functional phenotypes possible through modifications to the channel protein. Thus, models based on this dataset are not broadly applicable to other ion channels. The large structure/function dataset I have presented in this study provides necessary information on the packing tolerances within the voltage-

sensing domain, and provides further information about the environment around the S4 voltage sensor, that when reconciled with the current model of channel behavior should advance our understanding of the structural basis of voltage-sensitivity in voltage-gated potassium channels.

CHAPTER 7: REFERENCES

Abbott GW, Butler MH, Bendahhou S, Dalakas MC, Ptacek LJ, and Goldstein SA. MiRP2 forms potassium channels in skeletal muscle with Kv3.4 and is associated with periodic paralysis. *Cell* 104: 217-231, 2001.

Abbott GW, Butler MH, and Goldstein SA. Phosphorylation and protonation of neighboring MiRP2 sites: function and pathophysiology of MiRP2-Kv3.4 potassium channels in periodic paralysis. *Faseb J* 20: 293-301, 2006.

Abbott GW and Goldstein SA. A superfamily of small potassium channel subunits: form and function of the MinK-related peptides (MiRPs). *Q Rev Biophys* 31: 357-398, 1998.

Accili EA, Kuryshev YA, Wible B, and Brown AM. Separable effects of human Kvbeta1.2 N- and C-termini on inactivation and expression of human Kv1.4. *J Physiol* 512: 325-336, 1998.

Acharya KR and Lloyd MD. The advantages and limitations of protein crystal structures. *Trends in Pharmacol Sc* 26: 10-14, 2005.

Adachi J and Hasegawa M. MOLPHY Version 2.3, Programs for molecular phylogenetics based on maximum likelihood. *Computer Science Monographs* 28, 1996.

Aggarwal SK and MacKinnon R. Contribution of the S4 segment to gating charge in the Shaker K+ channel. *Neuron* 16: 1169-1177, 1996.

Ahern CA, Eastwood AL, Lester HA, Dougherty DA, and Horn R. A Cation-{pi} Interaction between Extracellular TEA and an Aromatic Residue in Potassium Channels. *J Gen Physiol* 128: 649-657, 2006.

Ahern CA and Horn R. Focused electric field across the voltage sensor of potassium channels. *Neuron* 48: 25-29, 2005.

Aiyar J, Rizzi JP, Gutman GA, and Chandy KG. The signature sequence of voltage-gated potassium channels projects into the external vestibule. *J Biol Chem* 271: 31013-31016, 1996.

Altschul SF, Madden TL, Schaffer AA, Zhang J, Zhang Z, Miller W, and Lipman DJ. Gapped BLAST and PSI-BLAST: a new generation of protein database search programs. *Nucleic Acids Res* 25: 3389-3402., 1997.

Anantharam A, Lewis A, Panaghie G, Gordon E, McCrossan ZA, Lerner DJ, and Abbott GW. RNA interference reveals that endogenous Xenopus MinK-related peptides govern mammalian K+ channel function in oocyte expression studies. *J Biol Chem* 278: 11739-11745, 2003.

Anderson PA and Greenberg RM. Phylogeny of ion channels: clues to structure and function. *Comp Biochem Physio B Biochem Mol Biol* 129: 17-28, 2001.

Armstrong CM. Voltage-dependent ion channels and their gating. *Trends Neurosci* 15: 403-408, 1992.

Asamoah OK, Wuskell JP, Loew LM, and Bezanilla F. A fluorometric approach to local electric field measurements in a voltage-gated ion channel. *Neuron* 37: 85-97, 2003.

Ausubel FM, Brent R, Kingston RE, Moore DD, Seidman JG, Smith JA, and Struhl K. Current Protocols in Molecular Biology. New York: John Wiley & Sons, 1987.

Baker OS, Larsson HP, Mannuzzu LM, and Isacoff EY. Three transmembrane conformations and sequence-dependent displacement of the S4 domain in shaker K+ channel gating. *Neuron* 20: 1283-1294, 1998.

Bao H, Hakeem A, Henteleff M, Starkus JG, and Rayner MD. Voltage-insensitive gating after charge-neutralizing mutations in the S4 segment of Shaker channels. *J Gen Physiol* 113: 139-151, 1999.

Barlow DJ and Thornton JM. Helix geometry in proteins. *J Mol Biol* 201: 601-619, 1988.

Berneche S and Roux B. Energetics of ion conduction through the K+ channel. *Nature* 414: 73-77, 2001.

Berneche S and Roux B. A microscopic view of ion conduction through the K+ channel. *Proc Natl Acad Sci U S A* 100: 8644-8648, 2003.

Bezanilla F. The voltage sensor in voltage-dependent ion channels. *Physiol Rev* 80: 555-592, 2000.

Bezanilla F, Perozo E, and Stefani E. Gating of Shaker K+ channels: II. The components of gating currents and a model of channel activation. *Biophys J* 66: 1011-1021, 1994.

Blair KL and Anderson PAV. Properties of voltage-activated ionic currents in cells from the brains of the triclad flatworm, Bdelloura candida. *J Exp Biol* 185: 267-286, 1993.

Blunck R, Cordero-Morales JF, Cuello LG, Perozo E, and Bezanilla F. Detection of the opening of the bundle crossing in KcsA with fluorescence lifetime spectroscopy reveals the existence of two gates for ion conduction. *J Gen Physiol* 128: 569-581, 2006.

Bouchard C, Price RB, Moneypenny CG, Thompson LF, Zillhardt M, Stalheim L, and Anderson PA. Cloning and functional expression of voltage-gated ion channel subunits from cnidocytes of the Portuguese Man O'War Physalia physalis. *J Exp Biol* 209: 2979-2989, 2006.

Bright JN and Sansom MS. Kv channel S6 helix as a molecular switch: simulation studies. *IEE Proc Nanobiotechnol* 151: 17-27, 2004.

Bright JN, Shrivastava IH, Cordes FS, and Sansom MS. Conformational dynamics of helix S6 from Shaker potassium channels: simulation studies. *Biopolymers* 64: 303-313, 2002.

Broomand A, Mannikko R, Larsson HP, and Elinder F. Molecular movement of the voltage sensor in a K channel. *J Gen Physiol* 122: 741-748, 2003.

Buckingham SD and Spencer AN. K(+) currents in cultured neurones from a polyclad flatworm. *J Exp Biol* 203: 3189-3198, 2000.

Buckingham SD and Spencer AN. Role of high-voltage activated potassium currents in high-frequency neuronal firing: evidence from a Basal metazoan. *J Neurophysiol* 88: 861-868, 2002.

Carlson JE, Tulsieram LK, Nance WL, and Menozzi P. Segregation of random amplified DNA markers in F1 progeny of conifers. *Theo App Gen* 83: 194-200, 1991.

Catterall WA. Cellular and molecular biology of voltage-gated sodium channels. *Physiol Rev* 72: S15-S48, 1992.

Catterall WA. Structure and function of voltage-gated sodium and calcium channels. *Curr Opin Neurobiol* 1: 5-13, 1991.

Catterall WA, Schmidt JW, Messner DJ, and Feller DJ. Structure and biosynthesis of neuronal of sodium channels. *Ann N Y Acad Sci* 479: 186-203, 1986.

Cha A, Snyder GE, Selvin PR, and Bezanilla F. Atomic scale movement of the voltage-sensing region in a potassium channel measured via spectroscopy. *Nature* 402: 809-813, 1999.

Chakrabartty A, Schellman JA, and Baldwin RL. Large differences in the helix propensities of alanine and glycine. *Nature* 351: 586-588, 1991.

Chanda B, Asamoah OK, Blunck R, Roux B, and Bezanilla F. Gating charge displacement in voltage-gated ion channels involves limited transmembrane movement. *Nature* 436: 852-856, 2005.

Chou PY and Fasman GD. Conformation parameters for amino acids in helical, beta-sheet, and random coil regions calculated from proteins. *Biochem* 13: 211-222, 1974.

Chou PY and Fasman GD. Prediction of protein conformation. *Biochem* 13: 222-245, 1974.

Christie MJ, North RA, Osborne PB, Douglass J, and Adelman JP. Heteropolymeric potassium channels expressed in Xenopus oocytes from cloned subunits. *Neuron* 2: 405-411, 1990.

Cole KC and Moore J. Potassium ion current in the squid giant axon:dynamic characteristics. *Biophys J* 1: 1-14, 1960.

Connor JA and Stevens CF. Prediction of repetitive firing behaviour from voltage clamp data on an isolated neurone soma. *J Physiol* 213: 31-53, 1971.

Cordero-Morales JF, Cuello LG, and Perozo E. Voltage-dependent gating at the KcsA selectivity filter. *Nat Struct Mol Biol* 13: 319-322, 2006.

Covarrubias M, Wei A, and Salkoff L. Shaker, Shal, Shab, and Shaw express independent K+ current systems. *Neuron* 7: 763-773, 1991.

Covarrubias M, Wei A, Salkoff L, and Vyas TB. Elimination of rapid potassium channel inactivation by phosphorylation of the inactivation gate. *Neuron* 13: 1403-1412, 1994.

Darman RB, Ivy AA, and Blaustein RO. Constraints on voltage sensor movement in the shaker k+ channel. *J Gen Physiol* 128: 687-699, 2006.

Day TA, Kim E, Bennett JL, and Pax RA. Analysis of the kinetics and voltage-dependency of transient and delayed K+ currents in muscle fibers isolated from the flatworm Schistosoma mansoni. *Comp Biochem Physiol A Physiol* 111: 79-87, 1995.

Del Camino D, Kanevsky M, and Yellen G. Status of the intracellular gate in the activated-not-open state of Shaker K+ channels. *J Gen Physiol* 126: 419-428, 2005.

Del Camino D and Yellen G. Tight steric closure at the intracellular activation gate of a voltage-gated K(+) channel. *Neuron* 2001: 4, 2001.

Derst C and Karschin A. Evolutionary link between prokaryotic and eukaryotic K+ channels. *J Exp Biol* 201: 2791-2799, 1998.

Deutsch C. Potassium channel ontogeny. *Annu Rev Physiol* 64: 19-46, 2002.

Ding S, Ingleby L, Ahern CA, and Horn R. Investigating the putative glycine hinge in shaker potassium channel. *J Gen Physiol* 126: 213-226, 2005.

Domene C, Doyle DA, and Venien-Bryan C. Modeling of an ion channel in its open conformation. *Biophys J* 89: L01-03, 2005.

Domene C and Sansom MS. Potassium channel, ions, and water: simulation studies based on the high resolution X-ray structure of KcsA. *Biophys J* 85: 2787-2800, 2003.

Dominguez I, Itoh K, and Sokol SY. Role of glycogen synthase kinase 3 beta as a negative regulator of dorsoventral axis formation in Xenopus embryos. *Proc Natl Acad Sci U S A* 92: 8498-8502, 1995.

Doyle DA, Cabral JM, Pfuetzner RA, Kuo A, Gulbis JM, Cohen SL, Chait BT, and MacKinnon R. The structure of the potassium channel: molecular basis of K+ conduction and selectivity. *Science* 280: 69-77, 1998.

Durell SR, Hao Y, and Guy HR. Structural models of the transmembrane region of voltage-gate and other K+ channels in open, closed and inactivated conformations. *J Struc Biol* 121: 263-284, 1998.

Durell SR, Shrivastava IH, and Guy HR. Models of the structure and voltage-gating mechanism of the shaker K+ channel. *Biophys J* 87: 2116-2130, 2004.

Edgar RC. MUSCLE: a multiple sequence alignment method with reduced time and space complexity. *BMC Bioinformatics* 5: 113, 2004.

Edgar RC. MUSCLE: multiple sequence alignment with high accuracy and high throughput. *Nucleic Acids Res* 32: 1792-1797, 2004.

Elinder F, Mannikko R, and Larsson HP. S4 charges move close to residues in the pore domain during activation in a K channel. *J Gen Physiol* 118: 1-10, 2001.

Erisir A, Lau D, Rudy B, and Leonard CS. Function of specific K(+) channels in sustained high-frequency firing of fast-spiking neocortical interneurons. *J Neurophysiol* 82: 2476-2489, 1999.

Fanger CM, Ghanshani S, Logsdon NJ, Rauer H, Kalman K, Zhou J, Beckingham K, Chandy KG, Cahalan MD, and Aiyar J. Calmodulin mediates calcium-dependent activation of the intermediate conductance
KCa channel, IKCa1. *J Biol Chem* 274: 5764-5754, 1999.

Fedida D, Maruoka ND, and Lin S. Modulation of slow inactivation in human cardiac Kv1.5 channels by extra- and intracellular permeant cations. *J Physiol* 515: 315-329, 1999.

Felsenstein J. PHYLIP (Phylogeny Inference Package) (3.57 ed.). Seattle: Department of Genetics, University of Washington, 1995.

Fitch WM and Margoliash E. Construction of phylogenetic trees. *Science* 155: 279-284, 1967.

Fleischhauer R, Davis MW, Dzhura I, Neely A, Avery L, and Joho RH. Ultrafast inactivation causes inward rectification in a voltage-gated K(+) channel from Caenorhabditis elegans. *J Neurosci* 20: 511-520, 2000.

Fleishman SJ, Yifrach O, and Ben-Tal N. An evolutionarily conserved network of amino acids mediates gating in voltage-dependent potassium channels. *J Mol Biol* 340: 307-318, 2004.

French RJ and Shoukimas JJ. An ion's view of the potassium channel. The structure of the permeation pathway as sensed by a variety of blocking ions. *J Gen Physiol* 85: 669-698, 1985.

Gandhi CS, Clark E, Loots E, Pralle A, and Isacoff EY. The orientation and molecular movement of a k(+) channel voltage-sensing domain. *Neuron* 40: 515-525, 2003.

Glauner KS, Mannuzzu LM, Gandhi CS, and Isacoff EY. Spectroscopic mapping of voltage sensor movement in the Shaker potassium channel. *Nature* 402: 813-817, 1999.

Goldstein SA. A structural vignette common to voltage sensors and conduction pores: canaliculli. *Neuron* 16: 717-722, 1996.

Goldstein SA, Price LA, Rosenthal DN, and Pausch MH. ORK1, a potassium-selective leak channel with two pore domains cloned from Drosophila melanogaster by

expression in Saccharomyces cerevisiae. *Proc Natl Acad Sci U S A* 93: 13256-13261, 1999.

Gonzalez C, Rosenman E, Bezanilla F, Alvarez O, and Latorre R. Periodic perturbations in Shaker K+ channel gating kinetics by deletions in the S3-S4 linker. *Proc Natl Acad Sci U S A* 98: 9617-9623, 2001.

Gordon E, Roepke TK, and Abbott GW. Endogenous KCNE subunits govern Kv2.1 K+ channel activation kinetics in Xenopus oocyte studies. *Biophys J* 90: 1223-1231, 2006.

Grabe M, Bichet D, Qian X, Jan YN, and Jan LY. K+ channel selectivity depends on kinetic as well as thermodynamic factors. *Proc Natl Acad Sci U S A* 103: 14361-14366, 2006.

Grigoriev NG, Spafford JD, Gallin WJ, and Spencer AN. Voltage sensing in jellyfish Shaker K+ channels. *J Exp Biol* 200: 2919-2926, 1997.

Gross A and MacKinnon R. Agitoxin footprinting the shaker potassium channel pore. *Neuron* 16: 399-406, 1996.

Grottesi A, Domene C, Hall B, and Sansom MS. Conformational dynamics of M2 helices in KirBac channels: helix flexibility in relation to gating via molecular dynamics simulations. *Biochem* 44: 14586-14594, 2005.

Guex N and Peitsch MC. SWISS-MODEL and the Swiss-Pdb Viewer: an environment for comparative protein modeling. *Electrophoresis* 18: 2714-2723, 1997.

Gutman GA, Chandy KG, Adelman JP, Aiyar J, Bayliss DA, Clapham DE, Covarriubias M, Desir GV, Furuichi K, Ganetzky B, Garcia ML, Grissmer S, Jan LY, Karschin A, Kim D, Kuperschmidt S, Kurachi Y, Lazdunski M, Lesage F, Lester HA, McKinnon D, Nichols CG, O'Kelly I, Robbins J, Robertson GA, Rudy B, Sanguinetti M, Seino S, W. S, Tamkun MM, Vandenberg CA, Wei A, Wulff H, and Wymore R. International Union of Pharmacology. XLI. Compendium of voltage-gated ion channels: potassium channels. *Pharm Rev* 55: 583-586, 2003.

Hackos DH, Chang TH, and Swartz KJ. Scanning the intracellular S6 gate in the shaker K+ channel. *J Gen Physiol* 119: 521-532, 2002.

Harris RE, Larsson HP, and Isacoff EY. A permeant ion binding site located between two gates of the Shaker K+ channel. *Biophys J* 74: 1808-1820, 1998.

Heginbotham L, Lu Z, Abramson T, and MacKinnon R. Mutations in the K+ channel signature sequence. *Biophys J* 66: 1061-1067, 1994.

Holman MA and Anderson PAV. Voltage-activated ionic currents in myoepithelial cells isolated from the sea anemone Calliactis tricolor. *J Exp Biol* 161: 333-346, 1991.

Hong KH and Miller C. The lipid-protein interface of a Shaker K(+) channel. *J Gen Physiol* 115: 51-58, 2000.

Hopkins WF, Demas V, and Tempel BL. Both N- and C-terminal regions contribute to the assembly and functional expression of homo- and heteromultimeric voltage-gated K+ channels. *J Neurosci* 14: 1385-1393, 1994.

Horovitz A. Double-mutant cycles: a powerful tool for analyzing protein structure and function. *Fold Des* 1: R121-126, 1996.

Hoshi T, Zagotta WN, and Aldrich RW. Biophysical and molecular mechanisms of Shaker potassium channel inactivation. *Science* 250, 1990.

Huang HY, Liao CW, Chen PH, and Tsaur ML. Transient expression of A-type K channel alpha subunits kv3.2 and Kv4.3 in rat spinal neurons during development. *Eur J Neurosci* 23: 1142-1150, 2006.

Huang QQ, Harvey CM, Paterson ARP, and Young JD. Functional expression of Na+-dependent nucleoside transport systems of rat intestine in isolated oocytes of Xenopus laevis. *J Biol Chem* 268: 20613-20619, 1993.

Huguenard JR and McCormick DA. Simulation of the currents involved in rhythmic oscillations in thalamic relay neurons. *J Neurophysiol* 68: 1373-1383, 1992.

Hurst RS, Latorre R, Toro L, and Stefani E. External barium block of Shaker potassium channels: evidence for two binding sites. *J Gen Physiol* 106: 1069-1087, 1995.

Islas LD and Sigworth FJ. Electrostatics and the gating pore of Shaker potassium channels. *J Gen Physiol* 117: 69-89, 2001.

Islas LD and Sigworth FJ. Voltage sensitivity and gating charge in Shaker and Shab family potassium channels. *J Gen Physiol* 114: 723-742, 1999.

Jan LY and Jan YN. Tracing the roots of ion channels. *Cell* 69: 715-719, 1992.

Jan LY and Jan YN. Voltage-gated and inwardly rectifying potassium channels. *J Physiol* 505 (Pt 2): 267-282, 1997.

Javadpour MM, Eilers M, Groesbeek M, and Smith SO. Helix packing in polytopic membrane proteins: role of glycine in transmembrane helix association. *Biophys J* 77: 1609-1618, 1999.

Jegla T, Grigoriev N, Gallin WJ, Salkoff L, and Spencer AN. Multiple Shaker potassium channels in a primitive metazoan. *J Neurosci* 15: 7989-7999, 1995.

Jegla T and Salkoff L. A Multigene Family Of Novel K+ Channels From Paramecium Tetraurelia. *Receptors and Channels* 3: 51-60, 1995.

Jegla T and Salkoff L. A novel subunit for shal K+ channels radically alters activation and inactivation. *J Neurosci* 17: 32-44, 1997.

Jiang Y, Lee A, Chen J, Cadene M, Chait BT, and MacKinnon R. Crystal structure and mechanism of a calcium-gated potassium channel. *Nature* 417: 515-522, 2002.

Jiang Y, Lee A, Chen J, Cadene M, Chait BT, and MacKinnon R. The open pore conformation of potassium channels. *Nature* 417: 523-526, 2002.

Jiang Y, Lee A, Chen J, Ruta V, Cadene M, Chait BT, and MacKinnon R. X-ray structure of a voltage-dependent K+ channel. *Nature* 423: 33-41, 2003.

Jiang Y and MacKinnon R. The barium site in a potassium channel by x-ray crystallography. *J Gen Physiol* 115: 269-272, 2000.

Jiang Y, Ruta V, Chen J, Lee A, and MacKinnon R. The principle of gating charge movement in a voltage-dependent K+ channel. *Nature* 423: 42-48, 2003.

Johnstone DB, Wei A, Butler A, Salkoff L, and Thomas JH. Behavioral defects in C. elegans egl-36 mutants results from potassium channels shifted in voltage-dependence of activation. *Neuron* 19: 151-164, 1997.

Keenan L and Koopowitz H. Ionic basis of action potentials in identified flatworm neurons. *J Comp Neurol A* 155: 197-208, 1984.

Kerr PM, Clement-Chomienne O, Thorneloe KS, Chen TT, Ishii K, Sontag DP, Walsh MP, and Cole WC. Heteromultimeric Kv1.2-Kv1.5 channels underlie 4-aminopyridine-sensitive delayed rectifier K(+) current of rabbit vascular myocytes. *Circ Res* 89: 1038-1044, 2001.

Kerschbaum HH, Grissmer S, Engle E, Richter K, Lehner C, and Jager H. A Shaker homologue encodes an A-type current in Xenopus laevis. *Brain Res* 927: 55-68, 2002.

Kerschensteiner D, Monje F, and Stocker M. Structural determinants of the regulation of the voltage-gated potassium channel Kv2.1 by the modulatory alpha-subunit Kv9.3. *J Biol Chem* 278: 18154-18161, 2003.

Keynes RD and Elinder F. The screw-helical voltage gating of ion channels. *Proc Biol Sci* 266: 843-852, 1999.

Kim E, Day TA, Bennett JL, and Pax RA. Cloning and functional expression of a Shaker-related voltage-gated potassium channel gene from Schistosoma mansoni (Trematoda: Digenea). *Parasitol* 110: 171-180, 1995.

Kiss L, LoTurco J, and Korn SJ. Contribution of the selectivity filter to inactivation in potassium channels. *Biophys J* 76: 253-263, 1999.

Klapper I, Hagstrom R, Fine R, Sharp K, and Honig B. Focusing of electric fields in the active site of Cu-Zn superoxide dismutase: effects of ionic strength and amino acid modification. *Proteins* 1: 47-59, 1986.

Klassen TL, Buckingham SD, Atherton DM, Dacks JB, Gallin WJ, and Spencer AN. Atypical Phenotypes from Flatworm Kv3 channels. *J Neurophysiol*, 2006.

Kosolapov A and Deutsch C. Folding of the voltage-gated K+ channel T1 recognition domain. *J Biol Chem* 278: 4305-4313, 2003.

Kusano K, Miledi R, and Stinnakre J. Cholinergic and catecholaminergic receptors in the Xenopus oocyte membrane. *J Physiol* 328: 143-170, 1982.

Labro AJ, Raes AL, Bellens I, Ottschytsch N, and Snyders DJ. Gating of shaker-type channels requires the flexibility of S6 caused by prolines. *J Biol Chem* 278: 50724-50731, 2003.

Laine M, Lin MC, Bannister JP, Silverman WR, Mock AF, Roux B, and Papazian DM. Atomic proximity between S4 segment and pore domain in Shaker potassium channels. *Neuron* 39: 467-481, 2003.

Laine M, Papazian DM, and Roux B. Critical assessment of a proposed model of Shaker. *FEBS Lett* 564: 257-263, 2004.

Larsson HP, Baker OS, Dhillon DS, and Isacoff EY. Transmembrane movement of the shaker K+ channel S4. *Neuron* 16: 387-397, 1996.

Larsson HP and Elinder F. A conserved glutamate is important for slow inactivation in K+ channels. *Neuron* 27: 573-583, 2000.

Lecar H, Larsson HP, and Grabe M. Electrostatic model of S4 movement in voltage-gated channels. *Biophys J* 85, 2003.

Ledwell JL and Aldrich RW. Mutations in the S4 region isolate the final voltage-dependent cooperative step in potassium channel activation. *J Gen Physiol* 113: 389-414, 1999.

Lee SY, Lee A, Chen J, and MacKinnon R. Structure of the KvAP voltage-dependent K+ channel and its dependence on the lipid membrane. *Proc Natl Acad Sci U S A* 102: 15441-15446, 2005.

Li-Smerin Y, Hackos DH, and Swartz KJ. alpha-helical structural elements within the voltage-sensing domains of a K(+) channel. *J GenPhys* 115: 33-50, 2000.

Li B and Gallin WJ. Computational identification of residues that modulate voltage sensitivity of voltage-gated potassium channels. *BMC Struct Biol* 5: 16, 2005.

Li B and Gallin WJ. VKCDB: voltage-gated potassium channel database. *BMC Bioinformatics* 5: 3, 2004.

Li SC and Deber CM. Glycine and beta-branched residues support and modulate peptide helicity in membrane environments. *FEBS Lett* 311: 217-220, 1992.

Liman ER, Hess P, Weaver F, and Koren G. Voltage-sensing residues in the S4 region of a mammalian K+ channel. *Nature* 353: 752-756, 1991.

Lin YL, Chen CY, Cheng CP, and Chang LS. Protein-protein interactions of KChIP proteins and Kv4.2. *Biochem Biophys Res Commun* 321: 606-610, 2004.

Loboda A and Armstrong CM. Resolving the gating charge movement associated with late transitions in K channel activation. *Biophys J* 81: 905-916, 2001.

Loboda A, Melishchuk A, and Armstrong CM. Dilated and defunct K channels in the absence of K+. *Biophys J* 80: 2704-2714, 2001.

Logothetis DE, Kammen BF, Lindpaintner K, Bisbas D, and Nadal-Ginard B. Gating charge differences between two voltage-gated K+ channels are due to the specific charge content of their respective S4 regions. *Neuron* 10: 1121-1129, 1993.

Logothetis DE, Movahedi S, Satler C, Lindpaintner K, and Nadal-Ginard B. Incremental reductions of positive charge within the S4 region of a voltage-gated K+ channel result in corresponding decreases in gating charge. *Neuron* 8: 531-540, 1992.

Long SB, Campbell EB, and Mackinnon R. Crystal structure of a mammalian voltage-dependent Shaker family K+ channel. *Science* 309: 897-903, 2005.

Long SB, Campbell EB, and Mackinnon R. Voltage sensor of Kv1.2: structural basis of electromechanical coupling. *Science* 309: 903-908, 2005.

Lopatin AN and Nichols CG. Internal Na+ and Mg2+ blockade of DRK1 (Kv2.1) potassium channels expressed in Xenopus oocytes. Inward rectification of a delayed rectifier. *J Gen Physiol* 103: 203-216, 1994.

Lu Z, Klem AM, and Ramu Y. Coupling between voltage sensors and activation gates in voltage-gated K+ channels. *J Gen Physiol* 120: 663-676, 2002.

Lu Z, Klem AM, and Ramu Y. Ion conduction pore is conserved among potassium channels. *Nature* 413: 809-813, 2001.

MacKinnon R, Cohen SL, Kuo A, Lee A, and Chait BT. Structural conservation in prokaryotic and eukaryotic potassium channels [comment] [see comments]. *Science* 280: 106-109, 1998.

Mannuzzu LM and Isacoff EY. Independence and cooperativity in rearrangements of a potassium channel voltage sensor revealed by single subunit fluorescence. *J Gen Physiol* 115: 257-268, 2000.

Mathur R, Zheng J, Yan Y, and Sigworth FJ. Role of the S3-S4 linker in Shaker potassium channel activation. *J Gen Physiol* 109: 191-199, 1997.

McCormack K, Tanouye MA, Iverson LE, Lin J-W, Ramaswami M, McCormack T, Campanelli JT, Mathew MK, and Rudy B. A role for hydrophobic residues in the voltage-dependent gating of Shaker K+ channels. *Proc Natl Acad Sci U S A* 88: 2931-2935, 1991.

Meech RW and Mackie GO. Potassium channel family in giant motor axons of Aglantha digitale. *J Neurophysiol* 69: 894-901, 1993.

Melishchuk A, Loboda A, and Armstrong CM. Loss of shaker K channel conductance in 0 K+ solutions: role of the voltage sensor. *Biophys J* 75: 1828-1835, 1998.

Miller AG and Aldrich RW. Conversion of a delayed rectifier K+ channel to a voltage-gated inward rectifier K+ channel by three amino acid substitutions. *Neuron* 16: 853-858, 1996.

Miller C. An overview of the potassium channel family. *Genome Biol* 1: REVIEWS0004, 2000.

Monks SA, Needleman DJ, and Miller C. Helical structure and packing orientation of the S2 segment in the Shaker K+ channel. *J Gen Physiol* 113: 415-423, 1999.

Morais Cabral J, Zhou Y, and MacKinnon R. Energetic optimization of ion conduction rate by the K+ selectivity filter. *Nature* 414: 37-42, 2001.

Morales MJ, Castellino RC, Crews AL, Rasmusson RL, and Strauss HC. A novel beta subunit increases rate of inactivation of specific voltage-gated potassium channel alpha subunits. *J Biol Chem* 270: 6272-6277, 1995.

Moulton G, Attwood TK, Parry-Smith DJ, and Packer JC. Phylogenomic analysis and evolution of the potassium channel gene family. 9: 363-377, 2003.

Muller-Rober B, Ellenberg J, Provart N, Willmitzer L, Busch H, Becker D, Dietrich P, Hoth S, and Hendrich R. Cloning and electrophyisological analysis of KST1, an inward rectifying K+ channel expressed in potato guard cells. *EMBO J* 14: 2409-2416, 1995.

Murrell-Lagnado RD and Aldrich RW. Interactions of amino terminal domains of Shaker K channels with a pore blocking site studied with synthetic peptides. *J Gen Physiol* 102: 949-975, 1993.

Nitabach MN, Llamas DA, Thompson IJ, Collins KA, and Holmes TC. Phosphorylation-dependent and phosphorylation-independent modes of modulation of shaker family voltage-gated potassium channels by SRC family protein tyrosine kinases. *J Neurosci* 22: 7913-7922, 2002.

Noda M and Numa S. Structure and function of sodium channel. *J Recept Res* 7: 467-497, 1987.

Noda M, Shimizu S, Tanabe T, Takai T, Kayano T, Ikeda T, Takahashi H, Nakayama H, Kanaoka Y, Minamino N, and et al. Primary structure of Electrophorus electricus sodium channel deduced from cDNA sequence. *Nature* 312: 121-127, 1984.

Noda M, Shimizu S, Tanabe T, Takai T, Kayano T, Ikeda T, Takahashi H, Nakayama H, Kanaoka Y, Minamino N, Kangawa K, Matsuo H, Raftery MA, Hirose T, Inayama S, Hayashida H, Miyata T, and Numa S. Primary structure of

Electrophorus electricus sodium channel deduced from cDNA sequence. *Nature* 312: 121-127, 1984.

O'Neil KT and Degrado WF. A thermodynamic scale for the helix-forming tendencies of the commonly occurring amino acids. *Science* 250: 646-651, 1990.

Ogielska EM and Aldrich RW. Functional consequences of a decreased potassium affinity in a potassium channel pore. Ion interactions and C-type inactivation. *J Gen Physiol* 113: 347-358, 1999.

Ohlenschlager O, Hojo H, Ramachandran R, Gorlach M, and Haris PI. Three-dimensional structure of the s4-s5 segment of the shaker potassium channel. *Biophys J* 82: 2995-3002, 2002.

Olcese R, Sigg D, Latorre R, Bezanilla F, and Stefani E. A conducting state with properties of a slow inactivated state in a shaker K(+) channel mutant. *J Gen Physiol* 117: 149-163, 2001.

Ottschytsch N, Raes AL, Timmermans JP, and Snyders DJ. Domain analysis of Kv6.3, an electrically silent channel. *J Physiol* 568: 737-747, 2005.

Papazian DM, Shao XM, Seoh SA, Mock AF, Huang Y, and Wainstock DH. Electrostatic interactions of S4 voltage sensor in Shaker K+ channel. *Neuron* 14: 1293-1301, 1995.

Papazian DM, Timpe LC, Jan YN, and Jan LY. Alteration of voltage-dependence of Shaker potassium channel by mutations in the S4 sequence. *Nature* 349: 305-310, 1991.

Peitsch MC, Wells TN, Stampf DR, and Sussman JL. The Swiss-3DImage collection and the PDB-Browser on the World-Wide Web. *Trends in Biochem Sci* 20: 82-84, 1995.

Peitsch MC, Wilkins MR, Tonella L, Sanchez JC, Appel RD, and Hochstrasser DF. Large-scale protein modelling and integration with the SWISS-PROT and SWISS-2DPAGE databases: the example of Escherichia coli. *Electrophoresis* 18: 498-501, 1997.

Perozo E. Structure and packing orientation of transmembrane segments in voltage-dependent channels. Lessons from pertubation analysis. *J Gen Physiol* 115: 29-32, 2000.

Perozo E, Santacruz-Toloza L, Stefani E, Bezanilla F, and Papazian DM. S4 mutations alter gating currents of Shaker K channels. *Biophys J* 66: 345-354, 1994.

Plane F, Johnson R, Kerr P, Wiehler W, Thorneloe K, Ishii K, Chen T, and Cole W. Heteromultimeric Kv1 channels contribute to myogenic control of arterial diameter. *Circ Res* 96: 216-224, 2005.

Przysiezniak J and Spencer AN. Voltage-activated potassium currents in isolated motor neurons from the jellyfish Polyorchis penicillatus. *J Neurophysiol* 72: 1010-1019, 1994.

Quattrocki EA, Marshall J, and Kaczmarek LK. A Shab potassium channel contributes to action potential broadening in peptidergic neurons. *Neuron* 12: 73-86, 1994.

Ranatunga KM, Law RJ, Smith GR, and Sansom MS. Electrostatics studies and molecular dynamics simulations of a homology model of the Shaker K+ channel pore. *Eur Biophys J* 30: 295-303, 2001.

Ranganathan R, Lewis JH, and MacKinnon R. Spatial localization of the K+ channel selectivity filter by mutant cycle-based structure analysis. *Neuron* 16: 131-139, 1996.

Rashin AA, Iofin M, and Honig B. Internal cavities and buried waters in globular proteins. *Biochem* 25: 3619-3625, 1986.

Rasmusson RL, Morales MJ, Castellino RC, Zhang Y, Cambell DL, and Strauss HC. C-type inactivation controls recovery in a fast inactivating cardiac K+ channel (Kv1.4) expressed in Xenopus oocytes. *J Physiol* 489: 709-721, 1995.

Richardson J, Blunck R, Ge P, Selvin PR, Bezanilla F, Papazian DM, and Correa AM. Distance measurements reveal a common topology of prokaryotic voltage-gated ion channels in the lipid biliayer. *Proc Natl Acad Sci U S A* 103: 15865-15870, 2006.

Ronquist F and Huelsenbeck JP. MrBayes 3: Bayesian phylogenetic inference under mixed models. *Bioinformatics* 19: 1572-1574, 2003.

Rost B, Liu J, Nair R, Wrzeszczynski KO, and Ofran Y. Automatic prediction of protein function. *Cell Mol Life Sci* 60: 2637-2650, 2003.

Rost B, Yachdav G, and Liu J. The PredictProtein server. *Nucleic Acids Res* 32: W321-326, 2004.

Roux B and Berneche S. On potential functions used in molecular dynamics simulations of ion channels. *Biophys J* 82: 1681-1684, 2002.

Rudy B and McBain CJ. Kv3 channels: voltage-gated K+ channels designed for high-frequency repetitive firing. *Trends Neurosci* 24: 517-526, 2001.

Russ WP and Engleman DM. The GxxxG motif: a framework for transmembrane helix-helix association. *J Mol Biol* 296: 911-919, 2000.

Ruta V, Chen J, and MacKinnon R. Calibrated measurement of gating-charge arginine displacement in the KvAP voltage-dependent K+ channel. *Cell* 123: 463-475, 2005.

Ruta V and MacKinnon R. Localization of the voltage-sensor toxin receptor on KvAP. *Biochem* 43: 10071-10079, 2004.

Sack JT, Aldrich RW, and Gilly WF. A gastropod toxin selectively slows early transitions in the Shaker K channel's activation pathway. *J Gen Physiol* 123: 685-696, 2004.

Saitou N and Nei M. The neighbor-joining method: a new method for reconstructing phylogenetic trees. *Mol Biol Evol* 4: 406-425, 1987.

Salkoff L, Baker K, Butler A, Covarrubias M, Pak MD, and Wei AG. An Essential Set of K+ Channels Conserved in Flies, Mice and Humans. *Trends Neurosci* 15: 161-166, 1992.

Salvador-Recatala V, Gallin WJ, Abbruzzese J, Ruben PC, and Spencer AN. A potassium channel (Kv4) cloned from the heart of the tunicate Ciona intestinalis and its modulation by a KChIP subunit. *J Exp Biol* 209: 731-747, 2006.

Sanguinetti MC, Jiang C, Curran ME, and Keating A. A mechanistic link between an inherited and an aquired cardiac arrhythmia: HERG encodes the IKr potassium channel. *Cell* 81: 229-307, 1995.

Schealy RT, Murphy AD, Ramarathnam R, Jakobsson E, and Subramaniam S. Sequence-function analysis of the K+ selective family of ion channels using a comprehensive alignment and the KcsA channel structure. *Biophys J* 84: 2929-2942, 2003.

Schmidt D, Jiang Q, and MacKinnon R. Phospholipids and the origin of cationic gating charges in voltage sensors. *Nature* 444: 775-779, 2006.

Schmidt HA, Strimmer K, Vingorn M, and von Haeseler A. TREE-PUZZLE: maximum likelihood phylogenetic analysis using quartets and parallel computing. *Bioinformatics* 18: 502-504, 2002.

Scholle A, Koopmann R, Leicher T, Ludwig J, Pongs O, and Benndorf K. Structural elements determining activation kinetics in Kv2.1. *Receptors and Channels* 7: 65-75, 2000.

Schoppa NE, Mccormack K, Tanouye MA, and Sigworth FJ. The size of gating charge in wild-type and mutant shaker potassium channels. *Science* 255: 1712-1715, 1992.

Schoppa NE and Sigworth FJ. Activation of Shaker potassium channels. I. Characterization of voltage-dependent transitions. *J Gen Physiol* 111: 271-294, 1998.

Schoppa NE and Sigworth FJ. Activation of Shaker potassium channels. II. Kinetics of the V2 mutant channel. *J Gen Physiol* 111: 295-311, 1998.

Schoppa NE and Sigworth FJ. Activation of Shaker potassium channels. III: An activation gating model for wild-type and V2 mutant channels. *J Gen Physiol* 111: 313-342, 1998.

Schwede T, Kopp J, Guex N, and Peitsch MC. SWISS-MODEL: An automated protein homology-modeling server. *Nucleic Acids Res* 31: 3381-3385, 2003.

Seoh SA, Sigg D, Papazian DM, and Bezanilla F. Voltage-sensing residues in the S2 and S4 segments of the Shaker K+ channel. *Neuron* 16: 1159-1167, 1996.

Serrano L, Neira JL, Sancho J, and Fersht AR. Effect of alanine versus glycine in alpha-helices on protein stability. *Nature* 356: 453-455, 1992.

Shrivastava IH and Baher I. Common mechanism of pore opening shared by five different potassium channels. *Biophys J* 90: 3929-3940, 2006.

Shrivastava IH, Capener CE, Forrest LR, and Sansom MS. Structure and dynamics of K channel pore-lining helices: a comparative simulation study. *Biophys J* 78: 79-92, 2000.

Silverman WR, Roux B, and Papazian DM. Structural basis of two-stage voltage-dependent activation in K+ channels. *Proc Natl Acad Sci U S A* 100: 2935-2940, 2003.

Smith-Maxwell CJ, Ledwell JL, and Aldrich RW. Role of the S4 in cooperativity of voltage-dependent potassium channel activation. *J Gen Physiol* 111: 399-420, 1998.

Smith-Maxwell CJ, Ledwell JL, and Aldrich RW. Uncharged S4 residues and cooperativity in voltage-dependent potassium channel activation. *J Gen Physiol* 111: 421-439, 1998.

Sokolov S, Scheuer T, and Catterall WA. Ion permeation through a voltage- sensitive gating pore in brain sodium channels having voltage sensor mutations. *Neuron* 47: 183-189, 2005.

Spencer AN, Przysiezniak J, Acosta-Urquidi J, and Basarsky TA. Presynaptic spike broadening reduces junctional potential amplitude. *Nature* 340: 636-638, 1989.

Splitt H, Meuser D, Borovok I, Betzler M, and Schrempf H. Pore mutations affecting tetrameric assembly and functioning of the potassium channel KcsA from Streptomyces lividans. *FEBS Lett* 472: 83-87, 2000.

Stanfield PR, Davies NW, Shelton PA, Sutcliffe MJ, Khan IA, Brammar WJ, and Conley EC. A single aspartate residue is involved in both intrinsic gating and blockage by Mg2+ of the inward rectifier, IRK1. *J Physiol* 478 (Pt 1): 1-6, 1994.

Starace DM and Bezanilla F. Histidine scanning mutagenesis of basic residues of the S4 segment of the shaker k+ channel. *J Gen Physiol* 117: 469-490, 2001.

Starace DM and Bezanilla F. A proton pore in a potassium channel voltage sensor reveals a focused electric field. *Nature* 427: 548-553, 2004.

Starace DM, Stefani E, and Bezanilla F. Voltage-dependent proton transport by the voltage sensor of the Shaker K+ channel. *Neuron* 1997: 1319-1327, 1997.

Strang C, Cushman SJ, DeRubeis D, Peterson D, and Pfaffinger PJ. A central role for the T1 domain in voltage-gated potassium channel formation and function. *J Biol Chem* 276: 28493-28502, 2001.

Strauss WM. Preparation of genomic DNA from mammalian tissue. In: *Current Protocols in Molecular Biology*, edited by F.M. A, Brent R, Kingston RE, Moore D, Seidman JG, Smith JA and Struhl K. New York: John Wiley & Sons, Inc., 1998, p. 2.2.1-2.2.3.

Strong M, Chandy KG, and Gutman GA. Molecular evolution of voltage-sensitive ion channel genes - on the origins of electrical excitability. *Mol Biol Evol* 10: 221-242, 1993.

Stuhmer W, Conti F, Suzuki H, Wang X, Noda M, Yahagi N, Kubo H, and Numa S. Structural parts involved in activation and inactivation of the sodium channel. *Nature* 339: 597-603, 1989.

Stuhmer W, Ruppersberg JP, Schroter KH, Sakmann B, Stocker M, Giese KP, Perschke A, Baumann A, and Pongs O. Molecular basis of functional diversity of voltage-gated potassium channels in mammalian brain. *Embo J* 8: 3235-3244, 1989.

Sukhareva M, Hackos DH, and Swartz KJ. Constitutive activation of the Shaker Kv channel. *J Gen Physiol* 122: 541-556, 2003.

Swartz KJ. Towards a structural view of gating in potassium channels. *Nat Rev Neurosci* 5: 905-916, 2004.

Taglialatela M, Wible BA, Caporaso R, and Brown AM. Specification of pore properties by the carboxyl terminus of inwardly rectifying K+ channels. *Science* 264: 844-847, 1994.

Teitelman G, Lee J, and Reis DJ. Differentiation of prospective mouse pancreatic islet cells during development in vitro and during regeneration. *Dev Biol* 120: 425-533, 1987.

Thorneloe K, Chen TT, Kerr P, Grier EF, Cole WC, and Walsh MP. Molecular composition of 4-aminopyridine-sensitive voltage-gated K(+) channels of vascular smooth muscle. *Circ Res* 89: 1030-1037, 2001.

Tieleman DP, Shrivastava IH, Ulmschneider MR, and Sansom MS. Proline-induced hinges in transmembrane helices: possible roles in ion channel gating. *Proteins* 44: 63-72, 2001.

Titus SA, Warmke JW, and Ganetzky B. The Drosophila erg K+ Channel Polypeptide Is Encoded by the Seizure Locus. *J Neurosci* 17: 875-881, 1997.

Tiwari-Woodruff SK, Lin MA, Schulteis CT, and Papazian DM. Voltage-dependent structural interactions in the Shaker K(+) channel. *J Gen Physiol* 115: 123-138, 2000.

Tiwari-Woodruff SK, Schulteis CT, Mock AF, and Papazian DM. Electrostatic interactions between transmembrane segments mediate folding of Shaker K+ channel subunits. *Biophys J* 72: 1489-1500, 1997.

Tombola F, Pathak MM, and Isacoff EY. How Does Voltage Open an Ion Channel? *Annu Rev Cell Dev Biol*, 2006.

Tombola F, Pathak MM, and Isacoff EY. Voltage-sensing arginines in a potassium channel permeate and occlude cation-selective pores. *Neuron* 45: 379-388, 2005.

Treptow W, Maigret B, Chipot C, and Tarek M. Coupled Motions between Pore and Voltage-Sensor Domains: A Model for Shaker B, a Voltage-Gated Potassium Channel. *Biophys J* 87: 2365-2379, 2004.

Treptow W and Tarek M. K+ conduction in the selectivity filter of potassium channels is monitored by the charge distribution along their sequence. *Biophys J* 91: L81-83, 2006.

Treptow W and Tarek M. Molecular restraints in the permeation pathway of ion channels. *Biophys J* 91: L26-28, 2006.

Varshney ASK and Mathew MK. Modulation of voltage sensitivity by N-terminal cytoplasmic residues in human Kv1.2 channels. *Eur Biophys J* 31: 365-372, 2002.

von Heinje G. Proline kinks in transmembrane alpha-helices. *J Mol Biol* 218: 499-503, 1991.

Vriend D. WHAT IF: a molecular modeling and drug design program. *J Mol Graph* 8: 52-59, 1990.

Wang MH, Yusaf SP, Elliott DJ, Wray D, and Sivaprasadarao A. Effect of cysteine substitutions on the topology of the S4 segment of the Shaker potassium channel: implications for molecular models of gating. *J Physiol* 521 Pt 2: 315-326, 1999.

Webster SM, Del Camino D, Dekker JP, and Yellen G. Intracellular gate opening in Shaker K+ channels defined by high-affinity metal bridges. *Nature* 428: 864-868, 2004.

Williamson IM, Alvis SJ, East JM, and Lee AG. The potassium channel KcsA and its interaction with the lipid bilayer. *Cell Mol Life Sci* 60: 1581-1590, 2003.

Wishart DS, Boyko RF, and Sykes BD. Constrained multiple sequence alignment using XALIGN. *Comp Appl Biosci* 10: 687-688, 1994.

Wu N, Hsiao CF, and Chandler SH. Membrane resonance and subthreshold membrane oscillations in mesencephalic V neurons: participants in burst generation. *J Neurosci* 21: 3729-3739, 2001.

Yarov-Yarovoy V, Baker D, and Catterall WA. Voltage sensor conformations in the open and closed states in ROSETTA structural models of K(+) channels. *Proc Natl Acad Sci U S A* 103: 7292-7297, 2006.

Yellen G. The moving parts of voltage-gated ion channels. *Q Rev Biophys* 31: 239-295, 1998.

Yifrach O and MacKinnon R. Energetics of pore opening in a voltage-gated K(+) channel. *Cell* 111: 231-239, 2002.

Yool AJ and Schwarz AL. Alteration of ionic selectivity of a K+ channel by mutation of the H5 region. *Nature* 349: 700-704, 1991.

Zagotta WN, Hishi T, and Aldrich RW. Restoration of inactivation in mutants of Shaker potassium channels by a peptide derived from ShB. *Science* 250: 568-571, 1990.

Zagotta WN, Hoshi T, and Aldrich RW. Shaker potassium channel gating. III: Evaluation of kinetic models for activation. *J Gen Physiol* 103: 321-362, 1994.

Zagotta WN, Hoshi T, Dittman J, and Aldrich RW. Shaker potassium channel gating. II: Transitions in the activation pathway. *J Gen Physiol* 103: 279-319, 1994.

Zhou Y and MacKinnon R. The occupancy of ions in the K+ selectivity filter: charge balance and coupling of ion binding to a protein conformational change underlie high conduction rates. *J Mol Biol* 333: 965-975, 2003.

Zhou Y, Morais Cabral J, Kaufman A, and MacKinnon R. Chemistry of ion coordination and hydration revealed by a K+ channel-Fab complex at 2.0 A resolution. *Nature* 414: 43-48, 2001.